

Control and limitations of microbial degradation in aromatic hydrocarbon plumes – experiments in 2-D model aquifers

Dissertation

zur Erlangung des Grades eines Doktors der Naturwissenschaften

der Geowissenschaftlichen Fakultät
der Eberhard-Karls-Universität Tübingen

vorgelegt von
Robert Bauer
aus München

2007

Tag der mündlichen Prüfung: 21.12.07

Dekan: Prof. Dr. Peter Grathwohl

1. Berichterstatter: Prof. Dr. Rainer Meckenstock

2. Berichterstatter: Prof. Dr. Peter Grathwohl

„Als Pythagoras seinen bekannten Lehrsatz entdeckte, brachte er den Göttern hundert Ochsen dar.
Seitdem zittern die Ochsen, so oft eine neue Wahrheit ans Licht kommt.“
(Ludwig Börne, 1786-1837)

Clarification:

The simulation data in Chapter 2 was provided by Prof. Dr. Piotr Maloszewski, GSF Research Center for Environment and Health – Institute of Groundwater Ecology, Neuherberg, Germany.

The simulation data in Chapter 3 was provided by Dr. Massimo Rolle (ZAG, University of Tübingen) as this part of the work was accomplished within the DFG-funded research group “Reactions in porous media” in the course of a close cooperational work between the GSF Research Center for Environment and Health – Institute of Groundwater Ecology, Neuherberg, Germany, and the Center of Applied Geosciences, University of Tübingen, Germany.

Acknowledgements:

This work was financed by a grant from the Federal Ministry of Education and Research (BMBF KORA No. 02WN0357) and supported by a grant from the Deutsche Forschungsgemeinschaft (DFG) within the subproject “Effects of mixing processes on microbial degradation and the distribution of microorganisms in stationary and non-stationary contaminant plumes” of the Research Unit “Analysis and Modelling of Diffusion/Dispersion-limited Reactions in Porous Media” (GR 2107/1-2).

I want to express my explicit gratitudes to my supervisor Dr. Christian Griebler who provided me with excellent support, ideas and inspiration, and for his readiness for spontaneous discussions.

Thanks to Prof. Dr. Rainer U. Meckenstock for mentoring, profound coaching, fundamental ideas, and the opportunity for being part of the IGÖ-team.

I also thank Prof. Dr. Piotr Maloszewski for his help on “the other side” of my interdisciplinary work and his patience in explaining.

A huge “Grazie” to Dr. Massimo Rolle at the Center of Applied Geosciences, Tübingen, with whom I shared a most productive and good time at the end of my thesis work.

I greatly appreciated fruitful discussions within the DFG founded project group “Reactions in porous media”, especially with Peter Grathwohl, Christina Eberhardt, and Sebastian Bauer, helping me to broaden my mind and inspiring me with new ideas.

Furthermore, I would like to thank Florian Einsiedl for discussions in the geochemical topic, Christine Stumpp for patiently helping me in the basics of hydrogeology, and Günther Teichmann, Michael Stöckl and Dietmar Jurrat for their competent technical assistance.

Thanks to all members of the Institute of Groundwater Ecology for their cooperativeness and the great working atmosphere.

My special thanks go to my wife Verena who is always there for me, supporting, guiding and motivating me at any time.

I want to thank my family for their endless support and faith.

Control and limitations of microbial degradation in aromatic hydrocarbon plumes – experiments in 2-D model aquifers

Robert Bauer

Several hundred thousand groundwater sites worldwide are contaminated with petroleum derivatives, particularly with monoaromatic hydrocarbons such as benzene, toluene, ethylbenzene, and xylenes (BTEX). As groundwater serves as a major drinking water resource, controlled removal of these widespread organic compounds from aquifers is necessary. Among the processes involved in natural attenuation of pollutants in steady state groundwater contaminant plumes, only the mineralization via microorganisms leads to a significant mass removal. General concepts hold that in porous aquifers microbial degradation activities are primarily limited by mixing processes. Based on this consideration, the plume fringe concept was raised prior to this work, *i.e.* the dominant biodegradation activity takes place at the fringes of steady-state contaminant plumes, governed by the dispersive mixing of electron donors from the plume core and dissolved electron acceptors from ambient groundwater. Objective of this thesis was to experimentally prove the plume fringe concept by providing evidence that the biodegradation of model pollutants in porous media is mainly mixing-controlled. Moreover, this work tackled the detection of new potential degradation-limiting factors. The degradation of toluene and ethylbenzene therefore was investigated in 2-D sediment microcosms. Aerobic (*Pseudomonas putida* strain F1 and strain mt-2) as well as anaerobic (*Aromatoleum aromaticum* strain EbN1) degradation in toluene and ethylbenzene plumes showed steep biogeochemical gradients, dominant microbial biomass and biodegradation activities at the plumes' fringes in homogeneous porous media. These data confirmed the plume fringe concept and showed that biodegradation in the sediment microcosms is above all controlled by transverse dispersive mixing. If this holds true, increased dispersion, *i. e.* transverse dispersion and macrodispersion, should lead to an enhanced biodegradation. This hypothesis was proved in experiments where transverse dispersion was increased by means of sediment heterogeneity, *i.e.* an alternating succession of low- (middle sand) and high- (coarse sand) conductivity zones. Indeed, in developing toluene plumes as well as in steady state toluene and ethylbenzene plumes, aerobic degradation activity exhibited a significantly higher net removal of toluene and ethylbenzene (up to 100%) when compared to a homogeneous setup. However, under mixing-controlled conditions, the plume's fringe also exhibited zones with overlapping reactants during anaerobic degradation experiments. This indicated additional limiting factors or processes besides mixing. The slower reaction kinetics of denitrification were suggested to be responsible as the faster aerobic degradation never showed overlaps during this work. Although biokinetics played a minor role when compared to transverse dispersive mixing, the data indicated that additional limiting factors may be of greater importance in the field.

Steuernde und limitierende Einflußfaktoren auf den mikrobiellen Abbau in mit aromatischen Kohlenwasserstoffen belasteten Schadstofffahnen – Experimente in 2-D Modellaquiferen

Robert Bauer

Weltweit gibt es hunderttausende von Standorten, an denen das Grundwasser mit Mineralölderivaten und insbesondere mit monoaromatischen Kohlenwasserstoffen wie Benzol, Toluol, Ethylbenzol und Xylole (BTEX) verschmutzt sind. Weil Grundwasser als wichtigste Trinkwasserquelle dient, ist eine kontrollierte Beseitigung von organischen Schadstoffen zwingend erforderlich. Der natürliche Schadstoffabbau stabiler Schadstofffahnen im Grundwasser unterliegt zahlreichen Prozessen, wobei ausschließlich mikrobieller Abbau zu einer deutlichen Schadstoffabnahme führt. Gemäß allgemein gültigen Konzepten wird die Abbauaktivität durch Mikroorganismen insbesondere von transversalen Mischungsprozessen limitiert. Basierend auf dieser Annahme wurde zu Beginn dieser Arbeit das Fahnenrandkonzept formuliert. Es besagt, daß die Hauptabbauaktivität am Rand von stationären Schadstofffahnen stattfindet. Dabei steuern hauptsächlich Dispersionsvorgänge die Vermischung von Elektronendonoren aus der schadstoffhaltigen Fahne mit löslichen Elektronenakzeptoren des umgebenden Grundwassers. Das Ziel dieser Arbeit ist der eindeutige, durch experimentelle Daten erbrachte Nachweis des Fahnenrandkonzepts. Zu diesem Zweck soll zweifelsfrei bewiesen werden, daß der mikrobielle Abbau von Schadstoffen in porösen Medien hauptsächlich mischungskontrolliert ist. Darüberhinaus soll aufgeklärt werden, welche anderen Faktoren das Potential besitzen, den mikrobiellen Abbau zusätzlich zu limitieren. Zu diesem Zwecke wurde der mikrobielle Abbau von toluol- und ethylbenzolhaltigen Schadstofffahnen in zweidimensionalen Modellaquifer-Mikrokosmen untersucht. Sowohl der aerobe (*Pseudomonas putida* Stamm F1 und Stamm mt-2) als auch der anaerobe (*Aromatoleum aromaticum* Stamm EbN1) Abbau im homogenen Sediment zeigte am Fahnenrand steile biogeochemische Gradienten sowie Biomasse- und Aktivitätsverteilungen auf. Die Ergebnisse bestätigten das Fahnenrandkonzept, und zeigten daß der mikrobielle Schadstoffabbau in den verwendeten Mikrokosmen hauptsächlich durch transversale Dispersion kontrolliert wird. Falls das tatsächlich zutreffen sollte, so führen erhöhte Dispersionsprozesse (transversale Dispersion und Makrodispersion) zu einem verstärkten Abbau. Diese Hypothese konnte experimentell bestätigt werden, wobei Sedimente mit abwechselnder Reihenfolge von niedrig- (Mittelsand) und hochdurchlässigen (Grobsand) Zonen eine erhöhte Durchmischung ermöglichten. Im Verlauf sich entwickelnder Schadstofffahnen zeigte die aerobe Abbauaktivität eine deutlich höhere Abnahme von Toluol/Ethylbenzol im heterogenen Sediment. In stabilen Fahnen mit stufenweise erhöhten Schadstoffkonzentrationen lag die Abbaueffizienz im heterogenen Sediment zu jedem Zeitpunkt höher (bis zu 100%) als im homogenen Sediment. Während anaerober Abbauexperimente unter mischungskontrollierten Bedingungen im homogenen Sediment jedoch wurde phasenweise festgestellt, daß Toluol/Ethylbenzol und der zugehörige Elektronenakzeptor Nitrat gleichzeitig vorkamen. Dieser Umstand könnte darauf hin deuten, dass der Abbau nicht ausschließlich durch Mischungsprozesse kontrolliert wird, sondern zusätzlich limitierende Faktoren beteiligt sein könnten. Diese wurden z. T. den langsamaren Reaktionskinetiken der Denitrifikation zugeschrieben, da ähnliche Versuche mit Aerobiern, die bekanntlich schnelle Abbaukinetiken vorweisen können, solche Überlappungen nicht zeigten. Obwohl reaktionskinetische Prozesse im Vergleich zu transversalen Mischungsprozessen bei der Limitierung des mikrobiellen Schadstoffabbaus eine untergeordnete Rolle spielen, deuten die erhaltenen Daten darauf hin, daß zusätzliche limitierende Faktoren im Feld eine größere Bedeutung besitzen könnten.

Contents

1	General introduction	1
1.1	Background	1
1.2	Mixing-controlled biodegradation	1
1.3	Major scope of the work	3
1.12	References	4
2	Mixing-controlled biodegradation in a toluene plume.....	9
2.1	Introduction.....	9
2.2	Experimental setup.....	10
2.2.1	Two-dimensional (2-D) sediment microcosm	10
2.2.2	Media	11
2.2.3	Strains, cultivation and inoculation.....	12
2.2.4	Calculation of toluene degradation	12
2.2.5	Analysis of physical-chemical parameters.....	12
2.2.6	Redox conditions.....	12
2.2.7	Stable isotope analysis and cell counts	12
2.2.8	Conservative tracer transport	13
2.2.9	Reactive tracer transport	14
2.3	Results.....	14
2.3.1	Estimation of hydrodynamic parameters	14
2.3.2	Estimation of reactive parameters.....	16
2.3.2.1	Aerobic conditions	16
2.3.2.2	Anaerobic conditions	17
2.3.3	Experimental determination of microbial processes.....	18
2.3.4	Aerobic degradation of toluene.....	18
2.3.5	Toluene degradation under denitrifying conditions.....	21
2.3.6	Spatial distribution of degradation activity and microbes	23
2.4	Discussion and conclusions	24
2.4.1	Aerobic toluene degradation	24
2.4.2	Anaerobic toluene degradation	25
2.4.2	Plume fringe concept – mixing and biokinetics.....	27
2.4.4	Conclusions.....	29
2.5	References.....	30
3	Enhanced biodegradation in contaminant plumes via increased transverse dispersion.....	33
3.1	Introduction.....	33
3.2	Experimental setup.....	34
3.2.1	Two-dimensional sediment microcosms.....	34
3.2.2	Media	34
3.2.3	Strains, cultivation and inoculation.....	34
3.2.4	Analysis of anionic species	34
3.2.5	Redox conditions and oxygen measurements	37
3.2.6	Stable isotope analysis	37
3.2.7	Cell counts.....	37
3.2.8	Hydraulic properties.....	37
3.2.9	Flow and transport modeling	38
3.2.9.1	Flow Simulation	38
3.2.9.2	Conservative Transport.....	39
3.2.9.3	Reactive Transport	39
3.2.9.4	Mass flux of electron donors and electron acceptors.....	40
3.3	Results.....	40
3.3.1	Simulated flow and conservative transport.....	40

3.3.2 Degradation of contaminants	42
3.3.3 Distribution of biodegradation activity	45
3.3.4 Reactive transport simulations	47
3.4 Discussion	49
3.4.1 Mixing-controlled biodegradation in porous media	49
3.4.2 Additional biodegradation-limiting factors	51
3.5 References	52
4 Two-dimensional sediment microcosms – versatile test systems to study biodegradation processes in porous aquifers	55
4.1 Introduction	55
4.2 The 2-D sediment microcosm experimental setup	56
4.3 Controls and limitations of biodegradation in BTEX plumes – exemplary results and discussion	57
4.3.1 From abiotic to biotic processes	58
4.3.2 From aerobic to anaerobic degradation	58
4.3.3 From single strains to plain mixed communities	60
4.3.4 From homogeneous to heterogeneous sediments	61
4.3.5 From stable to transient plumes	63
4.3.6 From experimental to modeling data	63
4.3.7 Versatility of 2-D microcosm and application possibilities	65
4.3.8 Conclusions	66
4.4 References	66
5 General conclusions and outlook	69
References:	71
Appendix	I-LXXIV
Wissenschaftlicher Bildungsgang	LXXV
Publications	LXXVI
Selected Posters and Presentations	LXXVII

1 General introduction

1.1 Background

Since the industrialization organic resources and its synthetically formed products pose the most important source of energy. They are applied for various purposes, and ever since we face a marked increase of environmental pollution. Among a large variety of organic compounds that are involved, groundwater contaminations often feature mono- or polycyclic aromatic hydrocarbons (MAH, PAH) as prominent compounds. These are of utmost significance from an (eco)toxicological viewpoint, especially the monoaromatic BTEX group (Benzene, Toluene, Ethylbenzene and *ortho-/meta-/para-Xylene*). Careless storage, transport, and handling of crude oil, tar-oil and refined petroleum products brought forth countless sites of anthropogenic pollution over the past decades and centuries. As the contaminants are highly toxic and partly carcinogenic, their release to the environment is not only a serious ecological threat to the indigenous fauna and flora, but also a severe risk to human health when entering the subsurface. Since groundwater constitutes the fundamental resource for drinking water supply worldwide (Griebler & Mösslacher, 2003) and global water resources are overall scarce, groundwater contamination is highly undesirable (Danielopol *et al.*, 2003).

Due to the moving groundwater body, the dissolution of BTEX compounds into the groundwater leads to the formation of a contaminant plume. The morphology of such plumes depends on the size of the pollution source, the hydrogeologic conditions of the aquifer comprising hydraulic conductivity and water flow velocity, and sediment heterogeneity and composition. Subject to the gradient of the hydraulic head and the sediment permeability, groundwater moves at a rate between a few millimeters (silt to fine sand) to several meters (gravel) per day in porous media (Wiedemeier *et al.*, 1999). The lengths of contaminant plumes containing aromatic hydrocarbons measure between several meters to a few hundred meters (Teutsch *et al.*, 1997; Stupp *et al.*, 2006) and the total expansion is particularly governed by natural attenuation (NA).

Therefore, NA plays a crucial role in the fate of polluted sites. Most abiotic attenuation processes, *i.e.* dilution, sorption, ion exchange, volatilisation, precipitation, chemical transformation and dispersion (Christensen *et al.*, 2001; Cirpka *et al.*, 2006; Klenk and Grathwohl, 2002; Martian *et al.*, 2003; Mayer *et al.*, 2001), only play a role during the early stages of contamination until microbial degradation establishes. Subsequently, microbial activity is the only process which effectively leads to a net loss of pollutants in plumes contaminated with petroleum hydrocarbons (Christensen *et al.*, 2001; Martian *et al.*, 2003; Mayer *et al.*, 2001). Evaluating the contribution and the potential of NA at contaminated sites is an important prerequisite for choosing the right remediation strategy which ideally is characterized by an efficient removal of the pollutants at low costs. Monitored natural attenuation (MNA) and monitored enhanced natural attenuation (MENA) are “low technology” strategies building on the natural purification potential present in aquifers. To optimize NA and bioremediation of polluted grounds, the quality of investigation of basic biodegradation processes occurring in contaminant plumes is essential.

1.2 Mixing-controlled biodegradation

A contaminant plume in porous aquifers emerging from a point-source (e.g. an oil spill) generally causes an organic overload and due to microbial activity a severe change of the redox conditions, at which soluble electron acceptors are successively depleted in the order of their thermodynamic yield. Hence, aerobic degradation prevails in the first instance before denitrification

overtakes, followed by manganese- and iron-reduction, sulfate-reduction, and finally methanogenesis. After depletion in the plume's center, dissolved electron acceptors in a mature contaminant plume are often exclusively found at the plume's fringe, replenished from ambient groundwater. This forces major microbial degradation activity to concentrate at the plumes' fringes where steep redox gradients develop, ideally arranged according to their energy yield (Fig. 1.1).

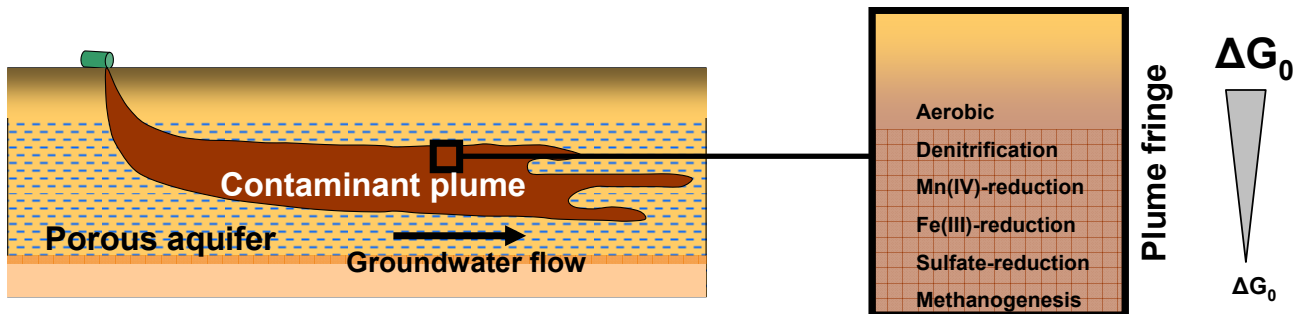


Figure 1.1: Conceptual scheme of a contaminant plume. The plume's fringe is characterized by a steep succession of individual redox processes according to their energy yield.

An overview of the Gibb's free energies of the respective terminal electron accepting processes (TEAPs) is given in Table 1.1.

Table 1.1: ΔG^0 [kJ eq⁻¹] in anaerobic and aerobic environments The transformation of contaminants entering the aquifer is subject to abiotic hydrolysis and subsequent respiration with O₂, NO₃⁻, Mn⁴⁺, Fe³⁺, SO₄²⁻ and methanogenesis as TEAPs, sometimes with intermittent fermentation (e.g. of sugars and amino acids) (modified from Christensen *et al.*, 2000; Watson *et al.*, 2003).

TEAP	ΔG^0 [kJ eq ⁻¹]
Aerobic:	-125
Denitrification:	-119
Mn ⁴⁺ -reduction:	-98
Fe ³⁺ -reduction:	-42
Fermentation:	(varies)
SO ₄ ²⁻ -reduction:	-25
CO ₂ -reduction/Methanogenesis:	-23

Given that the concentrations of organic pollutants do not reach toxic levels, degradation occurs at zones where both the electron donor and an adequate electron acceptor are concomitantly available which is generally at the fringe of contaminant plumes (Takahata *et al.*, 2006; Thornton *et al.*, 2001). Here, the mixing of electron donors from the contaminant plume with dissolved electron acceptors from pristine groundwater is warranted by hydrodynamic transverse dispersion, comprising pore-scale dispersion and diffusion (Jose & Cirpka, 2004; Maier & Grathwohl, 2006).

Due to the spatial separation of electron donor and acceptor the general concept holds that biodegradation in steady state contaminant plumes is primarily controlled by the mixing of reactants (e.g. Klenk & Grathwohl, 2002). Thus, the working hypothesis raised prior to this thesis was that

the contaminant removal is particularly located at the plume's fringe where, driven by transverse dispersion, the reactants mix, *i.e.* a theoretical concept that was termed the "plume fringe concept". However, in the case that mixing is the only driving force for microbial degradation in mature contaminant plumes, a concomitant presence of electron donor and acceptor can be excluded. Moreover, the redox zonation would be expected to be as steep as known from lake or marine sediments (in the micrometer range) (Kappler *et al.*, 2005). Here, oxygen is generally depleted within the first few millimeters from the sediment surface (Fenchel & Finlay, 1995; Frenzel, 1990; Hayes *et al.*, 1958) and the complete succession from aerobic to methanogenic conditions can be found within a few centimeters (Deming & Barros, 1993; Fenchel & Finlay, 1995; Jørgensen, 1977a, b; Sass *et al.*, 1997; Sørensen, 1979). In contrast to lake and sea sediments the groundwater flow in aquifers affects the pattern of biogeochemical gradients by complementing dispersion to diffusion as mixing process. The generally low transverse dispersivities in porous media which are in the order of millimeters or centimeters, of course depending on aquifer heterogeneity (Christensen *et al.*, 2001; Eberhardt & Grathwohl, 2002; Klenk and Grathwohl, 2002), narrow down the thickness of the plume's fringe and thus the zone of dominant microbial activity (Bekins *et al.*, 1999; Christensen *et al.*, 2000, 2001; Mayer *et al.*, 2001; Vieth *et al.*, 2005). However, in heterogeneous sediments the passing of a plume through domains of different conductivities may significantly increase transverse dispersion (Maier & Grathwohl, 2006; Werth *et al.*, 2006) which theoretically leads to an enhanced biodegradation. At contaminated groundwater sites, the resolution of sampling wells is usually not sufficient to detect steep biogeochemical gradients at the plume's fringe (Anneser *et al.*, 2007). The distribution of biodegradation and key factors limiting contaminant conversion are still not fully understood.

Although transverse mixing is suggested to constitute the main controlling factor for biodegradation in contaminant plumes, additional limiting parameters and processes were occasionally considered. Various field studies for instance documented an overlapping zone of electron donors and electron acceptors at the plume's fringe (Anneser *et al.*, 2007; Baéz-Cazull *et al.*, 2007; Bjerg *et al.*, 1995; Tuxen *et al.*, 2006; van Breukelen & Griffioen, 2004), pointing at secondary non mixing-dependent factors that limit microbial growth and biodegradation. Biokinetics as well as mass transfer limitations may be involved (Johnsen *et al.*, 2005; Wick *et al.*, 2001, 2002). This is supported by the fact that due to the slow growth and biodegradation rates of anaerobic processes, it takes several years or even decades until significant degradation or biomass increase takes place *in situ* (Bekins *et al.*, 2001; Lerner *et al.*, 2000; Mayer *et al.*, 2001).

1.3 Major scope of the work

Objective of this thesis work was to unambiguously prove the plume fringe concept and to evaluate if degradation in porous media in contaminant plumes carrying high loads of organic pollutants is exclusively mixing-controlled, or if additional limiting factors are involved. Mixing-controlled biodegradation was indicated by numerical simulations, reactive transport models (Cirpka *et al.*, 1999; Ham *et al.*, 2004; Jose & Cirpka, 2004; Maier & Grathwohl, 2006; Prommer *et al.*, 2000, 2002, 2006; Thullner *et al.*, 2004), and a few laboratory studies (e.g. Huang *et al.*, 2003; Oates *et al.*, 2005; Rees *et al.*, 2007; Thullner *et al.*, 2002). However, the use of extraordinary high concentrations of easy degradable carbon sources in the reported lab experiments questions the transferability of some findings to the situation in contaminated porous aquifers. Clear experimental evidence for the plume fringe concept, regarding the degradation of model pollutants (e.g. aromatic hydrocarbons), was missing. Also the spatial distribution of microbial activity, biomass and reactants according to the concept was hardly tackled in former studies. Furthermore, the effect of

sediment heterogeneity on dispersion processes (transverse dispersion and macrodispersion) and thus on biodegradation was hardly considered in model scenarios and lab studies published. So far, only a numerical modeling approach by Werth and coworkers (2006) showed that enhanced transverse dispersion, caused by high-conductivity sediment inclusions, has beneficial effects onto microbial degradation. Experimental data directly comparing biodegradation in homogeneous and heterogeneous sediments is lacking completely.

In addition, the role of limiting factors other than transverse dispersion was considered which was barely studied so far. This issue's significance is justified by the following statement: "On the one hand, bioclogging in contaminant plumes *in situ* has not been reported despite the obvious ample abundance of substrate and nutrients available in the mixing zone. On the other hand, broad overlapping zones of electron donors and electron acceptors were reported in field studies (e.g. Anneser *et al.*, 2007; Bjerg *et al.*, 1995; van Breukelen & Griffioen, 2004)". How does this come? So far, multidisciplinary bioreactive studies in mixing-controlled contaminant plumes focused on the validation of numerical models (e.g. Jose & Cirpka, 2004) rather than discerning limitation factors other than transverse dispersion. Still, such interdisciplinary approaches constitute invaluable work, connecting microbiological aspects with prediction models regarding the evaluation of the fate of contaminant plumes.

The experiments in this thesis work were conducted with laboratory-scale two-dimensional (2-D) sediment microcosms, reducing natural complexity and allowing to study individual processes in porous media under well-controlled conditions. In the first phase of my thesis, aerobic and anaerobic degradation of a toluene plume was investigated in homogeneous sediments to prove the plume fringe concept. Then, a comparative 2-D sediment microcosm experiment, where a contaminant plume passed through (a) homogeneous porous media and (b) a sediment packing with two consecutive quadrangular high-conductivity (*i.e.* coarse sand) lenses, was conducted. Here, first aerobic degradation of toluene and ethylbenzene was investigated in a developing plume till steady state, before turning to anaerobic degradation of ethylbenzene. The experiments were run with the aerobic strains *Pseudomonas putida* strain F1 and mt-2 and the anaerobic strain *Aromatoleum aromaticum* strain EbN1*. A number of highly sophisticated methods, such as compound-specific isotope analyses, direct counts of suspended and attached bacteria via flow cytometry, optode measurements for quantification of oxygen, contaminant analyses, among others were applied in an extraordinary temporal (daily) and spatial (cm-scale) resolution. Moreover, the experiments were prepared and accompanied by the application of a comprehensive contemporary modeling approach to interpret the data and identify factors other than transverse mixing that may play a role in the limitation of biodegradation in porous media.

1.12 References

Anneser B., Richters L., Griebler C. (2007) Identification and localization of redox processes in an aromatic hydrocarbon plume via high-resolution sampling of biotic and abiotic gradients. Candela, L.; Vadillo, I.; Aagaard, P.; Bedbur, E.; Trevisan, M.; Vanclooster, M.; Viotti, P.; López-Greta, J.A. (Eds.), Water Pollution in natural Porous media at different scales. Assessment of fate, impact and indicators. WAPO², Madrid, ISBN: 978-84-7840-676-0.

* According to Wöhlbrand *et al.*, 2007, strain EbN1 will follow the nomenclature "*Aromatoleum aromaticum*" strain EbN1, belonging to the proposed new genus "*Aromatoleum*". This will comprise a variety of denitrifying beta-Proteobacteria from the *Azoarcus/Thauera* cluster, which are capable of degrading aromatic compounds anaerobically.

- Baéz-Cazull S., McGuire J.T., Cozzarelli I.M., Raymond A., Welsh L. (2007) Centimeter-scale characterization of biogeochemical gradients at a wetland-aquifer interface using capillary electrophoresis. *Appl Geochem*, in press.
- Bekins B.A., Godsy E.M., Warren E. (1999) Distribution of microbial physiologic types in an aquifer contaminated by crude oil. *Microb Ecol* **37**: 263-75.
- Bekins B.A., Cozzarelli I.M., Godsy E.M., Warren E., Essaid H.I., Tuccillo M.E. (2001) Progression of natural attenuation processes at a crude oil spill site: II. Controls on spatial distribution of microbial populations. *J Contam Hydrol* **53**: 387-406.
- Bjerg P.B., Rügge K., Pedersen J.K., Christensen T.H. (1995) Distribution of redox-sensitive groundwater quality parameters downgradient of a landfill (Grindsted, Denmark). *Environ Sci Technol* **29**:1387-94.
- Christensen T.H., Bjerg P.L., Banwart S.A., Jakobsen R., Heron G., Albrechtsen H.J. (2000) Characterization of redox conditions in groundwater contaminant plumes. *J Contam Hydrol* **45**: 165-241.
- Christensen T.H., Kjeldsen P., Bjerg P.L., Jensen D.L., Christensen J.B., Baun A., Albrechtsen H.J., Heron G. (2001) Biogeochemistry of landfill leachate plumes. *Appl Geochem* **16**: 659-718.
- Cirpka O.A., Frind E.O., Helmig R. (1999) Numerical simulation of biodegradation controlled by transverse mixing. *J Contam Hydrol* **40**: 159-82.
- Cirpka O.A., Olsson Å., Ju Q., Rahman M.A., Grathwohl P. (2006) Determination of transverse dispersion coefficients from reactive plume lengths. *Ground Water* **44**: 212-21.
- Danielopol D.L., Griebler C., Gunatilaka A., Notenboom J. (2003) Present state and future prospects for groundwater ecosystems. *Environ Conserv* **30**: 104-30.
- Deming J.W. & Barros J.A. (1993) The early diagenesis of organic matter: bacterial activity. In: Engel, M.H., Macko S.A. (eds.) *Organic geochemistry – principles and applications*. Plenum Press, New York, pp.119-144.
- Eberhardt C. & Grathwohl P. (2002) Time scales of organic contaminant dissolution from complex source zones: coal tar pools vs. blobs. *J Contam Hydrol* **59**: 45-66.
- Fenchel T., Finlay B.J. (1995) Ecology and evolution in anoxic worlds. Chapter 1: Anaerobic environments, p. 1-31. Oxford series in ecology and evolution, University Press, Oxford. ISBN13: 978-0-19-854837-9, ISBN10: 0-19-854837-0.
- Frenzel P. (1990) The influence of chironomid larvae on the sediment oxygen microprofiles. *Arch Hydrobiol* **119**: 427-37.
- Griebler C., Mösslacher F. (2003) *Grundwasserökologie*, pp. 314ff. Facultas Verlags- und Buchhandels AG, Wien.
- Ham P.A., Schotting R.J., Prommer H., Davis G.B. (2004) Effects of hydrodynamic dispersion on plume lengths for instantaneous bimolecular reactions. *Advances Water Resour* **27**: 803-13.
- Hayes F.R., Reid B.L., Cameron M.L. (1958) Lake water sediment. 2. Oxidation-reduction relations at the mud-water interface. *Limnol Oceanogr* **3**: 308-17.
- Huang W.E., Oswald S.E., Lerner D.N., Smith C.C., Zheng C. (2003) Dissolved oxygen imaging in a porous medium to investigate biodegradation in a plume with limited electron acceptor supply. *Environ Sci Technol* **37**: 1905-11.
- Johnsen A.R., Wick L.Y., Harms H. (2005) Principles of microbial PAH-degradation in soil. *Environ Poll* **133**: 71-84.
- Jørgensen B.B. (1977a) Bacterial sulfate reduction within reduced microniches of oxidized marine sediments. *Marine Biol* **41**: 7-17.
- Jørgensen B.B. (1977b) Distribution of colorless sulfate bacteria (*Beggiatoa* spp.) in a coastal marine sediment. *Marine Biol* **41**: 19-28.

- Jose S.C. & Cirpka O.A. (2004) Measurement of mixing-controlled reactive transport in homogeneous porous media and its prediction from conservative tracer test data. *Environ Sci Technol* **38**: 2089-96.
- Kappler A., Emerson D., Edwards K., Amend J.P., Gralnick J.A., Grathwohl P., Hoehler T., Straub K.L. (2005) Microbial activity in biogeochemical gradients – new aspects of research. *Geobiol* **3**: 229-33.
- Klenk I.D. & Grathwohl P. (2002) Transverse vertical dispersion in groundwater and the capillary fringe. *J Contam Hydrol* **58**: 111-28.
- Lerner D.N., Thornton S.F., Spence M.J., Banwart S.A., Bottrell S.H., Higgs J., Mallinson H.E., Pickup R.W., Williams G.M. (2000) Ineffective natural attenuation of degradable organic compounds in a phenol-contaminated aquifer. *Ground Water* **38**: 922-8.
- Maier U. & Grathwohl P. (2006) Numerical experiments and field results on the size of steady state plumes. *J Contam Hydrol* **85**: 33-52.
- Martian P., Sorenson K.S., Peterson L.N. (2003) A critique of the internal tracer method for estimating contaminant degradation rates. *Ground Water* **41**: 632-9.
- Mayer K.U., Benner S.G., Frind E.O., Thornton S.F., Lerner D.N. (2001) Reactive transport modeling of processes controlling the distribution and natural attenuation of phenolic compounds in a deep sandstone aquifer. *J Contam Hydrol* **53**: 341-68.
- Oates P.M., Castenson C., Harvey C.F., Polz M., Culligan P. (2005) Illuminating reactive microbial transport in saturated porous media: demonstration of a visualization method and conceptual transport model. *J Contam Hydrol* **77**: 233-45.
- Prommer H., Barry D.A., Davis G.B. (2000) Numerical modelling for design and evaluation of groundwater remediation schemes. *Ecol Modelling* **128**: 181-95.
- Prommer H., Barry D.A., Davis G.B. (2002) Modelling of physical and reactive processes during biodegradation of a hydrocarbon plume under transient groundwater flow conditions. *J Contam Hydrol* **59**: 113-31.
- Prommer H., Tuxen N., Bjerg P.L. (2006) Fringe-controlled natural attenuation of phenoxy acids in a landfill plume: integration of field-scale processes by reactive transport modeling. *Environ Sci Technol* **40**: 4732-8.
- Rees H.C., Oswald S.E., Banwart S.A., Pickup R.W., Lerner D.N. (2007) Biodegradation processes in a laboratory-scale groundwater contaminant plume assessed by fluorescence imaging and microbial analysis. *Appl Environ Microbiol* **73**: 3865-76.
- Sass H., Cypionka H., Babenzien H.-B. (1997) Vertical distribution of sulfate-reducing bacteria at the oxic-anoxic interface in the sediments of the oligotrophic lake Stechlin. *FEMS Microb Ecol* **22**: 245-55.
- Sørensen J., Jørgensen B.B., Revsbech N.P. (1979) A comparison of oxygen, nitrate and sulfate respiration in coastal marine sediments. *Microb Ecol* **5**: 105-15.
- Stupp H.D., Bakenhaus A., Gass M., Schwaar I., Lorenz D. (2006) Ausbreitung von CKW und MTBE im Grundwasser – Grundwassertransport und Fahnenlängen – *Altlasten Spektrum* **5**: 256-66.
- Takahata Y., Kasai Y., Hoaki T., Watanabe K. (2006) Rapid intrinsic biodegradation of benzene, toluene, and xylenes at the boundary of a gasoline-contaminated plume under natural attenuation. *Appl Microbiol Biotechnol* **73**: 713-22.
- Teutsch G., Grathwohl P., Schiedek T. (1997) Literaturstudie zum natürlichen Rückhalt / Abbau von Schadstoffen im Grundwasser.- Bericht des Lehrstuhls für angewandte Geologie, Universität Tübingen (im Auftrag der Landesanstalt für Umweltschutz Baden-Württemberg).

- Thornton S.F., Quigley S., Spence M.J., Banwart S.A., Bottrell S., Lerner D.N. (2001) Processes controlling the distribution and natural attenuation of dissolved phenolic compounds in a deep sandstone aquifer. *J Contam Hydrol* **53**: 233-67.
- Thullner M., Mauclaire L., Schroth M.H., Kinzelbach W., Zeyer J. (2002) Interaction between water flow and spatial distribution of microbial growth in a two-dimensional flow field in saturated porous media. *J Contam Hydrol* **58**: 169-89.
- Thullner M., Schroth M.H., Zeyer J., Kinzelbach W. (2004) Modelling of a microbial growth experiment with bioclogging in a two-dimensional saturated porous media flow field. *J Contam Hydrol* **70**: 37-62.
- Tuxen N., Reitzel L.A., Albrechtsen H.J., Bjerg P.L. (2006) Oxygen-enhanced biodegradation of phenoxy acids in ground water at contaminated sites. *Ground Water* **44**: 256-65.
- Van Breukelen B.M. & Griffioen J. (2004) Biogeochemical processes at the fringe of a landfill leachate pollution plume: potential for dissolved organic carbon, Fe(II), Mn(II), NH₄ and CH₄ oxidation. *J Contam Hydrol* **73**: 181-205.
- Vieth A., Kästner M., Schirmer M., Weiss H., Gödeke S., Meckenstock R.U., Richnow H.H. (2005) Monitoring *in situ* biodegradation of benzene and toluene by stable carbon isotope fractionation. *Environ Toxicol Chem* **24**: 51-60.
- Watson I.A., Oswald S.E., Mayer K.U., Wu Y., Banwart S.A. (2003) Modeling kinetic processes controlling hydrogen and acetate concentrations in an aquifer-derived microcosm. *Environ Sci Technol* **37**: 3910-9.
- Werth C.J., Cirpka O.J., Grathwohl P. (2006) Enhanced mixing and reaction through flow focusing in heterogeneous porous media. *Water Resour Res* **42**, W12414, doi:10.1029/2005WR004511.
- Wick L.Y., Colangelo T., Harms H. (2001) Kinetics of mass-transfer limited bacterial growth on solid PAHs. *Environ Sci Technol* **35**: 354-61.
- Wick L.Y., de Ruiz M., Springael A., Harms H. (2002) Responses of *Mycobacterium* sp. 501T to the low bioavailability of solid anthracene. *Appl Microbiol Technol* **58**: 378-85.
- Wiedemeier T.H., Rifai H.S., Newell C.J., Wilson J.T. (1999) Natural attenuation of fuels and chlorinated solvents in the subsurface. John Wiley & Sons, Inc., New York, N.Y.
- Wöhlbrand L., Kallerhoff B., Lange D., Hufnagel P., Thiermann J., Reinhardt R., Rabus R. (2007) Functional proteomic view of metabolic regulation in „*Aromatoleum aromaticum*“ strain EbN1. *Proteomics* **7**: 2222-39.

2 Mixing-controlled biodegradation in a toluene plume

2.1 Introduction

Thousands of groundwater sites all over the world are polluted with organic chemicals such as petroleum hydrocarbons which are often spilled accidentally or escape by leakage from storage tanks into the environment as bulk NAPLs (non-aqueous phase lipids). After infiltrating the soil, these complex mixtures meet the groundwater table and, due to dissolution of individual compounds into the water, evolve into contaminant plumes. Effective remediation techniques for removal of these partly toxic compounds are cost- and time-intensive. However, in many cases, the length of mature contaminant plumes is stable. Therefore, monitored natural attenuation (MNA) or monitored enhanced natural attenuation (MENA) may be cost-effective strategies for the long-term management of sites polluted by petroleum hydrocarbons and the associated risks.

The processes of transport, distribution, and biodegradation of organic contaminants in porous aquifers are all determined by various physical, chemical and biological processes, such as advection, diffusion, dispersion, dissolution, volatilization, sorption and degradation. Whereas conservative contaminant transport and physico-chemical reactions in porous media have been studied extensively (e.g. Grathwohl, 1998; Jose & Cirpka, 2004; Maloszewski *et al.*, 2003; Ptak *et al.*, 2004; Zamfiresu & Grathwohl, 2001), how and where biodegradation takes place in contaminated porous aquifers is still not entirely known. During the development of contaminant plumes containing high organic loads, the available dissolved electron acceptors are successively depleted in the order of their thermodynamic energy yield; from oxygen to nitrate, Mn^{4+} , Fe^{3+} to SO_4^{2-} , before methanogenesis takes place. There is evidence from several field sites that biodegradation of oxidizable compounds at the core of mature anoxic plumes is low due to the depletion of dissolved electron acceptors and toxicity of contaminants (e.g. Takahata *et al.*, 2006; Thornton *et al.*, 2001). Thus, either only insoluble ferric iron phases may serve as electron acceptors or methanogenesis prevails (Watson *et al.*, 2005). Biodegradation activities in steady state contaminant plumes are often elevated at the transition zones between contaminated and uncontaminated areas in aquifers, *i.e.* the plume's fringes, where electron acceptors from ambient groundwater mix with contaminants (Tuxen *et al.*, 2006; Watson *et al.*, 2005). Here, transverse dispersion is the main process mixing dissolved terminal electron acceptors (TEAs) such as oxygen, nitrate and sulfate across the fringes of contaminant plumes (Cirpka *et al.*, 2006; Jose *et al.*, 2004; Klenk & Grathwohl, 2002; Rahman *et al.*, 2005; Schürmann *et al.*, 2003; Thornton *et al.*, 2001). Furthermore, dispersion might reduce toxic concentrations of contaminants and metabolic end products towards the plume's fringe zones. For a better understanding of *in situ* biodegradation and a targeted stimulation of pollutant transformation, it is crucial that the controlling processes as well as the distribution of active degradation zones in contaminated aquifers is fully understood.

Based on this knowledge the working hypothesis was raised that, for oxidizable compounds, biodegradation rates in steady state contaminant plumes are mainly controlled by transverse mixing of dissolved electron donors and acceptors. Support for this is partly found with reactive transport modeling assuming instantaneous reaction between the partners or microbial activity according to the Monod-equation (e.g. Cirpka *et al.*, 1999a, b; Jose & Cirpka, 2004; Maier & Grathwohl, 2006; Mayer *et al.*, 2001; Prommer *et al.*, 2000, 2002, 2006; Thornton *et al.*, 2001; Thullner *et al.*, 2002a, b, 2004). However, experimental evidence for a mixing-controlled biodegradation is still sparse (Tuxen *et al.*, 2006).

Numerous studies have examined the abiotic and biotic processes involved in contaminant degradation under well controlled lab conditions. However, there is often a discrepancy between

laboratory and field data stemming from a difference in growth conditions (Watson *et al.*, 2003). Unfortunately, most field studies lack detailed data at an appropriate scale (centimeter to decimeter resolution) to spatially resolve the real geochemical gradients and the microbial processes in the core and fringe zones of plumes (Anneser *et al.*, 2007). Such small scale information on geochemical and biological gradients and the dimensions of mixing zones are arguably the key to uncover limitations of biodegradation in porous groundwater systems. Laboratory two-dimensional sediment microcosms offer a valuable tool to investigate individual processes. Similarly to natural porous media, geochemically different flow lines can be maintained within a homogeneous flow field. 2-D sediment microcosms (in the following simply termed tanks) therefore mirror much better the typical conditions found in a contaminated porous sediment system. In recent years various 2-D flow-through systems have been developed and applied to study the transport and fate of contaminants in saturated sedimentary environments (e.g. Loveland *et al.*, 2003; MacKinnon *et al.*, 2002; Ptak *et al.*, 2004; Thullner *et al.*, 2002a). In order to test conceptual and numerical models, field data and experimental results from 2-D microcosm experiments are favourably used (Huang *et al.*, 2003; Cirpka *et al.*, 2006; Prommer *et al.*, 2006).

Here, 2-D tank experiments are reported on to elucidate key processes controlling biodegradation of toluene under oxic and denitrifying conditions. This study focused on the physical-chemical gradients across anoxic toluene plumes and the associated small-scale distribution of biodegradation activity and microbial biomass. To derive a conceptual understanding of factors controlling and limiting biodegradation, the experimental data were compared with results from a bioreactive transport model.

2.2 Experimental setup

2.2.1 Two-dimensional (2-D) sediment microcosm

The experiments presented in this study were carried out in two identical 2-D sediment microcosms (tank 1 and tank 2) with inner dimensions of 78.5 cm × 1,1 cm × 14 cm (Fig. 2.1). The tank is made of teflon, aluminium and two glass sheets, thus avoiding materials which sorb organic contaminants. Additionally, for the same purpose, only a minimum of silicon glue was used for sealing. The top of each tank could be closed with a lid. The inlet and outlet side is equipped with 11 ports each with a vertical spacing of 1.2 cm. This tank was packed with sterile quartz sand (heated at 450°C for 4 h) with a grain diameter of 200 – 300 µm (Aldrich, USA), and maintained in an upright position with a 0.5 cm thick unsaturated zone (Fig. 2.1). The inlet and outlet ports consist of stainless steel capillaries (1/16", Alltech, IL, USA) which were connected to tygon pump-tubing (ID: 1.02 mm; Ismatec, Glattbrugg, CH) fitted to two peristaltic pumps (MCP, Ismatec, Glattbrugg, CH). At the outflow side, the steel capillaries were tipped with steel wire gauzes inside the tanks to avoid plugging by sediment particles. The capillaries at the outlet were directly connected to brass T-fittings (1/16" A-Lok, Alltech, IL, USA), splitting the outflow for sampling purposes (Fig. 2.1). In general, 10 of the inlet ports were fed with artificial groundwater medium. Nine of the ports were fed with oxic medium containing nutrients and electron acceptors but no carbon source, while one of the ports (port 5) was fed with the anoxic plume medium containing toluene and bromide (see below). The plume medium was supplied to the tank via stainless steel capillaries and a ceramic piston pump (Ismatec, Glattbrugg, CH). An interposed brass T-fitting allowed subsampling of the plume medium immediately before the tank entrance. To maintain a constant flow, a second multi-channel peristaltic pump was connected to the 11 outflow ports. The adjusted flow rates resulted in

a flow velocity of 1.2 m d^{-1} (estimated with an artificial tracer test). To create an unsaturated zone ensuring a stable water table the uppermost port (*i.e.* port 1) at the inlet side was plugged with a stopper whereas surplus water and ambient gas from above the sediment was withdrawn by the uppermost port at the outlet side. Sampling of the outlet ports was done by a multi-channel syringe pump (WPI, Berlin, Germany) holding ten 10 mL glass syringes (Poulten & Graf, Wertheim, Germany) and maintaining the identical flow rate of the peristaltic pumps. All samples were aliquoted for subsequent analysis of different microbiological and chemical parameters.

Prior to each experiment, the tank was sterilized with a 12 g L^{-1} NaOH solution and rinsed with autoclaved ultra-pure MQ water (Millipore, MA, USA).

In a first experiment, the two tank systems were run in parallel, one inoculated with the denitrifying strain *Aromatoleum aromaticum* strain EbN1 (Wöhlbrand *et al.*, 2007) and the other with the aerobic strain *Pseudomonas putida* strain mt-2. With *A. aromaticum* strain EbN1 only, a similar follow-up experiment was conducted.

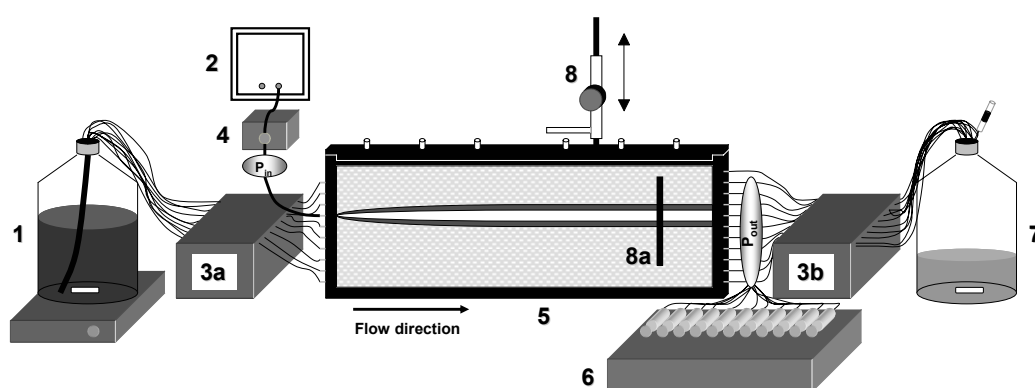


Figure 2.1: Schematic view of the two-dimensional aquifer microcosm indicating an artificially generated contaminant plume. (1) Reservoir containing organic carbon-free oxic medium; (2) reservoir for toluene-containing, anoxic medium (gas-tight Tedlar-Bag); (3a,b) peristaltic pumps maintaining a homogeneous flow regime; (4) ceramic piston pump transporting the anoxic plume medium; (5) 2-D sediment microcosm with 11 inlet and outlet ports and filled with quartz sand; (6) multi-channel syringe pump replacing 3b during sampling periods; (7) waste reservoir; (8) trim modulation device holding microsensors for vertical measurement; (8a) oxygen-sensitive sensor strip attached to the inner wall; (P_{in}) inlet sampling point; (P_{out}) outlet sampling ports.

2.2.2 Media

The oxic groundwater medium introduced to the tank at the inlet ports was based on bicarbonate-buffered freshwater medium (containing 2.52 g L^{-1} sodium-hydrocarbonate, 1.25 g L^{-1} disodium sulfate, 1 g L^{-1} NaCl, 0.5 g L^{-1} potassium chloride, 0.4 g L^{-1} magnesium-dichloride hexahydrate, 0.25 g L^{-1} ammonium chloride, 0.2 g L^{-1} potassium-dihydrophosphate, 0.15 g L^{-1} calcium-dichloride dihydrate, trace elements, and vitamins) (pH 7.2-7.4) (Widdel & Bak, 1992) amended with sodium nitrate (68.5 mg L^{-1}) and oxygen (8.45 mg L^{-1}) as electron acceptors. Furthermore, the medium contained resazurin (2 mg L^{-1}) as redox indicator (see below). A 5 L bottle (Schott, Mainz, Germany) served as medium reservoir, which was stirred constantly to guarantee oxygen saturation. At one inlet port of the tank (port no. 5), anoxic freshwater medium of similar composition but with toluene (8.7 mg L^{-1}) and bromide (50 mg L^{-1}) added as conservative tracer was continuously injected to generate an artificial contaminant plume (Fig. 2.1). Except for the disodium sulfate, no potential electron acceptor was added to the anoxic plume medium prepared under an N_2/CO_2 -atmosphere (80:20) and reduced with ascorbate at a final concentration

of 1.75 g L⁻¹. The plume medium reservoir was a gas-tight and inert 5 L Tedlar bag (SKC, PA, USA) without headspace and protected from light with aluminium foil.

2.2.3 Strains, cultivation and inoculation

The aerobic toluene-degrading strain *P. putida* mt-2 was obtained from J. R. van der Meer, Dübendorf, Switzerland and the denitrifying *A. aromaticum* strain EbN1 from F. Widdel, Bremen, Germany (Rabus & Widdel, 1995). Precultures of both strains were grown with toluene as the sole carbon and energy source at room temperature in the dark. Media were composed as reported above. All batch cultures were grown in half-filled 100 mL serum bottles, sealed with butyl rubber stoppers (Maag Technik, Switzerland). For EbN1, the headspace was flushed with N₂/CO₂ (80:20). Toluene (99.5%; Aldrich, USA) was injected with a sterile glass syringe through the rubber stopper to a final concentration of 20-50 mg L⁻¹.

Inoculation of the tank with the respective strains was performed over six hours at the two inlet ports adjacent to the plume medium port.

2.2.4 Calculation of toluene degradation

The degradation of toluene is based on the subtraction of the total mass flux detected at the outlet ports from the total mass flux entering the system given in mass per unit time where the standard deviation $s_{\bar{x}}$ is denoted as $s_{\bar{x}} = \sqrt{(s_{\bar{i}})^2 + (s_{\bar{o}})^2}$ with $s_{\bar{i}}$ and $s_{\bar{o}}$ representing the standard deviations of the inlet and outlet total mass fluxes, respectively.

2.2.5 Analysis of physical-chemical parameters

Concentrations of bromide, nitrate, and sulfate were determined by ion chromatography (Dionex AS3500, Idstein, Germany). Sulfide concentrations were determined photometrically following the protocol of Cline (1969).

Sample aliquots of two mL were used for the determination of toluene concentrations, first spiked with 0.5 mL cyclohexane containing 9.42 mg L⁻¹ ethylbenzene as internal standard, and then, after shaking for one hour, the cyclohexane phase was collected and toluene concentrations were measured by gas chromatography (Hewlett Packard 5890 series II; CA, USA) following a protocol as described previously in Griebler *et al.* (2004).

2.2.6 Redox conditions

For the visualization of reduced zones in the porous media, the redox indicator resazurin was added to all media (e.g. Bueno *et al.*, 2002; Tratnyek *et al.*, 2001). Therefore, oxic zones appeared bluish, while anoxic zones ($E_h \leq -100\text{mV}$) were colorless.

2.2.7 Stable isotope analysis and cell counts

In a second experiment with *Aromatoleum aromaticum* strain EbN1 a mixture of non-labelled toluene-*h*₈ and deuterium-labelled toluene-*d*₈ in a ratio of 10:1 was used as carbon source (8.6 mg L⁻¹ total conc.). The ratio of the two isotopomers in the residual (= non-degraded) toluene fraction was determined from 3 mL sample aliquots by headspace analysis with a GC-MS (Finnigan

Trace Ultra and Trace DSQ, Thermo Electron Cooperation, Waltham, MA, USA, with a DB-5MS column, 0.5 μm film thickness, 0.25 i.d., 30 m length, J & W Scientific, USA). Sample injection was on split mode (1:10 mL min^{-1}) and the flow rate of the carrier gas helium was 1 mL min^{-1} . The oven temperature was 40°C for 1 min, then ramped first at a rate of 15°C min^{-1} to 200°C and then at a rate of 25°C to 300°C where it was held for 1.33 min. The MS was operated at 350°C in the SIM scan mode for the masses 91.00 and 98.00.

At the end of the experiment, vertical sediment cores were collected from the tank across the toluene plume with a sterile aluminium tube (inner dimensions: 0.8 cm x 1.0 cm), partitioned into 0.5 cm aliquots which were then immediately fixed in 1 mL para-formaldehyde (4%) for 14 h, and then washed twice with 1xPBS (phosphate buffered saline, 7.6 g L^{-1} NaCl, 25 g L^{-1} Na_xPO_4 , pH 7.2-7.4). After washing and centrifugation (7000 X g, 10 min.), the supernatant was discarded and the solid was taken up in 250 μL 1xPBS buffer and 98% ethanol (50:50, vol/vol). Fixed sediment samples were shaken on a vortex mixer at maximum intensity for 1 min and subsequently treated in an ultrasonic bath (Branson Digital Sonifier, Branson, Danbury, CT, USA) at 20% amplitude for 1 min to disaggregate cells from the sediment, followed by a second treatment on a vortex mixer at maximum intensity for 0.5 min. Aliquots of the sample supernatant were stained with the fluorescent dye SYBR-Green I as previously described in Griebl *et al.* (2001). A defined amount of fluorescent beads (BD-Truecount Tubes, BD Biosciences, San Jose, USA) was added to each sample as an internal standard and the total number of cells was counted in duplicate in a LSR II flow cytometer (Becton Dickinson, NJ, USA).

2.2.8 Conservative tracer transport

In the flow-through system presented in this study, the transport of the non-reactive tracers toluene (only during the abiotic phase of the experiment) and bromide can be considered as two-dimensional (x, y) with the x-axis of the coordinate system being parallel to the flow direction (length of the tank) and the y-axis being parallel to the height of the system. The transport equation is then:

$$D_L \frac{\partial^2 C}{\partial x^2} + D_T \frac{\partial^2 C}{\partial y^2} - v \frac{\partial C}{\partial x} = \frac{\partial C}{\partial t} \quad (2.1)$$

where C is the solute concentration; v is the mean velocity of water; D_L and D_T are the longitudinal and transverse dispersion coefficients, respectively; t is the time variable; x is the flow distance and y is the transverse distance to the x-axis situated in the middle of the injection zone.

In our experiments, the injection was performed continuously with a constant toluene and bromide concentration ($C_{\text{in}} = C_0$) entering the system in $x = 0$ through the injection zone of the width (w) on the y-axis (between $y+w/2$, and $y-w/2$), described by the Heaviside function H(y):

$$C(x = 0, y) = C_0 [H(y + w/2) - H(y - w/2)] \quad (2.2)$$

The transverse distribution of the conservative tracers ($x = L$) was determined at the outlet after $(15-50) \times t_0$, (t_0 is the mean transit time of the water) and thus permitted to assume steady state conditions. For $P_D (= D_L/vx) < 0.03$ (valid for the experiments) longitudinal dispersion ($\alpha_L = D_L/v = 1.4$ mm) may be neglected, and the transport equation for non-reactive tracers in steady state reads:

$$D_T \frac{\partial^2 C}{\partial y^2} - v \frac{\partial C}{\partial x} = 0 \quad (2.3)$$

The solution of eq. (2.3) has the following form (*i.e.* Cirpka & Valocchi, 2007; Domenico and Palciauskas, 1982):

$$F(x, y) = \frac{C(x, y)}{C_0} = \frac{1}{2} \left[\operatorname{erf} \left(\frac{y + w/2}{\sqrt{4xD_T v}} \right) - \operatorname{erf} \left(\frac{y - w/2}{\sqrt{4xD_T v}} \right) \right] \quad (2.4)$$

where $F(x, y)$ is the relative tracer concentration $C(x, y)/C_0$ and $\operatorname{erf}(\eta)$ is the error function of argument (η).

2.2.9 Reactive tracer transport

The modeling of the experimental data was performed using the reactive transport model containing double Monod kinetics with first order biomass decay as introduced by Cirpka & Valocchi (2007). These authors assume an irreversible biotic reaction of compounds A and B reacting to compound C. Moreover, the model assumes an immobile and steady state biomass.

The three fitting parameters of the double Monod kinetic model with first order biomass decay under steady state conditions are the two Monod coefficients of compounds A and B (K_A , K_B), and the coefficient ε which is the ratio of the specific growth rate to the rate coefficient of biomass decay ($\mu_{\max}/k_{\text{dec}}$).

2.3 Results

2.3.1 Estimation of hydrodynamic parameters

The solution to equation (2.1) was used to determine the longitudinal dispersion coefficient (D_L) and the mean water velocity during a preliminary experiment in which bromide was injected as a pulse for the duration of 1 hour. The water velocity was found to be $v = 1.39 \times 10^{-5} \text{ m s}^{-1}$ (1.2 m d^{-1}) yielding a mean transit time of water $t_0 = L/v$ of approximately 15.5 h (L is the flow distance). The longitudinal dispersion coefficient was found to be $D_L = 1.95 \times 10^{-8} \text{ m}^2 \text{ s}^{-1}$, resulting in a dispersion parameter of $P_D = D_L/vx = 1.79 \times 10^{-3}$.

The transverse dispersion coefficient D_T was estimated using equation (2.4). The bromide data, stemming from the aerobic and the anaerobic experiment, was modeled during the abiotic phase (aerobic: day 8; anaerobic: day 6-9), the biotic phase (aerobic: day 20-28; anaerobic: day 22-32) and the biotic phase in the presence of sulfide (aerobic: day 30-34; anaerobic: day 34-38) (Fig. 2.2), yielding an identical value of $D_T = 1.85 \times 10^{-9} \text{ m}^2 \text{ s}^{-1}$. According to Grathwohl (1998) and Olsson (2005), the effective molecular diffusion coefficient in sediment is $D_S = D_{\text{aq}} \times n$, where $D_{\text{aq}}(\text{bromide}) = 2.08 \times 10^{-9} \text{ m}^2 \text{ s}^{-1}$ (Atkins, 1990) and $D_{\text{aq}}(\text{toluene}) = 8.49 \times 10^{-10} \text{ m}^2 \text{ s}^{-1}$ (Olesen *et al.*, 2001). For bromide, $D_S = 0.99 \times 10^{-9} \text{ m}^2 \text{ s}^{-1}$ revealed a transverse dispersivity of $\alpha_T = [(D_T - D_S)/v] = 0.06 \text{ mm}$. The effective diffusion coefficient for toluene $D_S = 0.45 \times 10^{-9} \text{ m}^2 \text{ s}^{-1}$ accounted for a transverse dispersion coefficient of $D_T = (D_S + \alpha_T \times v) = 1.31 \times 10^{-9} \text{ m}^2 \text{ s}^{-1}$. This value was used for the modeling of toluene data obtained from the experiments. A theoretical expansion of the toluene plume over the length of the flow-through system is depicted in Fig. 2.3.

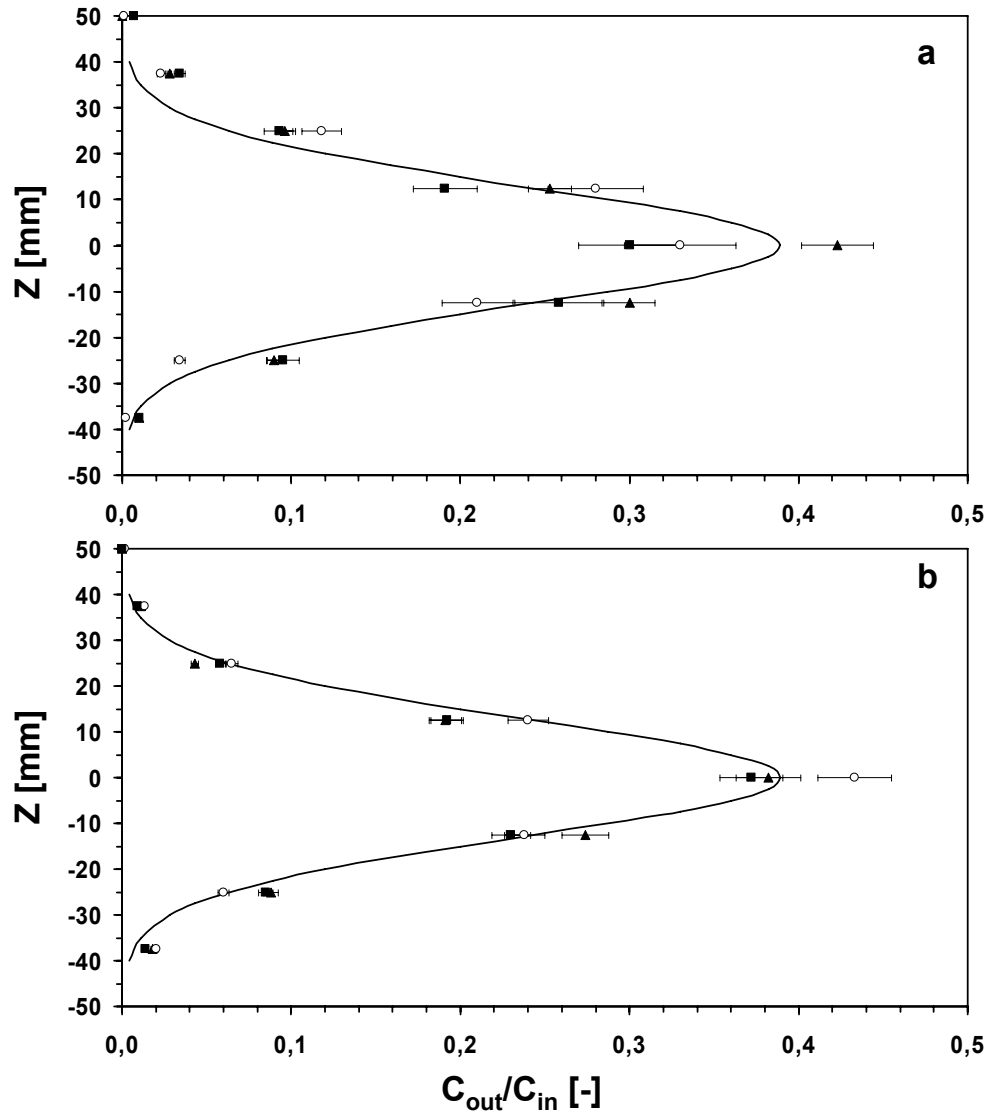


Figure 2.2: Relative bromide concentrations measured at the outlet ports during the abiotic phase on day 8 and 6-9 (triangles), the biotic phase on day 20-28 and 22-32 (circle), and the biotic phase with sulfide inside the plume on day 30-34 and 34-38 (squares) of the experiments conducted with *P. putida* mt-2 (a) and strain EbN1 (b), respectively. The solid line shows the modeled distribution.

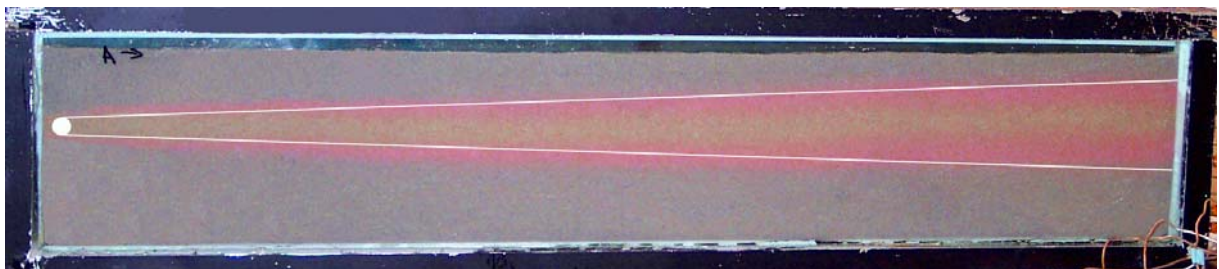


Figure 2.3: Photograph showing the shape of the anoxic toluene plume as was indicated by the redox indicator resazurin during the abiotic phase of the anaerobic experiment. The white spot depicts the infiltration point (source), and the white lines represent the theoretical expansion of the toluene plume based on $D_T = 1.31 \times 10^{-9} \text{ m}^2 \text{ s}^{-1}$.

2.3.2 Estimation of reactive parameters

The bioreactive transport modeling was based upon the hydraulic parameters described in the previous chapter and applied in our experiments for conditions that were assumed steady state. Toluene and oxygen, as well as toluene and nitrate, constitute the compounds A and B under aerobic and anaerobic conditions, respectively. The tank dimensions, hydraulic parameters, input concentrations of electron donor in the plume and electron acceptors in the ambient flow (C_A^{in} and C_B^{in}), as well as the stoichiometric coefficients (f_a , f_b , and f_c), are summarized in Table 2.1.

2.3.2.1 Aerobic conditions

The biokinetic parameters used in the model were determined in batch studies. Four batch experiments with *Pseudomonas putida* strain mt-2 (*P. putida* mt-2), an oxygen saturation of 7.8 mg L⁻¹ and different initial concentrations of toluene, yielded Monod half-saturation constants for toluene under aerobic conditions of $K_{Tol} = 0.8-25 \mu\text{mol L}^{-1}$ and maximum growth rates of $\mu_{max} = 7.3-20.2 \text{ d}^{-1}$ (data not shown). Assuming a mean value of $K_{Tol} = 10 \mu\text{mol L}^{-1}$ and of $\mu_{max} = 13.1 \text{ d}^{-1}$, the best fit was found for the parameters in Table 2.2 (Fig 2.2b). After the determination of μ_{max} and ϵ the decay rate k_{dec} was calculated. The results of aerobic reactive transport modeling of toluene are shown in Fig. 2.4. As the experimental oxygen data could not be measured, we applied a best fit according to the experimental toluene data and following the conservative and the bioreactive behavior of toluene and oxygen (Fig. 2.2a).

Table 2.1: Defined parameters used for modeling

Parameter	Symbol	Value
Length of the microcosm	L	0.785 m
Height of the microcosm	H	0.14 m
Width of the injection zone	w	0.0625 m
Water flow velocity	v	$1.39 \times 10^{-5} \text{ m s}^{-1}$
Mean transit time	t_0	15.5 h
Longitudinal dispersion coefficient for toluene	D_L	$1.95 \times 10^{-8} \text{ m}^2 \text{ s}^{-1}$
Transverse dispersion coefficient for toluene	D_T	$1.31 \times 10^{-9} \text{ m}^2 \text{ s}^{-1}$
Input concentration of toluene	C_{Tol}^{in}	8.7 mg L ⁻¹
Oxygen conc. in ambient flow (compound B; aerobic cond.)	C_{Oxy}^{in}	8.45 mg L ⁻¹
Nitrate conc. in ambient flow (compound B; anaerobic cond.)	C_{Nit}^{in}	68.5 mg L ⁻¹
Stoichiometric coefficient for toluene	f_{Tol}	1
Stoichiometric coefficient for oxygen	f_{Oxy}	9
Stoichiometric coefficient for nitrate	f_{Nit}	7.2
Stoichiometric coefficient for metabolite (inorganic carbon)	f_C	7.0

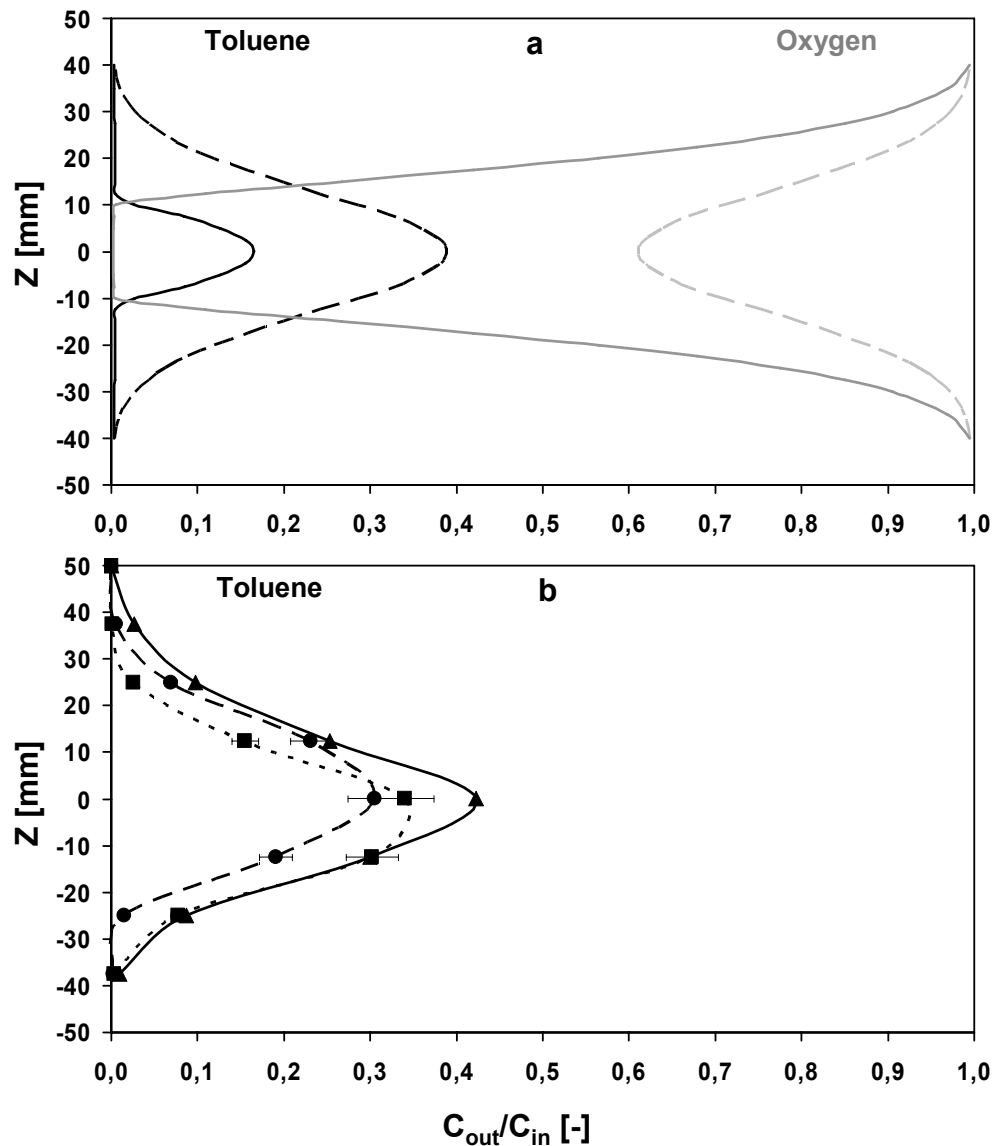


Figure 2.4: Aerobic degradation experiment. The modeled data (a) shows the conservative distribution (dashed lines) of toluene (black) and nitrate (grey). The solid lines illustrate the theoretical bioreactive distribution of the reactants in the absence of the reducing agent ascorbate (see text for further explanation). The experimental toluene data (b) was recorded during the three experimental phases, *i.e.* abiotic phase (triangles), biotic phase (circles), and biotic phase with the presence of sulfide in the plume medium (squares).

2.3.2.2 Anaerobic conditions

Three batch experiments with *Aromatoleum aromaticum* strain EbN1, a surplus of nitrate (0.62 g L^{-1}) and varying initial toluene concentrations revealed Monod half-saturation constants for toluene under anaerobic conditions of $K_{\text{Tol}} = 180\text{-}320 \text{ }\mu\text{mol L}^{-1}$ and maximum growth rates of $\mu_{\text{max}} = 0.34\text{-}0.98 \text{ d}^{-1}$ (data not shown). For modeling, a mean value of $K_{\text{Tol}} = 250 \text{ }\mu\text{mol L}^{-1}$ and of $\mu_{\text{max}} = 0.68 \text{ d}^{-1}$ was assumed. K_{Nit} and ε were used as fitting parameters. The parameters are defined as summarized in Table 2.2. The decay rate was then determined based upon the obtained values of ε and μ_{max} . The modeled toluene and nitrate distributions under anaerobic conditions during the different experimental phases are shown in Fig. 2.5.

Table 2.2: Reactive parameters defined for aerobic and anaerobic conditions.

Parameter	Symbol	Aerobic	Anaerobic
Biotic phase			
Monod coefficient for toluene (determined in batch experiments)	K_A	14 $\mu\text{mol L}^{-1}$	250 $\mu\text{mol L}^{-1}$
Monod coefficient for electron acceptor (estimation from values given in literature)	$K_B (K_{Oxy}; K_{Nit})$	10 $\mu\text{mol L}^{-1}$	70 $\mu\text{mol L}^{-1}$
Mean maximum growth rate (determined in batch experiments)	μ_{\max}	13.1 d^{-1}	0.68 d^{-1}
Decay rate (derived from $k_{\text{dec}} = \varepsilon \times \mu_{\max}$)	k_{dec}	0.262 d^{-1}	0.0007 d^{-1}
Rate coefficient of biomass decay ratio over the maximum specific growth rate ($k_{\text{dec}} / \mu_{\max}$) (fitted)	$\frac{1}{\varepsilon}$	0.02	0.001
Biotic phase + sulfide			
Monod coefficient for toluene	K_A	-	250 $\mu\text{mol L}^{-1}$
Monod coefficient for electron acceptor	$K_B (K_{Oxy}; K_{Nit})$	-	70 $\mu\text{mol L}^{-1}$
Rate coefficient of biomass decay ratio over the maximum specific growth rate ($k_{\text{dec}} / \mu_{\max}$) (fitted)	$\frac{1}{\varepsilon}$	-	0.045

2.3.3 Experimental determination of microbial processes

Data collected during the abiotic phase of each experiment indicated quasi-steady state conditions for bromide after 2-3 days. Probably due to sorption/desorption processes at quartz sand as well as with small areas of silicon glue used for sealing the inner tank components, the ratio of toluene outlet versus toluene inlet concentrations took about 8 days to become stable after launching the experiments (Fig. 2.6a). In the course of the degradation experiments, the distribution of bromide in the plume was stable indicating constant hydraulic conditions.

2.3.4 Aerobic degradation of toluene

The basic conditions of the aerobic degradation experiment in tank 1 were defined by a constant point source of toluene of $8.86 \pm 0.55 \text{ mg L}^{-1}$ (accounting for a total mass flux of $648.2 \pm 30.2 \mu\text{g d}^{-1}$) entering the tank at inlet port 5. This resulted in an anoxic plume surrounded by oxic artificial groundwater with a maximum oxygen mass flux of about 6.7 mg d^{-1} . Temperatures were kept steady at 18-20°C throughout the experiments. Furthermore, toluene was the only substrate, while the ascorbate used as reducing agent in the plume medium was not utilized by *P. putida* mt-2. Assuming perfect mixing, as in batch cultures, aerobic toluene degradation can be described according to equation 2.5.



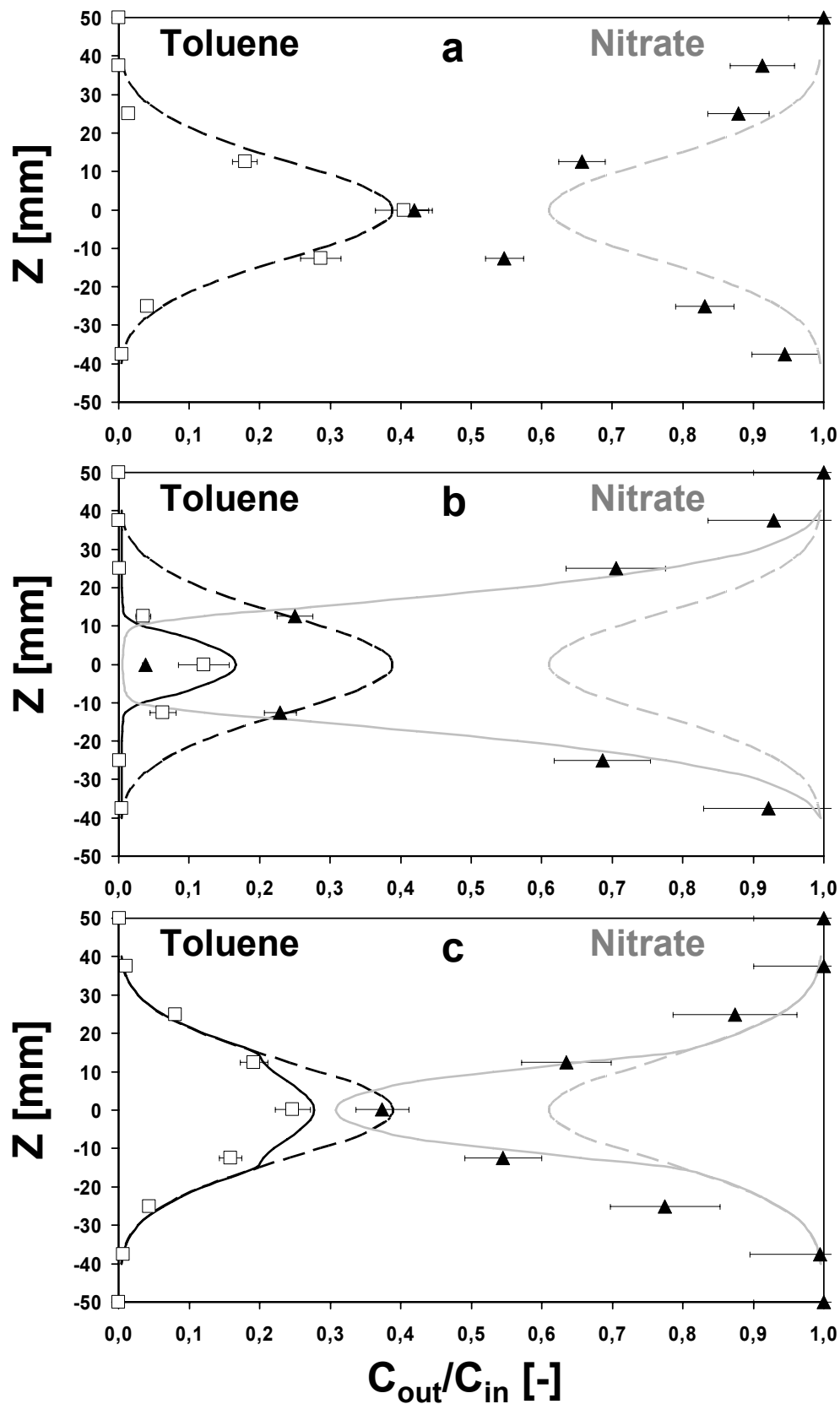


Figure 2.5: Anaerobic degradation experiment. Toluene (squares) and nitrate (triangles) concentrations as determined during the three experimental phases, *i.e.* abiotic phase (a), biotic phase (b), and biotic phase with the presence of sulfide in the plume medium (c), compared to modeled toluene (black lines) and nitrate (grey lines) concentration curves. The dashed lines indicate the conservative distribution of the reactants corresponding to the abiotic phase (a), and the solid lines represent the bioreactive data. For model input parameters see Tab. 2.2.

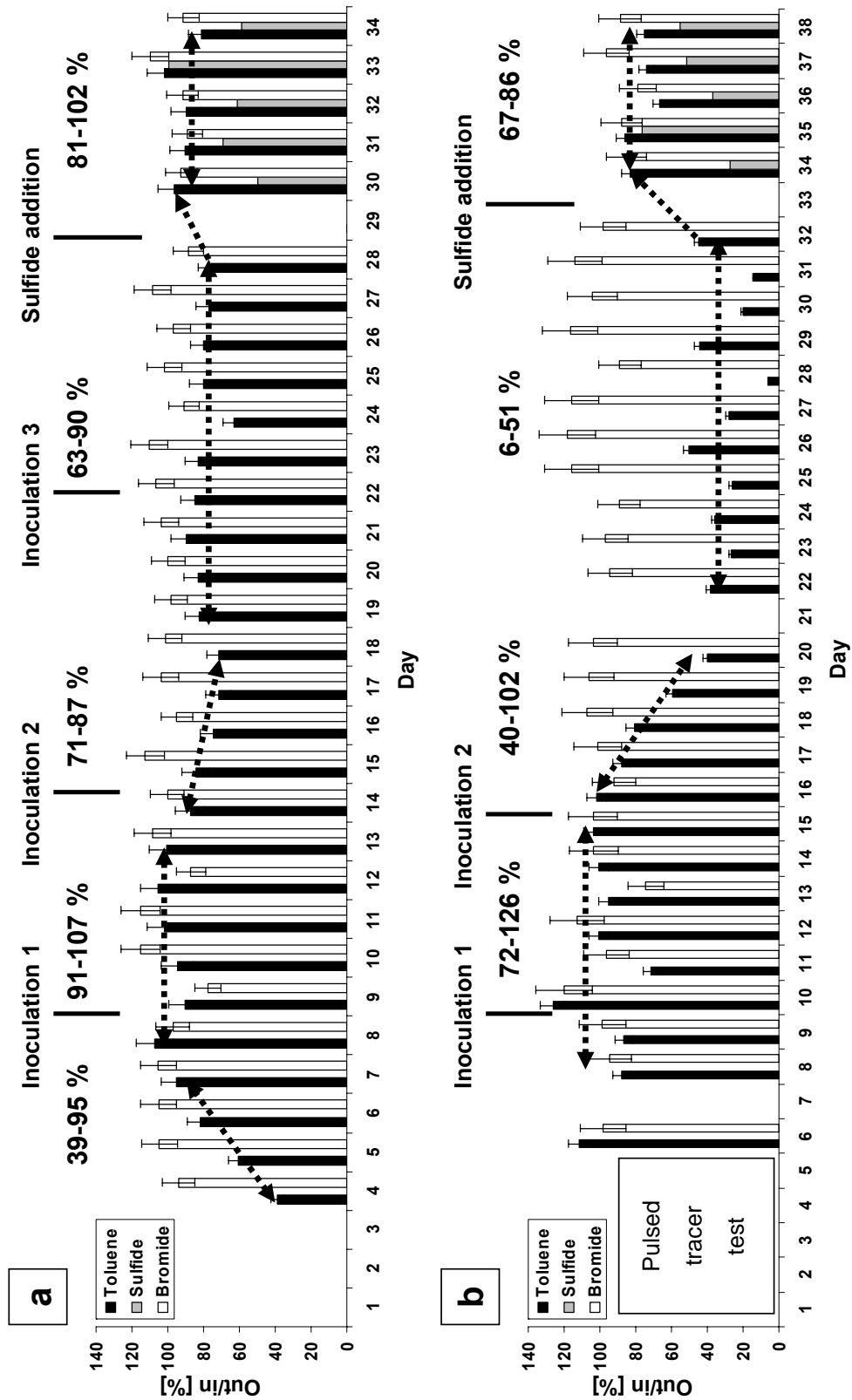


Figure 2.6: Mass balances for aerobic (a) and anaerobic (b) toluene degradation in the two-dimensional tank experiments conducted with *Pseudomonas putida* mt-2 and strain EbN1, respectively. Ratio of the outlet versus inlet concentration of toluene, sulfide, and bromide is depicted in % for each day of the experiment. Values highlighted above bars indicate the average percentage of the residual toluene during the different stages of the experiment. (SDs of daily balances were derived from SD of the mean inflow conc.).

After the abiotic equilibration phase of 8 days, the tank was inoculated with *P. putida* mt-2. However, this first inoculation was not sufficient to establish a bacterial population capable of actively degrading the substrate. Consequently, a second inoculation was performed six days later which led to the subsequent degradation of toluene (Fig. 2.6a). The first inoculation was a 15 hour pulse of a *P. putida* mt-2 culture infiltrated at the inlet ports 4 and 6 which are adjacent to the plume generated at port 5. The second inoculation was carried out at the inlet ports 3, 4, 6 and 7, and lasted for 10 hours. Thereafter, toluene degradation increased constantly for the following 5 days, before it levelled off at a remaining mass flux of $508.3 \pm 45.0 \mu\text{g d}^{-1}$ at the outlet ports of the system. Thus, $139.8 \pm 54.2 \mu\text{g d}^{-1}$ of toluene was degraded during transport through the tank, accounting for a mass removal of $21.7 \pm 8.4\%$. The comparison of the daily outlet versus inlet nitrate concentrations indicated that no nitrate was consumed and thus *P. putida* mt-2 used oxygen exclusively. Also in batch experiments, these organisms only used oxygen to degrade toluene when provided with nitrate in oxic, as well as in ascorbate-reduced medium (data not shown).

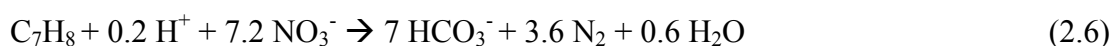
A third inoculation was performed at day 21, first, to refresh the bacterial population and second, to see if the active biomass in the tank could be increased. No long-term improvement of the degradation rate resulted (Fig. 2.6a).

The decrease of aerobic toluene degradation during day 18 and 19 can mainly be attributed to a reduced influx of dissolved oxygen into the tank, caused by fungal growth in the peristaltic tubes. Oxygen measurement in the oxic medium reservoir and at individual inlet ports showed a reduction in concentration of up to 70% at ports 8-11 on the last day of the experiment.

In the final stage of the experiment, sulfide was added to the plume medium to evaluate its inhibiting effects on microbial activity. In the corresponding batch experiments sulfide was repeatedly shown to be toxic at high concentrations (data not shown). Furthermore, the chemical oxidation of sulfide by dissolved oxygen at the fringe of the toluene plume was to be tested. This latter reaction resulted in steeper redox gradients, as indicated by a narrowing of the pink reactive zone (Fig. 2.7). The plume medium sulfide flow rate of $2,371.1 \pm 226.4 \mu\text{g d}^{-1}$ from day 28 on resulted in a stable outflow rate of $1,545.1 \pm 100.3 \mu\text{g d}^{-1}$ after 3 days. Concurrently, the total aerobic toluene degradation decreased significantly from $139.8 \pm 54.2 \mu\text{g d}^{-1}$ to $63.9 \pm 47.7 \mu\text{g d}^{-1}$ ($10.1 \pm 7.4\%$ total mass removal) and remained at that value (Fig. 2.6a). It was not possible to measure concentrations of SO_4^{2-} and S^0 , *i.e.* potential products of sulfide oxidation. However, based on stoichiometric calculations the observed loss of sulfide would require approximately 400 to $1,650 \mu\text{g d}^{-1}$ of oxygen for chemical reaction depending on whether sulfide is oxidized to either elemental sulfur or sulfate. Moreover, taking into account that 70% of the incoming oxygen was consumed by fungal growth in the tubing before reaching the tank, 360 to $1,610 \mu\text{g d}^{-1}$ of oxygen would still be available for aerobic toluene degradation and would allow oxidation of 40 to $180 \mu\text{g d}^{-1}$ of toluene. This range is in agreement with the measured data.

2.3.5 Toluene degradation under denitrifying conditions

The setup of the two anaerobic degradation experiments in tank 2 was identical to the aerobic experiment mentioned above, except that the denitrifying *Aromatoleum aromaticum* strain EbN1 (*A. aromaticum* EbN1) was used for inoculation. According to the reaction equation (2.6) the amount of nitrate supplied ($54,602 \pm 1,673 \mu\text{g d}^{-1}$) was in excess of that needed for the total oxidation of the $649.6 \pm 40.4 \mu\text{g d}^{-1}$ toluene source to CO_2 in perfectly mixed systems.



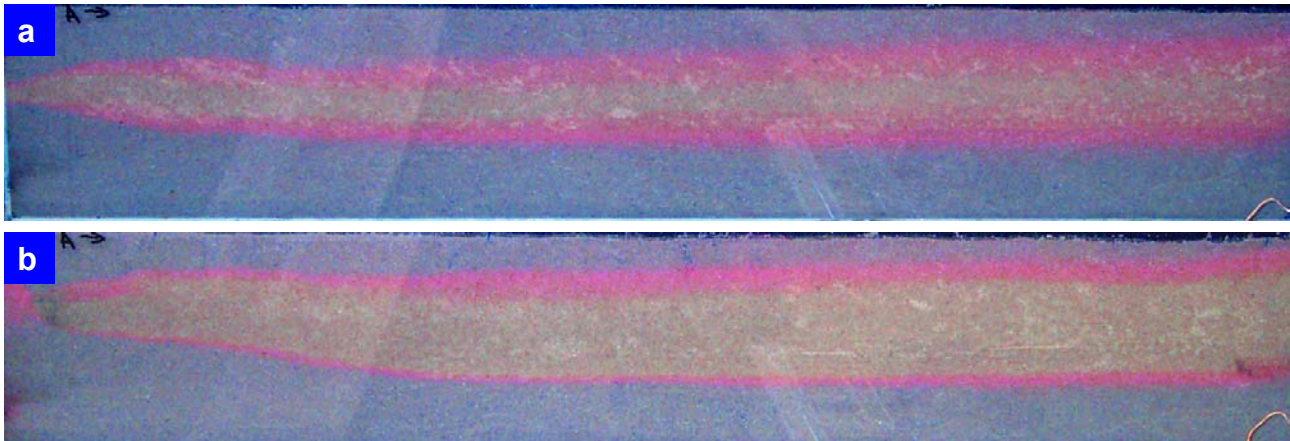


Figure 2.7: Comparison of the plume shape during different phases of toluene degradation by strain EbN1 before (a) and after (b) addition of sulfide to the plume medium, visualized by the redox indicator resazurin.

Although *A. aromaticum* EbN1 is described as a facultative anaerobe, the strain mineralized toluene exclusively via the well-described benzylsuccinate pathway (Rabus, 2005). Aerobic growth was excluded in previous batch culture experiments. Further batch experiments proved no growth on the organic redox indicator resazurin and the reducing agent ascorbate (data not shown).

During the initial abiotic phase (from day 1 to 5) in experiment one, a pulsed tracer test with bromide and uranine was conducted (see above), followed by a daily monitoring of the physical-chemical conditions from day 6 to 9 (Fig. 2.6b). Several further experiments under similar conditions always exhibited quasi steady state conditions in the initial abiotic phase after 6 to 9 days with respect to sorption/desorption processes of toluene at the sediment matrix and at the areas covered with silicon glue. The first inoculation of tank 2 with *A. aromaticum* EbN1 was conducted at day 9, whereupon no pronounced degradation of toluene could be achieved (Fig. 2.6b). After an intensive second inoculation (see above) at day 15, a rapid decrease in toluene and nitrate concentrations was observed at the tank outlet (Fig. 2.6b). Within 5 days, the toluene degradation stabilized at an average rate of $453.9 \pm 102.6 \mu\text{g d}^{-1}$, which accounted for $69.9 \pm 15.8\%$ of the substrate import (Fig. 2.6b). The high fluctuations in the daily toluene mass balances during this high activity period of the experiment can mainly be attributed to repeated disturbances of the tank sediments due to invasive oxygen measurements by means of Clark-type microsensors applied at that time. This method was later replaced by a non-invasive optode technique (see below). Assuming a constant total nitrate mass flux of $54,602 \pm 1,673 \mu\text{g d}^{-1}$ into the tank (consider port 1 was not active and 5 supplied nitrate-free plume medium), $28.8 \pm 6.4\%$ (i.e. $15,730 \pm 3,470 \mu\text{g d}^{-1}$) was consumed on average during this biotic phase. Later at day 32, sulfide ($2,356.2 \pm 226.4 \mu\text{g d}^{-1}$) was added to the anoxic plume medium (Fig. 2.6b). Concomitantly with the stabilization of the sulfide outflow concentrations at day 36 at $1,431.1 \pm 131.0 \mu\text{g d}^{-1}$, toluene degradation dropped to $140.0 \pm 68.2 \mu\text{g d}^{-1}$ which equaled a mass reduction of $21.6 \pm 10.5\%$ of the total inflow concentration. At the same time the total nitrate consumption dropped to $10,636 \pm 3,402 \mu\text{g d}^{-1}$ which accounted for $19.5 \pm 6.2\%$ of the total amount infiltrated (Fig. 2.6b). In complementing batch experiments, we found that the addition of $\geq 6.6 \text{ mg L}^{-1}$ of sulfide to *A. aromaticum* EbN1 cultures in the exponential growth phase significantly inhibited degradation of toluene and growth (data not shown). The actual sulfide concentration at the plume's center was approximately 8.25 mg L^{-1} with decreasing concentration towards the plume fringe.

2.3.6 Spatial distribution of degradation activity and microbes

In order to evaluate the hypothesis that the main biodegradation activities are restricted to the plume's fringe, a second anaerobic degradation experiment was performed with *A. aromaticum* EbN1 in tank 2. The experimental setup was identical to the experiments presented above, except that no sulfide was added. Moreover toluene was provided as a mixture of non-deuterated toluene and deuterated toluene (toluene- d_8) at a ratio of 10:1. *A. aromaticum* EbN1 significantly discriminates between the two isotopomers (Morasch *et al.*, 2001), *i.e.* non-deuterated toluene is transformed faster than the deuterated species. This leads to a subsequent shift of the toluene/toluene- d_8 ratio in the residual total toluene fraction in zones of pronounced biodegradation. No shift in the ratio of the toluene isotopomers was observed during the abiotic phase (Fig. 2.8). However, after inoculation with *A. aromaticum* EbN1 at day 8 in the second experiment, stable degradation activity was established underlined by a shift of the toluene/toluene- d_8 ratio in samples from the outlet ports 4 and 6, which clearly represented the plume's fringe zones (Fig. 2.8). This trend was even more striking at day 13 before a shift in the ratio of the isotopomers also started to occur in the plume center and toluene degradation activity was present all across the plume. As could be seen during the abiotic phase of this second anaerobic degradation experiment nitrate mixed into the plume center and reached concentrations of up to 25-28 mg L⁻¹. This provided enough electron accepting capacity to enable toluene degradation also in the plume core. However, the isotopic shift remained most pronounced at the plume's fringe zones (Fig. 2.8). A further independent indication for the localization of the main microbial activity at the plume's fringes was the continuous and increasing formation of gas bubbles in this area containing almost exclusively N₂ and traces of N₂O (Fig. 2.9a), partly rupturing the sediment.

Sediment samples collected over a vertical profile across the toluene plume at the end of the second anaerobic experiment exhibited two distinct peaks for total bacterial counts in the most reactive zones of the plume, *i.e.* the plume fringes (Fig. 2.9b). Here, the bacterial abundance accounted for 2.2 to 2.4 × 10¹⁰ cells cm⁻³, whereas a lower but significant amount of biomass (1.3 to 1.5 × 10¹⁰ cells cm⁻³) was present in the plume core. The oxic sediments outside the plume still contained 7.4 × 10⁸ to 2.7 × 10⁹ cells cm⁻³.

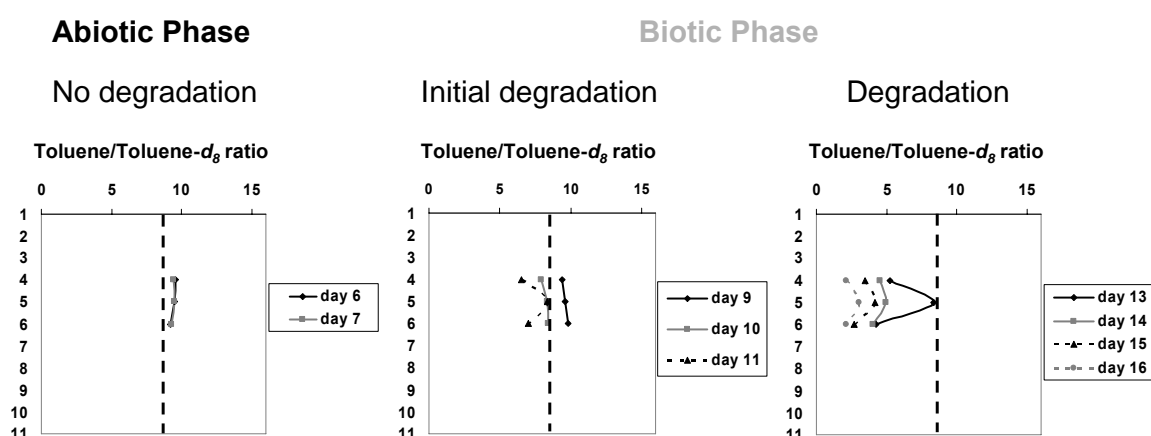


Figure 2.8: Ratio of toluene/ toluene- d_8 in the plume fringe zone, represented by port 4 and 6, and the plume core marked by port 5, over the course of an anaerobic degradation experiment with strain EbN1 under denitrifying conditions in tank two. The vertical dashed line shows the theoretical mean ratio of the toluene species before entering the tank, which was measured daily at P_{in} . Because of too small toluene concentrations no data could be obtained from port 3 and 7 samples.

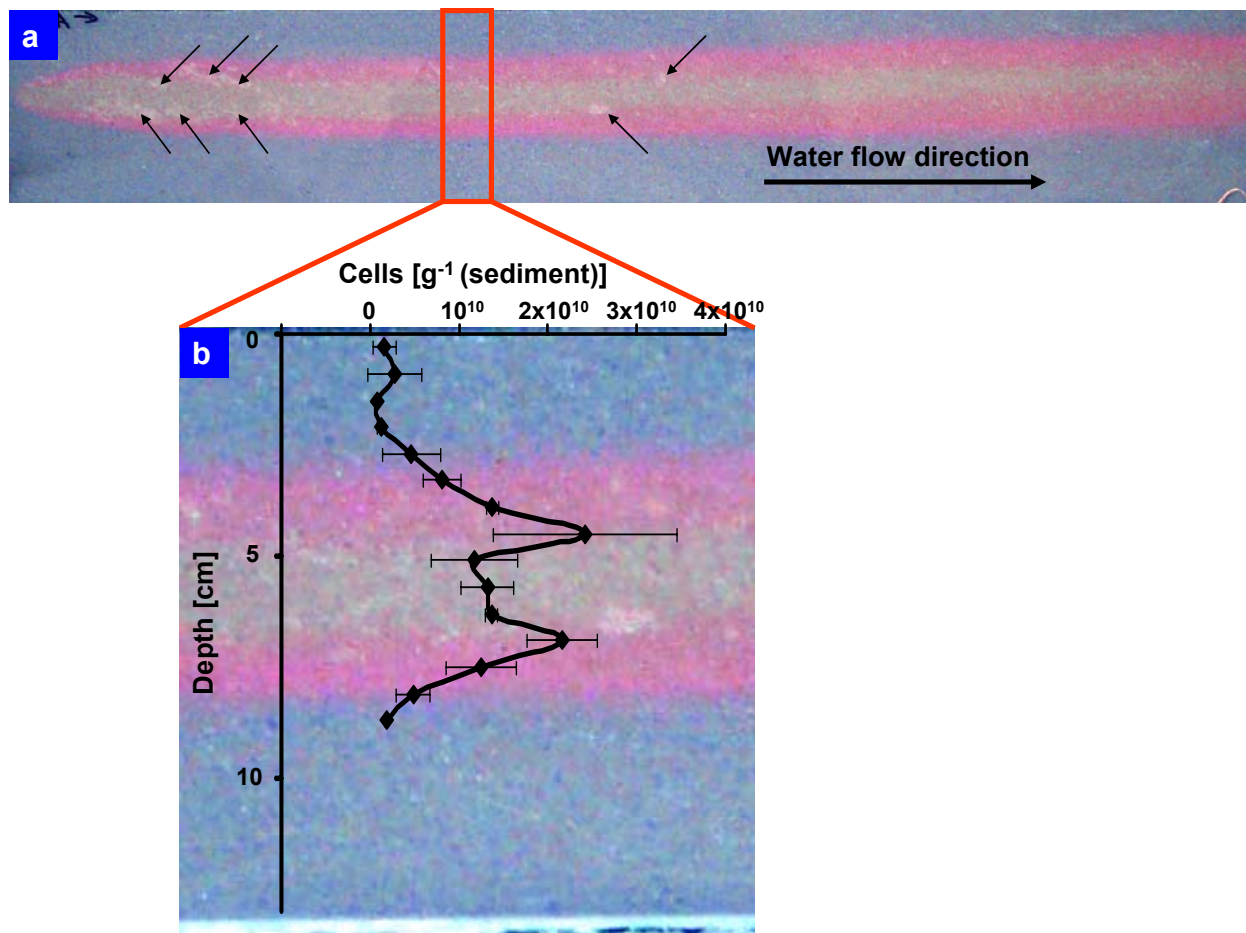


Figure 2.9: (a) Picture of a plume in tank two where *A. aromaticum* EbN1 degraded toluene under denitrifying conditions. Gas formation (arrows), as a result of denitrification, led to local ruptures of the sediment. The vertical profile of the cell abundance in the sediment (b), determined at day 18 of the anaerobic follow-up experiment, is shown.

2.4 Discussion and conclusions

The elucidation of the role of abiotic and biotic processes involved in the degradation of contaminant plumes in porous aquifers is especially important with respect to a better understanding of *in situ* natural attenuation potentials. The general concept that mixing of electron donors and electron acceptors driven by dispersion restricts main biodegradation activities to the plume's fringe was tested in a multidisciplinary approach combining data from 2-D microcosm experiments and data from reactive transport modeling.

2.4.1 Aerobic toluene degradation

To mimic the situation in the field, an oxygen-free reduced plume medium was applied in our degradation experiments. The measurements clearly show the effect of the bacteria on the toluene mass balance when comparing the abiotic and the biotic phases of the experiment. Biodegradation led to a pronounced reduction of the toluene mass flow. However, the application of a reducing agent, *i.e.* ascorbate, influenced the conservative transport and mixing of oxygen by transverse dispersion. Therefore, the experimental and modeling results have to be discussed separately for the aerobic degradation experiment.

Due to the transverse mixing of toluene from the reduced plume and oxygen from ambient flow the highest microbial activity was assumed to take place at the plume's fringe during the biotic

phase. The experimental data clearly support this working hypothesis. Later in the experiment, as was expected from the toxicity tests, the addition of sulfide to the plume medium reduced the biodegradation rates (Fig. 2.4b). At that point, the highly reduced center of the plume became significantly broader. This was due to a chemical reaction of sulfide with oxygen at the fringe which further reduced the mixing of oxygen into the plume (Fig. 2.7). An electron balance in this case was not feasible as the individual abiotic processes and end-products *i.e.* resulting oxidized sulfur species, outgassing, formation of metal sulfides, were not identified. Apart from this, the inhibitory effects of sulfide may account for part of the decrease in biodegradation. Thus, in conclusion, the experimental data obtained in the aerobic degradation experiment clearly showed that the presence of reduced sulfur compounds in contamination plumes restrict aerobic processes to the very external parts of the plume fringes. The data suggests that in steady state plumes contaminated with oxidizable compounds aerobic degradation will play a minor role when sulfide, which is formed by sulfate reduction, or other reducing agents such as Fe (II) from iron reduction, are present.

The theoretical behavior of toluene and oxygen in the simulations produced a slightly different picture. The bioreactive modeling data indicate mixing of oxygen into the plume center during conservative transport and its depletion during the biotic phase (Fig. 2.4a). This pattern seems realistic and has been observed in recent follow-up experiments (data not shown). However, as already mentioned, the presence of a reducing agent with the plume medium in this case limits the comparability of our experimental and modeling data. Support for the patterns observed in our experiment and the patterns obtained from the modeling is provided by Huang and coworkers (2003). These authors conducted degradation experiments with acetate-degrading aerobic bacteria in a two-dimensional flow cell filled with quartz sand. Here, a steepening of the oxygen gradients at the plume's fringe accompanied by a broadening of the anoxic plume core with biodegradation was observed, indicating preferred activity and growth in this area.

The simulations showed that oxygen at concentrations of several mg L^{-1} has the potential to mix into thin contaminant plumes. However, the presence of various reduced compounds may severely inhibit the formation of a significant contribution of aerobic degradation *in situ*. Still, oxygen may play an as yet underestimated role in the re-cycling of sulfur and iron species, which is the focus of current studies (F. Einsiedl, pers. comm.).

2.4.2 Anaerobic toluene degradation

The experimental data sets from the two anaerobic tank experiments seem ideal to test the plume fringe concept. In the first experiment, it was found that nitrate mixed into the plume during conservative transport (Fig. 2.5a). During the phase of highest biodegradation activities in the tank (duration ca. ten days), on days 23, 29 and 30 nitrate was almost completely depleted in the plume center and accompanied by a strong reduction in toluene (Fig. 2.5b). Additionally, the total plume width was significantly reduced. However, although nitrate values in the plume center occasionally declined to less than 5% of the import concentration, both toluene and nitrate could still be found all across the plume. Additional results from the second anaerobic degradation experiment clearly underlined earlier findings that the highest biodegradation activities were located in the fringe areas. Here, a continuous generation of N_2 gas and higher biomass of attached bacteria were observed. Both are likely to have some influence on local hydraulic conductivities and transverse dispersivity. However, the overall plume shape did not show significant changes as derived from the redox indicator.

Isotope fractionation data and the distribution of bacterial biomass proved the plume center also to be a highly active zone exhibiting pronounced degradation towards the end of the experiments. Similar to the aerobic degradation experiment, the introduction of sulfide with the plume medium led to a pronounced reduction of the biodegradation rates. In fact, sulfide caused a toluene plume broadening and a narrowing of the highly bioactive zones. In the case of the anaerobic degradation (experiment one), the negative effect of sulfide may be exclusively attributed to an inhibition of microbial activity.

The simulations for the first anaerobic degradation experiment revealed a mixing of nitrate into the plume center during conservative transport, but a complete depletion during the phase of biodegradation in the plume core. Furthermore, bioreactive zones were restricted to the upper and lower plume fringes, as indicated by ca. 5 mm wide overlaps (near the tank outlet) of toluene and nitrate (Fig. 2.5b). This is based on a double Monod model approach where toluene is degraded in the presence of nitrate. At a later stage of the experiment where the plume medium contained sulfide the model could be fitted to the experimentally derived data by adjusting the input parameter $k_{\text{dec}}/\mu_{\text{max}}$ (Fig. 2.5; see discussion below).

The modeled toluene data for the abiotic phase matched the measured data well, but indicated higher nitrate concentrations (Fig. 2.5a). Discrepancies between the experimental and modeling results were observed during the biotic phases of the experiment where the slope of the upper and lower nitrate gradients became steeper. The toluene gradients did not follow this pattern but became less sharp (Fig. 2.5b). During the last phase of the degradation experiment sulfide lowered the degradation rates. Moreover, although degradation showed steady state conditions, biomass, *i.e.* growth and decay of cells, perhaps still was not yet stable, therefore limiting the applicability of the analytical solution for this phase.

The applied model proved to be relatively congruent with the experimental results. Observed differences may be attributed to the various input variables required which doubtlessly hold uncertainties as especially the biokinetic parameters are difficult to determine. In addition, they would have had to be determined separately for the different conditions applied during the experiments.

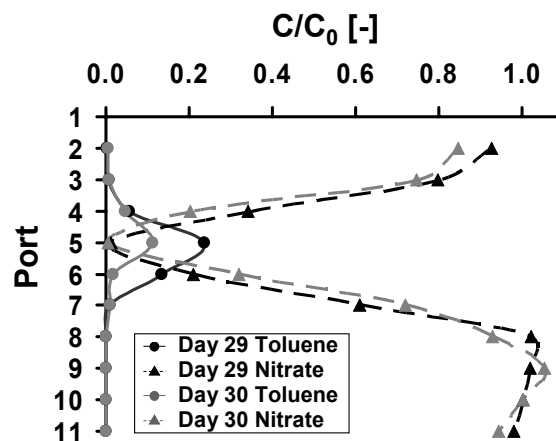


Figure 2.10: The vertical distribution of the electron donor (toluene) and acceptor (nitrate) on two subsequent days of the biotic phase shows the concomitant availability of both species between the ports 3 and 7, and therefore at two adjacent ports clearly representing the plume's fringe (ports 3 and 4, and ports 6 and 7).

The data sets of both anaerobic experiments imply a broad overlapping zone of electron donor and electron acceptor (Fig. 2.10). This somehow contradicts an instantaneous bioreaction frequently assumed in modeling (e.g. Borden & Bedient, 1986; Ham *et al.*, 2004). It is therefore

suggested that, besides dispersion, at least one additional factor contributed to the limitation of biodegradation in our experimental systems which did not allow a total degradation of reactants in the plume center (see below).

2.4.2 Plume fringe concept – mixing and biokinetics

If the plume fringe concept holds true, it is expected that, in comparison with the conservative transport, biodegradation would strongly narrow the zone where both substrate and dissolved electron acceptors are available (Cirpka *et al.*, 1999). The upper and the lower fringe zone where both toluene and nitrate was concomitantly present during the biotic phase of the anaerobic degradation experiments was somewhere between 0 to 1.2 cm. Both reactants could be detected permanently at one port above and below the plume center, *i.e.* the vertical convergence of flowlines spanning over ≤ 1.2 cm, at the upper and lower fringe at the tank outlet (Fig. 2.10). Due to the convergent mixing of flowlines at the outlet ports, a more detailed resolution of overlapping areas could not be pinpointed in this case. On two consecutive days during the period of maximum anaerobic degradation, this overlapping zone stretched over 2.4 cm (two ports) at the fringe and the flowline mixing between two adjacent ports in this case can be excluded (data not shown). It seems that the time-scale of other reactions or processes lag behind the time scale of the transport (advection and dispersion). On one hand, high strain-specific threshold concentrations of nitrate required to promote denitrification may be responsible for the residual concentrations of the electron acceptor in the plume center. Another explanation for the overlap could be, although unlikely, that the biomass in the microcosm was not sufficient to degrade the toluene available. If the attached bacteria are considered as reactive sites with a maximum degradation capacity, it requires a certain number of cells for complete contaminant degradation. This may also be valid for the situation in the field. Interestingly, no bacterial mass production and bioclogging is observed at the fringe of mature hydrocarbon plumes. In fact, quite the opposite is the case, contaminated aquifers display a limited carrying capacity for microbial biomass, of which only a part represents active degraders. Even in case of a perfectly mixed environment, a limited number of degraders would not be able to degrade high concentrations of organics to zero in a flow-through system, *i.e.* sediment columns. In our experiments bacterial cell densities were up to 2.4×10^{10} cells cm^{-3} (Fig. 2.9b). If we presume that a single cell covers one μm^2 of surface when attached to the sand and just a single layer biofilm is formed, up to 100% of the total sediment surface available for colonization, *i.e.* $45\text{-}225 \text{ cm}^2 \text{ g}^{-1}$ for a fine and middle sand fraction (Griebler & Mösslacher, 2003), would be covered by cells in the case of the maximum biomass found in the experiments. It is therefore assumed that biodegradation was not limited by the number of reactive sites. Although the colonization structure was not determined, the bacteria were possibly organized in microcolonies or biofilms reducing the populated area. Microorganisms were detected in all parts of the tank, even those with no toluene exposure. This indicates that the presence of microbes is not necessarily indicative of degradation activity. Still, the total number of bacteria increased by two orders of magnitude at the plume fringes compared to outside plume areas and was almost as high in the plume center during the end of the second anaerobic degradation experiment.

A further process which may limit biodegradation is the microscale diffusion of the substrate and/or electron acceptor from the bulk phase to the individual cells (= substrate availability). It is known that bacteria have the capability to enhance the mass flux by keeping the substrate concentrations very low at the cell surface (Johnsen *et al.*, 2005), which implies a high specific substrate affinity. And *vice versa*, a high affinity is indicated by steep concentration gradients and higher transfer rates (Wick *et al.*, 2001, 2002). However, microscale diffusion gradients may be

assumed to revoke stable isotope fractionation. The effect of discrimination between isotopomers is less pronounced at the moment the substrate becomes limiting and diminishes when single substrate molecules reach the microbial cell. The isotope fractionation data obtained from the second anaerobic degradation experiment contradicts microscale diffusion limitation in the plume.

At the field scale with its complex contamination patterns further mechanisms for limiting or suppressing biodegradation in plumes (cores) may come into play, such as chemotoxicity, substrate inhibition among others (Thornton *et al.*, 2001).

Existing mathematical models to date can not cope appropriately with biological processes and often are generated specifically for particular problems. Often, they are based on an instantaneous bioreaction implying infinitely fast enzymatic reaction kinetics. In cases where degradation is reaction-limited, rather than limited by transport processes, simulation models based on double Monod kinetics (Cirpka & Valocchi, 2007) provide a more adequate tool. However, several model input parameters need some further discussion from a microbiologist's point of view as there are discrepancies between definition and determination.

Microbially-mediated reactions are subject to enzymatic reaction kinetics, which can be described via the Michaelis-Menten coefficient. These are of a different time scale with different organisms and compounds. Furthermore, the total individual reaction kinetics comprise, for instance, individual uptake mechanisms, gene- and substrate-coupled regulations and degradation pathways coupled to different redox processes. Instead the Monod-term applied in contemporary models represents an expression comprised of various limiting factors. Therefore, the Monod half-saturation constant (K_S) is an empirical parameter which is not associated with enzyme kinetics. The K_S value is not constant reflecting the affinity of an uptake system or an enzyme system. However, to have a starting-point for modeling our experimental data, we determined Monod coefficients and the maximum specific growth rates for aerobic and anaerobic toluene degradation for the two strains used (Fig. 2.4, 2.5 and Tab. 2.2). They were further combined with literature values for K_{Nit} and K_{Ox} as model input parameters (Tab. 2.2). Although Monod half-saturation constants and growth rates can be assessed in perfectly mixed batch and chemostat experiments, it is questionable whether the values obtained from a handful of batch experiments properly reflect biokinetics in the sediment microcosms.

Among the parameters required for the model the decay rate is used as fitting parameter preventing an infinite formation of biomass and cannot be determined in simple experiments. Mathematically, a constant biomass over time would imply either a cell maintenance or a balance of growth and decay, in other words the coefficient ϵ must equal 1, yielding a pseudo-stationary phase (Johnsen *et al.*, 2005). However, in the simulations it turned out that the model used does not allow a balance between microbial growth and biomass decay. Interestingly, the rate coefficient of biomass decay had to be set very low (see Tab. 2.2) to obtain biokinetic model results for the whole vertical transect of the model aquifer. This is in accordance with values for maintenance coefficients published for other microorganisms (Müller *et al.*, 2007). Taking into account the maximum growth rates and the decay rates as set in the simulations (Tab. 2.2) as well as the optimal growth conditions, bioclogging should have been observed very early in our aerobic and anaerobic experiments. No extensive biomass production could be observed in the fringe zones during the experiments. However, bioclogging was indeed reported from a similar experiment with denitrification in a glucose plume (Thullner *et al.*, 2002a, 2004). It is not clear if the absence of bioclogging in our experiments is a characteristic of the contaminant degrading strains we applied, *i.e.* producing less biomass and exopolysaccharides per mol carbon converted, or a matter of absolute cell densities. Interestingly, as already mentioned above, bioclogging is rarely observed at sites impacted with petroleum hydrocarbons even after 50 or more years of contamination.

Compared to a multitude of the natural water transport velocities in aquifer sediments, the flow rates applied in the experimental systems were rather high. This allowed the impact of transverse dispersion on biodegradation under mixing-controlled conditions to be considered and avoided a situation where contaminant distribution is mainly driven by diffusion. Nevertheless, the flow velocity was within the typical range for quaternary gravel aquifers. The effective molecular diffusion coefficient of toluene in the quartz sand used still accounted for one third of the hydrodynamic dispersion. A slower flow rate probably would have increased the degradation potential due to an increased water residence time. A higher transport velocity would have instead decreased the total exposure time of toluene to the bacteria. This would have most probably resulted in a decrease of toluene consumption and an increased putative length of the toluene plume.

2.4.4 Conclusions

In conclusion, the aerobic and anaerobic degradation experiments in the 2-D tanks revealed several important results.

According to the initial working hypothesis, major biodegradation activities as well as the main microbial biomass were indeed located at the fringe of the contaminant plumes, indicating that biodegradation in homogeneous porous media is mixing-controlled. Although the experiments were characterized by thin contaminant plumes, the repeated observation of overlapping of both electron acceptors and electron donors indicated that there must be one or more additional factors limiting biodegradation.

Existing models, such as the double Monod model approach presented by Prommer and coworkers (2006) or that devised by Cirpka and Valocchi (2007), which was used in this study, are valuable in testing and simulating bioreactive transport under mixing-controlled steady state conditions. The model simulations helped to reconsider the working hypothesis and improved the perception of biodegradation in contaminant plumes. However, there is still a need to create valid analytical solutions to describe bioreactive processes in mixing-controlled environments. For instance, lumped-parameter extensions exist which can be used with double Monod approaches. These may cover, for instance, kinetic mass transfer (Kinzelbach *et al.*, 1991) and the restriction of biomass growth (Zysset *et al.*, 1994). For the experimental setup an improved sampling resolution would be advantageous in evaluating biogeochemical gradients at the plume fringe.

To investigate the 'new' limitations, research will have to be directed towards substrate uptake and transport rate constants at the microbe/pore space scale and/or the convertible threshold concentrations of electron donors and acceptors. It will have to be elucidated whether there is a dependence on mass transfer or biomass (active sites). This should verify whether aerobic degradation and growth kinetics are fast and may be transport-limited, while bacteria with slower kinetics are reaction-limited, or if the limitations imposed by microscale rate constants act in a comparable way for different redox processes and degraders present at contaminated sites.

2.5 References

- Anneser B., Richters L., Griebler C. (2007) Identification and localization of redox processes in an aromatic hydrocarbon plume via high-resolution sampling of biotic and abiotic gradients. Candela, L.; Vadillo, I.; Aagaard, P.; Bedbur, E.; Trevisan, M.; Vanclooster, M.; Viotti, P.; López-Greta, J.A. (Eds.), *Water Pollution in natural Porous media at different scales. Assessment of fate, impact and indicators. WAPO²*, Madrid, ISBN: 978-84-7840-676-0.
- Atkins P.W. (1990) *Physikalische Chemie. 2. korrigierter Nachdruck der. 1. Auflage*, VCH Verlagsgesellschaft mbH, Weinheim.
- Borden R.C. & Bedient P.B. (1986) Transport of dissolved hydrocarbons influenced by oxygen-limited biodegradation: 1. Theoretical development. *Water Resour Res* **22**:1973-82.
- Bueno C., Villegas M.L., Bertolotti S.G., Previtali C.M., Neumann M.G., Encinas M.V. (2002) The excited-state interaction of resazurin and resorufin with amines in aqueous solutions. Photophysics and photochemical reaction. *Photochem Photobiol* **76**: 385-90.
- Cirpka O.A., Windfuhr C., Bisch G., Granzow S., Scholz-Muramatsu H., Kobus H. (1999a) Microbial reductive chlorination in large-scale sandbox model. *J Environ Eng ASCE* **125**: 861-70.
- Cirpka O.A., Frind E.O., Helmig R. (1999b) Numerical simulation of biodegradation controlled by transverse mixing. *J Contam Hydrol* **40**: 159-82.
- Cirpka O.A., Olsson Å., Ju Q., Rahman M.A., Grathwohl P. (2006) Determination of transverse dispersion coefficients from reactive plume lengths. *Ground Water* **44**: 212-21.
- Cirpka O.A. & Valocchi A. (2007) Two-dimensional concentration distribution for mixing-controlled bioreactive transport in steady state. *Advances in Water Resources* **30**: 1668-79.
- Cline J.D. (1969) Spectrophotometric determination of hydrogen sulphide in natural waters. *Limnol Oceanogr* **14**: 454-8.
- Domenico P. & Palciauskas V. (1982) Alternative boundaries in solid waste management. *Ground Water* **20**: 303-11.
- Grathwohl, P. (1998) *Diffusion in natural porous media: Contaminant transport, sorption/desorption and dissolution kinetics*, pp. 207, Kluwer Academic Publ., Boston Dordrecht London.
- Griebler C., Mindl B., Slezak D. (2001) Combining DAPI and SYBR Green II for the enumeration of total bacterial numbers in aquatic sediments. *Int Rev Hydrobiol* **86**: 453-65.
- Griebler C., Mösslacher F. (2003) *Grundwasserökologie*, pp. 314ff. Facultas Verlags- und Buchhandels AG, Wien.
- Griebler C., Adrian L., Meckenstock R.U., Richnow H.H. (2004) Stable carbon isotope fractionation during aerobic and anaerobic transformation of trichlorobenzene. *FEMS Microbiol Ecol* **48**: 313-21.
- Ham P.A., Schotting R.J., Prommer H., Davis G.B. (2004) Effects of hydrodynamic dispersion on plume lengths for instantaneous bimolecular reactions. *Advances Water Resour* **27**: 803-13.
- Huang W.E., Oswald S.E., Lerner D.N., Smith C.C., Zheng C. (2003) Dissolved oxygen imaging in a porous medium to investigate biodegradation in a plume with limited electron acceptor supply. *Environ Sci Technol* **37**: 1905-11.
- Johnsen A.R., Wick L.Y., Harms H. (2005) Principles of microbial PAH-degradation in soil. *Environ Poll* **133**: 71-84.
- Jose S.C. & Cirpka O.A. (2004) Measurement of mixing-controlled reactive transport in homogeneous porous media and its prediction from conservative tracer test data. *Environ Sci Technol* **38**: 2089-96.

- Jose S.C., Rahman M.A., Cirpka O.A. (2004) Large-scale sandbox experiment on longitudinal effective dispersion in heterogeneous porous media. *Water Resour Res* **40**: doi:10.1029/2004WR003363.
- Kinzelbach W., Schäfer W., Herzer J. (1991) Numerical modeling of natural and enhanced denitrification processes in aquifers. *Water Resour Res* **27**: 1123-35.
- Klenk I.D. & Grathwohl P. (2002) Transverse vertical dispersion in groundwater and the capillary fringe. *J Contam Hydrol* **58**: 111-28.
- Loveland J.P., Bhattacharjee S., Ryan J.N., Elimelech M. (2003) Colloid transport in a geochemically heterogeneous porous medium: aquifer tank experiment and modelling. *J Contam Hydrol* **65**: 161-82.
- MacKinnon L.K. & Thomson N.R. (2002) Laboratory-scale *in situ* chemical oxidation of a perchloroethylene pool using permanganate. *J Contam Hydrol* **56**: 49-74.
- Maloszewski P., Zuber A., Bedbur E., Matthess G. (2003) Transport of three herbicides in ground water at Twin Lake test site, Chalk River, Ontario, Canada. *Ground Water* **41**: 376-86.
- Maier U. & Grathwohl P. (2006) Numerical experiments and field results on the size of steady state plumes. *J Contam Hydrol* **85**: 33-52.
- Mayer K.U., Benner S.G., Frind E.O., Thornton S.F., Lerner D.N. (2001) Reactive transport modeling of processes controlling the distribution and natural attenuation of phenolic compounds in a deep sandstone aquifer. *J Contam Hydrol* **53**: 341-68.
- Morasch B., Richnow H.H., Schink B., Meckenstock R.U. (2001) Stable hydrogen and carbon isotope fractionation during microbial toluene degradation: mechanistic and environmental aspects. *Appl Environ Microbiol* **67**: 4842-9.
- Müller R.H., Rohwerder T., Harms H. (2007) Carbon conversion efficiency and limits of productive bacterial degradation of methyl *tert*-butyl ether and related compounds. *Appl Environ Microbiol* **73**: 1783-91.
- Olesen T., Moldrup P., Yamaguchi T., Rolston D.E. (2001) Constant slope impedance factor model for predicting the solute diffusion coefficient in unsaturated soil. *Soil Sci* **166**: 89-96.
- Olsson, Å. (2005) Investigation and modeling of dispersion-reaction processes in natural attenuation groundwater. Ph.D-thesis, Center of Applied Geosciences, University of Tübingen, Germany.
- Prommer H., Barry D.A., Davis G.B. (2000) Numerical modelling for design and evaluation of groundwater remediation schemes. *Ecol Modelling* **128**: 181-95.
- Prommer H., Barry D.A., Davis G.B. (2002) Modelling of physical and reactive processes during biodegradation of a hydrocarbon plume under transient groundwater flow conditions. *J Contam Hydrol* **59**: 113-31.
- Prommer H., Tuxen N., Bjerg P.L. (2006) Fringe-controlled natural attenuation of phenoxy acids in a landfill plume: integration of field-scale processes by reactive transport modeling. *Environ Sci Technol* **40**: 4732-8.
- Ptak T., Piepenbrink M., Martac E. (2004) Tracer tests for the investigation of heterogeneous porous media and stochastic modelling of flow and transport – a review of some recent developments. *J Hydrol* **294**: 122-63.
- Rabus R. & Widdel F. (1995) Anaerobic degradation of ethylbenzene and other aromatic hydrocarbons by new denitrifying bacteria. *Arch Microbiol* **163**: 96-103.
- Rabus R. (2005) Functional genomics of an anaerobic aromatic-degrading denitrifying bacterium, strain EbN1. *Appl Microbiol Biotechnol* **68**: 580-7.
- Rahman M.A., Jose S.C., Nowak W., Cirpka O.A. (2005) Experiments on vertical transverse mixing in a large-scale heterogeneous model aquifer. *J Contam Hydrol* **80**: 130-48.

- Schürmann A., Schroth M.H., Saurer M., Bernasconi S.M., Zeyer J. (2003) Nitrate-consuming processes in a petroleum-contaminated aquifer quantified using push-pull tests combined with ^{15}N isotope and acetylene-inhibition methods. *J Contam Hydrol* **66**: 59-77.
- Takahata Y., Kasai Y., Hoaki T., Watanabe K. (2006) Rapid intrinsic biodegradation of benzene, toluene, and xylenes at the boundary of a gasoline-contaminated plume under natural attenuation. *Appl Microbiol Biotechnol* **73**: 713-22.
- Thornton S.F., Quigley S., Spence M.J., Banwart S.A., Bottrell S., Lerner D.N. (2001) Processes controlling the distribution and natural attenuation of dissolved phenolic compounds in a deep sandstone aquifer. *J Contam Hydrol* **53**: 233-67.
- Thullner M., Mauclaire L., Schroth M.H., Kinzelbach W., Zeyer J. (2002a) Interaction between water flow and spatial distribution of microbial growth in a two-dimensional flow field in saturated porous media. *J Contam Hydrol* **58**: 169-89.
- Thullner M., Zeyer J., Kinzelbach W. (2002b) Influence of microbial growth on hydraulic properties of pore networks. *Transp Por Med* **49**: 99-122.
- Thullner M., Schroth M.H., Zeyer J., Kinzelbach W. (2004) Modelling of a microbial growth experiment with bioclogging in a two-dimensional saturated porous media flow field. *J Contam Hydrol* **70**: 37-62.
- Tratnyek P.G., Reilkoff T.E., Lemon A.W., Scherer M.M., Balko B.A., Feik L.M., Henegar B.D. (2001) Visualizing redox chemistry: probing environmental oxidation-reduction reactions with indicator dyes. *Chem Educator* **6**: 172-9.
- Tuxen N., Albrechtsen H.-J., Bjerg P.L. (2006) Identification of a reactive degradation zone at a landfill leachate plume fringe using high resolution sampling and incubation techniques. *J Contam Hydrol* **85**: 179-94.
- Watson I.A., Oswald S.E., Mayer K.U., Wu Y., Banwart S.A. (2003) Modeling kinetic processes controlling hydrogen and acetate concentrations in an aquifer-derived microcosm. *Environ Sci Technol* **37**: 3910-9.
- Watson I.A., Oswald S.E., Banwart S.A., Crouch R.S., Thornton S.F. (2005) Modeling the dynamics of fermentation and respiratory processes in a groundwater plume of phenolic contaminants interpreted from laboratory- to field-scale. *Environ Sci Technol* **39**: 8829-39.
- Wick L.Y., Colangelo T., Harms H. (2001) Kinetics of mass-transfer limited bacterial growth on solid PAHs. *Environ Sci Technol* **35**: 354-61.
- Wick L.Y., de Ruiz M., Springael A., Harms H. (2002) Responses of *Mycobacterium* sp. 501T to the low bioavailability of solid anthracene. *Appl Microbiol Technol* **58**: 378-85.
- Widdel F. & Bak F. (1992) Gram negative mesophilic sulfate reducing bacteria. In H.G.T. A. Balows, M. Dworkin, W. Harder, and K. H. Schleifer (eds.). *The Prokaryotes. A handbook on the biology of bacteria: ecophysiology, isolation, identification, and applications*, pp. 3352-3378, Springer, New York.
- Wöhlbrand L., Kallerhoff B., Lange D., Hufnagel P., Thiermann J., Reinhardt R., Rabus R. (2007) Functional proteomic view of metabolic regulation in „*Aromatoleum aromaticum*“ strain EbN1. *Proteomics* **7**: 2222-39.
- Zamfirescu D., Grathwohl P. (2001) Occurrence and attenuation of specific organic compounds in the groundwater plume at a former gaswork site. *J Contam Hydrol* **53**: 407-27.
- Zysset A., Stauffer F., Dracos T. (1994) Modelling of reactive groundwater transport governed by biodegradation. *Water Resour Res* **30**: 2423-34.

3 Enhanced biodegradation in contaminant plumes via increased transverse dispersion

3.1 Introduction

Aquifers polluted with organic chemicals such as aromatic hydrocarbons (BTEX, PAH) do not only pose a threat to subsurface ecology but also to human health as the majority of the industrial countries uses groundwater as drinking water supply. The investigation of contaminant plumes in groundwater systems became a major scope of various disciplines in the past two decades and was approached by field studies, numerical modeling or laboratory based studies (Franzmann *et al.*, 2002; Röling & van Verseveld, 2002). The latter was ranging from batch tests over column systems to two- and three-dimensional sediment flow chambers. Understanding the processes controlling degradation of these compounds in porous aquifers is still a major challenge.

In organic contaminant plumes, microbial transformations are the most important processes for removal. To warrant oxidation of the carbon-load, the availability of an appropriate electron acceptor is required. Based on thermodynamics, oxygen is foremost consumed in the plume by indigenous aerobic bacteria (Christensen *et al.*, 2000). However, the contribution of aerobes to the overall degradation of contaminants is limited by the low solubility of oxygen in water (e.g. Brune *et al.*, 2000). Nevertheless, aerobic transformation processes may play a crucial role stimulating anaerobic degradation by forming oxygen-free areas. In mature plumes, a steep succession of redox processes develops together with the depletion of soluble electron acceptors in the plume core (Chapelle *et al.*, 1995; Christensen *et al.*, 2000). In a steady state contaminant plume, the dominant bacterial activity is thus confined to the fringe areas where the toxic concentration of contaminants is reduced and electron acceptors from ambient groundwater mix with the electron donor (*i.e.* the contaminants) by transverse dispersion (Hess *et al.*, 1997; Mayer *et al.*, 2001; Rahman *et al.*, 2005; Bauer *et al.*, 2007). Therefore, dispersive mixing at a pore-scale is supposed to constitute the main driving force for the degradation activity of the microorganisms (Cirpka *et al.*, 1999b; Maier & Grathwohl, 2006; Cirpka & Valocchi, 2007). However, natural sediments uncommonly reveal a uniform texture, but feature a heterogeneous matrix containing high- and low-conductivity zones (Jose *et al.*, 2004). Spatial variabilities of advection and streamline meandering, which was described as macrodispersion (Jose & Cirpka, 2004; Rahman *et al.*, 2005), increase the vertical spreading of a contaminant plume. The recent work of Werth *et al.* (2006) showed that the flow focusing in high permeability zones leads to a significant enhancement of transverse mixing. Consequently, the improved mixing processes can lead to a higher biodegradation potential. However, recent studies underline that additional factors other than mixing processes may play a role limiting biodegradation (Wick *et al.*, 2001, 2002; Bauer *et al.*, 2007).

The aim of this study is to demonstrate that biodegradation in porous media is predominantly mixing-controlled. To substantiate this hypothesis, two parallel two-dimensional sediment microcosms were run to compare biodegradation activity in homogeneous and heterogeneous sediments. The heterogeneous sediment carried two high-permeability lenses which increased the mixing of electron donor and acceptor and therefore were supposed to enhance biodegradation. Aerobic degradation of toluene and ethylbenzene by the strain *Pseudomonas putida* F1 was studied in a developing plume and later under steady state mixing-controlled conditions. Then, anaerobic degradation of ethylbenzene was initiated by inoculation of the denitrifying *Aromatoleum aromaticum* strain EbN1 (Wöhlbrand *et al.*, 2007). The experiments under well-controlled conditions were accompanied by a flow and reactive transport modeling study. This was to evaluate the applicability of the model used, and to find out if biodegradation in contaminant

plumes is exclusively mixing-controlled or if additional limiting factors such as biokinetics may be involved. This issue was tackled with respect to field observations where overlapping zones of electron donor and acceptor were indicated (Anneser *et al.*, 2007; Baéz-Cazull *et al.*, 2007; Bjerg *et al.*, 1995; Tuxen *et al.*, 2006; van Breukelen & Griffioen, 2004).

3.2 Experimental setup

3.2.1 Two-dimensional sediment microcosms

The 2-D sediment microcosm (in the following termed ‘microcosm’), its setup and the homogeneous sediment packing was performed as described in Bauer *et al.*, 2007 (Fig. 3.1a, HOM). The flow velocity was set at 1.2 m d^{-1} .

At the height of inlet port no. 5, where the hydrocarbon-loaded medium was introduced into the heterogeneous microcosm, two consecutive quadrangular coarse sand layers (sterile quartz sand, grain diameter 1 mm) with a dimension of $20 \text{ cm} \times 1.2 \text{ cm}$ each were embedded into the medium sand matrix (sterile quartz sand, grain diameter 200 – 300 μm) with the help of two sterilized aluminum disks defining the horizontal borders during packing. Both lenses, with an interspace of 7.5 cm to each other, were equidistant (15 cm) to the inlet and the outlet, respectively (Fig. 3.1a, HET).

3.2.2 Media

Oxic groundwater medium supplied with nitrate was permanently introduced to the microcosm through ports 2 to 4 and 6 to 11 (Tab. 3.1) (Bauer *et al.*, 2007). At inlet port number 5 oxic freshwater medium of identical composition but provided with increasing concentrations of toluene or ethylbenzene as sole electron donor (Tab. 3.1), and bromide (626 μM) as conservative tracer was continuously injected to generate an artificial contaminant plume (Bauer *et al.*, 2007).

3.2.3 Strains, cultivation and inoculation

The aerobic toluene-degrading strain *Pseudomonas putida* strain F1 was obtained from J. R. van der Meer, Dübendorf, Switzerland, and *Aromatoleum aromaticum* strain EbN1 from F. Widdel, Bremen, Germany (Rabus & Widdel, 1995). Precultures of both strains were grown with toluene and ethylbenzene, respectively (Bauer *et al.*, 2007).

P. putida F1 was inoculated into both microcosms at the two inlet ports (port 4 and 6) adjacent to the plume port (port 5) over seven hours upon launching the experiment. *A. aromaticum* EbN1 was inoculated at a later stage.

3.2.4 Analysis of anionic species

Concentrations of bromide, nitrate, and nitrite were determined by ion chromatography (Dionex AS3500, Idstein, Germany).

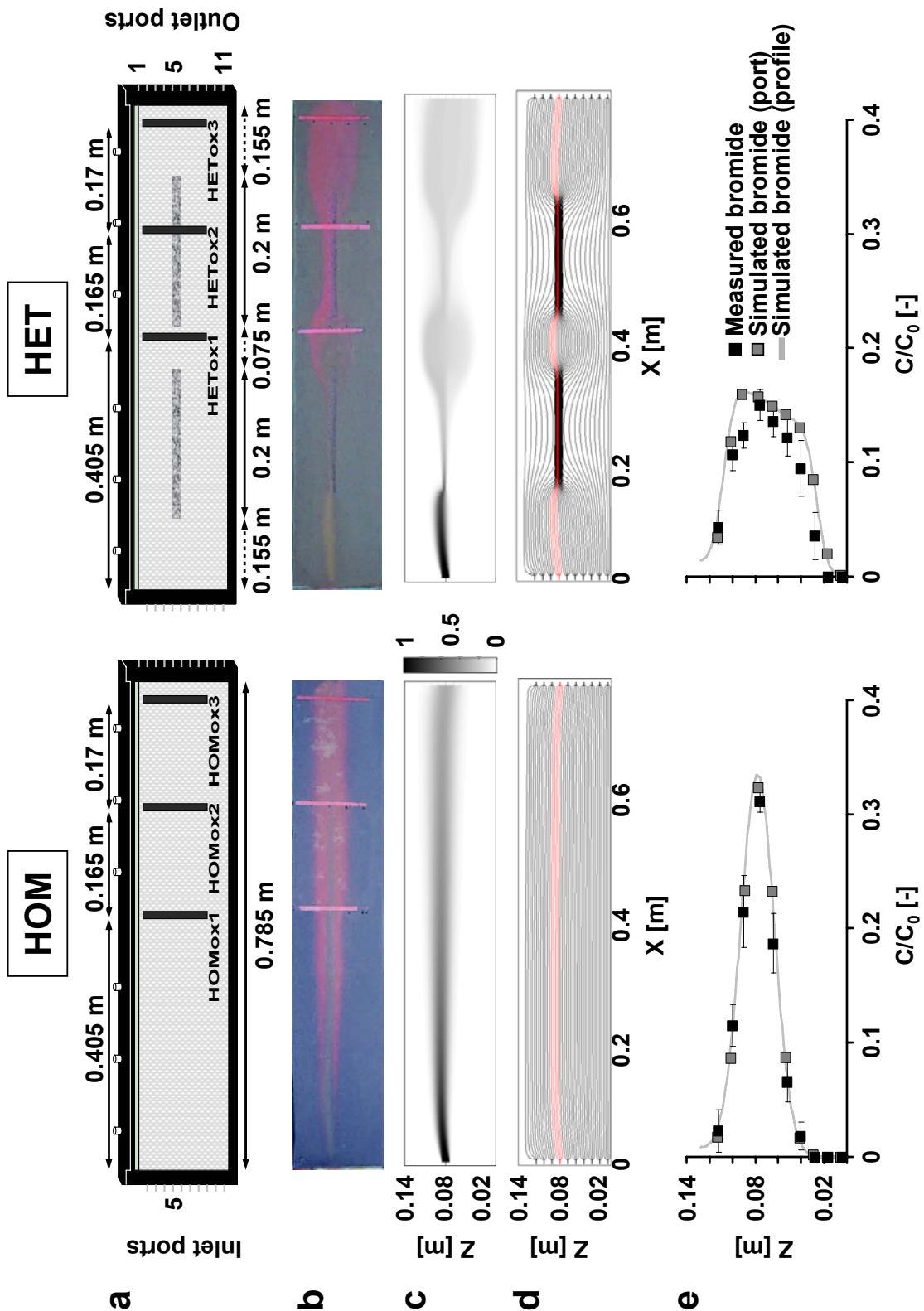


Figure 3.1: (a) Experimental design of the two 2-dimensional microcosms filled homogeneously with medium quartz sand (left side, HOM), or containing two high-conductivity coarse sand lenses (right side, HET). The positions of the three oxygen-sensitive strips are indicated (HOMox1-3, HETox1-3). (b) Photographs taken on day 70 (HOM) and day 64 (HET) of the experiment, illustrating oxic (blue), anoxic (colorless), and hypoxic (pink) areas, visualized by the redox indicator resazurin. (c) Steady-state distribution of the plumes and (d) flowlines in HOM and HET as derived from transport modeling. (e) Measured vs. simulated Br^- tracer concentrations at the microcosm outlet. The experimental data show the means of each day of the experiment (\pm SD).

Table 3.1: Concentrations of electron donors and electron acceptors in the plume and groundwater during different stages of the experiment.

Phase	Plume			Groundwater						
	Oxygen [$\times 10^{-5}$ M]	Nitrate [$\times 10^{-5}$ M]	Toluene [$\times 10^{-5}$ M]	Ethylbenzene [$\times 10^{-5}$ M]	Oxygen [$\times 10^{-5}$ M]	Nitrate [$\times 10^{-5}$ M]	Toluene [$\times 10^{-5}$ M]	Ethylbenzene [$\times 10^{-5}$ M]		
Growth of <i>Pseudomonas putida</i> F1										
I	27	9.4 ± 2.7	5.3 ± 0.2	0	27	11.2 ± 3.6	0	0		
II			7.4 ± 0.6							
III			10.7 ± 0.6							
IV			14.3 ± 1.4							
V			17.3 ± 1.4							
VI			20.6 ± 2.8							
VII			0						19.7 ± 4.9	
Growth of <i>Pseudomonas putida</i> F1 and <i>Aromatoleum aromaticum</i> EbN1										
VIII	27	9.4 ± 2.7	0	19.7 ± 4.9	27	131.6 ± 11.8	0	0		
IX									993.1 ± 63.7	
X									2.9 ± 0.2	41.7 ± 8.7
XI										

3.2.5 Redox conditions and oxygen measurements

For the visualization of a shift in the redox potential within the microcosms, the redox indicator resazurin was added to the media indicating oxic (blue), hypoxic (pink) and anoxic (colorless) conditions (Bauer *et al.*, 2007).

Oxygen concentrations across the plume were monitored via a non-invasive optode-array measuring system (Microx 1/FIBOX, PreSens, Regensburg, Germany) (e.g. Wittmann *et al.*, 2003). Here, oxygen-sensitive membrane strips (10 cm x 0.5 cm) were attached to the inner wall of the microcosms, located at 40.5 cm (HOMox1, HETox1), 57 cm (HOMox2, HETox2) and 74 cm (HOMox3, HETox3) distance from the inlet in both tank systems (Fig. 3.1a).

3.2.6 Stable isotope analysis

A mixture of non-labeled toluene- h_8 and deuterium labeled toluene- d_8 (3:1) was used as carbon source, which was maintained during the successive concentration increase during the experiment. At a later stage, the toluene mix was replaced by a mixture of ethylbenzene- h_{10} and ethylbenzene- d_{10} of the same ratio. Two mL sample aliquots were used for the determination of toluene and ethylbenzene concentrations and isotope ratio, first amended with 0.5 mL cyclohexane containing 100 μ M ethylbenzene and 100 μ M toluene as internal standards, respectively, and then, after shaking for one hour, the cyclohexane phase was collected and the toluene and ethylbenzene concentrations were measured by gas chromatography – mass spectrometry (Finnigan Trace Ultra and Trace DSQ, Thermo Electron Cooperation, Waltham, MA, USA, with a DB-5MS column, 0.5 μ m film thickness, 0.25 i.d., 30 m length, J & W Scientific, USA). Sample injection was on split mode (1:10 mL min⁻¹) and the flow rate of the carrier gas helium was 1 mL min⁻¹. The oven temperature was 40°C for 1 min, then ramped first at a rate of 15°C min⁻¹ to 200°C and then at a rate of 45°C to 300°C where it was held for 1.2 min. The MS was operated at 350°C in the SIM scan mode for the masses 91.00 and 98.00.

3.2.7 Cell counts

After the experiment, vertical sediment cores were extracted from the tanks at 14.5 and 17 cm (HOMsed1, HETsed1), 40.5 cm (HOMsed2, HETsed2), 57 cm (HOMsed3, HETsed3) and 74 cm (HOMsed4, HETsed4) after the tank inlet. The samples were proceeded following the protocol of Bauer *et al.* (2007), except the samples were fixed with 1 mL glutaraldehyde (4%).

The samples were provided with an internal standard prior to cell counting in a flow cytometer according to Bauer *et al.* (2007).

3.2.8 Hydraulic properties

The most sensitive flow and transport parameters such as hydraulic conductivities and transverse dispersivities were determined experimentally.

Column experiments were performed to estimate the hydraulic conductivity of the porous media used in both microcosms. By measuring the hydraulic gradients in the columns and applying Darcy's law, average values of 4.11×10^{-4} ms⁻¹ and 7.26×10^{-3} ms⁻¹ were calculated for the middle and coarse sand, respectively. Therefore, the ratio of the hydraulic conductivities in the heterogeneous system, which determines the amount of flow focused in the high-permeability inclusions, was 17.7.

Tracer experiments using bromide as a conservative solute were performed in both systems. Bromide concentrations measured at the outlet ports of the homogeneous microcosm were used to estimate the transverse dispersivity of the finer sand. In this system the simplifying assumption of uniform parallel flow can be considered valid and the two-dimensional steady state solution of the transport equation for a line source (Domenico & Palciauskas, 1982) can be applied:

$$\frac{C}{C_0} = \frac{1}{2} \left\{ \operatorname{erf} \left[\frac{(y+Y/2)}{2(xD_T/v)^{1/2}} \right] - \operatorname{erf} \left[\frac{(y-Y/2)}{2(xD_T/v)^{1/2}} \right] \right\} \quad (3.1)$$

where D_T = transverse hydrodynamic dispersion coefficient, C = tracer concentration, C_0 = tracer concentration at the source, Y = source width, y = distance in lateral direction, x = distance in longitudinal direction and v = pore water velocity.

A fitting procedure was applied to estimate D_T through the minimization of the sum of the squared error between the measured and simulated (eq. 3.1) concentrations. Then, the transverse dispersivity, α_T , was calculated with the formula:

$$D_T = D_p + \alpha_T v \quad (3.2)$$

where D_p is the effective pore diffusion coefficient: $D_p = D_{aq}n$, D_{aq} = aqueous diffusion coefficient and n = porosity (Grathwohl, 1998). A value of $\alpha_T = 7.6 \times 10^{-5}$ m was determined for the medium sediments. For the two coarse sand inclusions in the heterogeneous microcosm, a value of 8.0×10^{-5} m was extrapolated from an experimental dataset of bromide tracer experiments carried out in a similar setup (Olsson & Grathwohl, 2007).

Prior to the inoculation of the two 2-D microcosms with contaminant-degrading bacteria, non-reactive transport experiments have been conducted accompanied by additional column and batch tests to determine the principal transport and biokinetic parameters (Tab. 3.2).

3.2.9 Flow and transport modeling

Numerical modeling was performed to describe the flow and transport in the two flow-trough systems. Two-dimensional model grids with 35530 cells were constructed with a discretization of $\Delta z = 7.5 \times 10^{-4}$ m in the direction perpendicular to flow and a varying discretization ($\Delta x_{\min} = 1 \times 10^{-3}$ m, $\Delta x_{\max} = 5 \times 10^{-3}$ m) along the flow direction.

3.2.9.1 Flow Simulation

The flow field was simulated using the numerical model MODFLOW (McDonald and Harbaugh, 1988) and particle tracking simulations were performed using MODPATH (Pollock, 1994). The microcosms were simulated as unconfined aquifers using the hydraulic parameters reported in Table 3.2 as input values. Neumann boundary conditions were applied and active cells, with interspace equivalent to the ports spacing in the experimental setup, were used to simulate the inlet and outlet ports.

Table 3.2: Summary of transport and biokinetic parameters.

Flow and Transport Parameters		
Tank dimension [m]	0.785 x 0.011 x 0.14	
Average middle sand diameter [mm]	0.256	
Average coarse sand diameter [mm]	1	
Number of inlet/outlet ports [-]	10	
Vertical distance between ports [m]	0.012	
Total flow rate [mL s ⁻¹]	9.67 x 10 ⁻³	
Pore water velocity, homogeneous tank [m s ⁻¹]	1.39 x 10 ⁻⁵	
Average pore water velocity, heterogeneous tank [m s ⁻¹]	1.41 x 10 ⁻⁵	
Porosity [-]	0.48 ^a	
Hydraulic conductivity middle sand [m s ⁻¹]	4.11 x 10 ⁻⁴	
Hydraulic conductivity coarse sand [m s ⁻¹]	7.26 x 10 ⁻³	
Hydraulic conductivity ratio [-]	17.7	
Transverse dispersivity middle sand [mm]	7.6 x 10 ⁻²	
Transverse dispersivity coarse sand [mm]	8.0 x 10 ⁻²	
Longitudinal dispersivity middle sand [mm]	0.76 ^b	
Longitudinal dispersivity coarse sand [mm]	0.8 ^b	
Bromide aqueous diffusion coefficient [m ² s ⁻¹]	2.08 x 10 ⁻⁹	
Biokinetic Parameters		
	Aerobic Ethylbenzene eq. 6	Anaerobic Ethylbenzene eq. 7
μ_{\max} (d ⁻¹)	13.1	1.16
$K_{\text{Substrate}}$ (μM)	10	11.4
$K_{\text{electron acceptor}}$ (μM)	3	70
Decay coefficient (d ⁻¹)	0.1	0.1
Stoichiometric coefficient for ED	1	1
Stoichiometric coefficient for ED	10.5	8.4
Stoichiometric coefficient for metabolite	8	8

^a Based on the results of a tracer test and determined by calculating the porosity $n = \frac{Q}{A \times v}$, with the flow rate Q , the cross-sectional area A , and the flow velocity v .

^b Assumed 10 times α_T (at steady state it is not a sensitive parameter).

3.2.9.2 Conservative Transport

The non-reactive tracer experiments were simulated with the transport simulator MT3DMS (Zheng and Wang, 1999) using the parameters summarized in Table 3.2 and the total variation diminishing (TVD) scheme (Leonard, 1988) to solve the advection problem.

3.2.9.3 Reactive Transport

Reactive transport simulations were carried out to model the measured concentrations of dissolved electron donors (toluene and ethylbenzene) and acceptors (oxygen and nitrate) during the different phases of the experiment. An approach based on the recent work of Cirpka and Valocchi (2007) was followed. In a uniform two-dimensional flow field Cirpka and Valocchi derived closed

form analytical solutions for reactive transport in a system where an irreversible microbial transformation of reactants A and B (*i.e.* electron donor and acceptor) to compound C takes place. The analytical solutions consider both instantaneous and double Monod kinetics, and are based on the distribution of the normalized concentration or mixing ratio $X(x,z)$. The procedure assumes that the biomass is immobile and at steady-state and that the D_T is the same for the different dissolved species.

Under these assumptions the method has been adapted to describe the reactive transport of the present study. Due to the more complex flow patterns of the experimental settings, the distribution of $X(x,z)$ was computed numerically and the concentrations of the reactants have been calculating by post-processing, according to the stoichiometry of the oxidation-reduction reactions and to the biological parameters determined in batch experiments (Tab. 3.2).

The modeling strategy allowed the simulation of different experimental conditions based on the numerical computation of the distribution of a conservative species. Since the model assumes the same dispersion properties for the reactive partners, the molecular diffusion coefficient of oxygen ($D_{aq} = 2.1 \times 10^{-9} \text{ m}^2 \text{ s}^{-1}$) was selected as input data under the assumption that in a counter diffusion process the most mobile reactant determines the position of the reactive fringe (Appelo, 2007). Moreover, the initial concentrations were corrected by subtracting the stoichiometric amount of substrate consumed by the oxygen injected within the plume medium. This was performed in order to conform to the boundary conditions for which the analytical solutions were derived, *i.e.* the plume is right from the start depleted from dissolved oxygen (Cirpka and Valocchi, 2007).

3.2.9.4 Mass flux of electron donors and electron acceptors

Mass balances were calculated in order to quantify the microbial degradation activity in the sediment. The degradation mass balances were based on the mass fluxes determined at the inlet and outlet ports (Tab. 3.3). For each transported species the mass fluxes were calculated as:

$$m_i(n) = \sum_{i=1}^{N_{port}} C_i \cdot Q_i(n) \quad (3.3)$$

where m_i ($\mu\text{mol d}^{-1}$) is the mass flux of the i -species at the inlet/outlet of the tank, C_i is the concentration (μM) injected/extracted at each port and Q_i is the water flow rate (L d^{-1}) of each inlet/outlet port. As an example, applying (n), a mass flux of $225.5 \mu\text{mol d}^{-1}$ oxygen was continuously infiltrating the tanks during the entire term of the experiment.

3.3 Results

3.3.1 Simulated flow and conservative transport

Based on the transport parameters (Tab. 3.2), streamlines were computed for the homogeneous and heterogeneous sediments (Fig. 3.1c and 3.1d). The vertical height of the 2-D sediment microcosms is indicated with a 'Z' on the y-axis. The models predicted a rise of the flowlines immediately after the injection ports and a drop back towards the outlet ports. This effect was more significant for the upper ports due to geometry (e.g. ports spacing) and hydraulic properties (e.g. flow rates, initial head and hydraulic conductivity) of the unconfined aquifers.

Table 3.3: Mass fluxes of electron donors and electron acceptors at the inlet and the outlet of the homogeneous and the heterogeneous tank systems.

Phase	Day	Total in						Total out					
		Toluene [$\times 10^5 \text{ mol d}^{-1}$] HOM	Ethylbenzene [$\times 10^5 \text{ mol d}^{-1}$] HOM	Nitrate [$\times 10^5 \text{ mol d}^{-1}$] HOM	Nitrate [$\times 10^5 \text{ mol d}^{-1}$] HET	Toluene [$\times 10^5 \text{ mol d}^{-1}$] HOM	Ethylbenzene [$\times 10^5 \text{ mol d}^{-1}$] HOM	Nitrate [$\times 10^5 \text{ mol d}^{-1}$] HOM	Nitrate [$\times 10^5 \text{ mol d}^{-1}$] HET	Nitrite [$\times 10^5 \text{ mol d}^{-1}$] HOM	Nitrite [$\times 10^5 \text{ mol d}^{-1}$] HET		
Growth of <i>Pseudomonas putida</i> F1													
I	1-4	0.42 ± 0.02				0.05							
II	5-6	0.63 ± 0.05				0.05 ± 0.02							
III	7-15	0.92 ± 0.05				0.18 ± 0.11							
IV	16-22	1.25 ± 0.12	0	8.83 ± 1.43		0.56 ± 0.18	0	7.93 ± 0.76	7.71 ± 0.73	0	0	0	
V	23-27	1.46 ± 0.17				0.74 ± 0.35							
VI	28-37	1.75 ± 0.23				1.01 ± 0.25							
VII	38-46	0	1.67 ± 0.41			0		1.10 ± 0.32	0.52 ± 0.25				
Growth of <i>Pseudomonas putida</i> F1 and <i>Aromatoleum aromaticum</i> EbN1													
VIII	47-56		1.67 ± 0.41	99.62 ± 9.84				0.80 ± 0.44	0.19 ± 0.21	64.08 ± 11.57	65.15 ± 12.19	50.39 ± 4.76	38.56 ± 5.31
IX	57-63	0	3.22 ± 0.44	926.09 ± 55.46		0		0.12 ± 0.33	0.01 ± 0.04	603.06 ± 36.69	603.41 ± 26.5	117.23 ± 32.64	103.15 ± 27.41
X	64-69		3.47 ± 0.72	769.78 ± 90.35				0.11 ± 0.17	0	500.21 ± 18.32	504.54 ± 29.48	108.6 ± 5.1	106.7 ± 5.62
XI	70-74			1.56 ± 0.15				1.23 ± 0.84	1.11 ± 0.47	0.7 ± 0.09	0.7 ± 0.24	0	0

The standard deviation $s_{\bar{x}}$ is denoted as $s_{\bar{x}} = \sqrt{(s_i)^2 + (s_o)^2}$, where s_i and s_o represent the standard deviations of the inlet and outlet total mass flux rates, respectively.

The real plume exhibited a similar pattern with a raise of the plume immediately after the injection port 5 (Fig. 3.1b, c, d). In the heterogeneous sediment the flow was focused into the high conductivity lenses, which acted as a conduit for flow, collecting all plume streamlines together with streamlines from the surrounding inlet ports supplying fresh groundwater medium to the microcosm (Fig. 3.1d).

The computed steady state concentration distribution for the homogeneous and heterogeneous plumes are shown in Figure 3.1c, together with the simulated and measured tracer concentrations at the outlet (Fig. 3.1e).

3.3.2 Degradation of contaminants

To find out if biodegradation is mixing-controlled, the contaminant removal by *Pseudomonas putida* strain F1 in the homogeneous and heterogenous setup was compared based on the mass fluxes at the inlet and outlet of the microcosms (Tab. 3.3). Therefore, the toluene concentrations in the plume were raised successively from 50 μM to 210 μM (phase I-VI) (Tab. 3.1). Assuming steady state conditions for the bacterial biomass, the redox reaction describing toluene degradation can be expressed as:



In order to achieve mixing-controlled conditions without having to add interfering reducing agents to the plume, *P. putida* F1 was immediately inoculated. Figure 3.2 shows that instantly after launching the experiment, the oxygen concentration in the sediment at the oxygen measuring points HOM/HET1-3 decreased (day 1). This indicates that *P. putida* F1 was readily active in toluene degradation and utilized all oxygen available wherever toluene was present, *i.e.* in the plume. The following days (4, 6, 9), representing increasing toluene concentrations in the plume (50 μM , 75 μM , 110 μM), showed an oxygen-depletion inside the plume and a steepening of oxygen gradients at the plumes' fringes in both sediments. In the heterogeneous sediment increased mixing processes improved the replenishment of the electron acceptor, facilitating the complete degradation of toluene on day 9. Contrastingly, the oxygen-free area in the homogeneous sediment soon reached a maximum expansion. Here, the replenishment of oxygen from ambient medium was subsequently controlled by dispersive mixing since day 9, preventing complete toluene degradation.

Figure 3.3 shows that the aerobic degradation in the homogeneous sediment reached an upper limit which remained unsurpassed despite increased substrate concentrations (150, 175, 210 μM). In the same period, the heterogeneous sediment allowed higher toluene degradation. An entire contaminant removal was prevented by the low solubility of oxygen in water. On day 38, the carbon source was changed from toluene (210 μM) to ethylbenzene (200 μM), which did not significantly affect biodegradation in neither setup as both compounds follow the same degradation pathway. On day 46, the denitrifier *Aromatoleum aromaticum* strain EbN1 was inoculated to study the competitive degradation with *P. putida* F1 under changing ratios of ethylbenzene and nitrate. The selected nitrate concentrations in groundwater and plume media led to a complete degradation of the successively increased ethylbenzene concentrations (200 μM , 385 μM , 415 μM) in the heterogeneous setup. In contrast, though nitrate was provided to the groundwater in excess of the stoichiometric amount required for complete ethylbenzene oxidation (up to 10.5 mM), degradation in the homogeneous setup was mixing-controlled (phase VIII and X) (Tab. 3.1). Only with high nitrate concentrations in the plume (10 mM) complete substrate degradation could be observed (day 63). Finally, after adjusting nitrate concentrations close to natural conditions (20-30 μM) the overall

degradation decreased drastically, but did not reach a steady state within the last 5 days until the end of the experiment. A decline of the biodegradation by *A. aromaticum* EbN1 was accompanied by a simultaneous recovery of aerobic activity by *P. putida* F1. This was shown in both tanks by an ongoing biodegradation, in parallel to a color change of resazurin from pink to blue, indicating that a higher redox potential established (see below).

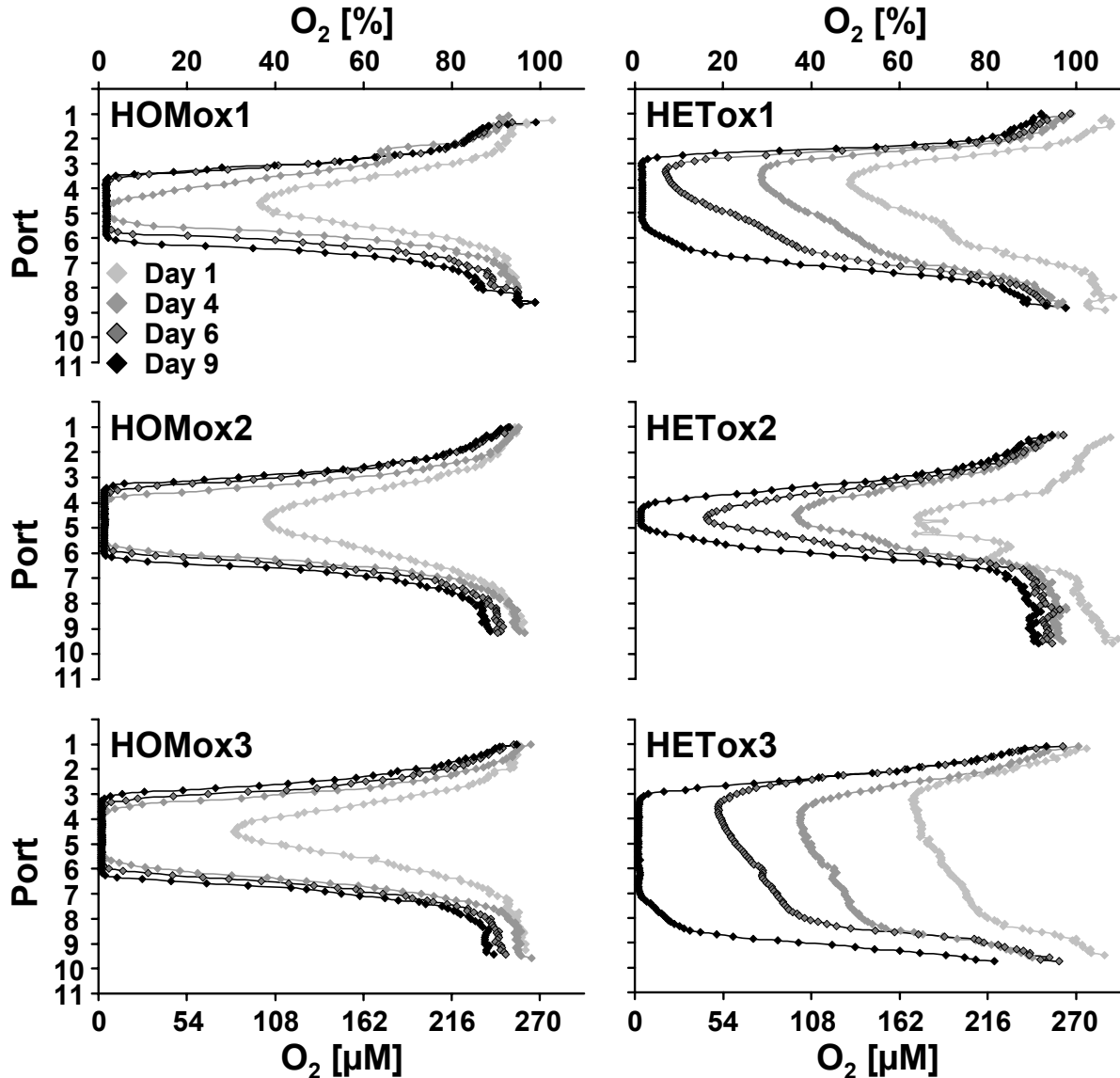


Figure 3.2: Vertical oxygen saturation profiles (given in %) recorded by means of a non-invasive optode measurement technique, during phases I to III at three positions in the microcosms as depicted in Fig. 3.1a. The oxygen distribution patterns show the successive oxygen depletion in the toluene plume in relation to the port positions.

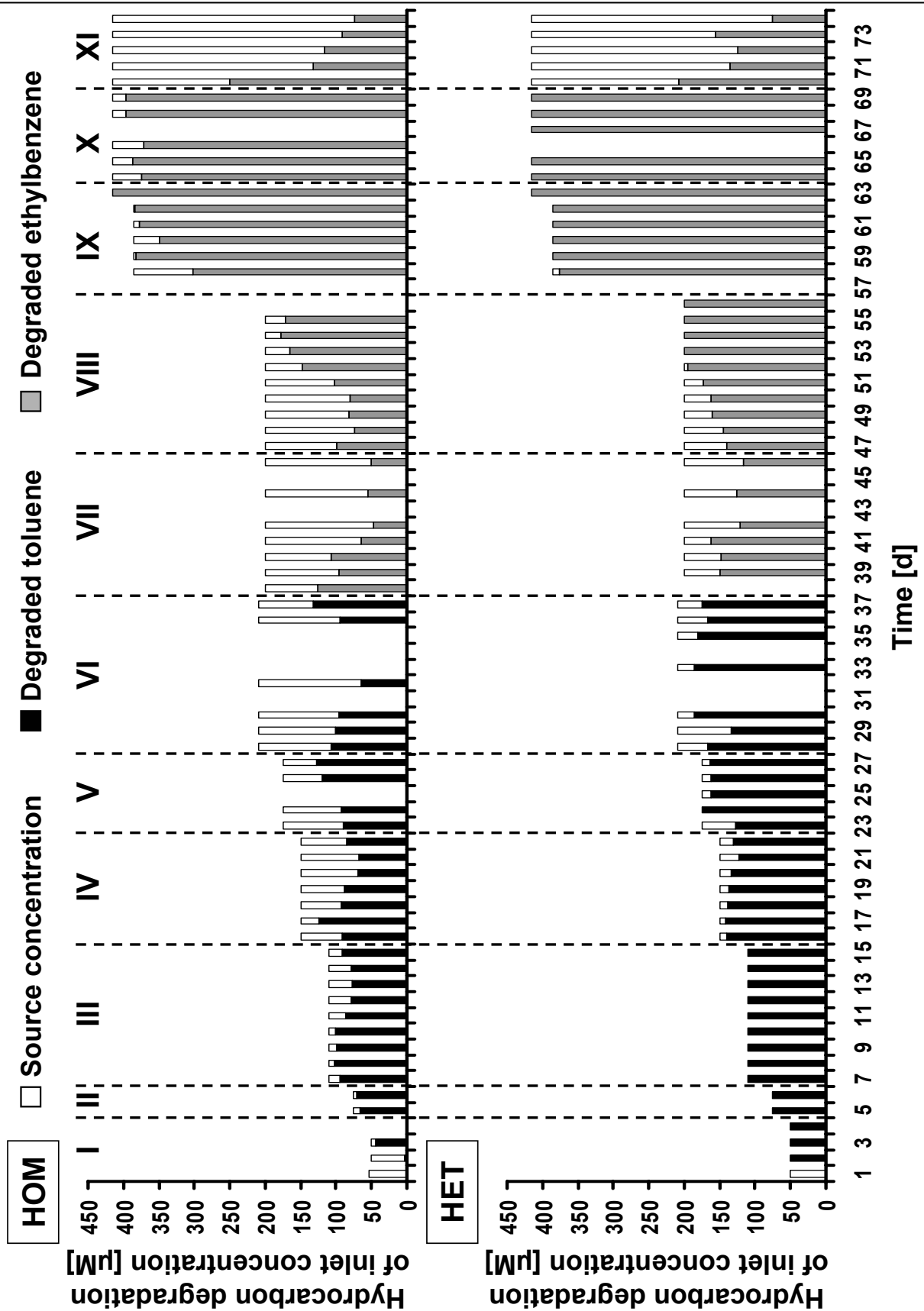


Figure 3.3: Total hydrocarbon degradation of the source concentration in the homogeneously and the heterogeneously filled microcosms during the course of the experiment. White bars show the hydrocarbon concentrations at the inlet, the total degraded portion at the outlets is indicated with black (toluene) and grey (ethylbenzene) filling. At day 38, the hydrocarbon source was changed from toluene to ethylbenzene, and at day 46 the denitrifying *Aromatoleum aromaticum* strain EbN1 was added.

In order to quantify the enhancement of biodegradation due to the high-conductivity lenses, a reaction enhancement factor (REF) based on the measured mass fluxes of toluene was calculated for the individual aerobic degradation phases (Tab. 3.3):

$$REF_{phase} = \frac{(m_{in} - m_{out})_{HET_{phase}}}{(m_{in} - m_{out})_{HOM_{phase}}} \quad (3.5)$$

where m_{in} = inlet mass flux and m_{out} = mean outlet mass flux during the respective degradation phase (Tab. 3.3). For the phases with stepwise increased toluene mass flux (III-VI), the REF increased from 1.23 to 1.63 to 1.79 to 1.82. This indicated a biodegradation enhancement in the heterogeneous sediment of 23% (III) up to 82% (VI), substantiating the beneficial effect of increased mixing onto biodegradation. When correlating the REF values to the respective toluene inlet concentrations a saturation curve like pattern is obtained (data not shown), indicating a finite biodegradation enhancement. In phase VII (200 μ M ethylbenzene) the REF was 2.01, meaning that a plus of 101% ethylbenzene was degraded in the heterogeneous sediment.

3.3.3 Distribution of biodegradation activity

In order to prove the mixing-controlled degradation of contaminants also in the presence of competitive denitrification activity, parameters indicative for microbial activity were investigated. Denitrification was dominant over aerobic degradation in the case of high nitrate concentrations provided (phase VIII-X), which was accompanied with the production of high nitrite concentrations (Tab. 3.3). Activity of *A. aromaticum* EbN1 first provoked a decline of the redox potential as indicated by a color change of the redox indicator resazurin from blue to pink, which was contained in groundwater and plume medium to make the plumes visible (Fig. 3.1b, 3.4). Then, N₂ gas bubbles formed in the sediments of both microcosms (data not shown). Areas of high denitrifying activity thus became visible: in the mixing-controlled homogeneous system both, the pink colour and the N₂ gas bubbles were clearly located at the plume's fringe where also dominant biomass peaks were detected after the experiment (Fig. 3.4a). The heterogeneous tank instead showed an overall pink plume after the first high-conductivity lens, and N₂ bubbles as well as total bacterial cells broadly distributed behind the second lens (Fig. 3.4b). This indicated that degradation activity distributed more evenly within the ethylbenzene plume.

The continuous injection of a mixture of unlabeled ethylbenzene and fully deuterium-labeled (ethylbenzene-*d*₁₀) ethylbenzene isotopomers (ratio 3:1) allowed to study the spatial distribution of anaerobic degradation activity of *A. aromaticum* EbN1. Whereas *P. putida* F1 does not discriminate between the isotopomers, *A. aromaticum* EbN1 metabolizes the unlabeled substrate quicker than the deuterium-labeled compound which leads to fractionation, *i.e.* the accumulation of ethylbenzene-*d*₁₀ in the undegraded residual. Figure 3.5 shows the spatial distribution of *A. aromaticum* EbN1 activity between day 47 and 58 at the outlet ports. Occurring fractionation was resolved in vertical profiles, where low ratios indicated high fractionation and thus degradation activity. Before the inoculation of *A. aromaticum* EbN1 on day 46, of course, no fractionation could be observed in the microcosms. Then, with the establishment of the denitrifier, degradation activity was particularly pronounced at the plume's fringe in the homogeneous setup (represented by the ports 3, 4 and 6, 7). The data measured at the following days showed that although fractionation in the plume's core increased (represented by port 5), it remained dominant at the fringes. In comparison, the faster contaminant depletion in the heterogeneous sediment entailed stronger fractionation which occurred on a wider range, and was according to the flow pattern of the plume. Despite the overall high activity between day 51 and 58, fractionation was less pronounced just below the high-conductivity

lenses, *i.e.* port 7 and 8, corresponding to the asymmetric pattern of the plume, which was supported by the simulated flow field of the heterogeneous system (Fig. 3.1c).

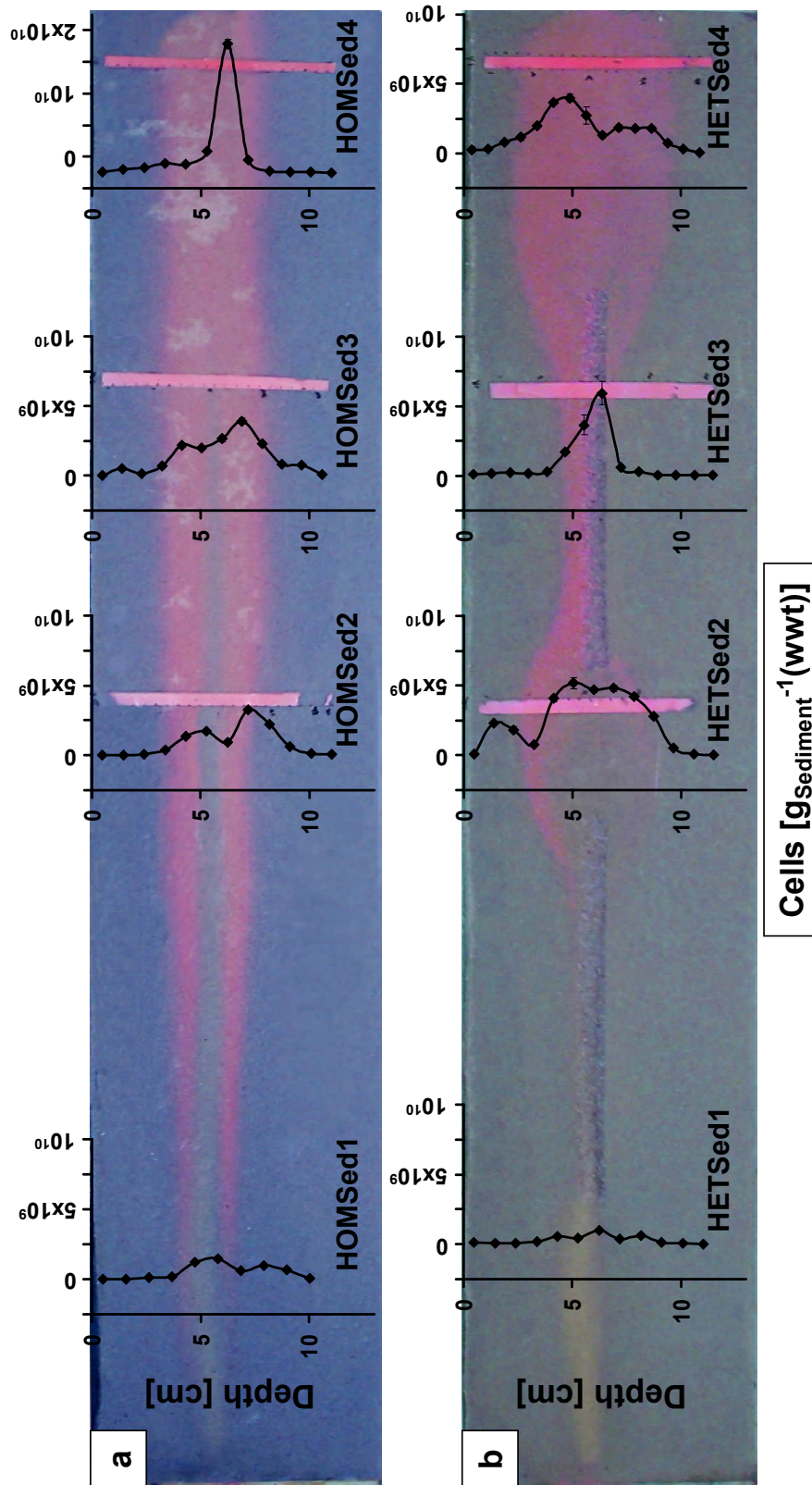


Figure 3.4: Vertical total cell counts given in per gramm sediment, wet weight, (\pm SD) in sediment cores extracted after the end of the experiment, according to the locations indicated on the photographs of (a) the homogeneous, and (b) the heterogeneous sediment, where HOMSed1 is located 14.5 cm, and HETSed1 17 cm from the inlet, and cores 2, 3, and 4 are located 40.5 cm, 57 cm, and 74 cm from the inlet, respectively.

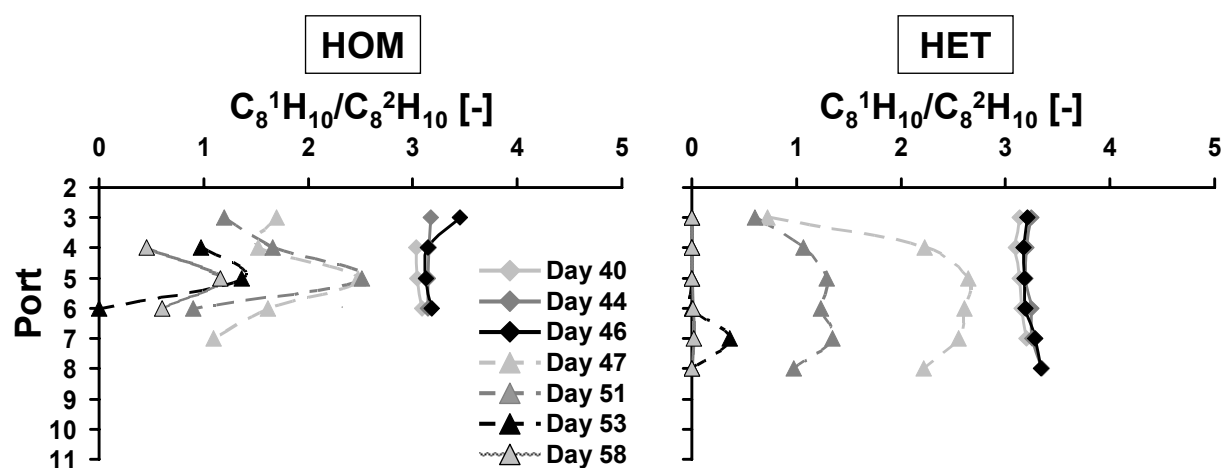
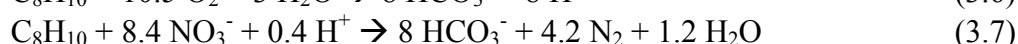
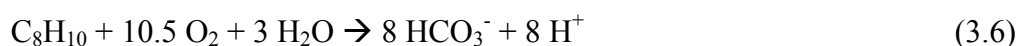


Figure 3.5: Ratio of unlabelled ethylbenzene ($C_8^1H_{10}$) to labelled ethylbenzene- d_{10} ($C_8^2H_{10}$) at the outlet ports in the homogeneous (HOM) and heterogeneous (HET) tanks during exclusive growth of the non-fractionating aerobic strain *P. putida* F1 (until day 46) and during additional growth of the fractionating *A. aromaticum* EbN1 (since day 47). Lower ratios denote higher fractionation activities which are dominant at the plume fringe area of HOM, represented by port 4 and 6.

3.3.4 Reactive transport simulations

Reactive transport modeling was applied to substantiate our experimental results and to elaborate factors controlling biodegradation. It was carried out for all experimental phases characterized by stable degradation and a steady state contaminant plume and biomass. Exemplarily, the results for phase VII and the end of phase VIII (Tab. 3.1) are shown to compare stages where the degradation of a 200 μM source concentration of ethylbenzene was dominated by aerobes (eq. 3.6) and denitrifiers (eq. 3.7), respectively (Fig. 3.6 and Fig. 3.7) and the degradation reactions for ethylbenzene can be written as:



To find out whether limitation factors other than transverse dispersion come into play, the simulations have been carried out using both, instantaneous and double Monod formulation for the degradation kinetics. The first assumes an instant reaction as soon as the reactants meet; the latter considers unspecified reaction rate limiting factors which are based on biokinetic parameters (Tab. 3.2). The slower the reaction effectively proceeds, the greater is the difference between both kinetic formulations.

The model results for aerobic ethylbenzene degradation are reported in Figure 3.6. In the upper plots (Fig. 3.6a) the simulated ethylbenzene profiles at 1 cm from the end of the tank, and the concentrations measured at the outlet ports of the homogeneous and heterogeneous microcosms are compared. Figures 3.6b, 3.6c, and 3.6d show the comparison between the measured oxygen data at the oxygen-sensitive membrane strips, and the simulated profiles of oxygen and ethylbenzene. Despite an overall good agreement between simulated and measured values in both microcosms, the model tended to slightly underestimate the concentrations of ethylbenzene at the outlet (Fig. 3.6a). Moreover, the measured data indicated oxygen consumption on a broader range in the heterogeneous microcosm (Fig. 3.6b, c, d). The congruency of the simulated kinetic formulations indicates fast aerobic degradation.

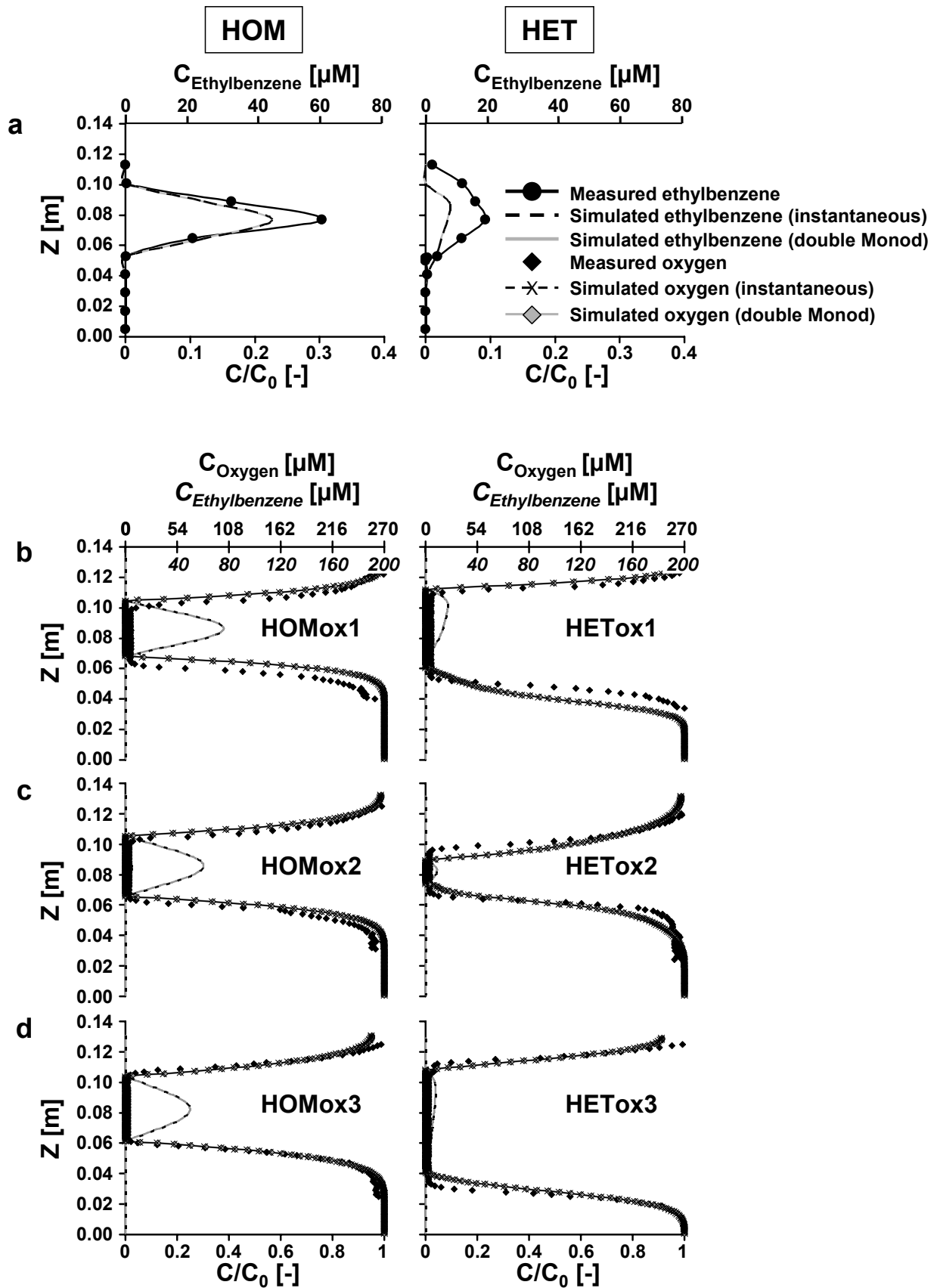


Figure 3.6: Average vertical distribution of the ethylbenzene (a) and oxygen (b, c, d) during aerobic degradation at day 39-46 (phase VII) for the homogeneous (HOM) and the heterogeneous (HET) setup. Experimental data as well as modeling results (considering double Monod kinetics and instantaneous reaction) are shown as concentrations (top axis) and normalized concentrations (ratio outlet/inlet, bottom axis) of ethylbenzene at the outlet (a), and oxygen and ethylbenzene located at the positions depicted in Fig. 3.1a (HOMox1-3, HETox1-3).

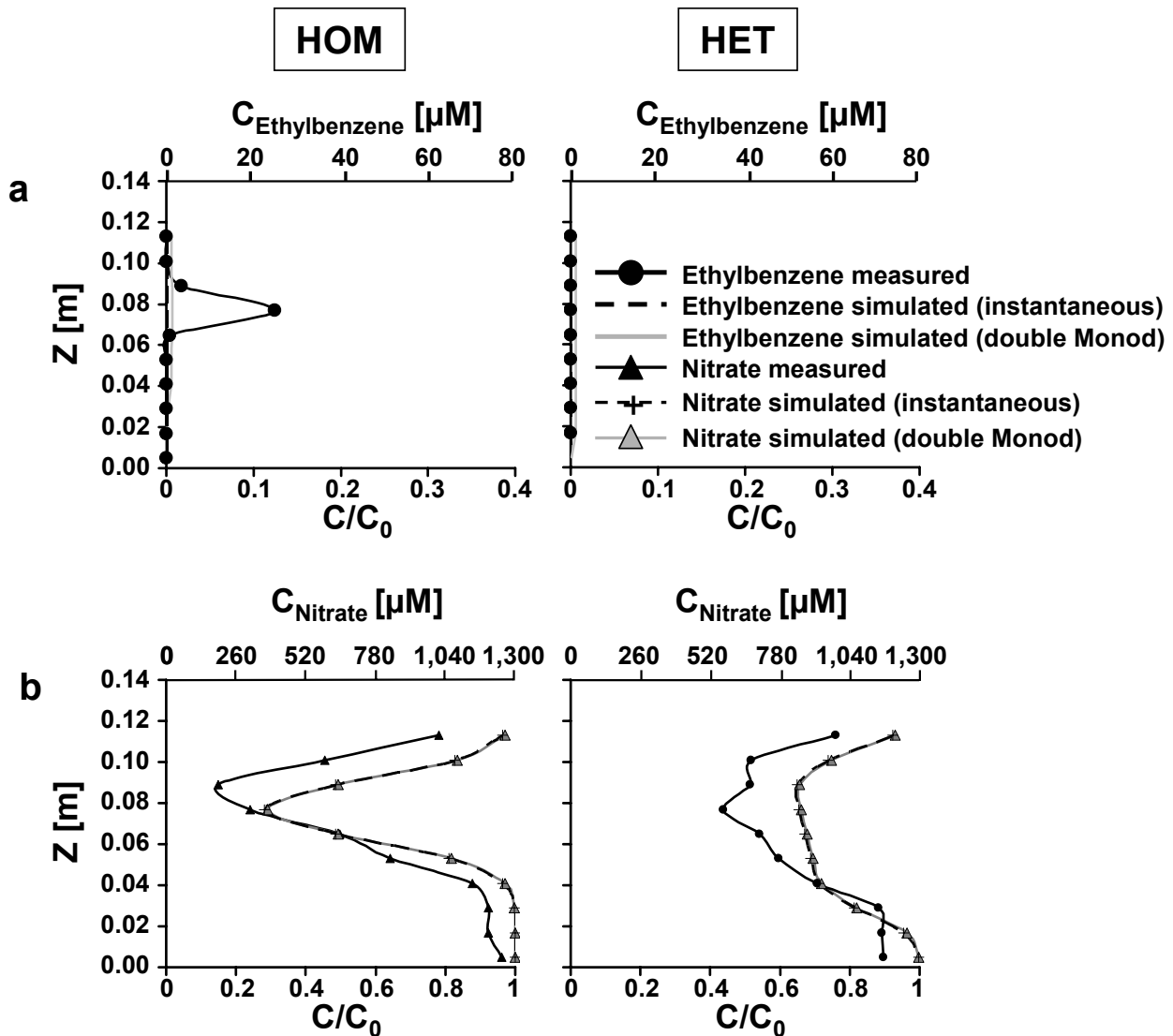


Figure 3.7: Vertical concentration profiles of ethylbenzene (a) and nitrate (b) during anaerobic degradation at the days 52-55 (end of phase VIII) in the homogeneous (HOM) and heterogeneous (HET) microcosms. Values obtained from experiments are compared with modeling data. Values are normalized to the outlet concentrations.

The model results for anaerobic ethylbenzene degradation are shown in Figure 3.7, where the measured vs. simulated ethylbenzene profiles are depicted in the upper plots (Fig. 3.7a), and the measured vs. simulated nitrate concentrations are compared in the lower plots (Fig. 3.7b). The simulated nitrate data shows a faint difference between the two kinetic models.

3.4 Discussion

3.4.1 Mixing-controlled biodegradation in porous media

In this study, it was demonstrated that the degradation of contaminants in porous media is particularly mixing-controlled (Hess *et al.*, 1997; Mayer *et al.*, 2001; Cirpka *et al.*, 1999b). It is therefore suggested that in homogeneous sediments biodegradation activity is predominantly located at the plume's fringe where, governed by transverse dispersion, electron donor and acceptor mix, *i.e.* the plume fringe concept (Bauer *et al.*, 2007). Aerobic degradation activity in homogeneous sediment was shown to form steep oxygen gradients at the toluene plume's fringes,

and led to the formation of an oxygen-free plume. Due to the successive increase of the electron donor and the low solubility of dissolved oxygen, the electron acceptor supply became limiting. Thus, oxygen was subsequently only provided from the ambient medium to the contaminant plume by transverse dispersion, but could not penetrate the plume's center. Therefore, dominant degradation activity was forced to shift to the plume's fringes. Also denitrification activity as well as total biomass (Fig. 3.4a) was located along the plume's fringe of the homogeneous system under mixing-controlled conditions. This was indicated by steep nitrate gradients (Fig. 3.7), stable isotope fractionation data (Fig. 3.5), and formation of N₂ bubbles. Thus, for the first time, the plume fringe concept was corroborated for aerobic and anaerobic degradation of model pollutants, *i.e.* toluene and ethylbenzene. Hitherto, the plume fringe concept was experimentally verified for aerobic degradation in acetate and salicylate plumes as well as for denitrification in glucose plumes in 2-D microcosms (Huang *et al.*, 2003; Oates *et al.*, 2005; Rees *et al.*, 2007; Thullner *et al.*, 2002). However, these studies were characterized by extraordinary high loads of easy degradable carbon-sources which do not reflect typical contamination situations encountered at polluted field sites (e.g. BTEX).

From the concept of mixing-controlled biodegradation it is followed that improved mixing should lead to an enhanced net removal of contaminants. This was proved particularly during aerobic degradation. Compared to the degradation in the homogeneous setup, the overall contaminant removal was up to 101% higher in the sediment where the contaminant plume passed through high-conductivity lenses (Fig. 3.3). Moreover, although gradients also established in the heterogeneous setup, the process was slower compared to the homogeneous sediment, and degradation activity was more evenly distributed within the contaminant plume. This was shown by the slower formation of an oxygen-free plume in the heterogeneous system (Fig. 3.2), which was accompanied by a higher toluene removal. Also after the inoculation of the denitrifier, the degradation response to changing electron donor and acceptor ratios was quicker and always higher in the heterogeneous setup. A reactive transport modeling approach additionally substantiated the fact that the heterogeneous setup significantly contributed to the biodegradation enhancement (Fig. 3.6, 3.7). This was due to flow focusing and spreading of the contaminant plume, which granted an improved mixing of reactants (Fig. 3.1c, 3.1d). The results of this study are in agreement with the postulation that the spatial vicinity of streamlines in the focused flow promotes the chance of streamline crossing of molecules by diffusion, thus favouring the mixing of compounds (Werth *et al.*, 2006). Therefore, the increased flow velocity in high-conductivity zones, such as the coarse sand inclusions of the heterogeneous experimental setup, enhanced the transverse mixing of reaction partners and thus biodegradation. The data therefore prove that transverse mixing is one of the most important factors governing the overall degradation potential in porous sediments. This was previously indicated in another 2-D microcosm experiment containing high-permeability lenses, where microbial dechlorination in heterogeneous sediments in general was focused on (Cirpka *et al.* 1999a). Further 2-D microcosm studies exist on biodegradation in sediments tackling the role of sediment heterogeneity, which particularly addressed the examination of transport and dispersion processes (Cirpka *et al.*, 1999b; Jose *et al.*, 2004). However, high-conductivity zones implicate less time available for the microorganisms to catalyze the degradation of compounds (Werth *et al.*, 2006). This effect implies that such areas benefit bacteria featuring fast kinetics. Regimes with a lower hydraulic conductivity, instead, can mean diffusion-controlled conditions, thus harboring also slower degraders. Such a general correlation could be observed in field studies (e.g. Cozzarelli *et al.*, 1999; Kao & Prosser, 1999). This aspect is of significant relevance to understand the distribution of microorganisms *in situ* as well as "hot-spots" of microbial activity (Vroblesky & Chapelle, 1994), particularly in heterogeneous sediments. Furthermore, the distribution of high- and

low-conductivity flow paths in sediments obviously has a major impact on the overall degradation activity and would be important to account for, rather than assume homogeneous transport and sediment.

3.4.2 Additional biodegradation-limiting factors

So far, no experimental studies dealt with the question of when additional limitation factors have to be taken into account and when biodegradation is exclusively mixing-controlled. Here, it was hypothesized that limiting factors other than transverse mixing are involved in the degradation of contaminants in porous aquifers.

Overlapping zones of nitrate and ethylbenzene during denitrifying activity in the homogeneous system indicated that biokinetics may be limiting. The reactive modelling data confirmed this observation (Fig. 3.7), though the concomitant presence of significant concentrations of the reactants could not be substantiated clearly by experimental data due to the low resolution of the sampling points at the microcosm's outlet (1.2 cm). Despite the presence of both reactants at the same outlet port, the convergence of flowlines mixed the reactants in the individual outlet ports, thus masking steep gradients (Fig. 3.1d), which were expected to follow a pattern similar to oxygen (Fig. 3.6). However, such overlaps were also reported in the field (e.g. Anneser *et al.*, 2007). Because traces of nitrate in the plume center were also detected despite the availability of ethylbenzene, mass transfer limitation (Wick *et al.*, 2001) and threshold concentrations of reactants (Schmidt *et al.*, 1985; Rapp & Timmis, 1999) cannot be excluded. Nevertheless, no significant difference in model results could be obtained for aerobic degradation, assuming instantaneous and double Monod kinetics (Fig. 3.6), which is likely due to the considerably fast reaction rates. The anaerobic transformation of ethylbenzene showed a faint difference between double Monod and instantaneous reaction kinetics, indicating kinetic limitations. Yet, this difference is likely to be underestimated as the biokinetic parameters used were determined in sediment-free batch experiments (Tab. 3.2).

Based on the discrepancy between the simulated and experimental data, it is suggested that the biokinetic parameters selected for modeling may have overestimated the real reaction rates in porous media (Fig. 3.7). This is due the fact, that the biokinetic parameters have been determined largely in batch experiments (Tab. 3.2). Kinetic limitations were further indicated by the detection of high abundances of nitrite when high nitrate concentrations were supplied during denitrification. This was previously reported from batch experiments with *A. aromaticum* EbN1 (Rabus & Widdel, 1995), and is typical when the electron donor is limiting (Jørgensen *et al.*, 1995). This suggests a rate-limiting step after the reduction from nitrate to nitrite which may be attributed to the different reaction sites (cytoplasm and periplasm) during denitrification (Zumft, 1997). It implies that enzymatically driven cell mechanisms (uptake, degradation, regulation) somehow may also control biodegradation and likely depend on the complexity and thermodynamics of the reaction chains of the electron acceptor. Batch experiments with representative strains from different terminal electron-accepting processes (TEAPs) showed a slower growth with lower energy yields of the degradation processes (Meckenstock *et al.*, 2004). Conclusively, also for field conditions a higher reaction-limitation with slower reaction kinetics is expected, although this apparently played a minor role in the experiments conducted.

3.5 References

- Appelo C.A. (2007) Multicomponent diffusion in clays. In *Water pollution in natural porous media*; Candela, L., Vadillo, I., Aagaard, P., Eds.; Instituto Geológico de España: Madrid, 2007, p. 3-13.
- Anneser B., Richters L., Griebler C. (2007) Identification and localization of redox processes in an aromatic hydrocarbon plume via high-resolution sampling of biotic and abiotic gradients. Candela, L.; Vadillo, I.; Aagaard, P.; Bedbur, E.; Trevisan, M.; Vanclooster, M.; Viotti, P.; López-Greta, J.A. (Eds.), *Water Pollution in natural Porous media at different scales. Assessment of fate, impact and indicators. WAPO²*, Madrid, ISBN: 978-84-7840-676-0.
- Baéz-Cazull S., McGuire J.T., Cozzarelli I.M., Raymond A., Welsh L. (2007) Centimeter-scale characterization of biogeochemical gradients at a wetland-aquifer interface using capillary electrophoresis. *Appl Geochem*, in press.
- Bauer R.D., Maloszewski P., Zhang Y., Meckenstock R.U., Griebler G. (2007) Mixing-controlled biodegradation in a toluene plume – results from two-dimensional laboratory experiments. *J Contam Hydrol*, in press.
- Bjerg P.B., Rügge K., Pedersen J.K., Christensen T.H. (1995) Distribution of redox-sensitive groundwater quality parameters downgradient of a landfill (Grindsted, Denmark). *Environ Sci Technol* **29**:1387-94.
- Brune A., Frenzel P., Cypionka H. (2000) Life at the oxic-anoxic interface: microbial activities and adaptations. *FEMS Microbiol Rev* **24**: 691-710.
- Chapelle F.H., McMahon P.B., Dubrovsky N.M., Fuji R.F., Oaksford E.T., Vroblesky D.A. (1995) Deducing the distribution of terminal electron-accepting processes in hydrologically diverse groundwater systems: *Water Resour Res* **31**: 359-371.
- Christensen T.H., Bjerg P.L., Banwart S.A., Jakobsen R., Heron G., Albrechtsen H.J. (2000) Characterization of redox conditions in groundwater contaminant plumes. *J Contam Hydrol* **45**: 165-241.
- Cirpka O.A., Windfuhr C., Bisch G., Granzow S., Scholz-Muramatsu H., Kobus H. (1999a) Microbial reductive chlorination in large-scale sandbox model. *J Environ Eng ASCE* **125**: 861-70.
- Cirpka O.A., Frind E.O., Helmig R. (1999b) Numerical simulation of biodegradation controlled by transverse mixing. *J Contam Hydrol* **40**: 159-82.
- Cirpka O.A. & Valocchi A.J. (2007) Two-dimensional concentration distribution for mixing-controlled bioreactive transport in steady state. *Advances in Water Resources* **30**: 1668-79, doi:10.1016/j.advwatres.2006.05.022
- Cozzarelli I., Herman J.S., Baedeker M.J., Fischer J.M. (1999) Geochemical heterogeneity of a gasoline-contaminated aquifer. *J Contam Hydrol* **40**: 261-84.
- Domenico P. & Palciauskas V. (1982) Alternative boundaries in solid waste management. *Ground Water* **20**: 303-11.
- Eckert P. & Appelo C.A. (2002) Hydrogeochemical modeling of enhanced benzene, toluene, ethylbenzene, xylene (BTEX) remediation with nitrate. *Water Resour Res* **38**: 1-10.
- Franzmann P.D., Robertson W.J., Zappia L.R., Davis G.B. (2002) The role of microbial populations in the containment of aromatic hydrocarbons in the subsurface. *Biodegrad* **13**: 65-78.
- Grathwohl P. (1998) *Diffusion in Natural Porous Media*. Kluwer Academic Publishers, Boston 224p.

- Hess A., Zarda B., Hahn D., Häner A., Stax D., Höhener P., Zeyer J. (1997) *In situ* analysis of denitrifying toluene- and m-xylene-degrading bacteria in a diesel fuel-contaminated laboratory aquifer column. *Appl Environ Microbiol* **63**: 2136-41.
- Huang W.E., Oswald S.E., Lerner D.N., Smith C.C., Zheng C. (2003) Dissolved oxygen imaging in a porous medium to investigate biodegradation in a plume with limited electron acceptor supply. *Environ Sci Technol* **37**: 1905-11.
- Jørgensen C., Flyvbjerg J., Arvin E., Jensen B.K. (1995) Stoichiometry and kinetics of microbial toluene degradation under denitrifying conditions. *Biodegrad* **6**: 147-56.
- Jose S.C. & Cirpka O.A. (2004) Measurement of mixing-controlled reactive transport in homogeneous porous media and its prediction from conservative tracer test data. *Environ Sci Technol* **38**: 2089-96.
- Jose S.C., Rahman M.A., Cirpka O.A. (2004) Large-scale sandbox experiment on longitudinal effective dispersion in heterogeneous porous media. *Water Resour Res* **40**: doi:10.1029/2004WR003363.
- Kao C.M. & Prosser J. (1999) Intrinsic bioremediation of trichloroethylene and chlorobenzene: field and laboratory studies. *J Hazard Mat B* **69**: 67-79.
- Kao C.M., Kota S., Ress B., Barlaz M.A., Borden R.C. (2001) Effects of subsurface heterogeneity on natural bioremediation at a gasoline spill site. *Water Sci Technol* **43**: 341-8.
- Leonard B.P. (1988). Universal Limiter for transient interpolation modeling of the advective transport equations: The ULTIMATE conservative difference scheme, NASA Technical Memorandum 100916 ICOMP-88-11, Washington, DC.
- Maier U. & Grathwohl P. (2005) Numerical experiments and field results on the size of steady state plumes. *J Contam Hydrol* **85**: 33-52.
- Mayer K.U., Benner S.G., Frind E.O., Thornton S.F., Lerner D.N. (2001) Reactive transport modeling of processes controlling the distribution and natural attenuation of phenolic compounds in a deep sandstone aquifer. *J Contam Hydrol* **53**: 341-68.
- McDonald M.G., Harbaugh, A.W. (1988) A modular three-dimensional finite-difference groundwater flow model. Technical Report, U.S. Geological Survey Techniques of Water Resources Investigations.
- Meckenstock R.U., Morasch B., Griebler C., Richnow H.H. (2004) Stable isotope fractionation analysis as a tool to monitor biodegradation in contaminated aquifers. *J Contam Hydrol* **75**: 215-55.
- Oates P.M., Castenson C., Harvey C.F., Polz M., Culligan P. (2005) Illuminating reactive microbial transport in saturated porous media: demonstration of a visualization method and conceptual transport model. *J Contam Hydrol* **77**: 233-45.
- Olsson A., Grathwohl P. (2007). Transverse dispersion of non reactive tracers in porous media: A new nonlinear relationship to predict dispersion coefficients. *J Contam Hydrol* **92**: 149-161.
- Pollock, D.W. (1994). User's guide for modpath/modpath-plot, version 3: A particle tracking post-processing package for modflow, the u.s. geological survey finite-difference ground-water flow model. Of 94-464, U.S. Geol. Survey, Reston, VA.
- Rabus R. & Widdel F. (1995) Anaerobic degradation of ethylbenzene and other aromatic hydrocarbons by new denitrifying bacteria. *Arch Microbiol* **163**: 96-103.
- Rahman M.A., Jose S.C., Nowak W., Cirpka O.A. (2005) Experiments on vertical transverse mixing in a large-scale heterogeneous model aquifer. *J Contam Hydrol* **80**: 130-48.
- Rapp P. & Timmis K.N. (1999) Degradation of chlorobenzenes at nanomolar concentrations by *Burkholderia* sp. Strain PS14 in liquid cultures and in soil. *Appl Environ Microbiol* **65**: 2547-52.

- Rees H.C., Oswald S.E., Banwart S.A., Pickup R.W., Lerner D.N. (2007) Biodegradation processes in a laboratory-scale groundwater contaminant plume assessed by fluorescence imaging and microbial analysis. *Appl Environ Microbiol* **73**: 3865-76.
- Röling W.F. & van Verseveld H.W. (2002) Natural attenuation: what does the subsurface have in store? *Biodegrad* **13**: 53-64.
- Schmidt S.K., Alexander M., Shuler M.L. (1985) Predicting threshold concentrations of organic substrates for bacterial growth. *J Theor Biol* **114** :1-8.
- Thullner M., Mauclaire L., Schroth M.H., Kinzelbach W., Zeyer J. (2002) Interaction between water flow and spatial distribution of microbial growth in a two-dimensional flow field in saturated porous media. *J Contam Hydrol* **58**: 169-89.
- Tuxen N., Reitzel L.A., Albrechtsen H.J., Bjerg P.L.. (2006) Oxygen-enhanced biodegradation of phenoxy acids in ground water at contaminated sites. *Ground Water* **44**: 256-65.
- Van Breukelen B.M. & Griffioen J. (2004) Biogeochemical processes at the fringe of a landfill leachate pollution plume: potential for dissolved organic carbon, Fe(II), Mn(II), NH₄ and CH₄ oxidation. *J Contam Hydrol* **73**: 181-205.
- Vroblesky D.A. & Chapelle F.H. (1994) Temporal and spatial changes of terminal electron-accepting processes in a petroleum hydrocarbon-contaminated aquifer and the significance for contaminant biodegradation. *Water Resour Res* **30**: 1561-70.
- Werth C.J., Cirpka O.J., Grathwohl P. (2006). Enhanced mixing and reaction through flow focusing in heterogeneous porous media. *Water Resour Res* **42**: W12414, doi:10.1029/2005WR004511.
- Wick L.Y., Colangelo T., Harms H. (2001) Kinetics of mass-transfer limited bacterial growth on solid PAHs. *Environ Sci Technol* **35**: 354-61.
- Wick L.Y., de Ruiz M., Springael A., Harms H. (2002) Responses of *Mycobacterium* sp. 501T to the low bioavailability of solid anthracene. *Appl Microbiol Technol* **58**: 378-85.
- Wittmann C., Kim H.M., John G., Heinzle E. (2003) Characterization and application of an optical sensor for quantification of dissolved O₂ in shake flasks. *Biotech Lett* **25**: 377-380.
- Wöhlbrand L., Kallerhoff B., Lange D., Hufnagel P., Thiermann J., Reinhardt R., Rabus R. (2007) Functional proteomic view of metabolic regulation in „*Aromatoleum aromaticum*“ strain EbN1. *Proteomics* **7**: 2222-39.
- Zheng C. and Wang P.P. (1999) MT3DMS: A Modular Three-Dimensional Multispecies Model for Simulation of Advection, Dispersion, and Chemical Reactions of Contaminants in Groundwater Systems. Documentation and User's Guide. Contract Report SERDP-99-1, U.S. Army Engineer Research and Development Center, Vicksburg, MS.
- Zumft W.G. (1997) Cell biology and molecular basis of denitrification. *Microbiol Mol Biol Rev* **61**: 533-616.

4 Two-dimensional sediment microcosms – versatile test systems to study biodegradation processes in porous aquifers

4.1 Introduction

Porous aquifers are a vital resource for drinking water, but nowadays subject to multiple threats such as the impact by various kinds of contaminations (Danielopol *et al.* 2003). Since the past three decades the fate of contaminants in aquifers is a major focus of various research disciplines, such as hydrogeology, geochemistry, and microbiology. Investigations of contamination scenarios in aquifers, especially at an appropriate micro- and mesoscale are often hampered by the limited accessibility and the structural and physical-chemical heterogeneity of the subsurface. Therefore, it is argued that it is important to have in hand versatile model systems which allow the researcher to study principal processes under well-controlled conditions.

Microcosms are, in the first instance, not designed to mimick natural systems but to simplify nature to an extent so that individual processes can be studied (Jessup *et al.*, 2004). An intelligent design of series of experiments, particularly when combined with mathematical modeling approach, allows to test theoretical concepts and hypotheses. The complex conditions in field instead often lead to vague interpretations and speculations which then require a fitting of parameters, hampering the evaluation of conceptual models.

The paradigm of a small-scale microcosm simplifying nature to a concise arrangement permits a target-oriented view. The simulation of a set of important basic environmental conditions in porous aquifers requires a number of preconditions. First, of course, the experimental system must contain a solid matrix such as sediments partly or fully saturated with a liquid phase, e.g. groundwater, passing through. Experiments in perfectly mixed, closed batch systems are in most cases inappropriate when investigating natural processes on a laboratory-scale. In a similar way, one dimensional flow-through systems, *i.e.* sediment columns, proved to be valuable for the enrichment of degradaers, the determination of transport characteristics of cells and particles (e.g. colloids), the qualitative proof of biodegradation and individual redox processes, and a first estimation of microbial growth rates (Hess *et al.*, 1996; Jose & Cirpka, 2004; Chi & Amy, 2004; Mailloux & Fuller, 2003). Column systems, however, are typically fed by a well-mixed medium which complicates the establishment of a 2-D or 3-D zonation of redox processes, among the general problem of wall and gravity effects with bottom to top columns (especially at flow velocities that are comparable to natural conditions). Columns show only limited applicability to capture processes in porous media in relation to its spatial distribution. But exactly this point proved to be of great importance (see below). 2-D model systems in this sense offer a valuable and versatile tool at manageable costs to challenge the investigation of abiotic and bioreactive processes in porous media under well-controlled conditions. Despite its artificial nature, selected basic conditions may be easily controlled, such as the sediment heterogeneity, and allow a natural microbial community from the infiltrating groundwater to establish. In other cases, well defined bacterial cultures may be inoculated to natural sediment material. Horizontal 2-D sediment microcosms, imitating a transect of an aquifer, are considerably qualified to investigate simple combinations of processes as they are arranged according to the natural flow direction.

Due to their versatility, 2-D microcosms of sizes ranging from millimeters to several meters grew popular in the past few years and were used to address various scientific questions. Selected studies dealt with the conservative transport of fluorescent dye tracers, colloids, and saline solutions (Huang *et al.*, 2002; Loveland *et al.*, 2003; Weisbrod *et al.*, 2004), the elucidation of hydrodynamic

parameters, such as the transverse dispersivities, in porous homogeneous and heterogeneous sediments (Jose *et al.*, 2004; Rahman *et al.*, 2005; Cirpka *et al.*, 2006), and the behavior of non-aqueous phase liquids (NAPLs) in saturated porous media (Zhang *et al.*, 2002, 2007). Research of biotic processes were directed to study bacterial transport and motility in porous media (Sharma & McInerney, 1994) and reactive microbial transport (Oates *et al.*, 2005) as well as on microbial growth in micropores at dispersion zones (Nambi *et al.*, 2003). The fate of contaminant plumes subject to microbial degradation in mixing-controlled environments characterized by a substrate plume were conducted in homogeneous sediments with glucose (Thullner *et al.*, 2002a, 2002b, 2004) or acetate, phenol, and toluene as model substrates (Huang *et al.*, 2003; Rees *et al.*, 2007; Bauer *et al.*, 2007). In an experiment with heterogeneous sediment the dechlorination of a tetrachloroethene plume was investigated (Cirpka *et al.*, 1999a). In the case of contaminant fate in porous aquifers, recent 2-D microcosm experiments substantially contributed to elucidate key processes involved in natural attenuation (Cirpka *et al.*, 1999b; Rahman *et al.*, 2005; Cirpka *et al.*, 2006; Jose *et al.*, 2004; Rees *et al.*, 2007; Bauer *et al.*, 2007).

The present paper introduces an all-round 2-D sediment microcosm constructed for the purpose of investigating key factors controlling aerobic as well as anaerobic degradation of aromatic hydrocarbons in porous aquifers. It provides an overview on data obtained from five years of biodegradation experiments which shall demonstrate the multifunctionality of this experimental system. Last but not least further fields of application are discussed. The frequent interest in this experimental setup by other working groups worldwide convinced us to introduce the 2-D model aquifer systems highlighting past and current experimental results to the scientific community.

4.2 The 2-D sediment microcosm experimental setup

The microcosm's outer/inner dimensions are 82.5 cm/ 78.5 cm × 16 cm/ 14 cm × 3 cm/ 1 cm (Fig. 4.1.5), and is composed of teflon, aluminum and two glass sheets minimizing the potential of sorption of organic contaminants. Nevertheless, a minimum of silicon glue was used for sealing. The top of the microcosm may be optionally closed with a lid. The microcosms were packed with either glass beads (212-300 μm grain diameter) or quartz sand with a grain diameters of 200-300 μm (Aldrich, USA) sterilized by heating at 450°C for 4 h, and maintained in upright position. Heterogeneous fillings additionally contained high-conductivity lenses of coarse quartz sand with a grain diameter of 1 mm. The inlet and outlet side of the microcosm is equipped with 11 ports each with a vertical spacing of 1.2 cm. The inlet and outlet ports consist of stainless steel capillaries (1/16", Alltech, IL, USA) which were connected to fluran pump-tubing (ID: 1.02 mm; Ismatec, Glattbrugg, CH) fitted in two peristaltic pumps (MCP, Ismatec, Glattbrugg, CH) (Fig. 4.1.4, 4.1.8). At the outflow side, the steel capillaries were tipped with steel wire gauzes inside the microcosms to avoid plugging by small sediment particles. The capillaries at the outlet were directly connected to brass T-fittings (1/16" A-Lok, Alltech, IL, USA), splitting the outflow for sampling purposes. In general, 10 of the inlet ports were fed with artificial groundwater medium (Fig. 4.1.2). Optionally, plume medium containing the contaminant (Fig. 4.1.1) was supplied to the microcosm via a stainless steel capillary and a ceramic piston pump (Ismatec, Glattbrugg, CH) (Fig. 4.1.3). An interposed brass T-fitting allowed subsampling of plume medium right before it entered the microcosm. To maintain a constant flow, a second multi-channel peristaltic pump was connected to the 11 outflow ports. Waste was collected in an outlet reservoir (Fig. 4.1.9). The flow rates were set slightly higher for the individual inlet ports than for the outlet ports in order to create a small unsaturated zone ensuring a stable water table. Therefore, the uppermost port (*i.e.* port 1) at the inlet

side was plugged with a stopper whereas surplus water and ambient gas from above the sediment was withdrawn by the uppermost port at the outlet side. Typically, the system was run at velocities of 1.2 m d^{-1} .

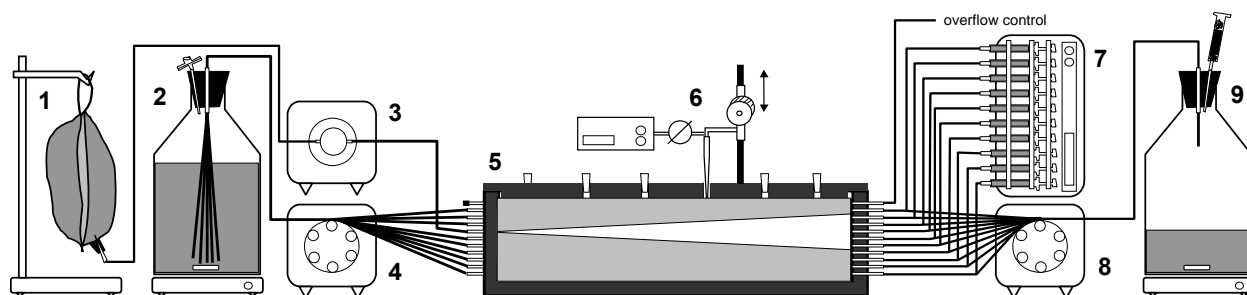


Figure 4.1: Experimental 2-D sediment microcosm setup. (1) Plume medium containing the contaminant and stored in Tedlar bag, (2) oxic groundwater medium, (3) piston pump, (4, 8) peristaltic pumps, (5) sediment-filled 2-D model aquifer (microcosm), (6) micromanipulator holding microsensor, (7) syringe pump, (9) waste collecting bottle.

Sampling at the outlet ports was done by a multi-channel syringe pump (WPI, Berlin, Germany) holding ten 10 mL glass syringes and maintaining the identical flow rate of the peristaltic pumps (Fig. 4.1.7). Subsequently, all samples were aliquoted for analysis of different microbiological and chemical parameters. Prior to each experiment, the microcosm was sterilized with a 0.3 M NaOH solution and rinsed twice with autoclaved ultra-pure MQ water (Millipore, MA, USA). Capillaries and tubings were autoclaved.

4.3 Controls and limitations of biodegradation in BTEX plumes – exemplary results and discussion

Most of the experiments presented in this work drew upon different aspects related to dealing with point-source contaminant plumes, with toluene and ethylbenzene representing oxidizable model pollutants. The elucidation of processes controlling and limiting microbial degradation was hereby of particular interest.

Conceptual and numerical reactive transport models as well as field and microcosm studies in stated and partly proved that biodegradation in contaminant plumes is mixing-controlled (e.g. Cirpka *et al.*, 1999a; Prommer *et al.*, 2000; Thornton *et al.*, 2001; Maier & Grathwohl, 2006; Cirpka *et al.*, 2006). Longitudinal and transverse dispersion are the physical processes which lead to a mixing of contaminated and uncontaminated water at the fringe of these plumes. In contrast to surface water systems, only limited mixing takes place in sediments which are characterized by laminar flow. In steady state contaminant plumes microbial degradation activity is thus suggested to be primarily localized at the fringe, where, governed by transverse dispersion, soluble electron acceptors, *i.e.* oxygen, nitrate, and sulfate, from ambient groundwater mix with electron donors, *i.e.* the contaminants. This was later explicitly referred to as the plume fringe concept (Bauer *et al.*, 2007). Therefore, steep physical-chemical and microbial gradients expand over a narrow zone (Bekins *et al.*, 1999; Christensen *et al.*, 2000, 2001; Huang *et al.*, 2003; Thullner *et al.*, 2002a, b; Mayer *et al.*, 2001; Vieth *et al.*, 2005, Anneser *et al.* 2007; Bauer *et al.*, 2007). In general it can be postulated that where gradients are, biological hot spots concerning activity and often also diversity can be found.

In the following, a selection of results obtained in a series of biodegradation experiments in

the 2-D microcosm used in this thesis is presented. To demonstrate the versatility of the 2-D system different aspects from aerobic to anaerobic degradation were touched, stepwise increasing the complexity of environmental conditions.

4.3.1 From abiotic to biotic processes

Characterizing hydrological properties of a flow-through bioreactor under abiotic conditions is fundamental to obtain detailed knowledge of basic conditions. This is a prerequisite to extrapolate evolving structures and processes involved, arising with the introduction of microbial activity.

Generally, non-reactive tracer tests are performed with either bromide and uranine, or a contaminant of choice (here: toluene) to describe hydrogeological properties of the flow-through sediment system. Depending on the aim of the experiment, either pulsed or continuous tracer tests are conducted. From these, important hydrodynamic parameters, such as transverse and longitudinal dispersion coefficients (D_T , D_L), water velocity (v) and the mean transit time (t_0) can be derived; a necessary data set when for example applying numerical reactive transport models to evaluate the working hypothesis. Table 3.2 summarizes the set of hydrodynamic data as determined for the experimental setup given in this paper.

In all degradation experiments, the established contaminant plume contained bromide as an internal conservative tracer. This way it was possible to make sure that stable hydraulic conditions prevailed during the experiment. In the following, the vertical distribution of bromide, the electron donor (toluene) and the electron acceptor (nitrate) at the outlet of the microcosm is captured on one selected day, *i.e.* without microbial activity, during the abiotic phase of experiment 1 (EXP1) (Fig. 4.2a). Subsequent to the inoculation of the microcosm with the denitrifying *Aromatoleum aromaticum* strain EbN1 degradation activity established, leading to a removal of both toluene and nitrate. In this phase of EXP1 *A. aromaticum* EbN1 was able to degrade up to 98% of the continuously infiltrated 80 μ M toluene along the travel distance of 78 cm from the inlet to the outlet of the microcosm at a mean transit time of 1.2 m d^{-1} . The conservative tracer distribution remained constant, indicating stable hydraulic conditions (Fig. 4.2b).

4.3.2 From aerobic to anaerobic degradation

In an experiment similar to the one introduced above, biodegradation in a toluene plume was investigated in two parallel microcosms, one inoculated with the aerobic strain *Pseudomonas putida* strain mt-2, and the other one with the denitrifying strain *A. aromatoleum* EbN1. These comparative studies of aerobic versus anaerobic (denitrifying) degradation revealed a lower toluene transformation efficiency of the aerobes, which were, without doubt, limited by the low solubility of oxygen in water when compared to nitrate. This situation is reflected in Fig. 4.2c and d, which show the vertical distribution of toluene and the corresponding electron acceptors oxygen (Fig. 4.2c) and nitrate (Fig. 4.2d) at the microcosm's outlet at the time point of experiment 2 (EXP2). Here, oxygen concentrations were recorded non-invasively with vertical resolution of millimeters using oxygen sensitive membrane strips combined with an optode technique (e.g. Wittmann *et al.*, 2003). These membrane strips were attached to the inner wall of the microcosms right before they were filled with sediment at several distances from the inlet. Data from the dissolved oxygen profile shown originate from a measurement close to the microcosm's outlet, and therefore may be compared against the outlet data of toluene and bromide.

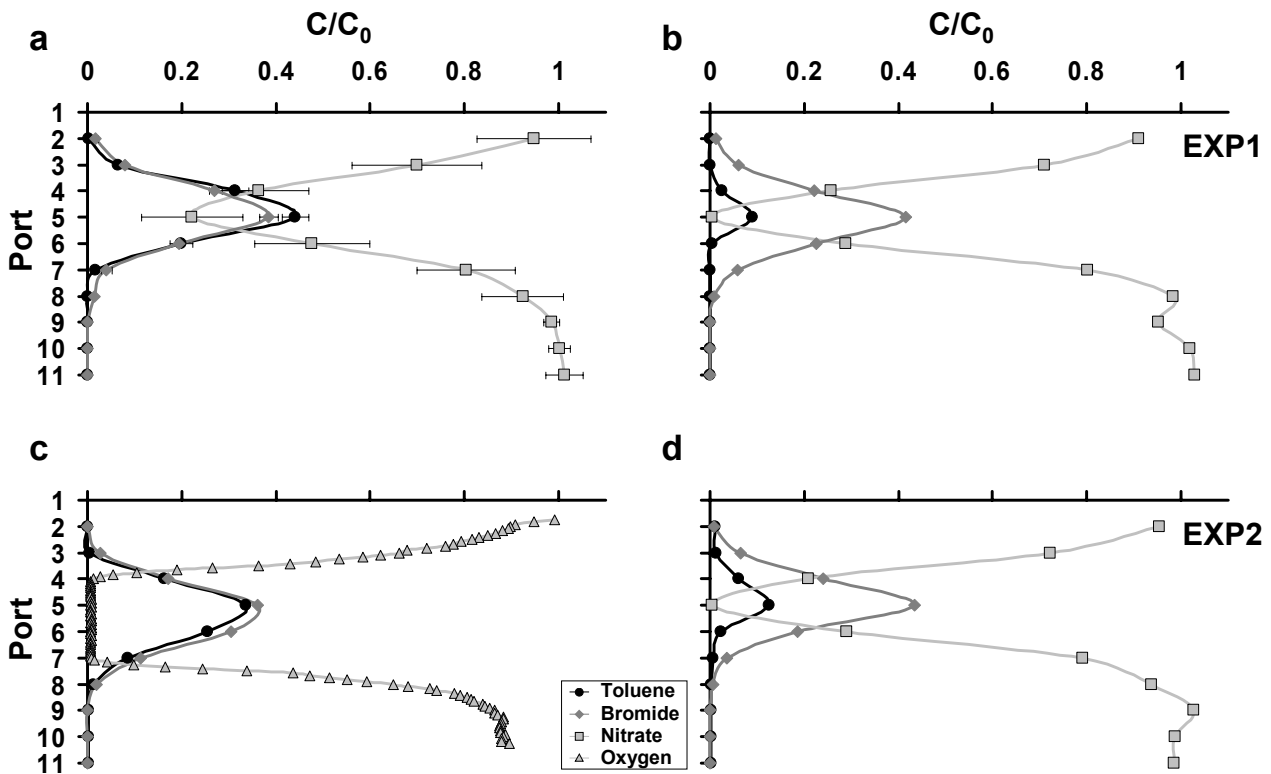


Figure 4.2: Vertical distribution of the conservative tracer bromide, the electron donor toluene, and the electron acceptors oxygen and nitrate at the outlet of the 2-D microcosm in the course of two aerobic/anaerobic degradation experiments. Outlet over inlet concentrations are depicted for the abiotic (conservative) phase (a) and a selected day of a biotic (reactive) phase showing denitrification activity by *A. aromaticum* EbN1 during experiment 1 (EXP1) (b). Accordingly, aerobic (c) and anaerobic (d) degradation of toluene, as investigated in two parallel microcosms in experiment 2 (EXP2), one inoculated with the aerobic *P. putida* mt-2 and the other with the denitrifying *A. aromaticum* EbN1, are shown for one selected day exhibiting full degradation activity.

In EXP2, aerobic degradation contributed to a maximum removal of 30% of an 80 μM toluene source. Due to the high solubility of nitrate, denitrification is not necessarily subjected to a limited availability of electron acceptor. It could be successfully demonstrated that the degradation efficiency by denitrification considerably exceeds aerobic degradation, in this case removing 95% of the toluene supplied (Bauer *et al.*, 2007). This aspect receives particular attention in the context of enhanced natural attenuation (Appelo, 2007).

Studying biodegradation efficiencies and the establishment of steep chemical gradients at the fringes of contaminant plumes in 2-D microcosms demands for measurement techniques with a high spatial and temporal resolution. These requirements are met by the 2-D microcosm here used and the selected techniques applied, and have also been successfully demonstrated in other studies where degradation was investigated at plumes with various easily oxidizable carbon-sources (Huang *et al.*, 2003; Oates *et al.*, 2005; Rees *et al.*, 2007; Thullner *et al.*, 2002a)

The conducted “well-controlled” lab experiments yielded further important information. Regarding the overall microbial degradation potential, aerobic contaminant oxidation of oxidizable compounds at mature organic contaminant plumes plays only a minor role compared to other electron-accepting processes. This is due to (1) the mixing-controlled replenishment of dissolved oxygen (DO) from groundwater into the plume, (2) the fast reaction of DO with reduced compounds, and (3) the potential omnipresence of reduced chemical species such as sulfide and Fe(II) in contaminated zones. However, during the initial development of a contaminant plume

aerobic degradation receives particular significance. The depletion of oxygen in the plume area by aerobic degradation activity grants anoxic domains, and thus the succession and establishment of sustainable anaerobic electron accepting processes.

4.3.3 From single strains to plain mixed communities

In situ biodegradation of contaminants is characterized by the activity of interacting microbial communities. Understanding the concerted action of degraders is crucial to unravel some general principles behind biodegradation in contaminant plumes; for instance is the establishment of individual redox processes reflected by the distribution of specific degraders. Therefore, the distribution of microbes in experiments was treated on where two degraders, *i.e.* the aerobic *Pseudomonas putida* strain F1 and the anaerobic *A. aromaticum* EbN1, interacted in an ethylbenzene plume. The results were compared against experiments containing only one degrader.

At the end of EXP1, which was carried out with a pure culture of *A. aromaticum* EbN1, growing in a steady state toluene plume, a sediment core was extracted and the distribution of cells attached to the sediment across the plume was determined by direct cell counts using flow cytometry (Fig. 4.3a). The vertical distribution of *A. aromaticum* EbN1 nicely reflected the distribution of degradation activity as determined via compound-specific isotope analysis (CSIA) (see below). Although cells were found all over in the microcosm, abundances clearly peaked at the upper and lower plume fringes (Fig. 4.3a). In a consecutive experiment (EXP2) with two strains of degraders, *i.e.* the aerobic *P. putida* F1 and the anaerobic *A. aromaticum* EbN1, again a sediment core was collected close to the microcosm's outlet. To spatially resolve the abundance and distribution of the two strains fluorescence *in situ* hybridization (FisH) was applied (Fig. 4.3b). Although the total cell numbers of *A. aromaticum* EbN1 were up to one order of magnitude higher compared to *P. putida* F1, both strains distributed likewise, peaking at the plume's fringe.

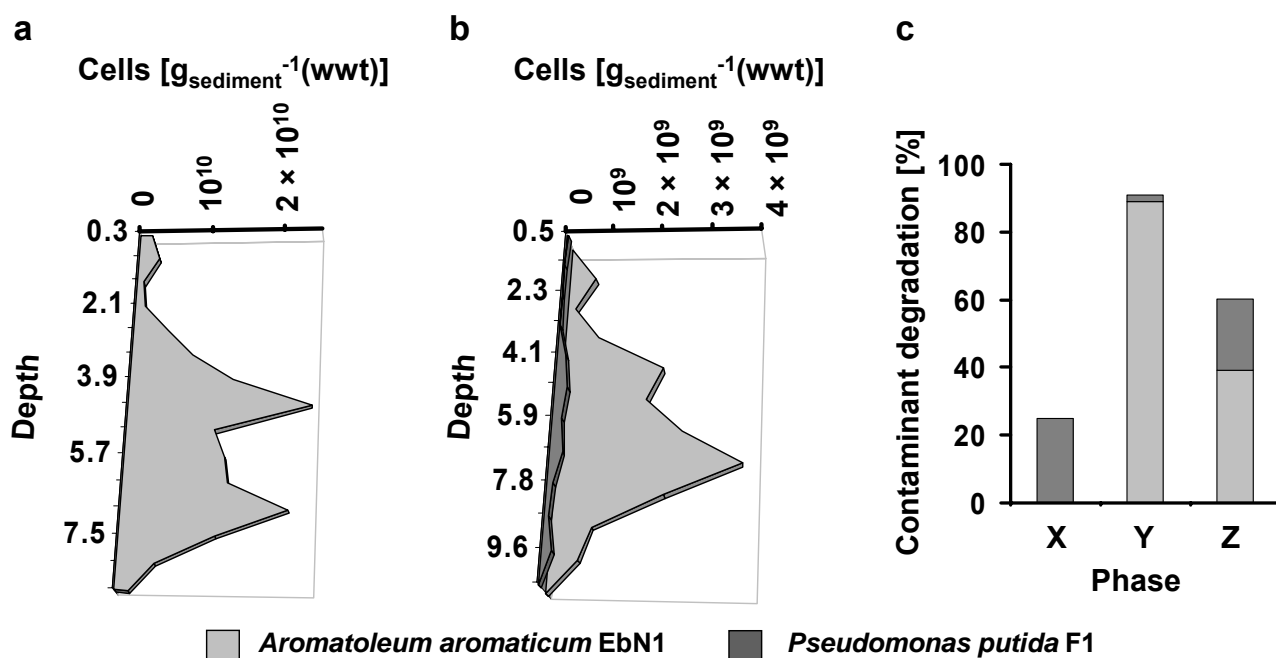


Figure 4.3: Depth-resolved biomass distribution patterns of attached bacteria in sediment cores extracted after (a) a degradation experiment (EXP1) in a steady state toluene plume by a pure culture of the denitrifying *A. aromaticum* EbN1, and (b) a degradation experiment (EXP2) with a steady state ethylbenzene plume harbored by a mixed community (*P. putida* F1 and *A. aromaticum* EbN1). The contribution of the individual strains to the overall degradation during different phases (X, Y, Z) of EXP2 as derived by stable isotope fractionation analyses (c); for further explanation see text.

An alternative and more direct way to differentiate the contribution of two strains to the overall contaminant degradation, compared to biomass distribution measurements, is the application of compound-specific isotope analysis (CSIA) (e.g. Meckenstock *et al.*, 2004). The right combination of strains allowed estimating the individual contribution to the total degradation of ethylbenzene in an anoxic plume. Here, *P. putida* F1 and *A. aromaticum* EbN1 were used, of which the first one does not discriminate between unlabelled and fully deuterium-labelled ethylbenzene. As a prerequisite, the plume medium contained a mixture of unlabelled (C_8H_{10}) and deuterium-labelled (C_8D_{10}) ethylbenzene in a ratio of 3:1. *A. aromaticum* EbN1 metabolizes the isotopically lighter compound several times faster than the heavier deuterium-labelled ethylbenzene species. This results in a shift of the ratio of the isotopomers in the residual compound fraction where degradation takes place. Thus, a measure of fractionation is a measure of microbial activity. The contribution of each strain to the overall degradation in EXP2 can be illustrated for experimental phases where (1) only *P. putida* F1 was present in the microcosm (Fig. 4.3c, X), and when concurrent degradation of both strains took place (2) under high (Fig. 4.3c, Y) and (3) low (limiting) (Fig. 4.3c, Z) nitrate concentrations. Over the distance of 78 cm and with a flow rate of 1.2 m d^{-1} in homogeneous sediment, *P. putida* F1 degraded 25% of a continuously injected ethylbenzene concentration of $200 \mu\text{M}$ in phase X. Two weeks after the inoculation of *A. aromaticum* EbN1 and the raise of the ethylbenzene concentration to $380 \mu\text{M}$, represented by phase Y, the contribution of the aerobe was merely 1.8%, whereas the denitrifier degraded 89.2%. Against the background of enhanced natural attenuation (ENA) (Eckert & Appelo, 2002), this was facilitated by adding high amounts of nitrate (11 mM), favoring denitrification. Immediately (one day) after limiting the nitrate concentration to natural abundance ($20 \mu\text{M}$, only in the groundwater medium), the aerobic degradation regained. This was indicated by contributing to a removal of 20.8% of the ethylbenzene (plume concentration: $415 \mu\text{M}$), whereas denitrification merely accounted for 39.3% with a further downward drift.

These results demonstrate how the 2-D microcosm setup may be used to address well-defined ecological questions related to biodegradation of organic contaminants in porous aquifers.

4.3.4 From homogeneous to heterogeneous sediments

Experiments in homogeneous porous media proved to be a strong simplification. The subsurface itself is generally inhomogeneous and characterized by a patchwork of sediment layers and lenses of different hydraulic conductivities. Therefore, a complex interaction of transport and mixing processes strongly determine biodegradation patterns. The natural attenuation of pollutants in heterogeneous sediments is complex and rarely addressed experimentally (Cirpka *et al.*, 1999a).

To prove the working hypothesis that increased mixing processes of water containing the contaminants and ambient groundwater carrying the dissolved electron acceptors enhances biodegradation, comparative experiments were conducted in parallel microcosms with different sediment textures. These comprised a homogeneous setup (Fig. 4.4a) and heterogeneous packings exhibiting an arrangement of two high-conductivity (coarse sand) lenses and one end-to-end high-conductivity layer, respectively (Fig. 4.4b, c). Different permeabilities lead to a focusing and spreading of streamlines and therefore to an increase of transverse dispersion (Werth *et al.*, 2006). The resulting shapes of the contaminant plumes emerging from the same inlet port as derived from conservative transport of the redox indicator resazurin (Bueno *et al.*, 2002) are sketched in Fig. 4.4. To detect zones of high microbial activity, the contaminant removal (Fig. 4.4, C/C_0) and the ratio of unlabelled to deuterium-labelled substrate (Fig. 4.4, $C(^1\text{H})/C(^2\text{H})$), were surveyed for selected time points at the outlet. The examples given show the abiotic phase and the succession of degradation

activity of *A. aromaticum* EbN1 in the two toluene plumes on consecutive days (Fig. 4.4a, c). Fig. 4.4b shows a similar situation from one experiment with an ethylbenzene plume (EXP2).

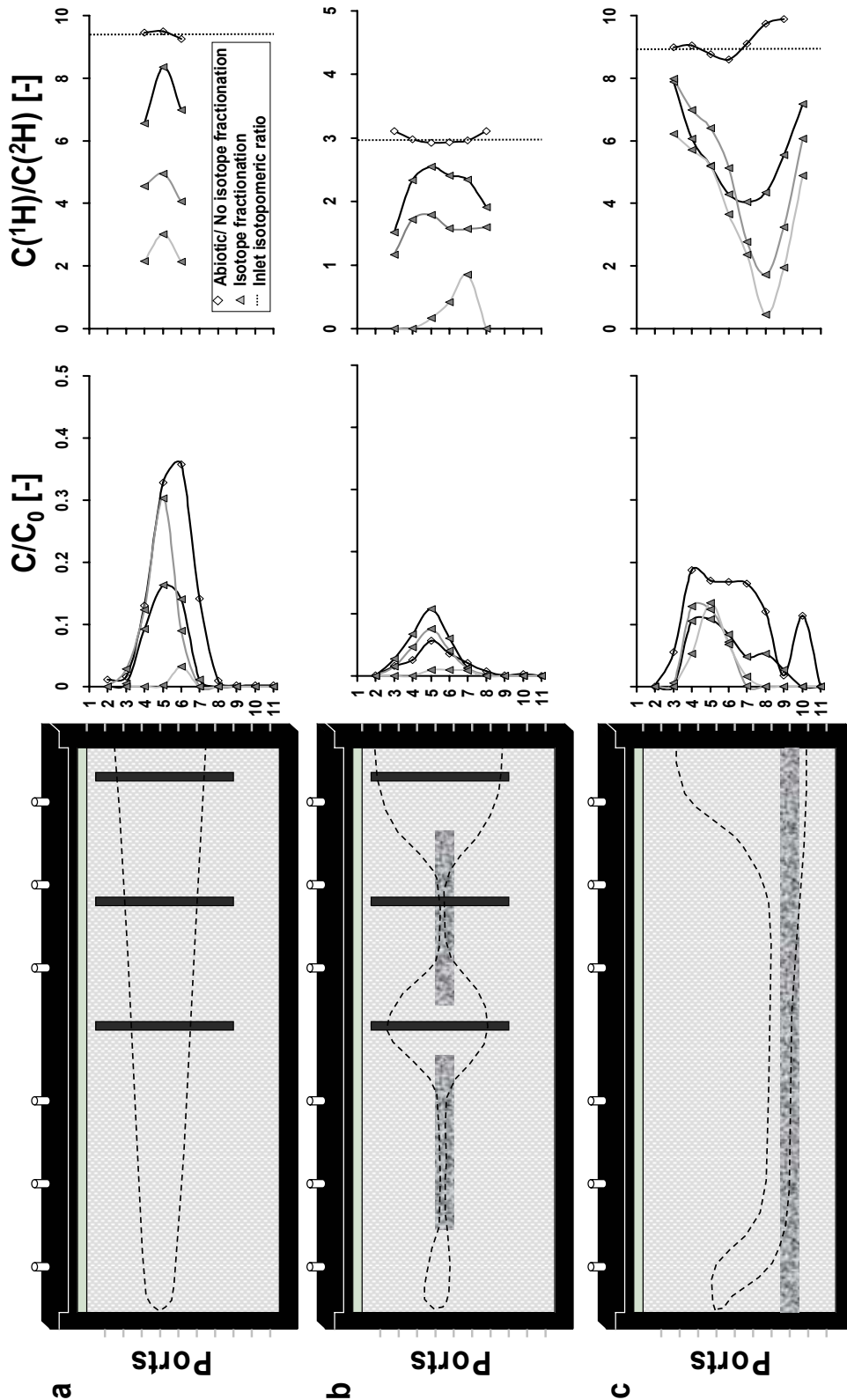


Figure 4.4: The observed shape of the contaminant plumes emerging from inlet port no. 5 are shown in relation to sediment heterogeneity, where (a) is characterized by a homogeneous sand packing, (b) by two consecutive, and (c) one continuous high-conductivity (coarse sand) lenses embedded in a middle sand matrix. The black bars indicate the locations of non-invasive oxygen concentration measurements (see data and discussion section “Aerobic and anaerobic degradation”). Adjoint, vertical contaminant distribution profiles (C/C_0) and the ratios of unlabelled and deuterium-labelled model contaminants ($C(^1H)/C(^2H)$) at successive days of the experiments are shown (dark grey to light grey).

The plume shapes clearly indicated that the heterogeneous sediment settings significantly increased the mixing of the electron donor and electron acceptors. During the plume development, but also when reaching a mature state, dissolved electron acceptors were depleted slower in the plume's center in heterogeneous packings due to a better replenishment from ambient water. Consequently, this resulted in higher biodegradation activities, as derived from CSIA data, compared to the homogeneous setup (Fig. 4.4). This could be substantiated by non-invasive optode-based measurements of the oxygen saturation at different distances from the plume source on selected days of a comparative homogeneous versus heterogeneous experiment, according to the setups of Fig. 4.4a and b (data not shown).

4.3.5 From stable to transient plumes

As observed in the microcosm studies with different hydrocarbon plumes, steep biogeochemical gradients at the plume's fringe, exhibiting very narrow spatial zonations measuring only few centimeters or decimeters, are also found in the field (e.g. Anneser *et al.*, 2007; Bekins *et al.*, 1999; Christensen *et al.*, 2000, 2001; Vieth *et al.*, 2005). These gradients are highly dynamic under transient conditions (Anneser *et al.*, 2007; Christensen *et al.*, 2000; Prommer *et al.*, 2002), as for instance provoked by groundwater level changes and sediment heterogeneities. However, so far little is known about the effects of transient hydraulic conditions onto the distribution and activity of degrading microorganisms.

Here, experiments were conducted focusing on aerobic degradation in a fluctuating toluene plume. (Fig. 4.5a, c). This way, the adaptation period of the microorganisms, *i.e.* the time required for the establishment and re-establishment of stable degradation patterns after each change, was conceptually issued. This was performed for a homogeneous (Fig. 4.5b) and heterogeneous (not shown) sediment packing similar to the setups depicted in Fig. 4.4a and b. First, a stable toluene plume was inoculated with the aerobic strain *P. putida* F1. After establishment of a stable degradation activity, estimated daily by mass balance calculations, it was commenced to switch the plume source from inlet port 5 to 8 and back again in 10-15 days intervals.

In brief, the results indicated that aerobic bacteria were able to cope with a plume change within the order of a few days in both, the homogeneous and the heterogeneous microcosm. A significant amount of attached cells remained when the plume was moved to a new position in the microcosm. They regained full degradation capacity much faster (about twofold) when compared to the first colonization of the plume. For further details see Kürzinger (2007).

4.3.6 From experimental to modeling data

The inaccessibility of the subsurface, the high costs with the installation of proper sampling infrastructure at contaminated sites, as well as the heterogeneity of porous aquifers makes it often rather difficult to obtain sufficient experimental data with an appropriate spatial and temporal resolution. On the one hand it is routine to apply numerical reactive transport models (Maier & Grathwohl, 2006; Prommer *et al.*, 2002; Watson *et al.*, 2003). On the other hand, to validate these models, experimental data are necessary. The 2-D microcosm turned out to be an ideal system producing high quality data which is then available for the validation and improvement of models and *vice versa*. Thus, the models help to test working hypotheses and evaluate obtained data in the shed of theoretical conception. This is demonstrated in the following example.

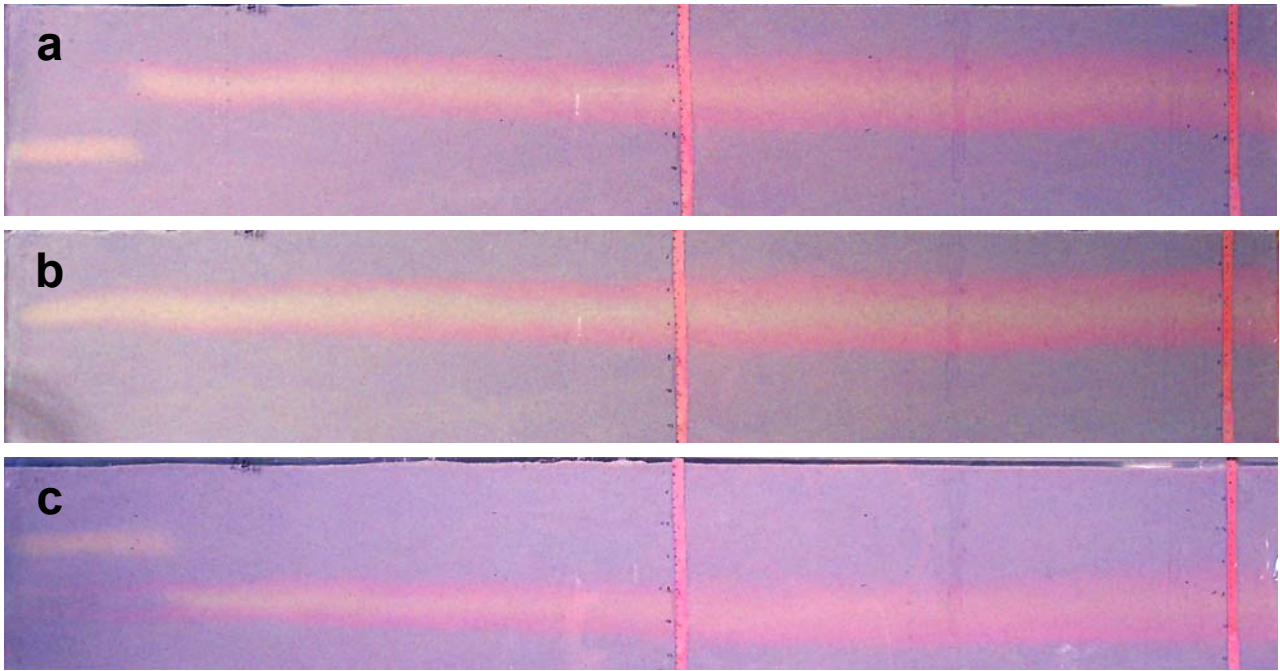


Figure 4.5: Pictures of the 2-D microcosms during an experiment with the aerobic *P. putida* F1. Transient flow conditions were accomplished by an alternate infiltration of the toluene plume through port 8 (a) and port 5 (b) and (c). In combination with the application of conservative or reactive dyes the 2-D shape of the microcosm and the glass walls allows to visualize non-reactive and reactive processes. Based on this principle the flow field of contaminant plumes was generally followed by adding the redox indicator resazurin to the media infiltrated (Bauer *et al.*, 2007).

At the end of an aerobic degradation experiment the distribution of the toluene-degrading strain *P. putida* F1 across a toluene plume was examined with increasing distance to the source. Based on the biokinetic data obtained in batch experiments, simulations were carried out in advance (Dr. Massimo Rolle, Center of Applied Geosciences, University of Tübingen) with the numerical reactive transport model PHT3D (Prommer *et al.*, 2003). It predicted two biomass peaks at the plume’s fringes independent from the distance to the inlet. Higher absolute cell numbers were predicted to be closer to the toluene source, but the peaks became wider with increasing distance (Fig. 4.6a). Despite differences in cell numbers, the experimental data perfectly matched the simulations (Fig. 4.6b).

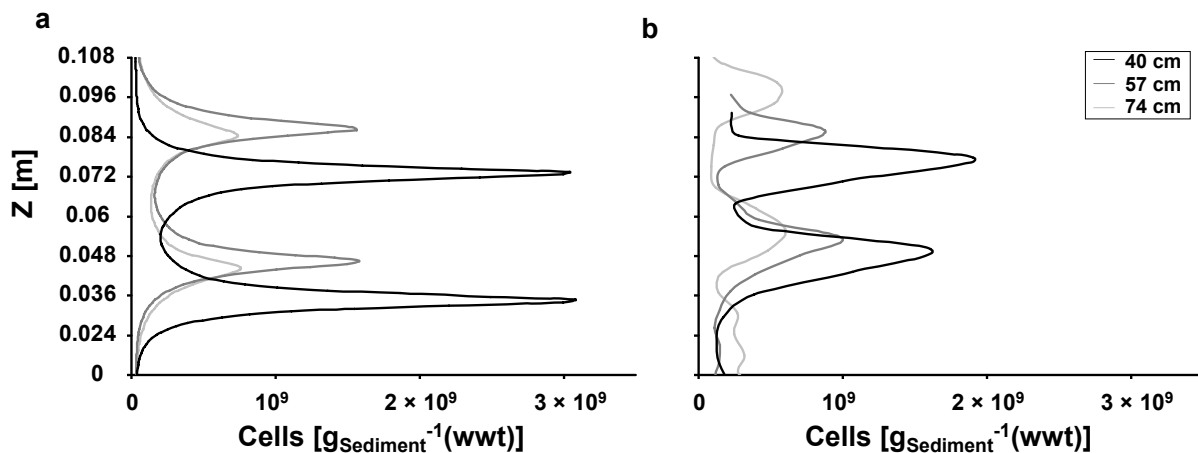


Figure 4.6: Vertical distribution of *P. putida* F1 cells attached to the sediment at the end of an aerobic degradation experiment with a steady state toluene plume. Cell concentration profiles at three distances from the microcosm inlet originate from (a) model simulations and (b) experimental measurement.

4.3.7 Versatility of 2-D microcosm and application possibilities

With the exemplary results from a series of degradation experiments presented in this work, the versatility of the 2-D sediment microcosm could be demonstrated. Besides the applications introduced, 2-D microcosms have been used for a variety of other scientific purposes.

A couple of conservative transport mechanisms in homogeneous and heterogeneous porous media, such as transverse and longitudinal dispersion as well as diffusion processes, were addressed in a couple of investigations and often combined with modeling approaches, to answer conceptual models (e.g. Cirpka *et al.*, 2006; Olsson & Grathwohl, 2007; Rahman *et al.*, 2005; Werth *et al.*, 2006). Therefore, pH-sensitive indicator chemicals and tracer dyes were commonly used. Furthermore, the behavior of dense saline solutions and organic chemicals, such as of highly concentrated (5 M) NaNO₃ and of NAPLs, was investigated in saturated porous media (Weisbrod *et al.*, 2004; Zhang *et al.*, 2002, 2007). For the investigation of oxygen transport and microbial oxygen depletion in 2-D microcosms that allow an interference-free transmission of fluorescent light, imaging techniques, here the application of O₂-reactive fluorescent dyes, proved to be efficient (Huang *et al.*, 2002, 2003; Rees *et al.*, 2007). Oates *et al.*, (2005) presented a study dealing with the illustration of the bioreactive transport of a genetically engineered bacterial strain emitting bioluminescence when aerobically metabolizing salicylate. The biodegradation of a variety of readily oxidizable substrates, such as glucose and acetate, was addressed in other experiments (Huang *et al.*, 2003; Thullner *et al.*, 2002a, Rees *et al.*, 2007). In some cases they were combined with modeling approaches to tackle concepts of bioclogging and biodegradation at field sites (Thullner *et al.*, 2004; Watson *et al.*, 2003).

Regarding the manifold combination of application possibilities it is imaginable that for instance the use of an image-based method which correlates the color of reactive dyes with prevailing conditions (e.g. temperature, redox potential) may be feasible. This would grant non-invasive and temporally high-resolved monitoring of physical parameters, which is particularly informative when microbial activity occurs. Because invasive measurements by microsensors in any case violate sensitive biogeochemical structures, non-invasive high-resolution techniques such as imaging methods or optode-based measurements are trend-setting. However, these techniques are still in the fledgling stages, though the potential would remain unsurpassed when covering different physical-chemical parameters (e.g. temperature, pH, redox potential, BTEX-concentrations). The implementation of microbiology anyhow opens up a wide horizon of application possibilities with respect to the investigation of bacterial behavior in porous media. Active migration, *i.e.* chemotaxis, of bacteria is yet poorly investigated, but can play a significant role with groundwater level changes. This may be approached by genetically engineered bacteria which, for instance, produce light when active. Oates *et al.* (2005) already were able to apply such a technique for aerobes. Likewise, efforts to engineer an anaerobic strain are currently in progress (pers. comm. T. Lüders, A. Feuchtinger). From a microbial ecologist's point of view, the 2-D system seems like a playground. Aerobic and anaerobic areas can be generated and maintained over a considerably long time. Therefore, the response to external influences of complex microbial communities may be investigated from most different aspects. Although demanding, trade-off relationships which allow competing organisms to coexist (Bohannan *et al.*, 2002), could be tackled in porous media. Moreover, protists may be introduced to bacterial communities, in order to study grazing and foodwebs. In field, the prediction of such complex ecological interactions is certainly very intricate. However, a combined model-based approach using the experimental data obtained from microcosm experiments can significantly facilitate the evaluation of conceptual working hypotheses and pinpoint most sensitive parameters and processes.

4.3.8 Conclusions

Geomicrobiological investigations necessitate strategies to be able to effectually follow various processes on a small scale. With the experimental studies presented in this paper versatile suitability of the 2-D microcosm was demonstrated, which is qualified for zooming into steep gradients of abiotic and biotic processes. The experimental flexibility, stability and reproducibility turn the 2-D microcosm to a highly authentic tool for various fields of research with a wide range of application possibilities and combined techniques. It constitutes an ideal lab-scale system where conceptual models and theoretical considerations can be tested under well-controlled conditions. Thereby, they offer the fundamental advantage that basic parameters required remain identical with a set of similar experiments. In summary, experiments conducted in 2-D microcosms warrant a valuable approach to identify the role of single scenes in a clockwork of concerting biogeochemical processes.

4.4 References

- Appelo C.A. (2007). Multicomponent diffusion in clays. In Water pollution in natural porous media; Candela, L., Vadillo, I., Aagaard, P., Eds.; Instituto Geológico de España: Madrid, 2007, p. 3-13.
- Anneser B., Richters L., Griebler C. (2007) Identification and localization of redox processes in an aromatic hydrocarbon plume via high-resolution sampling of biotic and abiotic gradients. Candela, L.; Vadillo, I.; Aagaard, P.; Bedbur, E.; Trevisan, M.; Vanclooster, M.; Viotti, P.; López-Greta, J.A. (Eds.), Water Pollution in natural Porous media at different scales. Assessment of fate, impact and indicators. WAPO², Madrid, ISBN: 978-84-7840-676-0.
- Bauer R. D., Maloszewski P., Zhang Y., Meckenstock R. U., Griebler G. (2007) Mixing-controlled biodegradation in a toluene plume – results from two-dimensional laboratory experiments. *J Contam Hydrol*, in press.
- Bekins B.A., Godsy E.M., Warren E. (1999) Distribution of microbial physiologic types in an aquifer contaminated by crude oil. *Microb Ecol* **37**: 263-75.
- Bohannan B.J., Kerr B., Jessup C.M., Hughes J.B., Sandvik G. (2002) Trade-offs and coexistence in microbial microcosms. *Antonie Van Leeuwenhoek* **81**: 107-15.
- Bueno C., Villegas M.L., Bertolotti S.G., Previtali C.M., Neumann M.G., Encinas M.V. (2002) The excited-state interaction of resazurin and resorufin with amines in aqueous solutions. Photophysics and photochemical reaction. *Photochem Photobiol* **76**: 385-90.
- Chi F.H. & Amy G.L. (2004) Transport of atracene and benz(a)anthracene through iron-quartz and three aquifer materials in laboratory columns. *Chemosphere* **55**: 515-24.
- Christensen T.H., Bjerg P.L., Banwart S.A., Jakobsen R., Heron G., Albrechtsen H.J. (2000) Characterization of redox conditions in groundwater contaminant plumes. *J Contam Hydrol* **45**: 165-241.
- Christensen T.H., Kjeldsen P., Bjerg P.L., Jensen D.L., Christensen J.B., Baun A., Albrechtsen H.J., Heron G. (2001) Biogeochemistry of landfill leachate plumes. *Appl Geochem* **16**: 659-718.
- Cirpka O.A., Windfuhr C., Bisch G., Granzow S., Scholz-Muramatsu H., Kobus H. (1999a) Microbial reductive chlorination in large-scale sandbox model. *J Environ Eng ASCE* **125**: 861-70.
- Cirpka O.A., Frind E.O., Helmig R. (1999b) Numerical simulation of biodegradation controlled by transverse mixing. *J Contam Hydrol* **40**: 159-82.

- Cirpka O.A., Olsson Å., Ju Q., Rahman M.A., Grathwohl P. (2006) Determination of transverse dispersion coefficients from reactive plume lengths. *Ground Water* **44**: 212-21.
- Cirpka O.A. & Valocchi A. (2007) Two-dimensional concentration distribution for mixing-controlled bioreactive transport in steady state. *Advances in Water Resources* **30**: 1668-79.
- Danielopol D.L., Griebler C., Gunatilaka A., Notenboom J. (2003) Present state and future prospects for groundwater ecosystems. *Environ Conserv* **30**: 104-30.
- Eckert P. & Appelo C.A. (2002) Hydrogeochemical modeling of enhanced benzene, toluene, ethylbenzene, xylene (BTEX) remediation with nitrate. *Water Resour Res* **38**: 1-10.
- Hess A., Höhener P., Hunkeler D., Zeyer J. (1996) Bioremediation of a diesel fuel contaminated aquifer columns. *J Contam Hydrol* **23**: 329-45.
- Huang W.E., Smith C.C., Lerner D.N., Thornton S.F., Oram A. (2002) Physical modelling of solute transport in porous media: evaluation of an imaging technique using UV excited fluorescent dye. *Water Res* **36**: 1843-53.
- Huang W.E., Oswald S.E., Lerner D.N., Smith C.C., Zheng C. (2003) Dissolved oxygen imaging in a porous medium to investigate biodegradation in a plume with limited electron acceptor supply. *Environ Sci Technol* **37**: 1905-11.
- Jessup C.M., Kassen R., Forde S.E., Kerr B., Buckling A., Rainey P.B., Bohannon B.J. (2004) Big questions, small worlds: microbial model systems in ecology. *Trends Ecol Evol* **19**: 189-97.
- Jose S.C., Rahman M.A., Cirpka O.A. (2004) Large-scale sandbox experiment on longitudinal effective dispersion in heterogeneous porous media. *Water Resour Res* **40**: doi:10.1029/2004WR003363.
- Jose S.C. & Cirpka O.A. (2004) Measurement of mixing-controlled reactive transport in homogeneous porous media and its prediction from conservative tracer test data. *Environ Sci Technol* **38**: 2089-96.
- Klenk I.D. & Grathwohl P. (2002) Transverse vertical dispersion in groundwater and the capillary fringe. *J Contam Hydrol* **58**: 111-28.
- Kürzinger P. (2007) Aerobic toluene degradation in porous media under transient flow conditions. Master's thesis, University of Tübingen.
- Loveland J.P., Bhattacharjee S., Ryan J.N., Elimelech M. (2003) Colloid transport in a geochemically heterogeneous porous medium: aquifer tank experiment and modelling. *J Contam Hydrol* **65**: 161-82.
- Meckenstock R.U., Morasch B., Griebler C., Richnow H.H. (2004) Stable isotope fractionation analysis as a tool to monitor biodegradation in contaminated aquifers. *J Contam Hydrol* **75**: 215-55.
- Maier U. & Grathwohl P. (2006) Numerical experiments and field results on the size of steady state plumes. *J Contam Hydrol* **85**: 33-52.
- Mailloux B.J. & Fuller M.E. (2003) Determination of in situ bacterial growth rates in aquifers and aquifer sediments. *Appl Environ Microbiol* **69**: 3798-808.
- Mayer K.U., Benner S.G., Frind E.O., Thornton S.F., Lerner D.N. (2001) Reactive transport modeling of processes controlling the distribution and natural attenuation of phenolic compounds in a deep sandstone aquifer. *J Contam Hydrol* **53**: 341-68.
- Nambi I.M., Werth C.J., Sanford R.A., Valocchi A.J. (2003) Pore-scale analysis of anaerobic halorespiring bacterial growth along the transverse mixing zone of an etched silicon pore network. *Environ Sci Technol* **37**: 5617-24.
- Oates P.M., Castenson C., Harvey C.F., Polz M., Culligan P. (2005) Illuminating reactive microbial transport in saturated porous media: demonstration of a visualization method and conceptual transport model. *J Contam Hydrol* **77**: 233-45.

- Olson M.S., Ford R.M., Smith J.A. Fernandez E.J. (2004) Quantification of bacterial chemotaxis in porous media using magnetic resonance imaging. *Environ Sci Technol* **38**: 3864-70.
- Olsson Å. & Grathwohl P. (2007) Transverse dispersion of non-reactive tracers in porous media: a new nonlinear relationship to predict dispersion coefficients. *J Contam Hydrol* **92**: 149-61.
- Prommer H., Barry D.A., Davis G.B. (2000) Numerical modelling for design and evaluation of groundwater remediation schemes. *Ecol Modelling* **128**: 181-95.
- Prommer H., Barry D.A., Davis G.B. (2002) Modelling of physical and reactive processes during biodegradation of a hydrocarbon plume under transient groundwater flow conditions. *J Contam Hydrol* **59**: 113-31.
- Prommer H., Barry D.A., Zheng C. (2003) PHT3D - A MODFLOW/MT3DMS based reactive multi-component transport model. *Ground Water* **42**: 247-257.
- Rahman M.A., Jose S.C., Nowak W., Cirpka O.A. (2005) Experiments on vertical transverse mixing in a large-scale heterogeneous model aquifer. *J Contam Hydrol* **80**: 130-48.
- Rees H.C., Oswald S.E., Banwart S.A., Pickup R.W., Lerner D.N. (2007) Biodegradation processes in a laboratory-scale groundwater contaminant plume assessed by fluorescence imaging and microbial analysis. *Appl Environ Microbiol* **73**: 3865-76.
- Sharma P.K. and McInerney M.J. (1994) Effect of grain size on bacterial penetration, reproduction, and metabolic activity in porous glass bead chambers. *Appl Environ Microbiol* **60**: 1481-6.
- Thornton S.F., Quigley S., Spence M.J., Banwart S.A., Bottrell S., Lerner D.N. (2001) Processes controlling the distribution and natural attenuation of dissolved phenolic compounds in a deep sandstone aquifer. *J Contam Hydrol* **53**: 233-67.
- Thullner M., Mauclaire L., Schroth M.H., Kinzelbach W., Zeyer J. (2002a) Interaction between water flow and spatial distribution of microbial growth in a two-dimensional flow field in saturated porous media. *J Contam Hydrol* **58**: 169-89.
- Thullner M., Zeyer J., Kinzelbach W. (2002b) Influence of microbial growth on hydraulic properties of pore networks. *Transp Por Med* **49**: 99-122.
- Thullner M., Schroth M.H., Zeyer J., Kinzelbach W. (2004) Modelling of a microbial growth experiment with bioclogging in a two-dimensional saturated porous media flow field. *J Contam Hydrol* **70**: 37-62.
- Tuxen N., Reitzel L.A., Albrechtsen H.J., Bjerg P.L. (2006) Oxygen-enhanced biodegradation of phenoxy acids in ground water at contaminated sites. *Ground Water* **44**: 256-65.
- Vieth A., Kästner M., Schirmer M., Weiss H., Gödeke S., Meckenstock R.U., Richnow H.H. (2005) Monitoring *in situ* biodegradation of benzene and toluene by stable carbon isotope fractionation. *Environ Toxicol Chem* **24**: 51-60.
- Weisbrod N., Niemet M.R., Rockhold M.L., McGinnis T., Selker J.S. (2004) Migration of saline solutions in variably saturated porous media. *J Contam Hydrol* **72**: 109-33.
- Werth C.J., Cirpka O.J., Grathwohl P. (2006). Enhanced mixing and reaction through flow focusing in heterogeneous porous media. *Water Resour Res* **42**: W12414, doi:10.1029/2005WR004511
- Wittmann C., Kim H.M., John G., Heinzle E. (2003) Characterization and application of an optical sensor for quantification of dissolved O₂ in shake flasks. *Biotech Lett* **25**: 377-380.
- Zhang C., Werth C.J., Webb A.G. (2002) A magnetic resonance imaging study of dense nonaqueous phase liquid dissolution from angular porous media. *Environ Sci Technol* **36**: 3310-7.
- Zhang C., Werth C.J., Webb A.G. (2007) Characterization of NAPL source zone architecture and dissolution kinetics in heterogeneous porous media using magnetic resonance imaging. *Environ Sci Technol* **41**: 3672-8.

5 General conclusions and outlook

General concepts strongly indicate that in mature steady state contaminant plumes transverse dispersive mixing of electron donors and dissolved electron acceptors at the plumes' fringes is the main driving force for biodegradation (e.g. Cirpka *et al.*, 2006; Jose *et al.*, 2004; Klenk & Grathwohl, 2002; Thornton *et al.*, 2001). On the other hand, experimental data proving the plume fringe concept formulated prior to this thesis, *i.e.* the unambiguous detection of dominant microbial degradation activities at the mixing-controlled contaminant plumes' fringes, were lacking so far. From here it was further hypothesized that enhanced dispersion processes lead, according to the plume fringe concept, to enhanced biodegradation, stressing the crucial role of mixing-control. And, besides mixing, additional factors limiting biodegradation were hardly tackled so far. This thesis, which builds upon the existing state of the art knowledge, therefore ties on the elucidation of key factors and processes controlling and limiting the microbial degradation of contaminant plumes in porous aquifers, based on experiments in two-dimensional (2-D) sediment microcosms.

The plume fringe concept was verified by aerobic and anaerobic degradation experiments in toluene and ethylbenzene plumes. An optode-based non-invasive technique for the measurement of oxygen in aerobic degradation experiments conducted with *Pseudomonas putida* strain F1 impressively showed how fast, *i.e.* within days, a stable anoxic plume center established. The validity of the concept, *i.e.* the restriction of aerobic degradation to the plumes fringes, could be pinpointed by the formation of steep oxygen gradients as well as the distribution of bacterial biomass, peaking at the fringe. In anaerobic degradation experiments with the denitrifying strain *Aromatoleum aromaticum* strain EbN1 similar patterns could be observed. N₂ formation, bacterial biomass as well as compound-specific isotope fractionation activities were found repeatedly located mainly at the plume's fringe. Further evidence for the validity of the plume fringe concept could also be obtained from experiments with a mixed bacterial community of aerobic (*P. putida* F1) and anaerobic (*A. aromatoleum* EbN1) degraders. Here, distribution profiles of biomass, degradation activity as well as of functional marker gene copies (*tod* for *P. putida* F1 and *bss* for *A. aromatoleum* EbN1, both coding for the degradation of toluene) showed two distinct peaks at the plume's fringe (Lüders *et al.*, unpublished data). The conducted experiments for the first time clearly demonstrated that microbial activity is indeed located at the fringes of organic plumes. Thus, evidence was provided that transverse dispersive mixing significantly governs the biodegradation of contaminant plumes.

Subsequent experiments with heterogeneous sediments, promoting an increased dispersive mixing of electron donors and acceptors, clearly showed biodegradation enhancement. Although a first experiment with an end-to-end high-conductivity layer indicated higher microbial degradation activity to occur only in highly permeable zones, the selected setup proved to complicate data interpretation. In a follow-up experiment, biodegradation in sediment containing two distinct high-permeability lenses showed a degradation enhancement of up to 100% when compared to a homogeneous setup which could be attributed to the increased replenishment of the electron acceptors and mixing of reactants. This was due to flow focusing of the plume into the high-conductivity lenses and re-infiltration into the low-conductivity sediment, *i.e.* macrodispersion, and an increased transverse dispersion in the high-permeability lenses. Although entrapped gas in porous media (observed in the experiments with *A. aromatoleum* EbN1) can also affect local hydraulic conductivities, it is particularly sediment heterogeneity that potentially leads to a change in the distribution patterns of degradation. However, the heterogeneous setups applied in this work were simple compared to natural sediments. The puzzle of heterogeneous porous media *in situ* becomes even more complex when zooming into the patchwork of different hydraulic

conductivities. High-conductivity zones on the one hand speed up the transit time of electron donors and dissolved electron acceptors, and lead to a focusing of flowlines which enhance mixing. However, the decreased residence time of nutrients leave the bacteria with less time for catalyzing the reaction. This could imply that such (reaction-controlled) areas are destined for microorganisms featuring fast reaction kinetics. On the other hand, low conductivity zones holding pores still big enough to harbor microorganisms, due to low transport velocities, stand for diffusion- (transport-) controlled environments where slow degraders may be dominant or at least present in relevant densities. Thus, regarding highly inhomogeneous natural sediments, microhabitats and microniches are suggested to determine microbial communities, TEAPs and overall physical-chemical conditions. It is therefore likely that the interplay of strain-specific biokinetics and/or microscale transport processes play a crucial role governing the efficiency of biodegradation. To further clarify this issue, different flow velocities and/or sediment permeabilities must be tested in future experiments.

This thesis work, for the first time, hinted at additional factors limiting biodegradation in mixing-controlled contaminant plumes. In experiments with toluene and ethylbenzene degradation under denitrifying conditions, the detection of the concomitant presence of electron donors and acceptors indicated further processes controlling degradation. By challenging the experimental dataset with a modeling approach, it could be derived that biokinetics may be involved in limitation as anaerobic degradation proceeded slower than aerobic degradation. Although biokinetics comprise enzymatic uptake-, and degradation kinetics, which are presumably strain-specific, the results obtained suggest following correlation: the slower the degradation kinetics are, *i.e.* the lower the energy yields and the more complex electron-acceptor half-reactions are (number of intermediates) the more does degradation shift from mixing-control to reaction-control. Also the accumulation of nitrite during the anaerobic degradation experiments indicated a rate-limiting step in the reaction chain of denitrification. By reducing the electron acceptors, the microorganisms have to cope with different reaction sites (cytoplasm and periplasm), transport or excretion of toxic metabolites or end products (e.g. nitrite, sulfide), long reaction chains, and thermodynamically unfavourable reaction steps. It is already known from batch experiments that growth rates decrease according to the energy yield of the terminal electron-accepting processes (TEAPs) (Tab. 1.1). Therefore, continuative experiments in both batch and 2-D sediment microcosms with strains representing various TEAPs (aerobic, nitrate-reducing and sulfate-reducing) and exhibiting different biokinetics should follow to elucidate this issue. Such studies could also help to determine the most important parameters required for predictive mathematical models.

Besides biokinetics, threshold concentrations of the reactants may be suggested to further limit biodegradation in porous sediments. However, this process could not be pinpointed experimentally, as a higher resolution of the distribution of reactants would be required to avoid convergent mixing of flowlines at each outlet (sampling) port. Still, further investigation may be feasible with non-invasive measurement techniques.

Miscellaneous limiting factors for biodegradation were considered exemplarily in this thesis, such as the general toxicity of contaminants and microbial intermediates or metabolites. Concentrations of up to 415 μM of ethylbenzene did not negatively influence the degradation activity of the aerobic and anaerobic strains applied. Higher concentrations were not applied in the 2-D microcosm experiments, but experience from batch experiments indicates concentrations of >1 mM to pose first inhibiting effects. The presence of sulfide on the other hand, representing the end product of sulfate-reduction, was demonstrated to significantly inhibit aerobic and anaerobic degradation in the microcosm experiments. Sulfate-reduction is known to occur at the majority of petroleum hydrocarbon-contaminated sites. Therefore, depending on the geochemical properties of

the aquifer (e.g. presence of metal species), sulfide-production has the potential to affect the overall degradation. Although investigation exclusively focused on the toxicity of sulfide and competition of chemical reoxidation with aerobic contaminant degradation, further microcosm experiments could contribute to the elucidation of the yet poorly understood cycle of sulfur species in contaminated porous aquifers.

This work showed that under the given experimental conditions biodegradation in mature contaminant plumes in porous media is essentially mixing-controlled, whereas the effects of additional limiting processes were marginal. Nevertheless, biokinetics are suggested to play a greater role in the presence of slow degraders. Consequently, this should also hold true *in situ* where much slower degradation rates occur. The outcomes of this thesis provide a profound basis for the comprehension of controlling factors for biodegradation in porous media. Continuing from here, future investigations should particularly deal with biokinetics, biomass formation and decay, and thermodynamic considerations to further clarify key processes involved as well as to contribute to the development of more accurate reactive transport models.

References:

- Cirpka O.A., Olsson Å., Ju Q., Rahman M.A., Grathwohl P. (2006) Determination of transverse dispersion coefficients from reactive plume lengths. *Ground Water* **44**: 212-21.
- Jose S.C., Rahman M.A., Cirpka O.A. (2004) Large-scale sandbox experiment on longitudinal effective dispersion in heterogeneous porous media. *Water Resour Res* **40**: doi:10.1029/2004WR003363.
- Klenk I.D. & Grathwohl P. (2002) Transverse vertical dispersion in groundwater and the capillary fringe. *J Contam Hydrol* **58**: 111-28.
- Thornton S.F., Quigley S., Spence M.J., Banwart S.A., Bottrell S., Lerner D.N. (2001) Processes controlling the distribution and natural attenuation of dissolved phenolic compounds in a deep sandstone aquifer. *J Contam Hydrol* **53**: 233-67.

Appendix

Mixing-controlled biodegradation in a toluene plume

Simulated and measured concentrations of the conservative tracer bromide during different phases of the experiment carried out with the aerobic *Pseudomonas putida* mt-2.

These data were used for Fig. 2.2a

Z [mm]	Bromide C/C ₀ [-]			
	Simulated Data	Measured Data		
		Abiotic (day 8)	Biotic (day 20-28)	Biotic + Sulfide (day 30-34)
-40.0	0.004			
-37.5		0.012	0.002	0.010
-35.0	0.011			
-30.0	0.028			
-27.5	0.043			
-25.0	0.063	0.087	0.034	0.095
-22.5	0.089			
-20.0	0.120			
-17.5	0.159			
-15.0	0.200			
-12.5	0.243	0.300	0.210	0.258
-10.0	0.287			
-7.5	0.330			
-5.0	0.360			
-2.5	0.382			
0.0	0.389	0.423	0.330	0.300
2.5	0.382			
5.0	0.360			
7.5	0.330			
10.0	0.287			
12.5	0.243	0.253	0.280	0.191
15.0	0.200			
17.5	0.159			
20.0	0.120			
22.5	0.089			
25.0	0.063	0.097	0.118	0.093
27.5	0.043			
30.0	0.028			
35.0	0.011			
37.5		0.028	0.023	0.034
40.0	0.004			
50.0		0.000	0.001	0.007

The error was determined 5% for the abiotic, and 10% for the biotic phases, reflecting the highest standard deviations observed during the respective phases.

Simulated and measured concentrations of the conservative tracer bromide during different phases of the experiment carried out with the anaerobic *A. aromaticum* EbN1.

These data were used for Fig. 2.2b

Z [mm]	Bromide C/C ₀ [-]			
	Simulated Data	Measured Data		
		Abiotic (day 6-9)	Biotic (day 22-32)	Biotic + Sulfide (day 34-38)
-40.0	0.004			
-37.5		0.018	0.020	0.014
-35.0	0.011			
-30.0	0.028			
-27.5	0.043			
-25.0	0.063	0.088	0.060	0.085
-22.5	0.089			
-20.0	0.120			
-17.5	0.159			
-15.0	0.200			
-12.5	0.243	0.274	0.238	0.230
-10.0	0.287			
-7.5	0.330			
-5.0	0.360			
-2.5	0.382			
0.0	0.389	0.382	0.433	0.372
2.5	0.382			
5.0	0.360			
7.5	0.330			
10.0	0.287			
12.5	0.243	0.191	0.240	0.192
15.0	0.200			
17.5	0.159			
20.0	0.120			
22.5	0.089			
25.0	0.063	0.043	0.065	0.058
27.5	0.043			
30.0	0.028			
35.0	0.011			
37.5		0.011	0.013	0.009
40.0	0.004			
50.0		0.000	0.001	0.000

The error was determined 5% for the abiotic, and 10% for the biotic phases, reflecting the highest standard deviations observed during the respective phases.

Simulated distribution of toluene and oxygen under abiotic (conservative) and bioreactive conditions where both reactants are subject to aerobic degradation.

These data were used for Fig. 2.4a

Z [mm]	C/C ₀ [-]			
	Conservative		Bioreactive	
	Toluene	Oxygen	Toluene	Oxygen
-40.0	0.004	0.996	0.004	0.995
-35.0	0.011	0.989	0.004	0.969
-30.0	0.028	0.972	0.004	0.906
-27.5	0.043	0.957	0.004	0.850
-25.0	0.063	0.937	0.004	0.776
-22.5	0.089	0.911	0.004	0.679
-20.0	0.120	0.880	0.004	0.564
-17.5	0.159	0.841	0.004	0.419
-15.0	0.200	0.800	0.004	0.267
-12.5	0.243	0.757	0.005	0.109
-10.0	0.287	0.713	0.027	0.006
-7.5	0.330	0.670	0.085	0.003
-5.0	0.360	0.640	0.126	0.002
-2.5	0.382	0.618	0.156	0.002
0.0	0.389	0.611	0.165	0.002
2.5	0.382	0.618	0.156	0.002
5.0	0.360	0.640	0.126	0.002
7.5	0.330	0.670	0.085	0.003
10.0	0.287	0.713	0.027	0.006
12.5	0.243	0.757	0.005	0.109
15.0	0.200	0.800	0.004	0.267
17.5	0.159	0.841	0.004	0.419
20.0	0.120	0.880	0.004	0.564
22.5	0.089	0.911	0.004	0.679
25.0	0.063	0.937	0.004	0.776
27.5	0.043	0.957	0.004	0.850
30.0	0.028	0.972	0.004	0.906
35.0	0.011	0.989	0.004	0.969
40.0	0.004	0.996	0.004	0.995

Experimentally determined distribution of toluene during the three phases of the experiment conducted with *P. putida* mt-2.

These data were used for Fig. 2.4b

Z [mm]	Toluene C/C ₀ [-]		
	Abiotic (day 8)	Biotic (day 20-28)	Biotic + Sulfide (day 30-34)
-37.5	0.010	0.002	0.003
-25.0	0.087	0.015	0.077
-12.5	0.300	0.191	0.302
0.0	0.423	0.305	0.340
12.5	0.253	0.231	0.155
25.0	0.097	0.069	0.025
37.5	0.027	0.005	0.001
50.0	0.000	0.000	0.000

The error was determined 10% for the biotic phases, reflecting the highest standard deviations observed during the respective phases.

Experimental and simulated distribution of toluene and nitrate during the abiotic phase of the experiment with *A. aromaticum* EbN1.

These data were used for Fig. 2.5a

Z [mm]	C/C ₀ [-]			
	Measured Data		Simulated Data	
	Toluene	Nitrate	Toluene	Nitrate
-40.0			0.004	0.996
-37.5	0.004	0.945		
-35.0			0.011	0.989
-30.0			0.028	0.972
-27.5			0.043	0.957
-25.0	0.040	0.831	0.063	0.937
-22.5			0.089	0.911
-20.0			0.120	0.880
-17.5			0.159	0.841
-15.0			0.200	0.800
-12.5	0.287	0.547	0.243	0.757
-10.0			0.287	0.713
-7.5			0.330	0.670
-5.0			0.360	0.640
-2.5			0.382	0.618
0.0	0.404	0.419	0.389	0.611
2.5			0.382	0.618
5.0			0.360	0.640
7.5			0.330	0.670

10.0			0.287	0.713
12.5	0.179	0.657	0.243	0.757
15.0			0.200	0.800
17.5			0.159	0.841
20.0			0.120	0.880
22.5			0.089	0.911
25.0	0.013	0.879	0.063	0.937
27.5			0.043	0.957
30.0			0.028	0.972
35.0			0.011	0.989
37.5	0.000	0.913		
40.0			0.004	0.996
50.0	0.000	1.000		

The error of the measured data was determined 10% for toluene and 5% for nitrate, reflecting the maximum standard deviations during the abiotic phase.

Experimental and simulated distribution of toluene and nitrate during the biotic phase of the experiment with *A. aromaticum* EbN1.

These data were used for Fig. 2.5b

Z [mm]	C/C ₀ [-]			
	Measured Data		Simulated Data	
	Toluene	Nitrate	Toluene	Nitrate
-40.0			0.004	0.994
-37.5	0.004	0.922		
-35.0			0.011	0.983
-30.0			0.028	0.957
-27.5			0.043	0.934
-25.0	0.001	0.686	0.063	0.903
-22.5			0.089	0.863
-20.0			0.120	0.816
-17.5			0.159	0.756
-15.0			0.200	0.693
-12.5	0.063	0.229	0.243	0.627
-10.0			0.287	0.560
-7.5			0.330	0.494
-5.0			0.360	0.448
-2.5			0.382	0.414
0.0	0.121	0.038	0.389	0.403
2.5			0.382	0.414
5.0			0.360	0.448
7.5			0.330	0.494
10.0			0.287	0.560
12.5	0.035	0.250	0.243	0.627

15.0			0.200	0.693
17.5			0.159	0.756
20.0			0.120	0.816
22.5			0.089	0.863
25.0	0.001	0.705	0.063	0.903
27.5			0.043	0.934
30.0			0.028	0.957
35.0			0.011	0.983
37.5	0.000	0.929		
40.0			0.004	0.994
50.0	0.000	1.000		

The error of the measured data was determined 10% for toluene and 5% for nitrate, reflecting the maximum standard deviations during the biotic phase.

Experimental and simulated distribution of toluene and nitrate during the biotic phase of the experiment with *A. aromaticum* EbN1 in the presence of sulfide.

These data were used for Fig. 2.5c

Z [mm]	C/C ₀ [-]			
	Measured Data		Simulated Data	
	Toluene	Nitrate	Toluene	Nitrate
-50.0	0.000	1.000		
-40.0			0.004	0.996
-37.5	0.006	0.995		
-35.0			0.011	0.989
-30.0			0.028	0.972
-27.5			0.043	0.957
-25.0	0.043	0.775	0.063	0.937
-22.5			0.089	0.911
-20.0			0.120	0.880
-17.5			0.159	0.841
-15.0			0.200	0.800
-12.5	0.159	0.545	0.243	0.757
-10.0			0.287	0.713
-7.5			0.330	0.670
-5.0			0.360	0.640
-2.5			0.382	0.618
0.0	0.247	0.374	0.389	0.611
2.5			0.382	0.618
5.0			0.360	0.640
7.5			0.330	0.670
10.0			0.287	0.713
12.5	0.192	0.635	0.243	0.757
15.0			0.200	0.800

17.5			0.159	0.841
20.0			0.120	0.880
22.5			0.089	0.911
25.0	0.080	0.874	0.063	0.937
27.5			0.043	0.957
30.0			0.028	0.972
35.0			0.011	0.989
37.5	0.011	1.000		
40.0			0.004	0.996
50.0	0.001	1.000		

The error of the measured data was determined 10% for toluene and 5% for nitrate, reflecting the maximum standard deviations during the biotic phase.

Mass balances including standard deviations of toluene, bromide and sulfide of the aerobic degradation experiment carried out with *P. putida* mt-2.

These data were used for Fig. 2.6a

Day	C/C ₀ [%]				
	Toluene	Toluene SD	Bromide	Bromide SD	Sulfide
1					
2					
3					
4	38.8	3.7	94.0	8.9	
5	60.3	5.7	104.6	9.9	
6	81.6	7.8	105.0	10.0	
7	94.9	9.0	105.4	10.0	
8	107.1	10.2	97.2	9.2	
9	90.6	8.6	77.5	7.4	
10	94.6	9.0	115.3	11.0	
11	101.6	9.7	115.0	10.9	
12	105.3	10.0	87.1	8.3	
13	100.7	9.6	108.4	10.3	
14	87.5	8.3	100.2	9.5	
15	84.3	8.0	112.5	10.7	
16	74.6	7.1	94.9	9.0	
17	71.8	6.8	103.9	9.9	
18	71.4	6.8	101.5	9.7	
19	82.6	7.8	98.2	9.3	
20	83.2	7.9	99.7	9.5	
21	89.8	8.5	103.5	9.8	
22	84.7	8.0	106.4	10.1	
23	82.7	7.9	110.4	10.5	
24	63.2	6.0	90.9	8.6	
25	80.3	7.6	101.7	9.7	

26	79.8	7.6	96.7	9.2	
27	77.0	7.3	108.6	10.3	
28	75.9	7.2	88.7	8.4	
29					
30	96.3	9.1	92.7	8.8	49.5
31	90.2	8.6	88.9	8.5	68.8
32	89.7	8.5	91.7	8.7	61.1
33	101.8	9.7	109.6	10.4	99.4
34	81.0	7.7	91.3	8.7	58.5

Mass balances including standard deviations of toluene, bromide and sulfide of the anaerobic degradation experiment carried out with *A. aromaticum* EbN1.

These data were used for Fig. 2.6b

Day	C/C ₀ [%]				
	Toluene	Toluene SD	Bromide	Bromide SD	Sulfide
1.0					
2.0					
3.0					
4.0					
5.0					
6.0	111.4	6.1	98.2	13.0	
7.0					
8.0	88.0	4.9	94.7	12.5	
9.0	86.5	4.8	98.8	13.0	
10.0	126.2	7.0	119.9	15.8	
11.0	71.6	3.9	96.4	12.7	
12.0	100.4	5.5	112.7	14.9	
13.0	95.2	5.2	74.3	9.8	
14.0	100.7	5.6	103.4	13.6	
15.0	103.7	5.7	103.7	13.7	
16.0	101.8	5.6	92.1	12.2	
17.0	88.1	4.9	101.4	13.4	
18.0	80.7	4.4	107.2	14.1	
19.0	59.6	3.3	105.9	14.0	
20.0	40.2	2.2	103.9	13.7	
21.0					
22.0	38.3	2.1	94.5	12.5	
23.0	26.5	1.5	96.8	12.8	
24.0	35.6	2.0	89.2	11.8	
25.0	26.3	1.4	115.8	15.3	
26.0	50.5	2.8	118.1	15.6	
27.0	28.0	1.5	115.6	15.2	
28.0	6.0	0.3	88.9	11.7	

29.0	44.5	2.5	116.5	15.4	
30.0	20.2	1.1	104.3	13.8	
31.0	14.0	0.8	113.8	15.0	
32.0	45.0	2.5	98.2	13.0	
33.0					
34.0	83.1	4.6	84.9	11.2	27.0
35.0	86.3	4.8	87.7	11.6	76.3
36.0	66.8	3.7	78.6	10.4	36.9
37.0	73.8	4.1	96.2	12.7	51.8
38.0	75.1	4.1	88.6	11.7	54.9

Isotope ratio data recorded in a follow-up experiment where *A. aromaticum* EbN1 was inoculated on day 10.

These data were used for Fig. 2.8

Port	Toluene/Toluene- d_8 [-]								
	Day 6	Day 7	Day 9	Day 10	Day 11	Day 13	Day 14	Day 15	Day 16
2									
3									
4	9.6	9.4	9.4	8.0	6.6	5.2	4.5	3.5	2.2
5	9.5	9.5	9.6	8.4	8.4	8.4	4.9	4.2	3.0
6	9.2	9.3	9.8	8.4	7.0	4.2	4.1	2.7	2.1
7									
8									
9									
10									
11									

The inlet ratio of the isotopomers was 8.4 ± 0.2 .

Biomass data determined in a vertical sediment core extracted 22.5 cm after the inlet at the end of a follow-up experiment with *A. aromaticum* EbN1.

These data were used for Fig. 2.9

Depth [cm]	Cells [$\text{g}_{\text{Sediment}}^{-1}$]	SD
0.3	1.58E+09	1.30E+09
0.9	2.75E+09	3.08E+09
1.5	7.40E+08	2.45E+08
2.1	1.18E+09	3.82E+08
2.7	4.65E+09	3.21E+09
3.3	8.14E+09	2.13E+09
3.9	1.37E+10	6.81E+08

4.5	2.42E+10	1.04E+10
5.1	1.17E+10	4.87E+09
5.7	1.32E+10	2.98E+09
6.3	1.36E+10	7.50E+08
6.9	2.16E+10	3.97E+09
7.5	1.25E+10	3.94E+09
8.1	4.84E+09	1.87E+09
8.7	1.80E+09	1.53E+08

Vertical distribution of the electron donor (toluene) and acceptor (nitrate) at the tank outlet on two subsequent days with anaerobic degradation by *A. aromaticum* EbN1.

These data were used for Fig. 2.10

Port	C/C ₀ [-]			
	Day 29		Day 30	
	Toluene	Nitrate	Toluene	Nitrate
2	0.001	0.926	0.005	0.846
3	0.007	0.797	0.007	0.747
4	0.057	0.342	0.045	0.203
5	0.236	0.012	0.113	0.004
6	0.134	0.210	0.018	0.319
7	0.010	0.609	0.009	0.719
8	0.000	1.021	0.001	0.930
9	0.000	1.019	0.001	1.055
10	0.000	1.002	0.001	1.001
11	0.000	0.980	0.001	0.944

Enhanced biodegradation in contaminant plumes passing zones of different hydraulic conductivity

Measured and simulated distribution of bromide at the end of the tanks featuring homogeneous and heterogeneous sediments.

These data were used for Fig. 3.1e

Z [m]	Bromide C/C ₀ [-]							
	HOM				HET			
	Measured		Simulated		Measured		Simulated	
	Port-resolved	SD	Port-resolved	Profile	Port-resolved	SD	Port-resolved	Profile
0.127875				0.00843				0.01447
0.127125				0.00847				0.01451
0.126375				0.00847				0.01471
0.125625				0.00861				0.01505
0.124875				0.00877				0.01553
0.124125				0.00898				0.01612
0.123375				0.00925				0.01691
0.122625				0.00963				0.01786
0.121875				0.01008				0.01901
0.121125				0.01057				0.02033
0.120375				0.01121				0.02185
0.119625				0.01193				0.02364
0.118875				0.01276				0.02566
0.118125				0.01375				0.02794
0.117375				0.01486				0.03050
0.116625				0.01608				0.03338
0.115875				0.01754				0.03660
0.115125				0.01918				0.04010
0.114375				0.02101				0.04404
0.113625				0.02299				0.04821
0.112875	0.02280	0.01872	0.01777	0.02527	0.04316	0.01491	0.03470	0.05272
0.112125				0.02783				0.05743
0.111375				0.03061				0.06256
0.110625				0.03358				0.06780
0.109875				0.03681				0.07328
0.109125				0.04045				0.07887
0.108375				0.04435				0.08461
0.107625				0.04866				0.09038
0.106875				0.05318				0.09605
0.106125				0.05796				0.10175
0.105375				0.06319				0.10737
0.104625				0.06877				0.11295

0.103875				0.07483				0.11825
0.103125				0.08125				0.12338
0.102375				0.08814				0.12829
0.101625				0.09560				0.13274
0.100875	0.11513	0.01845	0.08649	0.10308	0.10693	0.01406	0.11840	0.13695
0.100125				0.11087				0.14081
0.099375				0.11871				0.14422
0.098625				0.12768				0.14727
0.097875				0.13681				0.14979
0.097125				0.14580				0.15216
0.096375				0.15541				0.15424
0.095625				0.16508				0.15599
0.094875				0.17460				0.15745
0.094125				0.18489				0.15847
0.093375				0.19484				0.15946
0.092625				0.20518				0.16015
0.091875				0.21594				0.16073
0.091125	0.21471	0.03152	0.23346	0.22575	0.12377	0.01125	0.15960	0.16123
0.090375				0.23533				0.16128
0.089625				0.24522				0.16143
0.088875				0.25570				0.16145
0.088125				0.26495				0.16144
0.087375				0.27358				0.16141
0.086625				0.28307				0.16131
0.085875				0.29053				0.16099
0.085125				0.29783				0.16071
0.084375				0.30516				0.16058
0.083625				0.31031				0.16031
0.082875				0.31605				0.15992
0.082125				0.32129				0.15972
0.081375				0.32607				0.15928
0.080625				0.32902				0.15911
0.079875				0.33190				0.15853
0.079125				0.33422				0.15836
0.078375				0.33424				0.15794
0.077625				0.33372				0.15745
0.076875	0.31148	0.00987	0.32352	0.33306	0.15040	0.01345	0.15750	0.15717
0.076125				0.33231				0.15667
0.075375				0.32817				0.15618
0.074625				0.32593				0.15574
0.073875				0.32179				0.15519
0.073125				0.31639				0.15472
0.072375				0.31151				0.15427
0.071625				0.30475				0.15397
0.070875				0.29734				0.15341
0.070125				0.28920				0.15293

Appendix

0.069375				0.28120				0.15241
0.068625				0.27283				0.15187
0.067875				0.26353				0.15138
0.067125				0.25379				0.15067
0.066375				0.24387				0.15008
0.065625				0.23496				0.14970
0.064875	0.18709	0.02625	0.23297	0.22391	0.13577	0.01351	0.14990	0.14916
0.064125				0.21326				0.14874
0.063375				0.20275				0.14814
0.062625				0.19268				0.14753
0.061875				0.18206				0.14709
0.061125				0.17221				0.14661
0.060375				0.16156				0.14599
0.059625				0.15157				0.14544
0.058875				0.14228				0.14513
0.058125				0.13258				0.14476
0.057375				0.12363				0.14421
0.056625				0.11508				0.14357
0.055875				0.10635				0.14305
0.055125				0.09837				0.14269
0.054375				0.09067				0.14228
0.053625				0.08329				0.14175
0.052875	0.06549	0.01741	0.08720	0.07617	0.12185	0.01601	0.14180	0.14131
0.052125				0.06938				0.14076
0.051375				0.06330				0.14046
0.050625				0.05748				0.14004
0.049875				0.05218				0.13934
0.049125				0.04701				0.13894
0.048375				0.04252				0.13835
0.047625				0.03832				0.13795
0.046875				0.03437				0.13746
0.046125				0.03073				0.13672
0.045375				0.02753				0.13625
0.044625				0.02443				0.13561
0.043875				0.02176				0.13488
0.043125				0.01917				0.13426
0.042375				0.01691				0.13336
0.041625				0.01487				0.13253
0.040875	0.01815	0.01197	0.01700	0.01306	0.09467	0.02428	0.13070	0.13153
0.040125				0.01139				0.13022
0.039375				0.00992				0.12878
0.038625				0.00865				0.12722
0.037875				0.00751				0.12542
0.037125				0.00649				0.12334
0.036375				0.00561				0.12113
0.035625				0.00483				0.11880

0.034875				0.00416				0.11585
0.034125				0.00357				0.11279
0.033375				0.00306				0.10951
0.032625				0.00261				0.10581
0.031875				0.00221				0.10185
0.031125				0.00188				0.09770
0.030375				0.00158				0.09329
0.029625				0.00133				0.08846
0.028875	0.00013	0.00038	0.00172	0.00112	0.03577	0.02075	0.08534	0.08365
0.028125				0.00093				0.07857
0.027375				0.00078				0.07332
0.026625				0.00065				0.06812
0.025875				0.00054				0.06288
0.025125				0.00045				0.05776
0.024375				0.00037				0.05274
0.023625				0.00030				0.04786
0.022875				0.00025				0.04318
0.022125				0.00021				0.03872
0.021375				0.00017				0.03450
0.020625				0.00014				0.03056
0.019875				0.00011				0.02689
0.019125				0.00009				0.02347
0.018375				0.00007				0.02035
0.017625				0.00006				0.01752
0.016875	0.00000	0.00000	0.00009	0.00005	0.00000	0.00000	0.02020	0.01500
0.016125				0.00004				0.01276
0.015375				0.00003				0.01078
0.014625				0.00002				0.00905
0.013875				0.00002				0.00757
0.013125				0.00001				0.00629
0.012375				0.00001				0.00520
0.011625				0.00001				0.00428
0.010875				0.00001				0.00350
0.010125				0.00001				0.00285
0.009375				0.00000				0.00231
0.008625				0.00000				0.00185
0.007875				0.00000				0.00148
0.007125				0.00000				0.00118
0.006375				0.00000				0.00093
0.005625				0.00000				0.00073
0.004875	0.00000	0.00000	0.00000	0.00000	0.00000	0.00000	0.00129	0.00058
0.004125				0.00000				0.00045
0.003375				0.00000				0.00036
0.002625				0.00000				0.00029
0.001875				0.00000				0.00024
0.001125				0.00000				0.00021

0.000375				0.00000				0.00019
----------	--	--	--	---------	--	--	--	---------

The measured data consider the bromide concentrations of each day of the experiment.

Vertical oxygen profiles recorded at three distances from the tank inlet (40.5 cm, 57 cm, and 74 cm) during the first days of aerobic degradation by *P. putida* F1 in the homogeneous (HOMox) and heterogeneous (HETox) experiment.

These data were used for Fig. 3.2

Port	Z [cm]	Oxygen concentration [μ M]											
		HOMox1				HOMox2				HOMox3			
		Day 1	Day 4	Day 6	Day 9	Day 1	Day 4	Day 6	Day 9	Day 1	Day 4	Day 6	Day 9
0.583	0.9						263				273		
0.667	1						255				264		
0.75	1.1		250				254				259		
0.833	1.2		245			284	253			271	257		
0.917	1.3		248			260	251	260	256	259	256	275	268
1	1.4		248			249	249	250	248	252	254	254	256
1.083	1.5		246			248	249	247	244	251	253	247	245
1.167	1.6		242			244	248	246	243	250	253	247	243
1.25	1.7		244			247	247	246	241	248	250	245	241
1.333	1.8	264	243	253	268	246	245	241	235	246	247	239	238
1.417	1.9	252	238	245	250	243	244	238	239	244	242	239	234
1.5	2	242	238	239	238	242	242	235	233	247	238	235	230
1.583	2.1	240	235	235	235	239	242	233	229	242	235	234	224
1.667	2.2	240	229	236	233	239	238	231	228	239	231	229	221
1.75	2.3	240	223	236	231	235	238	228	225	240	224	226	214
1.833	2.4	241	218	233	229	237	232	227	223	235	219	223	210
1.917	2.5	239	205	230	227	236	229	221	219	235	215	218	205
2	2.6	235	189	227	226	233	223	217	213	231	206	213	194
2.083	2.7	238	177	225	224	232	217	211	209	228	200	205	183
2.167	2.8	237	172	222	223	230	209	209	205	222	192	197	179
2.25	2.9	236	173	219	218	227	201	199	199	221	180	192	168
2.333	3	234	178	214	213	225	197	193	191	219	173	185	158
2.417	3.1	235	179	212	209	222	189	184	179	216	166	174	144
2.5	3.2	232	177	204	203	217	181	175	170	213	146	163	131
2.583	3.3	231	174	197	192	214	171	170	161	210	132	154	116
2.667	3.4	229	170	185	181	209	154	159	148	206	113	145	98
2.75	3.5	228	163	170	169	203	140	151	139	202	102	133	71
2.833	3.6	221	154	157	157	198	131	137	123	197	87.4	115	51
2.917	3.7	218	141	145	148	192	121	124	100	192	62.3	91.6	28
3	3.8	215	134	128	134	189	104	111	85	188	39.9	66.9	15
3.083	3.9	208	123	110	107	179	84	94	64	184	26.9	45.5	7.3
3.167	4	209	111	103	76	172	67	79	45	178	19.1	24	3.6
3.25	4.1	198	103	79	66	166	50	57	16	168	9.82	16.9	2
3.333	4.2	196	93	60	46	154	29	35	8.7	163	5.46	7.6	1.9

3.417	4.3	189	83	31	22	158	15	24	4.6	157	3.12	4.02	1.6
3.5	4.4	181	77	24	11	142	7.1	11	3.3	151	2.69	2.81	1.7
3.583	4.5	174	66	12	5.7	137	5	6.7	3.3	145	2.32	2.28	1.7
3.667	4.6	167	55	7	4.5	129	3.8	4.4	3.2	138	2.25	1.89	1.8
3.75	4.7	160	46	5.1	4.4	119	3.5	3.3	3.1	132	2.15	1.91	1.9
3.833	4.8	147	39	4.9	4.3	115	3.4	3.2	3	126	2.15	2.14	1.9
3.917	4.9	137	33	4.7	4.4	108	3.4	3.1	3	118	2.3	1.96	2
4	5	129	27	4.7	4.4	102	3.5	3.1	3.1	108	2.27	2.01	1.9
4.083	5.1	118	18	4.9	4.6	95	3.6	3.3	3.1	105	2.37	2.16	2
4.167	5.2	106	12	4.7	4.6	91.4	3.5	3.2	3.3	103	2.12	2.14	1.9
4.25	5.3	99	9.1	4.8	4.4	88.2	3.6	3.5	3.4	102	2.2	2.08	2.2
4.333	5.4	90	5.9	4.8	4.6	84.8	3.9	3.3	3.2	101	2.1	2.28	1.9
4.417	5.5	85	5.3	4.7	4.7	82.9	3.6	3.4	3.2	101	2.2	1.96	2
4.5	5.6	79	4.9	4.9	4.8	80.4	3.7	3.3	3.4	104	2.37	1.99	2
4.583	5.7	74	4.9	4.7	4.7	78.9	3.4	3.4	3.3	105	2.12	1.99	2
4.667	5.8	69	4.9	4.6	4.7	80.1	3.5	3.4	3.4	109	2.2	2.11	2
4.75	5.9	65	5.7	5.1	4.7	80	3.4	3.5	3.4	113	2.15	1.86	2.1
4.833	6	64	6.6	4.9	4.9	81.2	3.1	3.4	3.5	121	1.88	2.06	2
4.917	6.1	63	9.5	5	4.7	84.7	3.2	3.2	3.4	118	1.88	2.08	2.1
5	6.2	64	15	4.8	4.9	88	3.3	3.3	3.1	126	2.05	2.04	2.1
5.083	6.3	64	23	4.9	4.7	90.2	3.2	3.1	3.3	134	2.39	2.04	2
5.167	6.4	66	34	4.9	4.8	95.2	3.1	3.1	3	138	2.99	2.01	1.9
5.25	6.5	70	52	4.8	4.8	101	3.5	3.1	3.2	147	4.3	2.01	1.9
5.333	6.6	74	86	4.8	4.5	108	4.9	3.2	3	153	7.9	2.06	2
5.417	6.7	80	111	4.9	4.8	116	10	3.1	3	167	12.5	1.84	1.8
5.5	6.8	88	122	4.7	4.7	121	19	3.1	3	161	19.9	1.94	2
5.583	6.9	97	138	5.6	4.6	129	30	2.9	3	172	28.4	1.86	1.9
5.667	7	104	152	7.8	4.5	136	44	3	3	180	36.4	1.86	1.9
5.75	7.1	113	170	12	4.4	144	62	3.4	2.9	184	49.7	1.94	2
5.833	7.2	123	183	21	4.4	149	85	4.7	3	188	60.8	2.58	1.8
5.917	7.3	136	191	54	4.8	155	107	8.8	2.9	194	81.4	3.77	1.8
6	7.4	150	202	85	5.8	160	127	20	3	199	103	6.5	1.8
6.083	7.5	162	211	108	10	164	137	34	4	204	112	15.1	1.9
6.167	7.6	167	219	125	22	169	149	51	7.7	208	127	30.3	2.4
6.25	7.7	176	219	137	38	175	168	73	17	213	142	45.1	3.9
6.333	7.8	183	226	150	65	180	180	96	29	213	159	64	11
6.417	7.9	189	232	166	95	186	190	110	53	215	169	79.6	27
6.5	8	196	237	183	123	193	196	128	79	221	176	99.4	44
6.583	8.1	199	242	188	139	197	206	142	102	223	186	116	66
6.667	8.2	203	242	199	157	203	212	156	122	227	197	132	91
6.75	8.3	210	245	206	169	205	219	167	138	232	205	146	118
6.833	8.4	213	248	214	180	210	222	181	150	237	212	157	127
6.917	8.5	218	248	218	191	212	226	191	162	237	219	160	139
7	8.6	218	248	220	200	213	229	195	171	238	226	174	149
7.083	8.7	222	246	225	203	218	232	204	180	239	231	188	160
7.167	8.8	225	250	227	211	221	236	208	186	241	237	192	175
7.25	8.9	228	251	232	217	223	240	211	195	241	242	201	184
7.333	9	230	254	238	220	226	240	215	199	245	246	204	196

7.417	9.1	231	251	238	225	227	243	221	206	243	245	213	200
7.5	9.2	233	256	238	227	229	244	223	211	244	249	219	210
7.583	9.3	232	256	241	230	229	249	227	214	247	250	226	214
7.667	9.4	234	256	241	231	232	248	229	220	246	250	225	217
7.75	9.5	239	256	241	229	233	250	233	221	249	252	229	220
7.833	9.6	236	256	240	234	235	252	236	225	246	255	233	221
7.917	9.7	238	256	242	234	233	254	237	226	250	255	236	227
8	9.8	237	256	250	232	237	252	235	232	250	257	240	228
8.083	9.9	234	257	256	235	238	252	238	229	249	256	239	231
8.167	10	238	255	256	246	239	253	241	233	253	258	240	233
8.25	10.1	239	267	256	256	241	253	241	233	250	254	241	234
8.333	10.2	237	258	256	256	242	253	241	233	254	256	242	235
8.417	10.3	244		257	257	244	251	242	231	251	256	243	239
8.5	10.4	240		255	255	246	253	242	234	254	255	245	238
8.583	10.5	241		267	267	243	253	240	234	263	257	244	237
8.667	10.6	239		258	258	251	254	241	235	256	258	244	237
8.75	10.7					248	256	244	233	258	257	245	236
8.833	10.8					246	258	244	236	257	255	244	236
8.917	10.9					248		245	236	260	257	243	236
9	11					249		242	236	260	257	245	236
9.083	11.1					244		244	237	258	258	246	239
9.167	11.2							242		252	259	247	238
9.25	11.3										265	246	237
9.333	11.4											248	237
9.417	11.5											249	242

Port	Z [cm]	Oxygen saturation [%]											
		HOMox1				HOMox2				HOMox3			
		Day 1	Day 4	Day 6	Day 9	Day 1	Day 4	Day 6	Day 9	Day 1	Day 4	Day 6	Day 9
0.583	0.9						97.3				100.9		
0.667	1						94.4				97.9		
0.750	1.1		92.8				94.2				95.8		
0.833	1.2		90.8			105.1	93.8			100.4	95.3		
0.917	1.3		91.9			96.3	93.1	96.1	94.7	95.8	94.8	101.9	99.2
1.000	1.4		91.8			92.2	92.1	92.4	92.0	93.3	94.2	94.2	94.8
1.083	1.5		91.1			92.0	92.3	91.5	90.3	93.1	93.6	91.5	90.9
1.167	1.6		89.5			90.3	91.8	91.0	90.1	92.6	93.7	91.6	89.8
1.250	1.7		90.5			91.5	91.6	91.2	89.4	91.8	92.4	90.8	89.4
1.333	1.8	97.6	90.1	93.6	99.1	91.0	90.8	89.4	87.1	91.0	91.5	88.6	88.0
1.417	1.9	93.3	88.3	90.6	92.7	89.8	90.3	88.2	88.4	90.3	89.6	88.4	86.7
1.500	2	89.6	88.1	88.6	88.3	89.6	89.5	86.9	86.2	91.6	88.3	86.9	85.0
1.583	2.1	89.0	87.0	87.1	87.0	88.6	89.6	86.4	84.8	89.5	87.2	86.5	83.1
1.667	2.2	88.9	84.8	87.4	86.3	88.7	88.0	85.5	84.4	88.6	85.5	84.9	81.7
1.750	2.3	88.9	82.5	87.3	85.6	87.0	88.0	84.6	83.4	88.8	83.1	83.6	79.3
1.833	2.4	89.3	80.7	86.1	84.8	87.8	86.0	84.0	82.5	86.9	81.0	82.7	77.7

1.917	2.5	88.4	75.8	85.1	84.0	87.4	84.7	81.8	81.3	86.9	79.8	80.7	76.1
2.000	2.6	87.1	70.2	84.2	83.8	86.4	82.5	80.5	78.9	85.6	76.4	79.0	72.0
2.083	2.7	88.2	65.6	83.2	82.9	86.0	80.4	78.2	77.5	84.6	74.1	75.9	67.7
2.167	2.8	87.8	63.8	82.2	82.7	85.1	77.6	77.6	75.9	82.3	71.3	72.8	66.2
2.250	2.9	87.4	64.0	80.9	80.6	84.1	74.3	73.8	73.6	81.9	66.5	71.2	62.2
2.333	3	86.6	65.8	79.3	78.9	83.2	72.8	71.4	70.9	81.1	64.2	68.7	58.4
2.417	3.1	87.0	66.2	78.5	77.3	82.2	70.0	68.1	66.2	79.9	61.5	64.3	53.4
2.500	3.2	86.0	65.7	75.4	75.1	80.3	67.0	65.0	63.1	79.1	54.2	60.5	48.5
2.583	3.3	85.7	64.5	73.0	71.2	79.4	63.2	63.1	59.6	77.9	49.0	57.1	42.9
2.667	3.4	84.7	63.0	68.4	67.2	77.4	57.0	59.0	54.9	76.2	41.8	53.5	36.3
2.750	3.5	84.5	60.4	63.0	62.5	75.0	51.9	55.9	51.4	74.7	37.6	49.4	26.4
2.833	3.6	81.8	57.1	58.2	58.0	73.2	48.4	50.7	45.6	72.9	32.4	42.5	19.1
2.917	3.7	80.8	52.3	53.5	54.7	71.0	44.9	46.0	37.1	71.2	23.1	33.9	10.5
3.000	3.8	79.7	49.6	47.4	49.8	69.8	38.7	41.0	31.4	69.8	14.8	24.8	5.4
3.083	3.9	77.2	45.6	40.6	39.8	66.5	31.2	34.7	23.6	68.2	9.9	16.9	2.7
3.167	4	77.3	41.2	38.2	28.0	63.6	24.7	29.1	16.7	65.9	7.1	8.9	1.3
3.250	4.1	73.5	38.0	29.2	24.6	61.5	18.6	21.0	5.8	62.1	3.6	6.3	0.7
3.333	4.2	72.6	34.4	22.1	16.9	57.0	10.7	13.1	3.2	60.4	2.0	2.8	0.7
3.417	4.3	70.0	30.9	11.4	8.1	58.4	5.7	8.9	1.7	58.3	1.2	1.5	0.6
3.500	4.4	67.2	28.4	8.8	3.9	52.7	2.6	4.2	1.2	55.9	1.0	1.0	0.6
3.583	4.5	64.5	24.5	4.5	2.1	50.9	1.9	2.5	1.2	53.8	0.9	0.8	0.6
3.667	4.6	61.8	20.4	2.6	1.7	47.7	1.4	1.6	1.2	50.9	0.8	0.7	0.7
3.750	4.7	59.1	17.2	1.9	1.6	44.1	1.3	1.2	1.1	48.8	0.8	0.7	0.7
3.833	4.8	54.5	14.5	1.8	1.6	42.6	1.3	1.2	1.1	46.7	0.8	0.8	0.7
3.917	4.9	50.6	12.2	1.8	1.6	40.2	1.3	1.1	1.1	43.8	0.9	0.7	0.8
4.000	5	47.7	9.9	1.7	1.6	37.7	1.3	1.2	1.1	40.0	0.8	0.7	0.7
4.083	5.1	43.9	6.7	1.8	1.7	35.2	1.3	1.2	1.2	39.1	0.9	0.8	0.7
4.167	5.2	39.4	4.5	1.7	1.7	33.8	1.3	1.2	1.2	38.1	0.8	0.8	0.7
4.250	5.3	36.6	3.4	1.8	1.6	32.7	1.4	1.3	1.3	37.9	0.8	0.8	0.8
4.333	5.4	33.2	2.2	1.8	1.7	31.4	1.4	1.2	1.2	37.4	0.8	0.8	0.7
4.417	5.5	31.3	2.0	1.7	1.7	30.7	1.3	1.3	1.2	37.5	0.8	0.7	0.7
4.500	5.6	29.2	1.8	1.8	1.8	29.8	1.4	1.2	1.2	38.5	0.9	0.7	0.8
4.583	5.7	27.3	1.8	1.8	1.7	29.2	1.2	1.3	1.2	39.0	0.8	0.7	0.7
4.667	5.8	25.6	1.8	1.7	1.7	29.6	1.3	1.3	1.3	40.3	0.8	0.8	0.8
4.750	5.9	24.1	2.1	1.9	1.7	29.6	1.2	1.3	1.3	41.8	0.8	0.7	0.8
4.833	6	23.6	2.4	1.8	1.8	30.1	1.1	1.3	1.3	45.0	0.7	0.8	0.7
4.917	6.1	23.3	3.5	1.8	1.7	31.4	1.2	1.2	1.3	43.6	0.7	0.8	0.8
5.000	6.2	23.5	5.6	1.8	1.8	32.6	1.2	1.2	1.2	46.7	0.8	0.8	0.8
5.083	6.3	23.7	8.7	1.8	1.8	33.4	1.2	1.2	1.2	49.5	0.9	0.8	0.7
5.167	6.4	24.6	12.5	1.8	1.8	35.3	1.1	1.2	1.1	51.3	1.1	0.7	0.7
5.250	6.5	26.0	19.2	1.8	1.8	37.3	1.3	1.2	1.2	54.4	1.6	0.7	0.7
5.333	6.6	27.3	31.8	1.8	1.7	39.9	1.8	1.2	1.1	56.7	2.9	0.8	0.8
5.417	6.7	29.8	41.0	1.8	1.8	43.1	3.7	1.1	1.1	62.0	4.6	0.7	0.7
5.500	6.8	32.4	45.3	1.7	1.7	44.9	7.0	1.2	1.1	59.5	7.4	0.7	0.7
5.583	6.9	35.8	51.2	2.1	1.7	47.9	11.1	1.1	1.1	63.9	10.5	0.7	0.7
5.667	7	38.5	56.3	2.9	1.7	50.5	16.2	1.1	1.1	66.7	13.5	0.7	0.7

Appendix

5.750	7.1	41.9	63.1	4.4	1.6	53.2	23.0	1.3	1.1	68.1	18.4	0.7	0.7
5.833	7.2	45.5	67.7	7.7	1.6	55.0	31.3	1.8	1.1	69.8	22.5	1.0	0.7
5.917	7.3	50.5	70.6	20.2	1.8	57.3	39.6	3.3	1.1	72.0	30.2	1.4	0.7
6.000	7.4	55.7	74.9	31.3	2.1	59.1	47.0	7.4	1.1	73.6	38.3	2.4	0.7
6.083	7.5	60.1	78.3	40.0	3.8	60.9	50.9	12.7	1.5	75.7	41.3	5.6	0.7
6.167	7.6	62.0	81.1	46.3	8.1	62.7	55.3	19.0	2.9	77.1	47.0	11.2	0.9
6.250	7.7	65.3	81.1	50.8	14.2	64.7	62.1	26.9	6.2	79.1	52.5	16.7	1.4
6.333	7.8	67.8	83.8	55.6	24.2	66.5	66.7	35.5	10.9	79.1	58.8	23.7	4.1
6.417	7.9	69.9	85.9	61.5	35.0	69.0	70.4	40.6	19.6	79.8	62.5	29.5	9.9
6.500	8	72.5	88.0	67.8	45.4	71.5	72.6	47.3	29.4	82.0	65.3	36.8	16.5
6.583	8.1	73.6	89.7	69.7	51.3	73.0	76.1	52.7	37.6	82.4	69.0	43.0	24.4
6.667	8.2	75.2	89.5	73.6	58.1	75.2	78.7	57.7	45.3	84.2	73.1	48.8	33.8
6.750	8.3	77.7	90.8	76.2	62.6	75.8	81.1	61.8	51.2	85.9	76.0	54.2	43.6
6.833	8.4	78.9	92.0	79.4	66.7	77.7	82.1	67.0	55.6	88.0	78.6	58.3	47.2
6.917	8.5	80.7	91.8	80.6	70.6	78.7	83.7	70.6	60.1	87.6	81.1	59.3	51.3
7.000	8.6	80.9	91.8	81.6	74.0	79.1	84.8	72.2	63.3	88.1	83.9	64.3	55.0
7.083	8.7	82.4	91.2	83.4	75.3	80.6	86.0	75.5	66.8	88.6	85.6	69.6	59.2
7.167	8.8	83.2	92.4	83.9	78.2	81.9	87.6	77.0	68.8	89.3	87.7	71.0	64.9
7.250	8.9	84.4	93.0	85.9	80.2	82.6	88.8	78.2	72.1	89.4	89.6	74.4	68.0
7.333	9	85.3	94.0	88.1	81.6	83.5	88.8	79.8	73.8	90.7	91.1	75.7	72.6
7.417	9.1	85.6	93.0	88.2	83.5	84.2	90.0	81.8	76.3	89.9	90.8	78.9	74.0
7.500	9.2	86.3	94.8	88.0	84.0	84.6	90.2	82.4	78.3	90.5	92.1	81.2	77.9
7.583	9.3	86.1	94.9	89.2	85.2	85.0	92.2	84.2	79.4	91.5	92.8	83.7	79.2
7.667	9.4	86.6	94.9	89.3	85.7	85.8	91.8	84.8	81.5	91.2	92.7	83.4	80.5
7.750	9.5	88.6	94.8	89.2	85.0	86.4	92.7	86.3	81.7	92.1	93.4	85.0	81.3
7.833	9.6	87.5	94.9	88.8	86.6	86.9	93.2	87.5	83.2	91.1	94.4	86.4	82.0
7.917	9.7	88.1	94.9	89.6	86.8	86.4	94.0	87.7	83.8	92.7	94.3	87.4	83.9
8.000	9.8	87.9	94.9	92.4	85.9	87.6	93.2	87.2	86.0	92.5	95.1	88.9	84.3
8.083	9.9	86.8	95.2	94.8	87.1	88.2	93.4	88.1	84.8	92.2	95.0	88.6	85.4
8.167	10	88.0	94.6	94.9	91.2	88.6	93.5	89.4	86.2	93.7	95.7	89.1	86.4
8.250	10.1	88.4	98.9	94.9	94.9	89.3	93.8	89.3	86.3	92.7	94.2	89.2	86.5
8.333	10.2	87.7	95.5	94.9	94.9	89.6	93.9	89.3	86.2	94.2	94.8	89.6	87.1
8.417	10.3	90.5		95.2	95.2	90.2	93.1	89.5	85.7	93.0	94.9	89.9	88.4
8.500	10.4	88.8		94.6	94.6	91.0	93.5	89.5	86.7	94.2	94.6	90.6	88.3
8.583	10.5	89.2		98.9	98.9	90.1	93.5	89.1	86.6	97.6	95.3	90.2	87.8
8.667	10.6	88.5		95.5	95.5	92.9	94.1	89.4	87.1	94.9	95.6	90.5	87.8
8.750	10.7					91.9	94.6	90.4	86.2	95.5	95.2	90.6	87.5
8.833	10.8					91.0	95.7	90.2	87.2	95.3	94.6	90.4	87.5
8.917	10.9					91.9		90.8	87.4	96.4	95.1	89.8	87.6
9.000	11					92.1		89.5	87.6	96.1	95.2	90.6	87.6
9.083	11.1					90.3		90.4	87.9	95.7	95.4	91.2	88.6
9.167	11.2							89.8		93.5	95.8	91.4	88.3
9.250	11.3										98.1	91.0	87.9
9.333	11.4											91.9	87.8
9.417	11.5											92.2	89.5

Port	Z [cm]	Oxygen concentration [μM]											
		HETox1				HETox2				HETox3			
		Day 1	Day 4	Day 6	Day 9	Day 1	Day 4	Day 6	Day 9	Day 1	Day 4	Day 6	Day 9
0.583	0.9	277	269		257								
0.667	1	267	267	267	248								
0.75	1.1	260	265	261	249					272	272	262	252
0.833	1.2	259	260	252	244					264	263	246	239
0.917	1.3	257	262	252	244					257	253	235	237
1	1.4	260	257	249	243	280	255	258	251	252	251	231	229
1.083	1.5	254	255	248	239	256	250	249	244	250	248	224	225
1.167	1.6	253	256	245	236	253	247	246	237	250	244	220	218
1.25	1.7	253	252	244	232	250	245	243	237	250	240	214	210
1.333	1.8	249	249	243	230	247	243	240	232	249	235	209	206
1.417	1.9	248	249	238	229	247	244	240	231	244	231	202	195
1.5	2	248	242	235	226	248	239	241	231	239	229	190	186
1.583	2.1	248	242	232	219	244	236	235	228	231	223	176	174
1.667	2.2	245	236	229	213	246	234	234	224	231	219	165	167
1.75	2.3	242	229	223	204	243	235	229	223	226	216	156	160
1.833	2.4	238	222	209	193	243	232	227	217	216	208	149	145
1.917	2.5	236	210	196	171	243	228	224	217	212	198	127	124
2	2.6	230	198	178	148	241	229	223	213	206	193	115	112
2.083	2.7	220	182	153	123	242	222	219	208	201	180	109	100
2.167	2.8	212	164	127	89	240	220	212	203	195	174	101	88
2.25	2.9	204	149	100	49	240	219	210	197	190	165	92	73
2.333	3	195	133	80	29	238	214	204	193	186	158	83	56
2.417	3.1	184	121	57	14	236	210	196	182	184	150	74	38
2.5	3.2	179	108	43	7.6	237	202	191	173	181	145	70	31
2.583	3.3	170	96	36	4.9	236	194	183	169	178	138	66	18
2.667	3.4	164	87	28	4.3	232	190	177	157	177	130	62	8.4
2.75	3.5	159	83	25	4.3	234	184	172	150	176	125	58	5.4
2.833	3.6	148	80	21	4.5	232	180	162	138	175	120	58	3.5
2.917	3.7	145	78	19	4.3	229	173	153	126	174	115	55	3.1
3	3.8	141	78	19	4.4	227	164	143	108	174	111	52	2.9
3.083	3.9	138	78	19	4.5	225	155	135	94	172	109	51	2.6
3.167	4	137	77	20	4.4	221	148	125	82	173	105	51	2.3
3.25	4.1	136	78	20	4.4	218	145	111	72	174	103	51	2.3
3.333	4.2	133	78	21	4.3	217	140	102	61	175	103	51	2.4
3.417	4.3	134	78	22	4.5	210	131	93	42	174	101	51	2.3
3.5	4.4	134	79	23	4.5	208	119	85	31	172	102	51	2.3
3.583	4.5	135	80	24	4.4	200	113	79	20	173	101	52	2.6
3.667	4.6	136	81	25	4.6	196	111	73	12	173	101	53	2.2
3.75	4.7	135	83	27	4.6	192	108	66	7.5	174	101	53	2.3
3.833	4.8	137	85	28	4.6	184	104	57	5	173	101	54	2.2
3.917	4.9	137	86	31	4.6	174	100	54	3.6	174	102	55	2.3
4	5	137	89	33	4.4	170	99	49	3.1	172	102	55	2.3
4.083	5.1	137	90	35	4.4	164	98	46	3.1	171	103	56	2.3

4.167	5.2	138	91	37	4.5	161	96	44	3.1	171	103	57	2.1
4.25	5.3	138	94	41	4.5	157	98	43	3	171	103	58	2.3
4.333	5.4	139	96	44	4.4	155	98	43	3.1	170	105	59	2.1
4.417	5.5	140	98	46	4.4	154	99	44	3	170	106	59	2
4.5	5.6	140	101	50	4.4	154	101	48	3.2	170	104	60	2
4.583	5.7	143	104	53	4.7	154	104	53	3.7	170	105	61	2.1
4.667	5.8	143	106	58	4.2	154	111	62	6.1	169	108	61	2.1
4.75	5.9	144	112	62	4.4	156	117	70	8.8	170	106	63	2
4.833	6	146	114	63	4.1	158	125	79	13	171	109	64	2.1
4.917	6.1	149	116	67	4.4	163	130	86	18	170	108	65	1.9
5	6.2	149	120	70	4.4	166	139	91	27	173	109	67	1.9
5.083	6.3	153	122	73	5.3	175	143	101	34	174	110	68	2.1
5.167	6.4	154	124	76	6.3	181	147	107	41	173	111	68	1.9
5.25	6.5	154	124	77	6.6	185	150	114	49	175	113	70	2
5.333	6.6	156	127	81	8.4	191	153	118	54	175	114	71	3
5.417	6.7	159	129	81	10	192	157	127	64	177	114	71	1.9
5.5	6.8	160	130	84	12	195	165	136	74	178	115	73	2
5.583	6.9	162	133	86	15	195	174	143	88	179	118	75	2.1
5.667	7	163	135	90	18	194	175	154	105	180	122	77	2.6
5.75	7.1	164	138	91	20	196	189	171	119	181	122	78	2.7
5.833	7.2	165	139	93	23	196	197	182	138	181	124	78	3.1
5.917	7.3	167	141	96	26	200	211	195	155	182	122	78	3.2
6	7.4	169	143	99	29	202	221	208	173	182	121	78	2.9
6.083	7.5	170	146	100	30	204	225	214	183	184	121	78	2.5
6.167	7.6	175	147	104	34	214	229	217	195	185	122	80	2.2
6.25	7.7	180	150	109	42	221	237	226	206	188	123	81	2.1
6.333	7.8	182	155	116	49	227	240	234	213	190	124	82	1.9
6.417	7.9	187	159	123	59	233	241	235	218	191	126	84	2.1
6.5	8	193	162	128	69	240	244	237	223	190	128	84	2.3
6.583	8.1	200	166	136	81	240	245	237	225	191	129	85	2.7
6.667	8.2	207	172	144	93	244	245	239	223	191	128	87	3.1
6.75	8.3	212	177	154	101	244	246	241	229	191	128	87	3.7
6.833	8.4	224	189	163	115	247	251	241	229	193	130	88	4.3
6.917	8.5	227	196	175	128	249	249	240	231	193	130	89	6.1
7	8.6	232	201	187	145	248	247	245	234	193	132	91	7.1
7.083	8.7	237	211	194	158	249	249	241	232	195	131	91	9.6
7.167	8.8	239	218	206	175	250	250	242	233	194	131	92	11
7.25	8.9	246	225	209	187	252	249	241	235	195	132	93	12
7.333	9	248	229	219	194	251	251	245	237	196	134	94	13
7.417	9.1	249	233	224	205	251	254	244	235	197	135	97	15
7.5	9.2	251	240	230	213	252	253	245	235	197	137	99	16
7.583	9.3	253	244	233	218	253	253	246	237	196	137	100	18
7.667	9.4	252	245	237	225	252	253	247	237	199	139	104	19
7.75	9.5	252	246	240	226	253	254	244	240	200	141	108	20
7.833	9.6	253	250	242	229	254	259	251	240	204	143	112	22
7.917	9.7	252	251	244	232	251	260	255	241	207	145	117	24
8	9.8	252	253	246	235	253	256	252	244	210	151	123	27
8.083	9.9	256	255	247	237	253	252	251	242	214	154	132	30

8.167	10	255	254	249	240	255	256	249	239	220	163	147	34
8.25	10.1	256	262	250	238	251	250	248	237	231	171	159	40
8.333	10.2	255	259	252	240	250	252	246	237	233	176	174	50
8.417	10.3	254	259	252	251	249	252	246	241	241	188	189	60
8.5	10.4	252	264	264	264	253	254	246	238	249	197	208	72
8.583	10.5	253				251	251	248	239	250	209	211	87
8.667	10.6	252				251	255	248	237	252	212	214	100
8.75	10.7					250	254	249	239	255	218	222	121
8.833	10.8					252	255	248	240	253	224	226	135
8.917	10.9					251	252	250	242	257	227	234	146
9	11					253	254	247	240	262	230	238	162
9.083	11.1					254	255	248	241	263	237	242	174
9.167	11.2					255	257	245	240	262	240	242	191
9.25	11.3					251		251	243	254	243	254	202
9.333	11.4										248	248	209
9.417	11.5										260	260	220

Port	Z [cm]	Oxygen saturation [%]											
		HETox1				HETox2				HETox3			
		Day 1	Day 4	Day 6	Day 9	Day 1	Day 4	Day 6	Day 9	Day 1	Day 4	Day 6	Day 9
0.917	1.3	102.6	99.6		95.1								
1.000	1.4	99.0	99.0	98.7	92.0								
1.083	1.5	96.4	98.1	96.8	92.4					100.9	100.6	97.0	93.3
1.167	1.6	96.0	96.3	93.3	90.4					97.7	97.4	91.0	88.5
1.250	1.7	95.3	97.2	93.4	90.3					95.4	93.6	86.9	87.6
1.333	1.8	96.3	95.3	92.3	89.9	103.5	94.3	95.5	93.0	93.2	92.8	85.6	84.8
1.417	1.9	94.2	94.4	91.7	88.7	95.0	92.6	92.3	90.4	92.7	91.7	83.0	83.2
1.500	2	93.8	94.9	90.8	87.5	93.6	91.5	91.3	87.8	92.6	90.5	81.3	80.8
1.583	2.1	93.8	93.3	90.5	86.1	92.5	90.8	89.9	87.9	92.7	88.9	79.4	77.7
1.667	2.2	92.4	92.4	90.0	85.2	91.5	89.9	88.9	86.1	92.2	87.2	77.4	76.3
1.750	2.3	91.7	92.2	88.2	84.9	91.3	90.3	88.9	85.6	90.5	85.4	74.8	72.3
1.833	2.4	91.8	89.6	87.2	83.7	91.8	88.7	89.3	85.4	88.4	84.9	70.4	68.8
1.917	2.5	91.8	89.6	86.0	81.2	90.4	87.6	86.9	84.5	85.6	82.6	65.1	64.5
2.000	2.6	90.9	87.5	84.7	78.8	91.2	86.8	86.6	82.9	85.5	81.1	61.2	61.7
2.083	2.7	89.6	84.9	82.4	75.7	90.2	87.0	84.8	82.5	83.8	80.0	57.7	59.4
2.167	2.8	88.0	82.3	77.4	71.4	89.9	86.0	84.2	80.5	80.0	76.9	55.0	53.8
2.250	2.9	87.3	77.9	72.5	63.3	89.8	84.5	83.0	80.2	78.5	73.4	47.2	46.1
2.333	3	85.0	73.3	65.9	54.8	89.2	84.9	82.6	78.8	76.2	71.4	42.5	41.6
2.417	3.1	81.5	67.5	56.7	45.7	89.5	82.4	81.1	77.1	74.5	66.8	40.2	37.1
2.500	3.2	78.6	60.6	47.0	32.8	88.9	81.7	78.4	75.1	72.3	64.6	37.3	32.8
2.583	3.3	75.6	55.1	36.9	18.3	88.8	81.0	77.7	73.1	70.3	61.2	34.2	27.0
2.667	3.4	72.2	49.4	29.7	10.8	88.2	79.3	75.4	71.6	69.0	58.5	30.8	20.6
2.750	3.5	68.1	44.9	21.2	5.1	87.5	77.7	72.7	67.5	68.0	55.6	27.4	14.2
2.833	3.6	66.3	40.1	16.0	2.8	87.9	75.0	70.8	64.0	67.0	53.7	25.9	11.5
2.917	3.7	63.0	35.5	13.4	1.8	87.3	71.9	67.9	62.6	66.0	51.2	24.4	6.5

3.000	3.8	60.8	32.3	10.4	1.6	86.1	70.5	65.4	58.3	65.5	48.3	23.1	3.1
3.083	3.9	58.9	30.7	9.2	1.6	86.6	68.1	63.6	55.4	65.0	46.3	21.5	2.0
3.167	4	55.0	29.7	7.6	1.7	85.8	66.5	60.0	51.3	64.7	44.4	21.4	1.3
3.250	4.1	53.6	29.1	7.1	1.6	84.8	64.1	56.7	46.6	64.5	42.7	20.2	1.2
3.333	4.2	52.3	28.9	6.9	1.6	83.9	60.6	53.0	40.2	64.4	40.9	19.3	1.1
3.417	4.3	51.2	28.8	7.0	1.7	83.4	57.4	49.9	34.9	63.8	40.4	19.0	1.0
3.500	4.4	50.8	28.5	7.2	1.6	81.8	54.8	46.3	30.3	64.1	38.8	18.9	0.8
3.583	4.5	50.5	28.8	7.5	1.6	80.7	53.6	41.2	26.5	64.5	38.2	18.9	0.9
3.667	4.6	49.4	28.7	7.8	1.6	80.4	51.9	37.8	22.7	64.7	38.0	19.0	0.9
3.750	4.7	49.8	29.0	8.1	1.7	77.9	48.4	34.4	15.7	64.3	37.5	18.9	0.9
3.833	4.8	49.7	29.1	8.5	1.7	76.9	44.0	31.6	11.4	63.9	37.7	19.0	0.8
3.917	4.9	50.0	29.7	8.9	1.6	74.0	42.0	29.3	7.4	64.2	37.5	19.2	0.9
4.000	5	50.4	29.9	9.3	1.7	72.6	41.0	26.9	4.3	64.1	37.6	19.5	0.8
4.083	5.1	50.2	30.7	9.9	1.7	71.2	39.9	24.6	2.8	64.6	37.4	19.7	0.9
4.167	5.2	50.7	31.4	10.5	1.7	68.2	38.6	21.0	1.9	63.9	37.4	19.9	0.8
4.250	5.3	50.8	31.9	11.4	1.7	64.6	37.0	19.9	1.3	64.3	37.7	20.2	0.9
4.333	5.4	50.6	32.9	12.1	1.6	63.1	36.7	18.1	1.1	63.9	37.9	20.5	0.9
4.417	5.5	50.8	33.3	12.9	1.6	60.6	36.2	17.1	1.1	63.3	38.3	20.6	0.8
4.500	5.6	51.3	33.8	13.6	1.7	59.6	35.7	16.1	1.1	63.5	38.2	21.0	0.8
4.583	5.7	51.2	34.7	15.3	1.7	58.1	36.3	15.9	1.1	63.4	38.0	21.3	0.8
4.667	5.8	51.4	35.4	16.1	1.6	57.4	36.4	16.0	1.1	63.1	38.8	21.7	0.8
4.750	5.9	51.7	36.4	17.1	1.6	57.1	36.7	16.4	1.1	63.1	39.1	21.8	0.8
4.833	6	51.7	37.2	18.4	1.6	57.2	37.5	17.6	1.2	62.8	38.5	22.1	0.7
4.917	6.1	52.9	38.5	19.8	1.7	56.9	38.5	19.7	1.4	63.0	38.8	22.6	0.8
5.000	6.2	53.0	39.3	21.6	1.6	57.2	41.3	22.8	2.3	62.7	40.0	22.7	0.8
5.083	6.3	53.4	41.5	22.9	1.6	57.8	43.4	26.1	3.3	62.9	39.3	23.4	0.8
5.167	6.4	54.2	42.3	23.4	1.5	58.7	46.3	29.1	4.8	63.2	40.2	23.7	0.8
5.250	6.5	55.0	42.9	25.0	1.6	60.3	48.2	31.9	6.6	63.0	40.0	24.1	0.7
5.333	6.6	55.1	44.3	25.8	1.6	61.5	51.3	33.5	10.1	64.1	40.2	24.7	0.7
5.417	6.7	56.8	45.2	27.0	2.0	64.8	52.8	37.3	12.8	64.6	40.8	25.0	0.8
5.500	6.8	56.9	45.9	28.0	2.3	67.1	54.3	39.8	15.2	64.0	41.0	25.4	0.7
5.583	6.9	57.2	46.1	28.7	2.4	68.6	55.7	42.1	18.0	65.0	41.9	25.8	0.8
5.667	7	57.9	46.9	29.9	3.1	70.8	56.6	43.6	20.1	64.8	42.1	26.2	1.1
5.750	7.1	58.8	47.8	30.1	3.8	71.0	58.2	46.9	23.6	65.4	42.3	26.4	0.7
5.833	7.2	59.4	48.3	31.2	4.6	72.1	61.1	50.5	27.4	65.9	42.4	26.9	0.7
5.917	7.3	60.0	49.3	31.9	5.5	72.2	64.5	53.1	32.4	66.5	43.7	27.9	0.8
6.000	7.4	60.5	50.1	33.2	6.6	71.9	64.7	57.0	39.0	66.8	45.2	28.7	0.9
6.083	7.5	60.7	51.0	33.6	7.5	72.4	70.0	63.4	44.1	67.0	45.1	29.0	1.0
6.167	7.6	61.0	51.4	34.4	8.5	72.7	73.0	67.5	51.3	66.9	45.8	29.0	1.1
6.250	7.7	61.7	52.1	35.7	9.5	74.0	78.2	72.2	57.5	67.3	45.1	28.9	1.2
6.333	7.8	62.6	53.1	36.6	10.6	74.9	81.9	76.9	64.2	67.4	44.9	28.8	1.1
6.417	7.9	62.9	54.1	37.1	11.2	75.7	83.4	79.1	67.8	68.1	44.7	29.0	0.9
6.500	8	64.9	54.5	38.6	12.7	79.3	85.0	80.4	72.2	68.7	45.2	29.5	0.8
6.583	8.1	66.6	55.7	40.3	15.7	81.9	88.0	83.8	76.2	69.5	45.5	29.9	0.8
6.667	8.2	67.3	57.4	43.1	18.3	84.1	88.7	86.6	78.9	70.3	46.1	30.3	0.7
6.750	8.3	69.4	58.9	45.5	21.7	86.4	89.2	86.9	80.7	70.9	46.5	31.0	0.8

6.833	8.4	71.6	60.1	47.5	25.4	88.8	90.2	87.8	82.6	70.3	47.3	31.2	0.8
6.917	8.5	74.0	61.5	50.5	29.9	89.0	90.6	88.0	83.2	70.8	47.6	31.6	1.0
7.000	8.6	76.8	63.9	53.5	34.3	90.5	90.6	88.6	82.7	70.8	47.5	32.2	1.1
7.083	8.7	78.5	65.6	56.9	37.5	90.5	91.0	89.3	84.6	70.6	47.6	32.3	1.4
7.167	8.8	82.8	69.9	60.2	42.6	91.5	93.0	89.4	84.8	71.3	48.2	32.6	1.6
7.250	8.9	84.0	72.4	64.8	47.5	92.3	92.1	88.8	85.7	71.5	48.3	33.0	2.3
7.333	9	85.8	74.6	69.3	53.8	91.9	91.4	90.7	86.8	71.3	49.0	33.6	2.6
7.417	9.1	87.7	78.1	72.0	58.6	92.2	92.2	89.3	86.0	72.3	48.4	33.5	3.5
7.500	9.2	88.4	80.7	76.2	64.9	92.5	92.6	89.5	86.2	72.0	48.6	34.1	3.9
7.583	9.3	91.2	83.5	77.6	69.2	93.3	92.3	89.2	86.9	72.4	49.0	34.6	4.6
7.667	9.4	91.7	85.0	81.3	71.8	93.1	93.1	90.9	87.6	72.7	49.6	35.0	4.9
7.750	9.5	92.2	86.4	82.9	75.8	93.1	94.0	90.4	87.1	73.0	49.9	35.8	5.4
7.833	9.6	92.9	88.8	85.0	78.7	93.4	93.8	90.7	86.9	73.1	50.8	36.7	6.1
7.917	9.7	93.7	90.5	86.4	80.8	93.8	93.7	91.1	87.6	72.8	50.8	37.2	6.6
8.000	9.8	93.3	90.8	88.0	83.3	93.5	93.8	91.4	87.8	73.8	51.5	38.5	7.0
8.083	9.9	93.5	91.1	88.9	83.8	93.8	94.0	90.3	88.7	74.1	52.2	39.8	7.5
8.167	10	93.8	92.5	89.6	84.9	94.0	96.0	92.8	89.1	75.5	52.9	41.5	8.2
8.250	10.1	93.4	93.1	90.4	85.9	93.1	96.1	94.6	89.3	76.7	53.7	43.5	8.9
8.333	10.2	93.5	93.7	91.1	86.9	93.6	94.9	93.4	90.4	77.7	55.8	45.7	10.2
8.417	10.3	95.0	94.4	91.3	87.8	93.9	93.3	93.1	89.5	79.4	56.9	49.0	11.2
8.500	10.4	94.3	93.9	92.1	89.0	94.4	94.7	92.2	88.6	81.4	60.2	54.4	12.6
8.583	10.5	94.8	96.9	92.5	88.0	93.1	92.5	92.0	87.9	85.7	63.3	58.8	14.8
8.667	10.6	94.6	96.0	93.5	88.9	92.6	93.4	91.0	88.0	86.3	65.3	64.3	18.5
8.750	10.7	94.0	95.9	93.5	93.1	92.2	93.2	91.1	89.4	89.2	69.8	70.1	22.3
8.833	10.8	93.4	97.7	97.7	97.7	93.6	94.3	91.3	88.0	92.1	73.0	76.9	26.8
8.917	10.9	93.8				92.9	93.1	91.8	88.5	92.7	77.2	78.0	32.3
9.000	11	93.3				92.8	94.3	91.7	87.8	93.2	78.5	79.2	37.1
9.083	11.1					92.6	94.2	92.1	88.4	94.3	80.9	82.3	44.8
9.167	11.2					93.2	94.5	91.8	88.7	93.8	82.9	83.8	50.0
9.250	11.3					93.0	93.5	92.7	89.7	95.1	84.3	86.5	54.2
9.333	11.4					93.9	94.1	91.4	88.8	97.0	85.1	88.0	60.1
9.417	11.5					94.0	94.6	91.8	89.2	97.6	87.6	89.6	64.6
9.500	11.6					94.5	95.3	90.7	88.9	97.1	89.0	89.5	70.6
9.583	11.7					93.1		93.0	89.9	94.1	90.1	94.0	74.7
9.667	11.8										91.9	91.9	77.3
9.750	11.9										96.2	96.2	81.6

Degradation of the infiltrated hydrocarbon concentration calculated by subtracting the measured total outlet concentration from the inlet concentration.

These data were used for Fig. 3.3

Day	Toluene in [μM]	Ethylbenzene in [μM]	HOM		HET	
			Toluene degraded [μM]	Ethylbenzene degraded [μM]	Toluene degraded [μM]	Ethylbenzene degraded [μM]
1	50		0.0		0.0	
2	50		3.6		50.0	
3	50		44.8		50.0	
4	50				50.0	
5	75		66.7		75.0	
6	75		70.2		75.0	
7	110		94.5		110.0	
8	110		102.5		109.8	
9	110		99.5		109.6	
10	110		101.3		110.0	
11	110		86.9		108.6	
12	110		79.3		110.0	
13	110		77.6		109.3	
14	110		79.2		110.0	
15	110		91.9		110.0	
16	150		91.6		140.6	
17	150		123.8		142.0	
18	150		92.8		139.2	
19	150		87.4		137.3	
20	150		69.2		133.2	
21	150		67.2		123.4	
22	150		84.6		130.9	

Appendix

23	175		90.4		128.1	
24	175		93.1		175.0	
25	175				162.2	
26	175		120.0		161.7	
27	175		128.2		163.0	
28	210		107.6		166.7	
29	210		101.1		134.0	
30	210		96.5		186.0	
31	210					
32	210		64.9			
33	210				186.1	
34	210					
35	210				181.5	
36	210		94.5		166.2	
37	210		131.5		174.9	
38		200		125.4		
39		200		96.7		149.0
40		200		106.2		148.5
41		200		65.1		162.6
42		200		46.5		121.2
43		200				
44		200		55.3		125.1
45		200				
46		200		49.8		117.0
47		200		99.4		140.0
48		200		73.3		144.8
49		200		81.5		159.9
50		200		80.5		161.7
51		200		101.5		173.6
52		200		147.8		194.6

Appendix

53		200		164.9		199.8
54		200		177.8		200.0
55		200		171.6		200.0
56		200				200.0
57		385				
58		385		302.3		375.4
59		385		382.9		385.0
60		385		350.0		385.0
61		385		377.4		385.0
62		385		384.1		385.0
63		415		415.0		415.0
64		415		374.2		415.0
65		415		387.5		415.0
66		415		371.3		
67		415				415.0
68		415		396.0		415.0
69		415		395.7		415.0
70		415		249.4		207.9
71		415		133.0		135.7
72		415		115.9		124.5
73		415		90.8		155.8
74		415		73.5		76.2

Biomass profiles as determined by flow cytometry from extracted sediment cores of the homogeneous and heterogeneous tank after the experiment.

These data were used for Fig. 3.4

HOM Cells [$\text{g}_{\text{Sediment}}^{-1}(\text{wwt})$]											
14.5 cm			38 cm			56 cm			73 cm		
Depth [cm]	Average	SD	Depth [cm]	Average	SD	Depth [cm]	Average	SD	Depth [cm]	Average	SD
0.525	2.93E+07	4.66E+06	0.48	6.46E+06	3.78E+06	0.46	2.97E+07	6.24E+06	0.48	6.04E+07	3.22E+06
1.58	3.04E+07	1.48E+06	1.44	4.19E+06	1.87E+07	1.38	5.41E+08	4.25E+07	1.44	4.47E+08	3.37E+07
2.635	9.66E+07	1.45E+07	2.4	5.47E+07	2.84E+06	2.3	1.48E+08	3.56E+06	2.4	8.05E+08	4.32E+07
3.69	1.75E+08	1.70E+07	3.36	4.01E+08	1.89E+07	3.22	6.76E+08	6.78E+07	3.36	1.49E+09	1.83E+08
4.745	1.23E+09	6.56E+07	4.32	1.37E+09	2.94E+07	4.14	2.21E+09	1.40E+08	4.32	1.36E+09	1.22E+07
5.8	1.48E+09	6.69E+07	5.28	1.72E+09	5.27E+07	5.06	1.99E+09	1.02E+08	5.28	3.36E+09	1.59E+08
6.855	5.98E+08	6.00E+07	6.24	9.16E+08	5.64E+07	5.98	2.66E+09	2.08E+08	6.24	2.04E+10	7.43E+08
7.91	9.74E+08	8.90E+07	7.2	3.29E+09	1.62E+08	6.9	3.93E+09	2.02E+08	7.2	1.98E+09	8.14E+07
8.965	6.42E+08	4.51E+07	8.16	2.25E+09	1.15E+08	7.82	2.27E+09	1.72E+08	8.16	1.89E+08	1.40E+07
10.02	8.98E+07	6.82E+06	9.12	6.14E+08	3.65E+07	8.74	8.56E+08	1.61E+07	9.12	8.51E+07	5.84E+06
			10.08	1.49E+08	1.62E+07	9.66	7.47E+08	3.86E+07	10.08	9.49E+07	1.65E+07
			11.04	5.64E+07	1.31E+07	10.58	9.76E+07	1.62E+07	11.04	1.55E+07	7.50E+06

Appendix

HET Cells [$\text{g}_{\text{Sediment}}^{-1}(\text{wwt})$]											
17 cm			38 cm			56 cm			73 cm		
Depth [cm]	Average	SD	Depth [cm]	Average	SD	Depth [cm]	Average	SD	Depth [cm]	Average	SD
0.48	1.45E+08	7.59E+07	0.46	8.94E+07	1.16E+07	0.425	6.90E+07	1.95E+07	0.375	2.64E+08	2.09E+08
1.44	5.69E+07	1.43E+07	1.38	2.29E+09	7.82E+07	1.275	1.73E+08	4.79E+07	1.125	3.11E+08	3.90E+07
2.4	5.97E+07	9.55E+06	2.3	1.82E+09	2.12E+08	2.125	1.92E+08	2.32E+07	1.875	7.97E+08	3.31E+07
3.36	1.86E+08	1.22E+07	3.22	7.58E+08	3.65E+07	2.975	1.56E+08	3.66E+07	2.625	1.14E+09	2.10E+08
4.32	5.40E+08	2.28E+07	4.14	4.07E+09	2.16E+08	3.825	3.13E+08	9.28E+07	3.375	2.00E+09	1.29E+08
5.28	4.56E+08	3.36E+07	5.06	5.17E+09	3.78E+08	4.675	1.71E+09	1.46E+08	4.125	3.67E+09	1.38E+08
6.24	9.76E+08	5.74E+07	5.98	4.68E+09	1.70E+08	5.525	3.64E+09	6.96E+08	4.875	3.99E+09	3.00E+08
7.2	3.94E+08	4.10E+07	6.9	4.81E+09	2.14E+08	6.375	5.94E+09	8.49E+08	5.625	2.74E+09	6.25E+08
8.16	6.31E+08	2.32E+07	7.82	4.23E+09	1.60E+08	7.225	5.72E+08	6.40E+07	6.375	1.28E+09	1.64E+08
9.12	1.10E+08	5.72E+06	8.74	2.77E+09	1.41E+08	8.075	2.72E+08	1.37E+07	7.125	1.84E+09	2.31E+08
10.08	6.57E+07	3.91E+06	9.66	5.06E+08	1.95E+07	8.925	6.32E+07	4.72E+06	7.875	1.78E+09	1.46E+08
11.04	4.15E+07	1.17E+06	10.58	1.09E+08	8.09E+06	9.775	2.09E+07	4.88E+06	8.625	1.77E+09	1.54E+08
			11.5	1.51E+07	0.00E+00	10.625	3.57E+07	3.95E+06	9.375	7.61E+08	8.63E+07
						11.475	9.69E+06	4.65E+06	10.125	2.91E+08	1.91E+07
									10.875	7.60E+07	1.59E+07

Ratio of the isotomeric species ethylbenzene and ethylbenzene- d_{10} , measured at the outlet of the homogeneous and heterogeneous tanks before and after (day 46) the introduction of the fractionating *A. aromaticum* EbN1.

These data were used for Fig. 3.5

Port	Ethylbenzene/Ethylbenzene- d_{10} [-]													
	HOM							HET						
	Day 40	Day 44	Day 46	Day 47	Day 51	Day 53	Day 58	Day 40	Day 44	Day 46	Day 47	Day 51	Day 53	Day 58
2														
3		3.2	3.5	1.7	1.2			3.1	3.2	3.2	0.7	0.6	0.0	0.0
4	3.0	3.2	3.1	1.5	1.7	1.0	0.5	3.1	3.2	3.2	2.2	1.1	0.0	0.0
5	3.0	3.1	3.1	2.5	2.5	1.4	1.2	3.1	3.2	3.2	2.6	1.3	0.0	0.0
6	3.1	3.1	3.2	1.6	0.9	0.0	0.6	3.1	3.2	3.2	2.6	1.2	0.0	0.0
7				1.1				3.2	3.3	3.3	2.6	1.3	0.4	0.0
8									3.4	3.3	2.2	1.0	0.0	0.0
9														
10														
11														

The inlet ratio of the isotopomers was 3.1 ± 0.1 .

Measured and simulated distribution of the electron donor (ethylbenzene) at the outlet of the homogeneous and heterogeneous tanks during aerobic degradation by *P. putida* F1 in phase VII. The concentration in [μM] equals the multiplication of the inlet concentration of ethylbenzene during phase VII (200 μM ; see Tab. 3.1) with the respective C/C_0 value given in the table below.

These data were used for Fig. 3.6a

Z [m]	Ethylbenzene C/C_0 [-]									
	HOM					HET				
	Measured Data	Simulated Data				Measured Data	Simulated Data			
		Double Monod		Instantaneous			Double Monod		Instantaneous	
Port-resolved		Profile	Port-resolved	Profile	Port-resolved		Profile	Port-resolved	Profile	
0.130125			0.00040		0.00000					
0.129375			0.00040		0.00000					
0.128625			0.00040		0.00000					
0.127875			0.00040		0.00000			0.00040		0.00000
0.127125			0.00040		0.00000			0.00040		0.00000
0.126375			0.00040		0.00000			0.00040		0.00000
0.125625			0.00040		0.00000			0.00040		0.00000
0.124875			0.00040		0.00000			0.00040		0.00000
0.124125			0.00040		0.00000			0.00040		0.00000
0.123375			0.00040		0.00000			0.00040		0.00000
0.122625			0.00040		0.00000			0.00040		0.00000
0.121875			0.00040		0.00000			0.00040		0.00000
0.121125			0.00040		0.00000			0.00040		0.00000
0.120375			0.00040		0.00000			0.00040		0.00000
0.119625			0.00040		0.00000			0.00040		0.00000
0.118875			0.00040		0.00000			0.00040		0.00000
0.118125			0.00040		0.00000			0.00040		0.00000
0.117375			0.00040		0.00000			0.00040		0.00000

Appendix

0.116625			0.00040		0.00000			0.00040		0.00000
0.115875			0.00040		0.00000			0.00040		0.00000
0.115125			0.00040		0.00000			0.00040		0.00000
0.114375			0.00040		0.00000			0.00040		0.00000
0.113625			0.00040		0.00000			0.00040		0.00000
0.112875	0.00001	0.00040	0.00040	0.00000	0.00000	0.02649	0.00040	0.00040	0.00000	0.00000
0.112125			0.00040		0.00000			0.00050		0.00000
0.111375			0.00040		0.00000			0.00050		0.00000
0.110625			0.00040		0.00000			0.00050		0.00000
0.109875			0.00040		0.00000			0.00050		0.00000
0.109125			0.00040		0.00000			0.00050		0.00000
0.108375			0.00040		0.00000			0.00050		0.00000
0.107625			0.00040		0.00000			0.00050		0.00000
0.106875			0.00040		0.00000			0.00050		0.00000
0.106125			0.00050		0.00000			0.00050		0.00000
0.105375			0.00050		0.00000			0.00050		0.00000
0.104625			0.00050		0.00000			0.00050		0.00000
0.103875			0.00050		0.00000			0.00050		0.00000
0.103125			0.00050		0.00000			0.00060		0.00000
0.102375			0.00050		0.00000			0.00100		0.00000
0.101625			0.00050		0.00000			0.00500		0.00480
0.100875	0.00195	0.00050	0.00050	0.00000	0.00000	0.02175	0.00050	0.00970	0.00000	0.00960
0.100125			0.00050		0.00000			0.01410		0.01410
0.099375			0.00050		0.00000			0.01800		0.01800
0.098625			0.00140		0.00000			0.02150		0.02150
0.097875			0.01250		0.00070			0.02440		0.02440
0.097125			0.02370		0.01240			0.02710		0.02710
0.096375			0.03290		0.02370			0.02950		0.02950
0.095625			0.04490		0.03290			0.03150		0.03150

Appendix

0.094875			0.05690		0.04480			0.03320		0.03310
0.094125			0.06760		0.05680			0.03440		0.03430
0.093375			0.07830		0.06750			0.03550		0.03550
0.092625			0.09050		0.07830			0.03630		0.03620
0.091875			0.10260		0.09050			0.03700		0.03690
0.091125			0.11420		0.10260			0.03750		0.03750
0.090375			0.12380		0.11420			0.03760		0.03750
0.089625			0.13870		0.12380			0.03770		0.03770
0.088875	0.18775	0.12040	0.14900	0.12040	0.13870	0.03156	0.03560	0.03780	0.03560	0.03770
0.088125			0.15910		0.14900			0.03780		0.03770
0.087375			0.17010		0.15910			0.03770		0.03770
0.086625			0.17930		0.17010			0.03760		0.03760
0.085875			0.19080		0.17920			0.03720		0.03720
0.085125			0.20280		0.19080			0.03690		0.03690
0.084375			0.20630		0.20280			0.03680		0.03670
0.083625			0.21320		0.20630			0.03650		0.03640
0.082875			0.22110		0.21320			0.03600		0.03600
0.082125			0.22510		0.22110			0.03580		0.03580
0.081375			0.23000		0.22510			0.03530		0.03520
0.080625			0.23390		0.23000			0.03510		0.03510
0.079875			0.23740		0.23390			0.03440		0.03440
0.079125			0.23930		0.23740			0.03420		0.03420
0.078375			0.23980		0.23930			0.03370		0.03370
0.077625			0.23980		0.23980			0.03320		0.03310
0.076875	0.34822	0.22680	0.23840	0.22680	0.23980	0.02825	0.03330	0.03290	0.03330	0.03280
0.076125			0.23660		0.23840			0.03230		0.03230
0.075375			0.23340		0.23650			0.03170		0.03170
0.074625			0.22890		0.23340			0.03120		0.03120
0.073875			0.22360		0.22890			0.03060		0.03060

Appendix

0.073125			0.21790		0.22360			0.03010		0.03000
0.072375			0.21170		0.21790			0.02950		0.02950
0.071625			0.20430		0.21170			0.02920		0.02920
0.070875			0.19510		0.20430			0.02850		0.02850
0.070125			0.18800		0.19510			0.02800		0.02800
0.069375			0.17730		0.18800			0.02740		0.02740
0.068625			0.16650		0.17720			0.02680		0.02670
0.067875			0.15570		0.16650			0.02620		0.02620
0.067125			0.14370		0.15570			0.02540		0.02540
0.066375			0.13160		0.14370			0.02470		0.02470
0.065625			0.11970		0.13150			0.02430		0.02430
0.064875	0.11967	0.12080	0.11000	0.12080	0.11970	0.02483	0.02450	0.02370	0.02440	0.02360
0.064125			0.09550		0.11000			0.02320		0.02320
0.063375			0.08600		0.09550			0.02250		0.02250
0.062625			0.07320		0.08600			0.02180		0.02180
0.061875			0.05890		0.07310			0.02130		0.02130
0.061125			0.04750		0.05890			0.02080		0.02070
0.060375			0.03510		0.04750			0.02000		0.02000
0.059625			0.02380		0.03510			0.01940		0.01940
0.058875			0.01420		0.02370			0.01910		0.01900
0.058125			0.00510		0.01410			0.01860		0.01860
0.057375			0.00050		0.00490			0.01800		0.01800
0.056625			0.00050		0.00000			0.01730		0.01720
0.055875			0.00050		0.00000			0.01670		0.01660
0.055125			0.00050		0.00000			0.01630		0.01620
0.054375			0.00050		0.00000			0.01580		0.01570
0.053625			0.00050		0.00000			0.01520		0.01510
0.052875	0.00100	0.00050	0.00050	0.00000	0.00000	0.01219	0.01520	0.01470	0.01520	0.01460
0.052125			0.00050		0.00000			0.01410		0.01400

Appendix

0.051375			0.00050		0.00000			0.01370		0.01360
0.050625			0.00050		0.00000			0.01320		0.01320
0.049875			0.00040		0.00000			0.01240		0.01240
0.049125			0.00040		0.00000			0.01200		0.01190
0.048375			0.00040		0.00000			0.01130		0.01120
0.047625			0.00040		0.00000			0.01090		0.01080
0.046875			0.00040		0.00000			0.01030		0.01020
0.046125			0.00040		0.00000			0.00950		0.00940
0.045375			0.00040		0.00000			0.00890		0.00880
0.044625			0.00040		0.00000			0.00820		0.00810
0.043875			0.00040		0.00000			0.00740		0.00720
0.043125			0.00040		0.00000			0.00670		0.00650
0.042375			0.00040		0.00000			0.00570		0.00550
0.041625			0.00040		0.00000			0.00470		0.00460
0.040875	0.00013	0.00040	0.00040	0.00000	0.00000	0.00257	0.00270	0.00360	0.00240	0.00340
0.040125			0.00040		0.00000			0.00230		0.00190
0.039375			0.00040		0.00000			0.00120		0.00020
0.038625			0.00040		0.00000			0.00080		0.00000
0.037875			0.00040		0.00000			0.00060		0.00000
0.037125			0.00040		0.00000			0.00060		0.00000
0.036375			0.00040		0.00000			0.00050		0.00000
0.035625			0.00040		0.00000			0.00050		0.00000
0.034875			0.00040		0.00000			0.00050		0.00000
0.034125			0.00040		0.00000			0.00050		0.00000
0.033375			0.00040		0.00000			0.00050		0.00000
0.032625			0.00040		0.00000			0.00050		0.00000
0.031875			0.00040		0.00000			0.00050		0.00000
0.031125			0.00040		0.00000			0.00050		0.00000
0.030375			0.00040		0.00000			0.00050		0.00000

Appendix

0.029625			0.00040		0.00000			0.00050		0.00000
0.028875	0.00000	0.00040	0.00040	0.00000	0.00000	0.00000	0.00050	0.00050	0.00000	0.00000
0.028125			0.00040		0.00000			0.00050		0.00000
0.027375			0.00040		0.00000			0.00050		0.00000
0.026625			0.00040		0.00000			0.00050		0.00000
0.025875			0.00040		0.00000			0.00050		0.00000
0.025125			0.00040		0.00000			0.00050		0.00000
0.024375			0.00030		0.00000			0.00040		0.00000
0.023625			0.00030		0.00000			0.00040		0.00000
0.022875			0.00020		0.00000			0.00040		0.00000
0.022125			0.00020		0.00000			0.00040		0.00000
0.021375			0.00010		0.00000			0.00040		0.00000
0.020625			0.00010		0.00000			0.00040		0.00000
0.019875			0.00010		0.00000			0.00040		0.00000
0.019125			0.00010		0.00000			0.00040		0.00000
0.018375			0.00010		0.00000			0.00040		0.00000
0.017625			0.00010		0.00000			0.00040		0.00000
0.016875	0.00000	0.00010	0.00000	0.00000	0.00000	0.00000	0.00040	0.00040	0.00000	0.00000
0.016125			0.00000		0.00000			0.00040		0.00000
0.015375			0.00000		0.00000			0.00040		0.00000
0.014625			0.00000		0.00000			0.00040		0.00000
0.013875			0.00000		0.00000			0.00040		0.00000
0.013125			0.00000		0.00000			0.00040		0.00000
0.012375			0.00000		0.00000			0.00040		0.00000
0.011625			0.00000		0.00000			0.00040		0.00000
0.010875			0.00000		0.00000			0.00040		0.00000
0.010125			0.00000		0.00000			0.00040		0.00000
0.009375			0.00000		0.00000			0.00040		0.00000
0.008625			0.00000		0.00000			0.00040		0.00000

Appendix

0.007875			0.00000		0.00000			0.00040		0.00000
0.007125			0.00000		0.00000			0.00040		0.00000
0.006375			0.00000		0.00000			0.00040		0.00000
0.005625			0.00000		0.00000			0.00040		0.00000
0.004875	0.00000	0.00000	0.00000	0.00000	0.00000	0.00000	0.00040	0.00040	0.00000	0.00000
0.004125			0.00000		0.00000			0.00040		0.00000
0.003375			0.00000		0.00000			0.00040		0.00000
0.002625			0.00000		0.00000			0.00030		0.00000
0.001875			0.00000		0.00000			0.00020		0.00000
0.001125			0.00000		0.00000			0.00020		0.00000
0.000375			0.00000		0.00000			0.00020		0.00000

Measured and simulated distribution of the electron acceptor (oxygen), and simulated distribution of the electron donor (ethylbenzene) at 40.5 cm distant to the inlet of the homogeneous and heterogeneous tanks during aerobic degradation by *P. putida* F1 in phase VII. The concentrations in [μM] equal the multiplication of the inlet concentrations of oxygen (270 μM ; see Tab. 3.1) and ethylbenzene (200 μM ; see Tab. 3.1) during phase VII with the respective C/C_0 value given in the tables below.

These data were used for Fig. 3.6b

Z [m]	HOM				
	Measured Data	Oxygen		Ethylbenzene	
		Simulated Data			
		Double Monod	Instantaneous	Double Monod	Instantaneous
0.13275		0.99970	0.99800	0.00030	0.00000
0.13205		0.99970	0.99800	0.00030	0.00000
0.13125		0.99970	0.99780	0.00030	0.00000
0.13055		0.99970	0.99740	0.00030	0.00000
0.12975		0.99960	0.99700	0.00040	0.00000
0.12905		0.99930	0.99630	0.00040	0.00000
0.12825		0.99840	0.99540	0.00040	0.00000
0.12755		0.99730	0.99430	0.00040	0.00000
0.12675	0.89702	0.99590	0.99280	0.00040	0.00000
0.12605	0.85155	0.99400	0.99100	0.00040	0.00000
0.12525	0.84344	0.99170	0.98870	0.00040	0.00000
0.12455	0.83226	0.98910	0.98610	0.00040	0.00000
0.12375	0.82831	0.98550	0.98250	0.00040	0.00000
0.12305	0.81970	0.98150	0.97850	0.00040	0.00000
0.12225	0.80205	0.97660	0.97360	0.00040	0.00000
0.12155	0.79528	0.97040	0.96740	0.00040	0.00000
0.12075	0.78561	0.96330	0.96030	0.00040	0.00000
0.12005	0.76314	0.95500	0.95190	0.00040	0.00000
0.11925	0.75254	0.94490	0.94190	0.00040	0.00000
0.11855	0.72986	0.93340	0.93040	0.00040	0.00000
0.11775	0.69706	0.91980	0.91680	0.00040	0.00000
0.11705	0.65168	0.90420	0.90120	0.00040	0.00000
0.11625	0.61195	0.88560	0.88250	0.00040	0.00000
0.11555	0.55898	0.86380	0.86080	0.00040	0.00000
0.11475	0.50182	0.83740	0.83430	0.00040	0.00000
0.11405	0.40885	0.80860	0.80550	0.00040	0.00000
0.11325	0.28296	0.77590	0.77290	0.00040	0.00000
0.11255	0.19501	0.73860	0.73550	0.00040	0.00000
0.11175	0.11729	0.69580	0.69280	0.00040	0.00000
0.11105	0.08335	0.65150	0.64840	0.00040	0.00000
0.11025	0.03679	0.59780	0.59470	0.00040	0.00000
0.10955	0.02083	0.54210	0.53900	0.00050	0.00000

Appendix

0.10875	0.01756	0.47650	0.47340	0.00050	0.00000
0.10805	0.01622	0.40260	0.39950	0.00050	0.00000
0.10725	0.01727	0.32530	0.32220	0.00050	0.00000
0.10655	0.01737	0.24090	0.23770	0.00050	0.00000
0.10575	0.01679	0.14950	0.14620	0.00050	0.00000
0.10505	0.01756	0.05030	0.04660	0.00050	0.00000
0.10425	0.01737	0.00070	0.00000	0.00820	0.00810
0.10355	0.01746	0.00030	0.00000	0.02530	0.02520
0.10275	0.01756	0.00020	0.00000	0.04280	0.04280
0.10205	0.01775	0.00020	0.00000	0.06120	0.06110
0.10125	0.01794	0.00010	0.00000	0.08000	0.08000
0.10055	0.01842	0.00010	0.00000	0.09810	0.09810
0.09975	0.01804	0.00010	0.00000	0.12030	0.12020
0.09905	0.01861	0.00010	0.00000	0.14060	0.14060
0.09825	0.01832	0.00010	0.00000	0.16210	0.16200
0.09755	0.01813	0.00010	0.00000	0.18220	0.18210
0.09675	0.01784	0.00010	0.00000	0.20240	0.20240
0.09605	0.01813	0.00010	0.00000	0.22320	0.22320
0.09525	0.01919	0.00010	0.00000	0.24260	0.24260
0.09455	0.01842	0.00010	0.00000	0.26250	0.26250
0.09375	0.01842	0.00010	0.00000	0.27820	0.27820
0.09305	0.01938	0.00010	0.00000	0.29700	0.29700
0.09225	0.01804	0.00010	0.00000	0.31500	0.31490
0.09155	0.01890	0.00010	0.00000	0.32850	0.32850
0.09075	0.01813	0.00010	0.00000	0.34210	0.34210
0.09005	0.01890	0.00010	0.00000	0.35370	0.35360
0.08925	0.01794	0.00010	0.00000	0.36270	0.36270
0.08855	0.01775	0.00010	0.00000	0.37040	0.37040
0.08775	0.01737	0.00010	0.00000	0.37530	0.37530
0.08705	0.01679	0.00010	0.00000	0.37880	0.37870
0.08625	0.01727	0.00010	0.00000	0.37970	0.37970
0.08555	0.01670	0.00010	0.00000	0.37810	0.37810
0.08475	0.01613	0.00010	0.00000	0.37400	0.37400
0.08405	0.01756	0.00010	0.00000	0.36830	0.36830
0.08325	0.02093	0.00010	0.00000	0.36010	0.36010
0.08255	0.03257	0.00010	0.00000	0.35070	0.35070
0.08175	0.06275	0.00010	0.00000	0.33900	0.33890
0.08105	0.11615	0.00010	0.00000	0.32570	0.32570
0.08025	0.20857	0.00010	0.00000	0.31060	0.31060
0.07955	0.34619	0.00010	0.00000	0.29360	0.29360
0.07875	0.40850	0.00010	0.00000	0.27480	0.27480
0.07805	0.47841	0.00010	0.00000	0.25750	0.25750
0.07725	0.53675	0.00010	0.00000	0.23740	0.23740
0.07655	0.61131	0.00010	0.00000	0.21800	0.21800
0.07575	0.65987	0.00010	0.00000	0.19660	0.19660
0.07505	0.68742	0.00010	0.00000	0.17640	0.17640

0.07425	0.71374	0.00010	0.00000	0.15600	0.15600
0.07355	0.74058	0.00010	0.00000	0.13550	0.13550
0.07275	0.75799	0.00010	0.00000	0.11500	0.11500
0.07205	0.77881	0.00010	0.00000	0.09450	0.09450
0.07125	0.79059	0.00020	0.00000	0.07530	0.07530
0.07055	0.81947	0.00020	0.00000	0.05670	0.05670
0.06975	0.81560	0.00020	0.00000	0.03920	0.03920
0.06905	0.82886	0.00030	0.00000	0.02140	0.02130
0.06825	0.82415	0.00100	0.00000	0.00610	0.00600
0.06755	0.83679	0.06950	0.06600	0.00050	0.00000
0.06675	0.82808	0.16850	0.16530	0.00050	0.00000
0.06605	0.83839	0.25800	0.25480	0.00050	0.00000
0.06525	0.86836	0.33960	0.33650	0.00050	0.00000
0.06455		0.41350	0.41040	0.00050	0.00000
0.06375		0.48420	0.48120	0.00050	0.00000
0.06305		0.54880	0.54570	0.00050	0.00000
0.06225		0.60560	0.60250	0.00040	0.00000
0.06155		0.65690	0.65390	0.00040	0.00000
0.06075		0.70280	0.69980	0.00040	0.00000
0.06005		0.74320	0.74020	0.00040	0.00000
0.05925		0.78160	0.77860	0.00040	0.00000
0.05855		0.81240	0.80940	0.00040	0.00000
0.05775		0.84050	0.83740	0.00040	0.00000
0.05705		0.86690	0.86390	0.00040	0.00000
0.05625		0.88870	0.88570	0.00040	0.00000
0.05555		0.90580	0.90280	0.00040	0.00000
0.05475		0.92210	0.91910	0.00040	0.00000
0.05405		0.93470	0.93160	0.00040	0.00000
0.05325		0.94640	0.94340	0.00040	0.00000
0.05255		0.95640	0.95340	0.00040	0.00000
0.05175		0.96490	0.96190	0.00040	0.00000
0.05105		0.97190	0.96890	0.00040	0.00000
0.05025		0.97780	0.97480	0.00040	0.00000
0.04955		0.98260	0.97950	0.00040	0.00000
0.04875		0.98650	0.98340	0.00040	0.00000
0.04805		0.98960	0.98660	0.00040	0.00000
0.04725		0.99230	0.98930	0.00040	0.00000
0.04655		0.99450	0.99140	0.00040	0.00000
0.04575		0.99630	0.99320	0.00040	0.00000
0.04505		0.99770	0.99470	0.00040	0.00000
0.04425		0.99880	0.99580	0.00040	0.00000
0.04355		0.99960	0.99670	0.00040	0.00000
0.04275		0.99970	0.99740	0.00030	0.00000
0.04205		0.99970	0.99800	0.00030	0.00000
0.04125		0.99980	0.99850	0.00020	0.00000
0.04055		0.99980	0.99880	0.00020	0.00000

Appendix

0.03975		0.99990	0.99910	0.00010	0.00000
0.03905		0.99990	0.99930	0.00010	0.00000
0.03825		0.99990	0.99950	0.00010	0.00000
0.03755		0.99990	0.99960	0.00010	0.00000
0.03675		1.00000	0.99970	0.00000	0.00000
0.03605		1.00000	0.99980	0.00000	0.00000
0.03525		1.00000	0.99980	0.00000	0.00000
0.03455		1.00000	0.99990	0.00000	0.00000
0.03375		1.00000	0.99990	0.00000	0.00000
0.03305		1.00000	0.99990	0.00000	0.00000
0.03225		1.00000	0.99990	0.00000	0.00000
0.03155		1.00000	1.00000	0.00000	0.00000
0.03075		1.00000	1.00000	0.00000	0.00000
0.03005		1.00000	1.00000	0.00000	0.00000
0.02925		1.00000	1.00000	0.00000	0.00000
0.02855		1.00000	1.00000	0.00000	0.00000
0.02775		1.00000	1.00000	0.00000	0.00000
0.02705		1.00000	1.00000	0.00000	0.00000
0.02625		1.00000	1.00000	0.00000	0.00000
0.02555		1.00000	1.00000	0.00000	0.00000
0.02475		1.00000	1.00000	0.00000	0.00000
0.02405		1.00000	1.00000	0.00000	0.00000
0.02325		1.00000	1.00000	0.00000	0.00000
0.02255		1.00000	1.00000	0.00000	0.00000
0.02175		1.00000	1.00000	0.00000	0.00000
0.02105		1.00000	1.00000	0.00000	0.00000
0.02025		1.00000	1.00000	0.00000	0.00000
0.01955		1.00000	1.00000	0.00000	0.00000
0.01875		1.00000	1.00000	0.00000	0.00000
0.01805		1.00000	1.00000	0.00000	0.00000
0.01725		1.00000	1.00000	0.00000	0.00000
0.01655		1.00000	1.00000	0.00000	0.00000
0.01575		1.00000	1.00000	0.00000	0.00000
0.01505		1.00000	1.00000	0.00000	0.00000
0.01425		1.00000	1.00000	0.00000	0.00000
0.01355		1.00000	1.00000	0.00000	0.00000
0.01275		1.00000	1.00000	0.00000	0.00000
0.01205		1.00000	1.00000	0.00000	0.00000
0.01125		1.00000	1.00000	0.00000	0.00000
0.01055		1.00000	1.00000	0.00000	0.00000
0.00975		1.00000	1.00000	0.00000	0.00000
0.00905		1.00000	1.00000	0.00000	0.00000
0.00825		1.00000	1.00000	0.00000	0.00000
0.00755		1.00000	1.00000	0.00000	0.00000
0.00675		1.00000	1.00000	0.00000	0.00000
0.00605		1.00000	1.00000	0.00000	0.00000

0.00525		1.00000	1.00000	0.00000	0.00000
0.00455		1.00000	1.00000	0.00000	0.00000
0.00375		1.00000	1.00000	0.00000	0.00000
0.00305		1.00000	1.00000	0.00000	0.00000
0.00225		1.00000	1.00000	0.00000	0.00000
0.00155		1.00000	1.00000	0.00000	0.00000
0.00075		1.00000	1.00000	0.00000	0.00000

Z [m]	HET				
	Measured Data	Oxygen		Ethylbenzene	
		Simulated Data			
		Double Monod	Instantaneous	Double Monod	Instantaneous
0.13275		0.99990	0.99920	0.00010	0.00000
0.13205		0.99990	0.99910	0.00010	0.00000
0.13125		0.99990	0.99890	0.00010	0.00000
0.13055		0.99980	0.99830	0.00020	0.00000
0.12975		0.99970	0.99750	0.00030	0.00000
0.12905	0.93644	0.99920	0.99620	0.00040	0.00000
0.12825	0.91143	0.99740	0.99430	0.00040	0.00000
0.12755	0.88217	0.99460	0.99160	0.00040	0.00000
0.12675	0.86385	0.99070	0.98770	0.00040	0.00000
0.12605	0.85731	0.98520	0.98220	0.00040	0.00000
0.12525	0.83018	0.97770	0.97470	0.00040	0.00000
0.12455	0.79513	0.96760	0.96460	0.00040	0.00000
0.12375	0.75697	0.95440	0.95140	0.00040	0.00000
0.12305	0.72166	0.93730	0.93430	0.00040	0.00000
0.12225	0.66991	0.91510	0.91210	0.00040	0.00000
0.12155	0.61697	0.88790	0.88490	0.00040	0.00000
0.12075	0.51763	0.85370	0.85070	0.00040	0.00000
0.12005	0.33818	0.81320	0.81020	0.00040	0.00000
0.11925	0.21900	0.76480	0.76170	0.00040	0.00000
0.11855	0.12785	0.70900	0.70600	0.00040	0.00000
0.11775	0.05901	0.64450	0.64140	0.00040	0.00000
0.11705	0.02627	0.57360	0.57050	0.00050	0.00000
0.11625	0.01927	0.49590	0.49290	0.00050	0.00000
0.11555	0.01966	0.41190	0.40880	0.00050	0.00000
0.11475	0.02045	0.32330	0.32020	0.00050	0.00000
0.11405	0.01966	0.23280	0.22970	0.00050	0.00000
0.11325	0.01897	0.13870	0.13550	0.00050	0.00000
0.11255	0.01819	0.04580	0.04210	0.00050	0.00000
0.11175	0.01878	0.00080	0.00000	0.00700	0.00690
0.11105	0.01917	0.00040	0.00000	0.01900	0.01900
0.11025	0.01819	0.00020	0.00000	0.03080	0.03070

Appendix

0.10955	0.01819	0.00020	0.00000	0.04150	0.04150
0.10875	0.01917	0.00020	0.00000	0.05100	0.05100
0.10805	0.01887	0.00020	0.00000	0.05950	0.05950
0.10725	0.01868	0.00020	0.00000	0.06630	0.06630
0.10655	0.01819	0.00020	0.00000	0.07160	0.07160
0.10575	0.01819	0.00020	0.00000	0.07590	0.07590
0.10505	0.01799	0.00010	0.00000	0.07970	0.07970
0.10425	0.01868	0.00010	0.00000	0.08290	0.08290
0.10355	0.01887	0.00010	0.00000	0.08500	0.08490
0.10275	0.01868	0.00010	0.00000	0.08560	0.08550
0.10205	0.01897	0.00010	0.00000	0.08580	0.08580
0.10125	0.01956	0.00010	0.00000	0.08570	0.08570
0.10055	0.01956	0.00010	0.00000	0.08590	0.08590
0.09975	0.01887	0.00010	0.00000	0.08570	0.08570
0.09905	0.01878	0.00010	0.00000	0.08530	0.08530
0.09825	0.01809	0.00010	0.00000	0.08420	0.08420
0.09755	0.01897	0.00010	0.00000	0.08340	0.08340
0.09675	0.01927	0.00010	0.00000	0.08290	0.08290
0.09605	0.01878	0.00010	0.00000	0.08180	0.08180
0.09525	0.01848	0.00010	0.00000	0.08050	0.08050
0.09455	0.01848	0.00010	0.00000	0.07980	0.07980
0.09375	0.01946	0.00010	0.00000	0.07880	0.07880
0.09305	0.01878	0.00010	0.00000	0.07750	0.07750
0.09225	0.01868	0.00020	0.00000	0.07650	0.07650
0.09155	0.01789	0.00020	0.00000	0.07580	0.07580
0.09075	0.01858	0.00020	0.00000	0.07430	0.07430
0.09005	0.01828	0.00020	0.00000	0.07330	0.07320
0.08925	0.01809	0.00020	0.00000	0.07170	0.07170
0.08855	0.01809	0.00020	0.00000	0.07060	0.07060
0.08775	0.01779	0.00020	0.00000	0.06950	0.06950
0.08705	0.01858	0.00020	0.00000	0.06840	0.06830
0.08625	0.01672	0.00020	0.00000	0.06710	0.06710
0.08555	0.01760	0.00020	0.00000	0.06560	0.06560
0.08475	0.01848	0.00020	0.00000	0.06430	0.06430
0.08405	0.01828	0.00020	0.00000	0.06250	0.06240
0.08325	0.01868	0.00020	0.00000	0.06070	0.06070
0.08255	0.01858	0.00020	0.00000	0.05880	0.05880
0.08175	0.01976	0.00020	0.00000	0.05680	0.05680
0.08105	0.02006	0.00020	0.00000	0.05460	0.05450
0.08025	0.02026	0.00020	0.00000	0.05250	0.05240
0.07955	0.01858	0.00020	0.00000	0.05040	0.05030
0.07875	0.01927	0.00020	0.00000	0.04800	0.04800
0.07805	0.01779	0.00020	0.00000	0.04610	0.04610
0.07725	0.01682	0.00020	0.00000	0.04360	0.04350
0.07655	0.01760	0.00020	0.00000	0.04120	0.04120
0.07575	0.02194	0.00020	0.00000	0.03890	0.03890

0.07505	0.04525	0.00020	0.00000	0.03650	0.03650
0.07425	0.09189	0.00020	0.00000	0.03430	0.03430
0.07355	0.17384	0.00020	0.00000	0.03200	0.03200
0.07275	0.25224	0.00030	0.00000	0.03000	0.03000
0.07205	0.36363	0.00030	0.00000	0.02760	0.02760
0.07125	0.44731	0.00030	0.00000	0.02540	0.02540
0.07055	0.52260	0.00030	0.00000	0.02300	0.02290
0.06975	0.57083	0.00030	0.00000	0.02120	0.02110
0.06905	0.63481	0.00030	0.00000	0.01940	0.01940
0.06825	0.67965	0.00040	0.00000	0.01740	0.01730
0.06755	0.72696	0.00040	0.00000	0.01540	0.01540
0.06675	0.76470	0.00050	0.00000	0.01330	0.01330
0.06605	0.77756	0.00050	0.00000	0.01170	0.01160
0.06525	0.81014	0.00060	0.00000	0.00990	0.00980
0.06455	0.82550	0.00070	0.00000	0.00850	0.00840
0.06375	0.84202	0.00090	0.00000	0.00660	0.00650
0.06305	0.86303	0.00110	0.00000	0.00520	0.00500
0.06225	0.86715	0.00170	0.00000	0.00350	0.00330
0.06155	0.87378	0.00300	0.00000	0.00210	0.00170
0.06075	0.90010	0.00810	0.00100	0.00110	0.00000
0.06005	0.91231	0.01540	0.01020	0.00080	0.00000
0.05925	0.94057	0.02570	0.02140	0.00060	0.00000
0.05855		0.03490	0.03090	0.00060	0.00000
0.05775		0.04580	0.04200	0.00050	0.00000
0.05705		0.05740	0.05380	0.00050	0.00000
0.05625		0.06870	0.06520	0.00050	0.00000
0.05555		0.07800	0.07460	0.00050	0.00000
0.05475		0.09090	0.08750	0.00050	0.00000
0.05405		0.10100	0.09770	0.00050	0.00000
0.05325		0.11180	0.10850	0.00050	0.00000
0.05255		0.12500	0.12170	0.00050	0.00000
0.05175		0.13680	0.13350	0.00050	0.00000
0.05105		0.14860	0.14540	0.00050	0.00000
0.05025		0.16110	0.15790	0.00050	0.00000
0.04955		0.17500	0.17180	0.00050	0.00000
0.04875		0.19050	0.18740	0.00050	0.00000
0.04805		0.20690	0.20380	0.00050	0.00000
0.04725		0.22520	0.22200	0.00050	0.00000
0.04655		0.24400	0.24080	0.00050	0.00000
0.04575		0.26570	0.26260	0.00050	0.00000
0.04505		0.28830	0.28520	0.00050	0.00000
0.04425		0.31470	0.31160	0.00050	0.00000
0.04355		0.34350	0.34040	0.00050	0.00000
0.04275		0.37380	0.37070	0.00050	0.00000
0.04205		0.40490	0.40180	0.00050	0.00000
0.04125		0.43990	0.43680	0.00050	0.00000

Appendix

0.04055		0.47650	0.47340	0.00050	0.00000
0.03975		0.51380	0.51070	0.00050	0.00000
0.03905		0.55350	0.55040	0.00050	0.00000
0.03825		0.59390	0.59090	0.00040	0.00000
0.03755		0.63280	0.62980	0.00040	0.00000
0.03675		0.67170	0.66860	0.00040	0.00000
0.03605		0.70900	0.70600	0.00040	0.00000
0.03525		0.74640	0.74330	0.00040	0.00000
0.03455		0.78060	0.77750	0.00040	0.00000
0.03375		0.81250	0.80940	0.00040	0.00000
0.03305		0.84120	0.83820	0.00040	0.00000
0.03225		0.86810	0.86510	0.00040	0.00000
0.03155		0.89180	0.88880	0.00040	0.00000
0.03075		0.91200	0.90900	0.00040	0.00000
0.03005		0.92960	0.92660	0.00040	0.00000
0.02925		0.94470	0.94170	0.00040	0.00000
0.02855		0.95720	0.95420	0.00040	0.00000
0.02775		0.96770	0.96470	0.00040	0.00000
0.02705		0.97600	0.97290	0.00040	0.00000
0.02625		0.98270	0.97970	0.00040	0.00000
0.02555		0.98790	0.98490	0.00040	0.00000
0.02475		0.99200	0.98900	0.00040	0.00000
0.02405		0.99500	0.99200	0.00040	0.00000
0.02325		0.99730	0.99430	0.00040	0.00000
0.02255		0.99900	0.99600	0.00040	0.00000
0.02175		0.99960	0.99720	0.00040	0.00000
0.02105		0.99980	0.99810	0.00020	0.00000
0.02025		0.99980	0.99870	0.00020	0.00000
0.01955		0.99990	0.99920	0.00010	0.00000
0.01875		0.99990	0.99950	0.00010	0.00000
0.01805		1.00000	0.99970	0.00000	0.00000
0.01725		1.00000	0.99980	0.00000	0.00000
0.01655		1.00000	0.99990	0.00000	0.00000
0.01575		1.00000	0.99990	0.00000	0.00000
0.01505		1.00000	1.00000	0.00000	0.00000
0.01425		1.00000	1.00000	0.00000	0.00000
0.01355		1.00000	1.00000	0.00000	0.00000
0.01275		1.00000	1.00000	0.00000	0.00000
0.01205		1.00000	1.00000	0.00000	0.00000
0.01125		1.00000	1.00000	0.00000	0.00000
0.01055		1.00000	1.00000	0.00000	0.00000
0.00975		1.00000	1.00000	0.00000	0.00000
0.00905		1.00000	1.00000	0.00000	0.00000
0.00825		1.00000	1.00000	0.00000	0.00000
0.00755		1.00000	1.00000	0.00000	0.00000
0.00675		1.00000	1.00000	0.00000	0.00000

0.00605		1.00000	1.00000	0.00000	0.00000
0.00525		1.00000	1.00000	0.00000	0.00000
0.00455		1.00000	1.00000	0.00000	0.00000
0.00375		1.00000	1.00000	0.00000	0.00000
0.00305		1.00000	1.00000	0.00000	0.00000
0.00225		1.00000	1.00000	0.00000	0.00000
0.00155		1.00000	1.00000	0.00000	0.00000
0.00075		1.00000	1.00000	0.00000	0.00000

Measured and simulated distribution of the electron acceptor (oxygen), and simulated distribution of the electron donor (ethylbenzene) at 57 cm distant to the inlet of the homogeneous and heterogeneous tanks during aerobic degradation by *P. putida* F1 in phase VII. The concentrations in [μM] equal the multiplication of the inlet concentrations of oxygen (270 μM ; see Tab. 3.1) and ethylbenzene (200 μM ; see Tab. 3.1) during phase VII with the respective C/C_0 value given in the tables below.

These data were used for Fig. 3.6c

Z [m]	HOM				
	Measured Data	Oxygen		Ethylbenzene	
		Simulated Data			
		Double Monod	Instantaneous	Double Monod	Instantaneous
0.13205		0.98750	0.98450	0.00040	0.00000
0.13125		0.98750	0.98450	0.00040	0.00000
0.13055	0.92238	0.98690	0.98390	0.00040	0.00000
0.12975	0.90343	0.98580	0.98270	0.00040	0.00000
0.12905	0.89040	0.98410	0.98110	0.00040	0.00000
0.12825	0.86836	0.98180	0.97880	0.00040	0.00000
0.12755	0.85677	0.97880	0.97570	0.00040	0.00000
0.12675	0.83975	0.97490	0.97190	0.00040	0.00000
0.12605	0.83282	0.97040	0.96740	0.00040	0.00000
0.12525	0.81692	0.96500	0.96200	0.00040	0.00000
0.12455	0.81076	0.95850	0.95550	0.00040	0.00000
0.12375	0.78890	0.95160	0.94860	0.00040	0.00000
0.12305	0.76920	0.94230	0.93930	0.00040	0.00000
0.12225	0.75710	0.93280	0.92980	0.00040	0.00000
0.12155	0.73563	0.92140	0.91830	0.00040	0.00000
0.12075	0.71293	0.90810	0.90510	0.00040	0.00000
0.12005	0.67673	0.89260	0.88950	0.00040	0.00000
0.11925	0.64154	0.87550	0.87240	0.00040	0.00000
0.11855	0.60094	0.85680	0.85380	0.00040	0.00000
0.11775	0.56130	0.83420	0.83120	0.00040	0.00000
0.11705	0.51104	0.81320	0.81020	0.00040	0.00000
0.11625	0.45573	0.78520	0.78220	0.00040	0.00000

Appendix

0.11555	0.39499	0.75490	0.75190	0.00040	0.00000
0.11475	0.30384	0.72610	0.72310	0.00040	0.00000
0.11405	0.21597	0.68810	0.68510	0.00040	0.00000
0.11325	0.08671	0.64910	0.64610	0.00040	0.00000
0.11255	0.04929	0.60710	0.60410	0.00040	0.00000
0.11175	0.02704	0.55970	0.55660	0.00050	0.00000
0.11105	0.01813	0.50750	0.50450	0.00050	0.00000
0.11025	0.01291	0.45160	0.44850	0.00050	0.00000
0.10955	0.01216	0.39090	0.38780	0.00050	0.00000
0.10875	0.01207	0.32560	0.32250	0.00050	0.00000
0.10805	0.01226	0.25800	0.25480	0.00050	0.00000
0.10725	0.01282	0.18630	0.18320	0.00050	0.00000
0.10655	0.01282	0.10890	0.10560	0.00050	0.00000
0.10575	0.01198	0.02840	0.02420	0.00060	0.00000
0.10505	0.01235	0.00060	0.00000	0.00930	0.00920
0.10425	0.01292	0.00030	0.00000	0.02240	0.02240
0.10355	0.01301	0.00020	0.00000	0.03620	0.03610
0.10275	0.01367	0.00020	0.00000	0.05020	0.05020
0.10205	0.01338	0.00020	0.00000	0.06500	0.06500
0.10125	0.01282	0.00010	0.00000	0.08000	0.08000
0.10055	0.01329	0.00010	0.00000	0.09490	0.09490
0.09975	0.01433	0.00010	0.00000	0.11020	0.11020
0.09905	0.01423	0.00010	0.00000	0.12530	0.12530
0.09825	0.01461	0.00010	0.00000	0.14070	0.14060
0.09755	0.01423	0.00010	0.00000	0.15590	0.15590
0.09675	0.01367	0.00010	0.00000	0.17120	0.17120
0.09605	0.01386	0.00010	0.00000	0.18680	0.18670
0.09525	0.01395	0.00010	0.00000	0.19970	0.19970
0.09455	0.01254	0.00010	0.00000	0.21510	0.21510
0.09375	0.01320	0.00010	0.00000	0.22740	0.22740
0.09305	0.01301	0.00010	0.00000	0.23940	0.23930
0.09225	0.01348	0.00010	0.00000	0.25020	0.25020
0.09155	0.01226	0.00010	0.00000	0.26190	0.26190
0.09075	0.01245	0.00010	0.00000	0.26960	0.26960
0.09005	0.01263	0.00010	0.00000	0.27850	0.27850
0.08925	0.01235	0.00010	0.00000	0.28650	0.28650
0.08855	0.01142	0.00010	0.00000	0.29290	0.29290
0.08775	0.01245	0.00010	0.00000	0.29670	0.29670
0.08705	0.01170	0.00010	0.00000	0.30000	0.30000
0.08625	0.01217	0.00010	0.00000	0.30200	0.30200
0.08555	0.01207	0.00010	0.00000	0.30240	0.30240
0.08475	0.01086	0.00010	0.00000	0.30110	0.30110
0.08405	0.01198	0.00010	0.00000	0.29870	0.29860
0.08325	0.01794	0.00010	0.00000	0.29490	0.29490
0.08255	0.03783	0.00010	0.00000	0.28960	0.28950
0.08175	0.07459	0.00010	0.00000	0.28280	0.28270

0.08105	0.14954	0.00010	0.00000	0.27530	0.27530
0.08025	0.23013	0.00010	0.00000	0.26740	0.26730
0.07955	0.33528	0.00010	0.00000	0.25640	0.25640
0.07875	0.40885	0.00010	0.00000	0.24630	0.24630
0.07805	0.53863	0.00010	0.00000	0.23520	0.23520
0.07725	0.55449	0.00010	0.00000	0.22100	0.22100
0.07655	0.57544	0.00010	0.00000	0.20780	0.20780
0.07575	0.61569	0.00010	0.00000	0.19420	0.19420
0.07505	0.64629	0.00010	0.00000	0.18010	0.18000
0.07425	0.67256	0.00010	0.00000	0.16560	0.16560
0.07355	0.69755	0.00010	0.00000	0.15050	0.15050
0.07275	0.72835	0.00010	0.00000	0.13490	0.13490
0.07205	0.75587	0.00010	0.00000	0.12000	0.12000
0.07125	0.77808	0.00010	0.00000	0.10420	0.10410
0.07055	0.79582	0.00010	0.00000	0.08900	0.08890
0.06975	0.81021	0.00020	0.00000	0.07420	0.07420
0.06905	0.82103	0.00020	0.00000	0.05970	0.05970
0.06825	0.83282	0.00020	0.00000	0.04600	0.04600
0.06755	0.84159	0.00020	0.00000	0.03200	0.03200
0.06675	0.83919	0.00040	0.00000	0.01890	0.01890
0.06605	0.85867	0.00090	0.00000	0.00650	0.00630
0.06525	0.85620	0.04580	0.04210	0.00050	0.00000
0.06455	0.85538	0.12610	0.12290	0.00050	0.00000
0.06375	0.86280	0.20030	0.19720	0.00050	0.00000
0.06305	0.86695	0.27120	0.26810	0.00050	0.00000
0.06225	0.87113	0.33820	0.33510	0.00050	0.00000
0.06155	0.85374	0.40030	0.39720	0.00050	0.00000
0.06075	0.85867	0.45860	0.45550	0.00050	0.00000
0.06005	0.86114	0.51380	0.51070	0.00050	0.00000
0.05925	0.85702	0.56440	0.56130	0.00050	0.00000
0.05855	0.87029	0.60950	0.60640	0.00040	0.00000
0.05775		0.65300	0.65000	0.00040	0.00000
0.05705		0.69190	0.68890	0.00040	0.00000
0.05625		0.72770	0.72460	0.00040	0.00000
0.05555		0.75960	0.75650	0.00040	0.00000
0.05475		0.78800	0.78500	0.00040	0.00000
0.05405		0.81560	0.81250	0.00040	0.00000
0.05325		0.83890	0.83590	0.00040	0.00000
0.05255		0.85990	0.85690	0.00040	0.00000
0.05175		0.87860	0.87550	0.00040	0.00000
0.05105		0.89570	0.89270	0.00040	0.00000
0.05025		0.91050	0.90740	0.00040	0.00000
0.04955		0.92370	0.92070	0.00040	0.00000
0.04875		0.93550	0.93250	0.00040	0.00000
0.04805		0.94510	0.94210	0.00040	0.00000
0.04725		0.95340	0.95040	0.00040	0.00000

Appendix

0.04655		0.96130	0.95820	0.00040	0.00000
0.04575		0.96760	0.96460	0.00040	0.00000
0.04505		0.97310	0.97010	0.00040	0.00000
0.04425		0.97790	0.97490	0.00040	0.00000
0.04355		0.98190	0.97890	0.00040	0.00000
0.04275		0.98520	0.98220	0.00040	0.00000
0.04205		0.98840	0.98540	0.00040	0.00000
0.04125		0.99090	0.98790	0.00040	0.00000
0.04055		0.99300	0.99000	0.00040	0.00000
0.03975		0.99470	0.99170	0.00040	0.00000
0.03905		0.99620	0.99320	0.00040	0.00000
0.03825		0.99740	0.99440	0.00040	0.00000
0.03755		0.99840	0.99540	0.00040	0.00000
0.03675		0.99930	0.99630	0.00040	0.00000
0.03605		0.99960	0.99700	0.00040	0.00000
0.03525		0.99970	0.99750	0.00030	0.00000
0.03455		0.99970	0.99800	0.00030	0.00000
0.03375		0.99980	0.99840	0.00020	0.00000
0.03305		0.99980	0.99870	0.00020	0.00000
0.03225		0.99990	0.99900	0.00010	0.00000
0.03155		0.99990	0.99920	0.00010	0.00000
0.03075		0.99990	0.99930	0.00010	0.00000
0.03005		0.99990	0.99950	0.00010	0.00000
0.02925		0.99990	0.99960	0.00010	0.00000
0.02855		1.00000	0.99970	0.00000	0.00000
0.02775		1.00000	0.99970	0.00000	0.00000
0.02705		1.00000	0.99980	0.00000	0.00000
0.02625		1.00000	0.99980	0.00000	0.00000
0.02555		1.00000	0.99990	0.00000	0.00000
0.02475		1.00000	0.99990	0.00000	0.00000
0.02405		1.00000	0.99990	0.00000	0.00000
0.02325		1.00000	0.99990	0.00000	0.00000
0.02255		1.00000	1.00000	0.00000	0.00000
0.02175		1.00000	1.00000	0.00000	0.00000
0.02105		1.00000	1.00000	0.00000	0.00000
0.02025		1.00000	1.00000	0.00000	0.00000
0.01955		1.00000	1.00000	0.00000	0.00000
0.01875		1.00000	1.00000	0.00000	0.00000
0.01805		1.00000	1.00000	0.00000	0.00000
0.01725		1.00000	1.00000	0.00000	0.00000
0.01655		1.00000	1.00000	0.00000	0.00000
0.01575		1.00000	1.00000	0.00000	0.00000
0.01505		1.00000	1.00000	0.00000	0.00000
0.01425		1.00000	1.00000	0.00000	0.00000
0.01355		1.00000	1.00000	0.00000	0.00000
0.01275		1.00000	1.00000	0.00000	0.00000

0.01205		1.00000	1.00000	0.00000	0.00000
0.01125		1.00000	1.00000	0.00000	0.00000
0.01055		1.00000	1.00000	0.00000	0.00000
0.00975		1.00000	1.00000	0.00000	0.00000
0.00905		1.00000	1.00000	0.00000	0.00000
0.00825		1.00000	1.00000	0.00000	0.00000
0.00755		1.00000	1.00000	0.00000	0.00000
0.00675		1.00000	1.00000	0.00000	0.00000
0.00605		1.00000	1.00000	0.00000	0.00000
0.00525		1.00000	1.00000	0.00000	0.00000
0.00455		1.00000	1.00000	0.00000	0.00000
0.00375		1.00000	1.00000	0.00000	0.00000
0.00305		1.00000	1.00000	0.00000	0.00000
0.00225		1.00000	1.00000	0.00000	0.00000
0.00155		1.00000	1.00000	0.00000	0.00000
0.00075		1.00000	1.00000	0.00000	0.00000

Z [m]	HET				
	Measured Data	Oxygen		Ethylbenzene	
		Simulated Data			
		Double Monod	Instantaneous	Double Monod	Instantaneous
0.13125		0.98850	0.98550	0.00040	0.00000
0.13055		0.98840	0.98540	0.00040	0.00000
0.12975		0.98800	0.98500	0.00040	0.00000
0.12905		0.98730	0.98430	0.00040	0.00000
0.12825		0.98630	0.98330	0.00040	0.00000
0.12755		0.98510	0.98210	0.00040	0.00000
0.12675	0.94466	0.98370	0.98060	0.00040	0.00000
0.12605	0.91937	0.98190	0.97880	0.00040	0.00000
0.12525	0.88809	0.97970	0.97670	0.00040	0.00000
0.12455	0.89065	0.97720	0.97420	0.00040	0.00000
0.12375	0.88132	0.97430	0.97130	0.00040	0.00000
0.12305	0.86057	0.97110	0.96810	0.00040	0.00000
0.12225	0.85650	0.96730	0.96430	0.00040	0.00000
0.12155	0.84841	0.96340	0.96030	0.00040	0.00000
0.12075	0.83253	0.95880	0.95580	0.00040	0.00000
0.12005	0.81242	0.95400	0.95100	0.00040	0.00000
0.11925	0.79291	0.94860	0.94560	0.00040	0.00000
0.11855	0.77829	0.94260	0.93960	0.00040	0.00000
0.11775	0.75627	0.93580	0.93280	0.00040	0.00000
0.11705	0.74383	0.92870	0.92570	0.00040	0.00000
0.11625	0.70990	0.92140	0.91830	0.00040	0.00000
0.11555	0.68211	0.91280	0.90980	0.00040	0.00000

Appendix

0.11475	0.64858	0.90350	0.90040	0.00040	0.00000
0.11405	0.60827	0.89390	0.89080	0.00040	0.00000
0.11325	0.57485	0.88320	0.88020	0.00040	0.00000
0.11255	0.50389	0.87310	0.87010	0.00040	0.00000
0.11175	0.44695	0.86150	0.85840	0.00040	0.00000
0.11105	0.36238	0.84820	0.84520	0.00040	0.00000
0.11025	0.29542	0.83500	0.83200	0.00040	0.00000
0.10955	0.18176	0.82100	0.81800	0.00040	0.00000
0.10875	0.10625	0.80550	0.80240	0.00040	0.00000
0.10805	0.05666	0.78960	0.78650	0.00040	0.00000
0.10725	0.02485	0.77280	0.76980	0.00040	0.00000
0.10655	0.01604	0.75570	0.75260	0.00040	0.00000
0.10575	0.01420	0.73780	0.73480	0.00040	0.00000
0.10505	0.01449	0.71840	0.71530	0.00040	0.00000
0.10425	0.01391	0.69890	0.69590	0.00040	0.00000
0.10355	0.01333	0.67790	0.67490	0.00040	0.00000
0.10275	0.01449	0.65560	0.65250	0.00040	0.00000
0.10205	0.01400	0.63280	0.62980	0.00040	0.00000
0.10125	0.01400	0.60950	0.60640	0.00040	0.00000
0.10055	0.01381	0.58460	0.58150	0.00040	0.00000
0.09975	0.01400	0.55810	0.55510	0.00050	0.00000
0.09905	0.01410	0.53090	0.52790	0.00050	0.00000
0.09825	0.01497	0.50370	0.50060	0.00050	0.00000
0.09755	0.01429	0.47180	0.46870	0.00050	0.00000
0.09675	0.01372	0.44130	0.43820	0.00050	0.00000
0.09605	0.01372	0.40570	0.40260	0.00050	0.00000
0.09525	0.01430	0.36840	0.36530	0.00050	0.00000
0.09455	0.01430	0.32720	0.32410	0.00050	0.00000
0.09375	0.01458	0.28670	0.28360	0.00050	0.00000
0.09305	0.01429	0.24010	0.23690	0.00050	0.00000
0.09225	0.01372	0.19110	0.18800	0.00050	0.00000
0.09155	0.01449	0.14110	0.13790	0.00050	0.00000
0.09075	0.01420	0.09040	0.08700	0.00050	0.00000
0.09005	0.01391	0.03990	0.03610	0.00060	0.00000
0.08925	0.01372	0.00260	0.00000	0.00240	0.00210
0.08855	0.01410	0.00060	0.00000	0.01020	0.01010
0.08775	0.01401	0.00040	0.00000	0.01720	0.01720
0.08705	0.01458	0.00030	0.00000	0.02420	0.02420
0.08625	0.01497	0.00020	0.00000	0.03060	0.03050
0.08555	0.02737	0.00020	0.00000	0.03580	0.03570
0.08475	0.04610	0.00020	0.00000	0.04060	0.04060
0.08405	0.09641	0.00020	0.00000	0.04430	0.04430
0.08325	0.19906	0.00020	0.00000	0.04480	0.04480
0.08255	0.32159	0.00020	0.00000	0.04450	0.04440
0.08175	0.48885	0.00020	0.00000	0.04440	0.04440
0.08105	0.54255	0.00020	0.00000	0.04430	0.04420

0.08025	0.59760	0.00020	0.00000	0.04080	0.04080
0.07955	0.67659	0.00020	0.00000	0.03630	0.03630
0.07875	0.73974	0.00020	0.00000	0.03390	0.03390
0.07805	0.76329	0.00020	0.00000	0.03110	0.03110
0.07725	0.79143	0.00030	0.00000	0.02590	0.02580
0.07655	0.80636	0.00030	0.00000	0.02110	0.02100
0.07575	0.82317	0.00040	0.00000	0.01470	0.01470
0.07505	0.82163	0.00070	0.00000	0.00830	0.00820
0.07425	0.83963	0.00130	0.00000	0.00450	0.00430
0.07355	0.84043	0.01390	0.00850	0.00080	0.00000
0.07275	0.84761	0.03560	0.03170	0.00060	0.00000
0.07205	0.85487	0.04780	0.04410	0.00050	0.00000
0.07125	0.85568	0.05070	0.04700	0.00050	0.00000
0.07055	0.85976	0.06220	0.05870	0.00050	0.00000
0.06975	0.85812	0.07500	0.07160	0.00050	0.00000
0.06905	0.85812	0.09100	0.08760	0.00050	0.00000
0.06825	0.85164	0.11330	0.11000	0.00050	0.00000
0.06755	0.85406	0.13670	0.13340	0.00050	0.00000
0.06675	0.86880	0.16910	0.16590	0.00050	0.00000
0.06605	0.87212	0.20770	0.20450	0.00050	0.00000
0.06525	0.88048	0.24630	0.24320	0.00050	0.00000
0.06455	0.88385	0.28830	0.28520	0.00050	0.00000
0.06375	0.86880	0.33260	0.32950	0.00050	0.00000
0.06305	0.87796	0.37930	0.37620	0.00050	0.00000
0.06225	0.86632	0.42670	0.42360	0.00050	0.00000
0.06155	0.86632	0.47340	0.47030	0.00050	0.00000
0.06075	0.86632	0.51780	0.51480	0.00050	0.00000
0.06005	0.86797	0.55890	0.55590	0.00050	0.00000
0.05925	0.86632	0.59780	0.59470	0.00040	0.00000
0.05855	0.87629	0.63440	0.63130	0.00040	0.00000
0.05775	0.86715	0.66620	0.66320	0.00040	0.00000
0.05705	0.87880	0.69660	0.69350	0.00040	0.00000
0.05625	0.87629	0.72300	0.72000	0.00040	0.00000
0.05555	0.87964	0.74640	0.74330	0.00040	0.00000
0.05475	0.87378	0.76740	0.76430	0.00040	0.00000
0.05405	0.88724	0.78630	0.78320	0.00040	0.00000
0.05325	0.86550	0.80310	0.80010	0.00040	0.00000
0.05255		0.81870	0.81570	0.00040	0.00000
0.05175		0.83190	0.82890	0.00040	0.00000
0.05105		0.84470	0.84160	0.00040	0.00000
0.05025		0.85600	0.85300	0.00040	0.00000
0.04955		0.86690	0.86390	0.00040	0.00000
0.04875		0.87700	0.87400	0.00040	0.00000
0.04805		0.88640	0.88330	0.00040	0.00000
0.04725		0.89570	0.89270	0.00040	0.00000
0.04655		0.90350	0.90040	0.00040	0.00000

Appendix

0.04575		0.91200	0.90900	0.00040	0.00000
0.04505		0.91900	0.91600	0.00040	0.00000
0.04425		0.92620	0.92320	0.00040	0.00000
0.04355		0.93270	0.92970	0.00040	0.00000
0.04275		0.93890	0.93590	0.00040	0.00000
0.04205		0.94480	0.94170	0.00040	0.00000
0.04125		0.95010	0.94710	0.00040	0.00000
0.04055		0.95500	0.95200	0.00040	0.00000
0.03975		0.95980	0.95680	0.00040	0.00000
0.03905		0.96410	0.96100	0.00040	0.00000
0.03825		0.96800	0.96500	0.00040	0.00000
0.03755		0.97170	0.96870	0.00040	0.00000
0.03675		0.97510	0.97210	0.00040	0.00000
0.03605		0.97810	0.97510	0.00040	0.00000
0.03525		0.98090	0.97780	0.00040	0.00000
0.03455		0.98340	0.98040	0.00040	0.00000
0.03375		0.98570	0.98270	0.00040	0.00000
0.03305		0.98780	0.98480	0.00040	0.00000
0.03225		0.98960	0.98660	0.00040	0.00000
0.03155		0.99140	0.98830	0.00040	0.00000
0.03075		0.99290	0.98990	0.00040	0.00000
0.03005		0.99420	0.99110	0.00040	0.00000
0.02925		0.99540	0.99230	0.00040	0.00000
0.02855		0.99640	0.99340	0.00040	0.00000
0.02775		0.99730	0.99430	0.00040	0.00000
0.02705		0.99810	0.99510	0.00040	0.00000
0.02625		0.99880	0.99580	0.00040	0.00000
0.02555		0.99940	0.99640	0.00040	0.00000
0.02475		0.99960	0.99700	0.00040	0.00000
0.02405		0.99970	0.99740	0.00030	0.00000
0.02325		0.99970	0.99780	0.00030	0.00000
0.02255		0.99980	0.99820	0.00020	0.00000
0.02175		0.99980	0.99850	0.00020	0.00000
0.02105		0.99980	0.99870	0.00020	0.00000
0.02025		0.99990	0.99890	0.00010	0.00000
0.01955		0.99990	0.99910	0.00010	0.00000
0.01875		0.99990	0.99930	0.00010	0.00000
0.01805		0.99990	0.99940	0.00010	0.00000
0.01725		0.99990	0.99950	0.00010	0.00000
0.01655		0.99990	0.99960	0.00010	0.00000
0.01575		1.00000	0.99970	0.00000	0.00000
0.01505		1.00000	0.99970	0.00000	0.00000
0.01425		1.00000	0.99980	0.00000	0.00000
0.01355		1.00000	0.99980	0.00000	0.00000
0.01275		1.00000	0.99990	0.00000	0.00000
0.01205		1.00000	0.99990	0.00000	0.00000

0.01125		1.00000	0.99990	0.00000	0.00000
0.01055		1.00000	0.99990	0.00000	0.00000
0.00975		1.00000	0.99990	0.00000	0.00000
0.00905		1.00000	1.00000	0.00000	0.00000
0.00825		1.00000	1.00000	0.00000	0.00000
0.00755		1.00000	1.00000	0.00000	0.00000
0.00675		1.00000	1.00000	0.00000	0.00000
0.00605		1.00000	1.00000	0.00000	0.00000
0.00525		1.00000	1.00000	0.00000	0.00000
0.00455		1.00000	1.00000	0.00000	0.00000
0.00375		1.00000	1.00000	0.00000	0.00000
0.00305		1.00000	1.00000	0.00000	0.00000
0.00225		1.00000	1.00000	0.00000	0.00000
0.00155		1.00000	1.00000	0.00000	0.00000
0.00075		1.00000	1.00000	0.00000	0.00000

Measured and simulated distribution of the electron acceptor (oxygen), and simulated distribution of the electron donor (ethylbenzene) at 74 cm distant to the inlet of the homogeneous and heterogeneous tanks during aerobic degradation by *P. putida* F1 in phase VII. The concentrations in [μM] equal the multiplication of the inlet concentrations of oxygen (270 μM ; see Tab. 3.1) and ethylbenzene (200 μM ; see Tab. 3.1) during phase VII with the respective C/C_0 value given in the tables below.

These data were used for Fig. 3.6d

Z [m]	HOM				
	Measured Data	Oxygen		Ethylbenzene	
		Simulated Data			
		Double Monod	Instantaneous	Double Monod	Instantaneous
0.13055	0.95458	0.95300	0.95000	0.00040	0.00000
0.12975	0.92059	0.95250	0.94950	0.00040	0.00000
0.12905	0.88809	0.95110	0.94800	0.00040	0.00000
0.12825	0.87618	0.94870	0.94560	0.00040	0.00000
0.12755	0.86197	0.94550	0.94250	0.00040	0.00000
0.12675	0.84562	0.94150	0.93850	0.00040	0.00000
0.12605	0.82886	0.93630	0.93330	0.00040	0.00000
0.12525	0.81406	0.93000	0.92700	0.00040	0.00000
0.12455	0.79134	0.92290	0.91990	0.00040	0.00000
0.12375	0.75377	0.91440	0.91130	0.00040	0.00000
0.12305	0.71177	0.90420	0.90120	0.00040	0.00000
0.12225	0.68305	0.89380	0.89080	0.00040	0.00000
0.12155	0.63305	0.88090	0.87790	0.00040	0.00000
0.12075	0.57595	0.86770	0.86470	0.00040	0.00000
0.12005	0.49060	0.85210	0.84910	0.00040	0.00000

Appendix

0.11925	0.44642	0.83580	0.83280	0.00040	0.00000
0.11855	0.38560	0.81710	0.81410	0.00040	0.00000
0.11775	0.31166	0.79610	0.79310	0.00040	0.00000
0.11705	0.19087	0.77360	0.77050	0.00040	0.00000
0.11625	0.11359	0.74950	0.74640	0.00040	0.00000
0.11555	0.06507	0.72380	0.72080	0.00040	0.00000
0.11475	0.03534	0.69500	0.69200	0.00040	0.00000
0.11405	0.01689	0.66470	0.66160	0.00040	0.00000
0.11325	0.00947	0.62890	0.62590	0.00040	0.00000
0.11255	0.00763	0.59550	0.59240	0.00040	0.00000
0.11175	0.00736	0.55500	0.55200	0.00050	0.00000
0.11105	0.00772	0.51540	0.51230	0.00050	0.00000
0.11025	0.00781	0.47100	0.46800	0.00050	0.00000
0.10955	0.00726	0.42280	0.41970	0.00050	0.00000
0.10875	0.00745	0.37460	0.37150	0.00050	0.00000
0.10805	0.00717	0.32330	0.32020	0.00050	0.00000
0.10725	0.00772	0.27150	0.26840	0.00050	0.00000
0.10655	0.00763	0.21500	0.21180	0.00050	0.00000
0.10575	0.00791	0.15100	0.14780	0.00050	0.00000
0.10505	0.00800	0.08760	0.08420	0.00050	0.00000
0.10425	0.00846	0.02680	0.02250	0.00060	0.00000
0.10355	0.00800	0.00080	0.00000	0.00740	0.00720
0.10275	0.00791	0.00040	0.00000	0.01740	0.01740
0.10205	0.00827	0.00030	0.00000	0.02770	0.02770
0.10125	0.00846	0.00020	0.00000	0.03850	0.03850
0.10055	0.00855	0.00020	0.00000	0.05100	0.05100
0.09975	0.00929	0.00020	0.00000	0.06190	0.06190
0.09905	0.00929	0.00020	0.00000	0.07260	0.07260
0.09825	0.00919	0.00010	0.00000	0.08370	0.08370
0.09755	0.00873	0.00010	0.00000	0.09620	0.09620
0.09675	0.00901	0.00010	0.00000	0.10850	0.10850
0.09605	0.00873	0.00010	0.00000	0.11950	0.11950
0.09525	0.00864	0.00010	0.00000	0.13110	0.13110
0.09455	0.00892	0.00010	0.00000	0.14170	0.14170
0.09375	0.00873	0.00010	0.00000	0.15300	0.15300
0.09305	0.00864	0.00010	0.00000	0.16390	0.16380
0.09225	0.00883	0.00010	0.00000	0.17370	0.17370
0.09155	0.00892	0.00010	0.00000	0.18510	0.18510
0.09075	0.00791	0.00010	0.00000	0.19320	0.19310
0.09005	0.00883	0.00010	0.00000	0.20220	0.20210
0.08925	0.00827	0.00010	0.00000	0.21040	0.21040
0.08855	0.00809	0.00010	0.00000	0.21870	0.21870
0.08775	0.00791	0.00010	0.00000	0.22660	0.22660
0.08705	0.00800	0.00010	0.00000	0.23160	0.23160
0.08625	0.00791	0.00010	0.00000	0.23690	0.23690
0.08555	0.00763	0.00010	0.00000	0.24200	0.24200

0.08475	0.00827	0.00010	0.00000	0.24550	0.24550
0.08405	0.00763	0.00010	0.00000	0.24780	0.24780
0.08325	0.00717	0.00010	0.00000	0.24900	0.24900
0.08255	0.00772	0.00010	0.00000	0.24980	0.24970
0.08175	0.01273	0.00010	0.00000	0.24970	0.24970
0.08105	0.01996	0.00010	0.00000	0.24840	0.24840
0.08025	0.04257	0.00010	0.00000	0.24610	0.24610
0.07955	0.10966	0.00010	0.00000	0.24270	0.24270
0.07875	0.18350	0.00010	0.00000	0.23860	0.23850
0.07805	0.27824	0.00010	0.00000	0.23390	0.23380
0.07725	0.34799	0.00010	0.00000	0.22780	0.22770
0.07655	0.42869	0.00010	0.00000	0.22210	0.22200
0.07575	0.49060	0.00010	0.00000	0.21350	0.21350
0.07505	0.55498	0.00010	0.00000	0.20630	0.20630
0.07425	0.59676	0.00010	0.00000	0.19700	0.19700
0.07355	0.63533	0.00010	0.00000	0.18730	0.18720
0.07275	0.67809	0.00010	0.00000	0.17690	0.17680
0.07205	0.70981	0.00010	0.00000	0.16630	0.16630
0.07125	0.75237	0.00010	0.00000	0.15540	0.15530
0.07055	0.77808	0.00010	0.00000	0.14370	0.14370
0.06975	0.78615	0.00010	0.00000	0.13190	0.13190
0.06905	0.80108	0.00010	0.00000	0.11970	0.11970
0.06825	0.81175	0.00010	0.00000	0.10860	0.10860
0.06755	0.81947	0.00010	0.00000	0.09710	0.09700
0.06675	0.82415	0.00010	0.00000	0.08370	0.08360
0.06605	0.84400	0.00020	0.00000	0.07130	0.07120
0.06525	0.84886	0.00020	0.00000	0.05940	0.05940
0.06455	0.85456	0.00020	0.00000	0.04780	0.04770
0.06375	0.85867	0.00020	0.00000	0.03610	0.03610
0.06305	0.87029	0.00030	0.00000	0.02490	0.02490
0.06225	0.86362	0.00050	0.00000	0.01370	0.01370
0.06155	0.86197	0.00180	0.00000	0.00340	0.00310
0.06075	0.86445	0.05840	0.05480	0.00050	0.00000
0.06005	0.87281	0.12610	0.12290	0.00050	0.00000
0.05925	0.87871	0.18990	0.18680	0.00050	0.00000
0.05855	0.87449	0.25190	0.24880	0.00050	0.00000
0.05775	0.87281	0.31010	0.30700	0.00050	0.00000
0.05705	0.86945	0.37130	0.36820	0.00050	0.00000
0.05625	0.87449	0.42360	0.42050	0.00050	0.00000
0.05555	0.87449	0.47180	0.46870	0.00050	0.00000
0.05475	0.87197	0.51770	0.51460	0.00050	0.00000
0.05405	0.87956	0.56280	0.55970	0.00050	0.00000
0.05325		0.60400	0.60100	0.00040	0.00000
0.05255		0.64370	0.64060	0.00040	0.00000
0.05175		0.67640	0.67330	0.00040	0.00000
0.05105		0.70900	0.70600	0.00040	0.00000

Appendix

0.05025		0.73780	0.73480	0.00040	0.00000
0.04955		0.76580	0.76280	0.00040	0.00000
0.04875		0.79380	0.79080	0.00040	0.00000
0.04805		0.81870	0.81570	0.00040	0.00000
0.04725		0.83970	0.83670	0.00040	0.00000
0.04655		0.85910	0.85610	0.00040	0.00000
0.04575		0.87550	0.87240	0.00040	0.00000
0.04505		0.88950	0.88640	0.00040	0.00000
0.04425		0.90420	0.90120	0.00040	0.00000
0.04355		0.91670	0.91370	0.00040	0.00000
0.04275		0.92750	0.92450	0.00040	0.00000
0.04205		0.93720	0.93420	0.00040	0.00000
0.04125		0.94590	0.94280	0.00040	0.00000
0.04055		0.95350	0.95050	0.00040	0.00000
0.03975		0.96030	0.95730	0.00040	0.00000
0.03905		0.96640	0.96340	0.00040	0.00000
0.03825		0.97210	0.96900	0.00040	0.00000
0.03755		0.97640	0.97340	0.00040	0.00000
0.03675		0.98030	0.97730	0.00040	0.00000
0.03605		0.98380	0.98080	0.00040	0.00000
0.03525		0.98670	0.98370	0.00040	0.00000
0.03455		0.98930	0.98620	0.00040	0.00000
0.03375		0.99130	0.98830	0.00040	0.00000
0.03305		0.99310	0.99000	0.00040	0.00000
0.03225		0.99460	0.99160	0.00040	0.00000
0.03155		0.99600	0.99300	0.00040	0.00000
0.03075		0.99720	0.99420	0.00040	0.00000
0.03005		0.99830	0.99530	0.00040	0.00000
0.02925		0.99900	0.99600	0.00040	0.00000
0.02855		0.99960	0.99670	0.00040	0.00000
0.02775		0.99970	0.99730	0.00030	0.00000
0.02705		0.99970	0.99780	0.00030	0.00000
0.02625		0.99980	0.99820	0.00020	0.00000
0.02555		0.99980	0.99850	0.00020	0.00000
0.02475		0.99980	0.99880	0.00020	0.00000
0.02405		0.99990	0.99900	0.00010	0.00000
0.02325		0.99990	0.99920	0.00010	0.00000
0.02255		0.99990	0.99930	0.00010	0.00000
0.02175		0.99990	0.99950	0.00010	0.00000
0.02105		0.99990	0.99960	0.00010	0.00000
0.02025		1.00000	0.99960	0.00000	0.00000
0.01955		1.00000	0.99970	0.00000	0.00000
0.01875		1.00000	0.99980	0.00000	0.00000
0.01805		1.00000	0.99980	0.00000	0.00000
0.01725		1.00000	0.99990	0.00000	0.00000
0.01655		1.00000	0.99990	0.00000	0.00000

0.01575		1.00000	0.99990	0.00000	0.00000
0.01505		1.00000	0.99990	0.00000	0.00000
0.01425		1.00000	0.99990	0.00000	0.00000
0.01355		1.00000	1.00000	0.00000	0.00000
0.01275		1.00000	1.00000	0.00000	0.00000
0.01205		1.00000	1.00000	0.00000	0.00000
0.01125		1.00000	1.00000	0.00000	0.00000
0.01055		1.00000	1.00000	0.00000	0.00000
0.00975		1.00000	1.00000	0.00000	0.00000
0.00905		1.00000	1.00000	0.00000	0.00000
0.00825		1.00000	1.00000	0.00000	0.00000
0.00755		1.00000	1.00000	0.00000	0.00000
0.00675		1.00000	1.00000	0.00000	0.00000
0.00605		1.00000	1.00000	0.00000	0.00000
0.00525		1.00000	1.00000	0.00000	0.00000
0.00455		1.00000	1.00000	0.00000	0.00000
0.00375		1.00000	1.00000	0.00000	0.00000
0.00305		1.00000	1.00000	0.00000	0.00000
0.00225		1.00000	1.00000	0.00000	0.00000
0.00155		1.00000	1.00000	0.00000	0.00000
0.00075		1.00000	1.00000	0.00000	0.00000

Z [m]	HET				
	Measured Data	Oxygen		Ethylbenzene	
		Simulated Data			
		Double Monod	Instantaneous	Double Monod	Instantaneous
0.12905	0.95390	0.91360	0.91050	0.00040	0.00000
0.12825	0.89407	0.91280	0.90980	0.00040	0.00000
0.12755	0.85568	0.90970	0.90670	0.00040	0.00000
0.12675	0.81395	0.90270	0.89970	0.00040	0.00000
0.12605	0.77901	0.89430	0.89120	0.00040	0.00000
0.12525	0.72762	0.88320	0.88020	0.00040	0.00000
0.12455	0.67842	0.86850	0.86540	0.00040	0.00000
0.12375	0.62582	0.85140	0.84840	0.00040	0.00000
0.12305	0.56089	0.83180	0.82870	0.00040	0.00000
0.12225	0.48131	0.80940	0.80630	0.00040	0.00000
0.12155	0.39833	0.78370	0.78070	0.00040	0.00000
0.12075	0.24210	0.75490	0.75190	0.00040	0.00000
0.12005	0.15032	0.72380	0.72080	0.00040	0.00000
0.11925	0.08809	0.68880	0.68580	0.00040	0.00000
0.11855	0.04036	0.65150	0.64840	0.00040	0.00000
0.11775	0.02974	0.61180	0.60870	0.00040	0.00000
0.11705	0.03400	0.56900	0.56600	0.00050	0.00000
0.11625	0.03716	0.52310	0.52010	0.00050	0.00000

Appendix

0.11555	0.03421	0.47650	0.47340	0.00050	0.00000
0.11475	0.02749	0.42900	0.42600	0.00050	0.00000
0.11405	0.02075	0.38080	0.37770	0.00050	0.00000
0.11325	0.01623	0.33100	0.32800	0.00050	0.00000
0.11255	0.01400	0.28130	0.27820	0.00050	0.00000
0.11175	0.01189	0.23230	0.22920	0.00050	0.00000
0.11105	0.01046	0.18330	0.18010	0.00050	0.00000
0.11025	0.01008	0.13540	0.13220	0.00050	0.00000
0.10955	0.01065	0.08970	0.08640	0.00050	0.00000
0.10875	0.01084	0.04670	0.04300	0.00050	0.00000
0.10805	0.01027	0.00780	0.00050	0.00110	0.00000
0.10725	0.01142	0.00110	0.00000	0.00530	0.00000
0.10655	0.01122	0.00060	0.00000	0.01040	0.00510
0.10575	0.01113	0.00040	0.00000	0.01500	0.01030
0.10505	0.01142	0.00040	0.00000	0.01910	0.01500
0.10425	0.01056	0.00030	0.00000	0.02260	0.01900
0.10355	0.01037	0.00030	0.00000	0.02590	0.02250
0.10275	0.01132	0.00030	0.00000	0.02860	0.02590
0.10205	0.01056	0.00020	0.00000	0.03100	0.02860
0.10125	0.01103	0.00020	0.00000	0.03290	0.03100
0.10055	0.01094	0.00020	0.00000	0.03430	0.03280
0.09975	0.01132	0.00020	0.00000	0.03590	0.03420
0.09905	0.01094	0.00020	0.00000	0.03710	0.03580
0.09825	0.01065	0.00020	0.00000	0.03760	0.03710
0.09755	0.01056	0.00020	0.00000	0.03820	0.03760
0.09675	0.01056	0.00020	0.00000	0.03830	0.03810
0.09605	0.01113	0.00020	0.00000	0.03850	0.03830
0.09525	0.01027	0.00020	0.00000	0.03870	0.03850
0.09455	0.00970	0.00020	0.00000	0.03850	0.03870
0.09375	0.00999	0.00020	0.00000	0.03860	0.03840
0.09305	0.00933	0.00020	0.00000	0.03870	0.03850
0.09225	0.00970	0.00020	0.00000	0.03800	0.03870
0.09155	0.00999	0.00020	0.00000	0.03820	0.03800
0.09075	0.01008	0.00020	0.00000	0.03810	0.03810
0.09005	0.00999	0.00020	0.00000	0.03760	0.03810
0.08925	0.01027	0.00020	0.00000	0.03710	0.03750
0.08855	0.01027	0.00020	0.00000	0.03670	0.03700
0.08775	0.00914	0.00020	0.00000	0.03680	0.03670
0.08705	0.00980	0.00020	0.00000	0.03630	0.03680
0.08625	0.00914	0.00020	0.00000	0.03580	0.03630
0.08555	0.00857	0.00020	0.00000	0.03550	0.03580
0.08475	0.01008	0.00020	0.00000	0.03510	0.03540
0.08405	0.01247	0.00020	0.00000	0.03480	0.03500
0.08325	0.01343	0.00020	0.00000	0.03460	0.03480
0.08255	0.01391	0.00020	0.00000	0.03390	0.03460
0.08175	0.01304	0.00020	0.00000	0.03370	0.03380

0.08105	0.01151	0.00020	0.00000	0.03290	0.03370
0.08025	0.01018	0.00020	0.00000	0.03260	0.03290
0.07955	0.01027	0.00020	0.00000	0.03210	0.03260
0.07875	0.00961	0.00020	0.00000	0.03150	0.03200
0.07805	0.00999	0.00020	0.00000	0.03080	0.03150
0.07725	0.01046	0.00030	0.00000	0.03030	0.03080
0.07655	0.01075	0.00030	0.00000	0.03010	0.03030
0.07575	0.01046	0.00030	0.00000	0.02950	0.03010
0.07505	0.01008	0.00030	0.00000	0.02850	0.02950
0.07425	0.01027	0.00030	0.00000	0.02850	0.02850
0.07355	0.01037	0.00030	0.00000	0.02780	0.02850
0.07275	0.01056	0.00030	0.00000	0.02740	0.02780
0.07205	0.00914	0.00030	0.00000	0.02690	0.02730
0.07125	0.00904	0.00030	0.00000	0.02620	0.02680
0.07055	0.00942	0.00030	0.00000	0.02570	0.02620
0.06975	0.00980	0.00030	0.00000	0.02480	0.02570
0.06905	0.00952	0.00030	0.00000	0.02430	0.02480
0.06825	0.01008	0.00030	0.00000	0.02410	0.02430
0.06755	0.01008	0.00030	0.00000	0.02340	0.02400
0.06675	0.01094	0.00030	0.00000	0.02260	0.02340
0.06605	0.01018	0.00030	0.00000	0.02170	0.02250
0.06525	0.01180	0.00030	0.00000	0.02130	0.02170
0.06455	0.01065	0.00030	0.00000	0.02070	0.02130
0.06375	0.00961	0.00030	0.00000	0.02010	0.02070
0.06305	0.00914	0.00030	0.00000	0.01960	0.02000
0.06225	0.01104	0.00040	0.00000	0.01910	0.01960
0.06155	0.01132	0.00040	0.00000	0.01890	0.01900
0.06075	0.01180	0.00040	0.00000	0.01830	0.01880
0.06005	0.01400	0.00040	0.00000	0.01750	0.01820
0.05925	0.01877	0.00040	0.00000	0.01700	0.01750
0.05855	0.03231	0.00040	0.00000	0.01640	0.01700
0.05775	0.05494	0.00040	0.00000	0.01610	0.01640
0.05705	0.09911	0.00040	0.00000	0.01540	0.01600
0.05625	0.16324	0.00040	0.00000	0.01480	0.01530
0.05555	0.27892	0.00040	0.00000	0.01450	0.01470
0.05475	0.37412	0.00040	0.00000	0.01420	0.01440
0.05405	0.43707	0.00050	0.00000	0.01340	0.01420
0.05325	0.50393	0.00050	0.00000	0.01320	0.01330
0.05255	0.60943	0.00050	0.00000	0.01240	0.01310
0.05175	0.66580	0.00050	0.00000	0.01230	0.01240
0.05105	0.70295	0.00050	0.00000	0.01140	0.01220
0.05025	0.74878	0.00060	0.00000	0.01090	0.01130
0.04955	0.77629	0.00060	0.00000	0.01040	0.01080
0.04875	0.82182	0.00060	0.00000	0.00990	0.01030
0.04805		0.00060	0.00000	0.00950	0.00980
0.04725		0.00070	0.00000	0.00880	0.00940

Appendix

0.04655		0.00070	0.00000	0.00790	0.00870
0.04575		0.00080	0.00000	0.00760	0.00780
0.04505		0.00090	0.00000	0.00660	0.00750
0.04425		0.00100	0.00000	0.00580	0.00640
0.04355		0.00110	0.00000	0.00510	0.00570
0.04275		0.00140	0.00000	0.00410	0.00500
0.04205		0.00190	0.00000	0.00320	0.00390
0.04125		0.00310	0.00000	0.00210	0.00300
0.04055		0.00910	0.00240	0.00100	0.00160
0.03975		0.02150	0.01690	0.00070	0.00000
0.03905		0.03480	0.03080	0.00060	0.00000
0.03825		0.04940	0.04570	0.00050	0.00000
0.03755		0.06890	0.06540	0.00050	0.00000
0.03675		0.08970	0.08630	0.00050	0.00000
0.03605		0.11360	0.11030	0.00050	0.00000
0.03525		0.13890	0.13560	0.00050	0.00000
0.03455		0.16620	0.16300	0.00050	0.00000
0.03375		0.19780	0.19460	0.00050	0.00000
0.03305		0.23190	0.22870	0.00050	0.00000
0.03225		0.26880	0.26570	0.00050	0.00000
0.03155		0.30690	0.30380	0.00050	0.00000
0.03075		0.34890	0.34580	0.00050	0.00000
0.03005		0.38940	0.38630	0.00050	0.00000
0.02925		0.43210	0.42910	0.00050	0.00000
0.02855		0.47490	0.47190	0.00050	0.00000
0.02775		0.51850	0.51540	0.00050	0.00000
0.02705		0.56050	0.55740	0.00050	0.00000
0.02625		0.60170	0.59860	0.00040	0.00000
0.02555		0.64140	0.63830	0.00040	0.00000
0.02475		0.68020	0.67720	0.00040	0.00000
0.02405		0.71600	0.71300	0.00040	0.00000
0.02325		0.75020	0.74720	0.00040	0.00000
0.02255		0.78140	0.77830	0.00040	0.00000
0.02175		0.81010	0.80710	0.00040	0.00000
0.02105		0.83660	0.83350	0.00040	0.00000
0.02025		0.85990	0.85690	0.00040	0.00000
0.01955		0.88090	0.87790	0.00040	0.00000
0.01875		0.89960	0.89650	0.00040	0.00000
0.01805		0.91590	0.91290	0.00040	0.00000
0.01725		0.93000	0.92700	0.00040	0.00000
0.01655		0.94200	0.93900	0.00040	0.00000
0.01575		0.95250	0.94950	0.00040	0.00000
0.01505		0.96130	0.95830	0.00040	0.00000
0.01425		0.96880	0.96580	0.00040	0.00000
0.01355		0.97510	0.97210	0.00040	0.00000
0.01275		0.98040	0.97740	0.00040	0.00000

0.01205		0.98470	0.98170	0.00040	0.00000
0.01125		0.98830	0.98530	0.00040	0.00000
0.01055		0.99120	0.98820	0.00040	0.00000
0.00975		0.99360	0.99060	0.00040	0.00000
0.00905		0.99560	0.99260	0.00040	0.00000
0.00825		0.99720	0.99410	0.00040	0.00000
0.00755		0.99840	0.99540	0.00040	0.00000
0.00675		0.99940	0.99640	0.00040	0.00000
0.00605		0.99960	0.99720	0.00040	0.00000
0.00525		0.99970	0.99780	0.00030	0.00000
0.00455		0.99980	0.99830	0.00020	0.00000
0.00375		0.99980	0.99870	0.00020	0.00000
0.00305		0.99990	0.99890	0.00010	0.00000
0.00225		0.99990	0.99910	0.00010	0.00000
0.00155		0.99990	0.99920	0.00010	0.00000
0.00075		0.99990	0.99930	0.00010	0.00000

Measured and simulated distribution of the electron donor (ethylbenzene) at the outlet of the homogeneous and heterogeneous tanks during anaerobic degradation by *A. aromaticum* EbN1 in phase VIII. The concentration in [μM] equals the multiplication of the inlet concentration of ethylbenzene during phase VIII (200 μM ; see Tab. 3.1) with the respective C/C_0 value given in the tables below.

These data were used for Fig. 3.7a

Z [m]	HOM		
	Measured Data	Simulated Data	
		Double Monod	Instantaneous
0.112875	0.00000	0.00600	0.00000
0.100875	0.00000	0.00610	0.00000
0.088875	0.01765	0.00640	0.00000
0.076875	0.12415	0.00690	0.00000
0.064875	0.00382	0.00640	0.00000
0.052875	0.00000	0.00610	0.00000
0.040875	0.00000	0.00600	0.00000
0.028875	0.00000	0.00160	0.00000
0.016875	0.00000	0.00010	0.00000
0.004875	0.00000	0.00000	0.00000

Z [m]	HET		
	Measured Data	Simulated Data	
		Double Monod	Instantaneous
0.112875	0.00000	0.00610	0.00000
0.100875	0.00000	0.00610	0.00000
0.088875	0.00000	0.00620	0.00000

0.076875	0.00000	0.00620	0.00000
0.064875	0.00000	0.00620	0.00000
0.052875	0.00026	0.00620	0.00000
0.040875	0.00000	0.00620	0.00000
0.028875	0.00000	0.00610	0.00000
0.016875	0.00000	0.00600	0.00000
0.004875	0.00000	0.00130	0.00000

Measured and simulated distribution of the electron acceptor (nitrate) at the outlet of the homogeneous and heterogeneous tanks during anaerobic degradation by *A. aromaticum* EbN1 in phase VIII. The concentration in [μM] equals the multiplication of the inlet concentration of nitrate in the groundwater medium (1316 μM ; see Tab. 3.1) during phase VIII with the respective C/C_0 value given in the tables below.

These data were used for Fig. 3.7b

Z [m]	HOM		
	Measured Data	Simulated Data	
		Double Monod	Instantaneous
0.112875	0.78226	0.97140	0.96410
0.100875	0.45511	0.83350	0.82620
0.088875	0.14956	0.49350	0.48580
0.076875	0.23973	0.28980	0.28150
0.064875	0.49706	0.49260	0.48490
0.052875	0.64210	0.81770	0.81030
0.040875	0.87825	0.97180	0.96450
0.028875	0.92416	0.99840	0.99650
0.016875	0.92309	0.99990	0.99980
0.004875	0.96181	1.00000	1.00000

Z [m]	HET		
	Measured Data	Simulated Data	
		Double Monod	Instantaneous
0.112875	0.76023	0.93090	0.92360
0.100875	0.51711	0.74640	0.73900
0.088875	0.51546	0.65600	0.64850
0.076875	0.43863	0.66040	0.65300
0.064875	0.54081	0.67740	0.66990
0.052875	0.59550	0.69510	0.68770
0.040875	0.70755	0.71960	0.71220
0.028875	0.88301	0.81950	0.81210
0.016875	0.89064	0.96280	0.95550
0.004875	0.89647	0.99870	0.99720

Two-dimensional sediment microcosms – versatile test systems to study biodegradation processes in porous media

Distribution of bromide (tracer), the electron donor (toluene), and electron acceptor (nitrate) during the abiotic (conservative) and biotic (reactive) phase of an experiment conducted with the denitrifying *A. aromaticum* EbN1.

These data were used for Fig. 4.2a and 4.2b

Port	C/C ₀ [-]								
	Conservative						Reactive		
	Toluene		Nitrate		Bromide		Toluene	Nitrate	Bromide
	Average	SD	Average	SD	Average	SD			
2	0.003	0.001	0.947	0.121	0.017	0.005	0.000	0.909	0.012
3	0.065	0.007	0.699	0.138	0.080	0.003	0.001	0.709	0.060
4	0.314	0.028	0.364	0.106	0.270	0.003	0.025	0.256	0.221
5	0.441	0.028	0.222	0.108	0.385	0.020	0.090	0.005	0.416
6	0.199	0.024	0.477	0.122	0.194	0.004	0.005	0.289	0.226
7	0.018	0.003	0.804	0.105	0.040	0.012	0.000	0.801	0.057
8	0.000	0.000	0.924	0.087	0.014	0.001	0.000	0.984	0.008
9	0.000	0.000	0.985	0.017	0.000	0.000	0.000	0.952	0.000
10	0.000	0.000	1.002	0.022	0.000	0.000	0.000	1.019	0.000
11	0.000	0.000	1.013	0.039	0.000	0.000	0.000	1.029	0.000

The data of the abiotic phase was determined by taking the average of three subsequent days, whereas only one selected day was considered for representing the biotic phase.

Distribution of bromide (tracer), the electron donor (toluene), and electron acceptors (oxygen, nitrate) during a selected day of the biotic phase of a simultaneous experiment carried out with the aerobic *P. putida* mt-2 in the one tank and the denitrifying *A. aromaticum* EbN1 in the other tank.

These data were used for Fig. 4.2c and 4.2d

Port	C/C ₀ [-]					
	Aerobic			Anaerobic		
	Toluene	Oxygen	Bromide	Toluene	Nitrate	Bromide
	Average	Average	Average			
1.750						
1.833		0.992				
1.917		0.948				
2.000	0.000	0.909	0.000	0.009	0.954	0.008
2.083		0.898				
2.167		0.894				
2.250		0.880				
2.333		0.867				

2.417		0.850				
2.500		0.831				
2.583		0.817				
2.667		0.793				
2.750		0.777				
2.833		0.761				
2.917		0.720				
3.000	0.004	0.677	0.028	0.012	0.721	0.064
3.083		0.662				
3.167		0.622				
3.250		0.584				
3.333		0.534				
3.417		0.485				
3.500		0.429				
3.583		0.363				
3.667		0.264				
3.750		0.191				
3.833		0.105				
3.917		0.054				
4.000	0.163	0.027	0.172	0.060	0.208	0.240
4.083		0.013				
4.167		0.007				
4.250		0.007				
4.333		0.006				
4.417		0.006				
4.500		0.006				
4.583		0.007				
4.667		0.007				
4.750		0.007				
4.833		0.008				
4.917		0.007				
5.000	0.336	0.007	0.360	0.125	0.003	0.434
5.083		0.007				
5.167		0.008				
5.250		0.007				
5.333		0.007				
5.417		0.008				
5.500		0.007				
5.583		0.008				
5.667		0.008				
5.750		0.007				
5.833		0.008				
5.917		0.008				
6.000	0.254	0.007	0.304	0.024	0.290	0.185
6.083		0.007				
6.167		0.007				

6.250		0.008				
6.333		0.007				
6.417		0.007				
6.500		0.007				
6.583		0.007				
6.667		0.007				
6.750		0.007				
6.833		0.007				
6.917		0.007				
7.000	0.086	0.007	0.114	0.006	0.791	0.036
7.083		0.009				
7.167		0.014				
7.250		0.041				
7.333		0.099				
7.417		0.165				
7.500		0.244				
7.583		0.338				
7.667		0.436				
7.750		0.472				
7.833		0.513				
7.917		0.550				
8.000	0.013	0.592	0.018	0.001	0.937	0.006
8.083		0.649				
8.167		0.680				
8.250		0.726				
8.333		0.740				
8.417		0.779				
8.500		0.792				
8.583		0.805				
8.667		0.813				
8.750		0.820				
8.833		0.839				
8.917		0.843				
9.000	0.001	0.854	0.000	0.001	1.027	0.000
9.083		0.864				
9.167		0.865				
9.250		0.871				
9.333		0.884				
9.417		0.883				
9.500		0.878				
9.583		0.878				
9.667		0.875				
9.750		0.875				
9.833		0.876				
9.917		0.876				
10.000	0.002	0.886	0.000	0.001	0.987	0.000

10.083		0.883				
10.167		0.879				
10.250		0.878				
10.333		0.895				
10.417						
10.500						
10.583						
10.667						
10.750						
10.833						
10.917						
11.000	0.001		0.000	0.001	0.986	0.000

Vertical distribution of *A. aromaticum* EbN1 cells in an extracted sediment core 22.5 cm after the tank inlet, as determined after an experiment by flow cytometry.

These data were used for Fig. 4.3a

Depth [cm]	Cells [g _{Sediment} ⁻¹ (wwt)]
	<i>A. aromaticum</i> EbN1
0.3	1.58E+09
0.9	2.75E+09
1.5	7.40E+08
2.1	1.18E+09
2.7	4.65E+09
3.3	8.14E+09
3.9	1.37E+10
4.5	2.42E+10
5.1	1.17E+10
5.7	1.32E+10
6.3	1.36E+10
6.9	2.16E+10
7.5	1.25E+10
8.1	4.84E+09
8.7	1.80E+09

Vertical distribution of *P. putida* F1 and *A. aromaticum* EbN1 cells in an extracted sediment core 57 cm after the tank inlet, as determined after an experiment by fluorescence *in situ* hybridization.

These data were used for Fig. 4.3b

Depth [cm]	Cells [$\text{g}_{\text{Sediment}}^{-1}(\text{wwt})$]	
	<i>A. aromaticum</i> EbN1	<i>Pseudomonas putida</i> F1
0.5	0.00E+00	2.97E+07
1.4	5.41E+08	0.00E+00
2.3	1.48E+08	0.00E+00
3.2	6.76E+08	0.00E+00
4.1	2.05E+09	1.64E+08
5.1	1.73E+09	2.58E+08
5.9	2.48E+09	1.81E+08
6.9	3.68E+09	2.45E+08
7.8	2.17E+09	1.00E+08
8.7	7.87E+08	6.85E+07
9.6	5.60E+08	1.87E+08
10.6	0.00E+00	0.00E+00

Theoretical contribution of *P. putida* F1 and *A. aromaticum* EbN1 to the overall degradation on selected days of an experiment, representing different conditions, based on stable isotope fractionation data.

These data were used for Fig. 4.3c

Phase	Degradation [%]	
	<i>A. aromaticum</i> EbN1	<i>Pseudomonas putida</i> F1
X	0.0	24.9
Y	89.2	1.8
Z	39.3	20.8

Toluene distribution and isotope fractionation, as measured at the outlet of a tank featuring homogeneous sediment filling, of an experiment conducted with *A. aromaticum* EbN1.

These data were used for Fig. 4.4a

Port	Homogeneous sediment							
	Toluene C/C_0 [-]				Toluene $C(^1\text{H})/(^2\text{H})$ [-]			
	Abiotic		Isotope fractionation		Abiotic		Isotope fractionation	
2	0.012	0.000	0.000	0.000				
3	0.016	0.000	0.000	0.000				

4	0.130	0.005	0.028	0.000	9.4	6.6	4.5	2.2
5	0.328	0.093	0.124	0.002	9.5	8.4	4.9	3.0
6	0.357	0.163	0.303	0.032	9.3	7.0	4.1	2.1
7	0.141	0.141	0.089	0.000				
8	0.010	0.011	0.000	0.000				
9	0.002	0.000	0.000	0.000				
10	0.002	0.000	0.000	0.000				
11	0.001	0.000	0.000	0.000				

Toluene distribution and isotope fractionation of an experiment, conducted with the non-fractionating strain *P. putida* F1 and the fractionating *A. aromaticum* EbN1, as measured at the outlet of a tank featuring two consecutive quadrangular coarse sand layers embedded in a middle sand matrix.

These data were used for Fig. 4.4b

Port	Heterogeneous sediment (two lenses)							
	Ethylbenzene C/C_0 [-]				Ethylbenzene $C(^1H)/(^2H)$ [-]			
	Abiotic	Isotope fractionation			Abiotic	Isotope fractionation		
2	0.001	0.000	0.000	0.000				
3	0.016	0.028	0.015	0.000	3.1	1.5	1.2	0.0
4	0.026	0.067	0.046	0.000	3.0	2.3	1.7	0.0
5	0.057	0.107	0.076	0.009	2.9	2.5	1.8	0.2
6	0.036	0.060	0.040	0.009	2.9	2.4	1.6	0.4
7	0.021	0.013	0.012	0.008	3.0	2.3	1.6	0.9
8	0.008	0.001	0.002	0.000	3.1	1.9	1.6	0.0
9	0.001	0.000	0.000	0.000				
10	0.002	0.000	0.000	0.000				
11	0.000	0.000	0.000	0.000				

Toluene distribution and isotope fractionation of an experiment, conducted with the *A. aromaticum* EbN1, as measured at the outlet of a tank featuring one continuous coarse sand layer in a middle sand matrix.

These data were used for Fig. 4.4c

Port	Heterogeneous sediment (one lens)							
	Toluene C/C_0 [-]				Toluene $C(^1H)/(^2H)$ [-]			
	Abiotic	Isotope fractionation			Abiotic	Isotope fractionation		
2	0.000	0.000	0.426	0.331	9.0	7.9	8.0	6.2
3	0.056	0.000	0.000	0.000	9.0	6.1	7.0	5.7
4	0.187	0.000	0.005	0.053	8.8	5.2	6.4	5.2
5	0.170	0.106	0.129	0.134	8.6	4.3	5.1	3.6

6	0.168	0.108	0.125	0.068	9.1	4.0	2.8	2.4
7	0.165	0.084	0.072	0.016	9.7	4.4	1.7	0.4
8	0.121	0.048	0.001	0.000	9.9	5.5	3.2	2.0
9	0.018	0.053	0.000	0.000		7.2	6.1	4.9
10	0.114	0.027	0.000	0.000				
11	0.000	0.000	0.000	0.000				

Measured and simulated distribution of *P. putida* F1 cells at three distances from the tank inlet.

These data were used for Fig. 4.6

Z [m]	Cells [g _{Sediment} ⁻¹ (wwt)]					
	Experimental Data			Simulated Data		
	40 cm	57 cm	74 cm	40 cm	57 cm	74 cm
10.875			5.25E+08	2.13E+08	2.31E+08	1.60E+08
10.805				2.58E+08	2.68E+08	1.78E+08
10.725				3.17E+08	3.16E+08	1.97E+08
10.655		3.58E+08		3.99E+08	3.76E+08	2.21E+08
10.575	2.32E+08			5.02E+08	4.52E+08	2.48E+08
10.505				6.40E+08	5.47E+08	2.79E+08
10.425				8.44E+08	6.70E+08	3.14E+08
10.355			1.61E+08	1.16E+09	8.32E+08	3.57E+08
10.275				1.60E+09	1.04E+09	4.03E+08
10.205		8.74E+08		2.29E+09	1.29E+09	4.55E+08
10.125				3.04E+09	1.53E+09	5.20E+08
10.055	2.81E+08			3.00E+09	1.57E+09	5.84E+08
9.975				2.42E+09	1.36E+09	6.54E+08
9.905				1.79E+09	1.08E+09	7.13E+08
9.825			1.02E+08	1.32E+09	8.42E+08	7.37E+08
9.755		5.84E+08		9.81E+08	6.65E+08	7.04E+08
9.675				7.67E+08	5.43E+08	6.25E+08
9.605				6.26E+08	4.55E+08	5.33E+08
9.525				5.34E+08	3.94E+08	4.54E+08
9.455	1.91E+09			4.67E+08	3.46E+08	3.86E+08
9.375				4.15E+08	3.11E+08	3.35E+08
9.305		1.80E+08	8.79E+07	3.74E+08	2.82E+08	2.97E+08
9.225				3.41E+08	2.60E+08	2.66E+08
9.155				3.12E+08	2.42E+08	2.42E+08
9.075				2.88E+08	2.24E+08	2.23E+08
9.005				2.68E+08	2.10E+08	2.07E+08
8.925	1.00E+09			2.50E+08	1.98E+08	1.94E+08
8.855				2.35E+08	1.89E+08	1.82E+08
8.775		1.36E+08		2.22E+08	1.80E+08	1.72E+08
8.705			1.20E+08	2.13E+08	1.73E+08	1.63E+08

8.625				2.06E+08	1.68E+08	1.56E+08
8.555				2.01E+08	1.64E+08	1.50E+08
8.475				2.00E+08	1.61E+08	1.45E+08
8.405		2.56E+08		2.02E+08	1.61E+08	1.41E+08
8.325	2.55E+08			2.06E+08	1.62E+08	1.38E+08
8.255				2.13E+08	1.64E+08	1.36E+08
8.175			3.92E+08	2.23E+08	1.68E+08	1.35E+08
8.105				2.36E+08	1.74E+08	1.35E+08
8.025				2.51E+08	1.81E+08	1.36E+08
7.955				2.70E+08	1.90E+08	1.37E+08
7.875		4.22E+08		2.91E+08	2.01E+08	1.40E+08
7.805				3.15E+08	2.13E+08	1.45E+08
7.725	4.07E+08			3.42E+08	2.27E+08	1.50E+08
7.655			6.01E+08	3.77E+08	2.44E+08	1.57E+08
7.575				4.20E+08	2.63E+08	1.64E+08
7.505				4.74E+08	2.88E+08	1.73E+08
7.425		9.94E+08		5.43E+08	3.16E+08	1.84E+08
7.355				6.40E+08	3.54E+08	1.97E+08
7.275				7.85E+08	4.00E+08	2.11E+08
7.205	1.61E+09			1.01E+09	4.70E+08	2.29E+08
7.125			4.83E+08	1.36E+09	5.66E+08	2.50E+08
7.055				1.86E+09	6.99E+08	2.78E+08
6.975		7.07E+08		2.49E+09	8.85E+08	3.14E+08
6.905				3.08E+09	1.14E+09	3.59E+08
6.825				3.00E+09	1.41E+09	4.23E+08
6.755				2.20E+09	1.58E+09	5.03E+08
6.675				1.55E+09	1.50E+09	5.97E+08
6.605	1.07E+09		1.68E+08	1.11E+09	1.24E+09	6.92E+08
6.525		3.93E+08		8.23E+08	1.00E+09	7.53E+08
6.455				6.27E+08	8.04E+08	7.55E+08
6.375				4.90E+08	6.44E+08	6.99E+08
6.305				3.86E+08	5.30E+08	6.31E+08
6.225				3.10E+08	4.38E+08	5.58E+08
6.155				2.53E+08	3.63E+08	4.87E+08
6.075			1.39E+08	2.09E+08	3.07E+08	4.25E+08
6.005	3.84E+08	2.17E+08		1.72E+08	2.60E+08	3.73E+08
5.925				1.45E+08	2.23E+08	3.24E+08
5.855				1.23E+08	1.91E+08	2.86E+08
5.775				1.05E+08	1.66E+08	2.53E+08
5.705				9.11E+07	1.45E+08	2.23E+08
5.625		1.47E+08		7.91E+07	1.27E+08	1.98E+08
5.555			2.67E+08	6.97E+07	1.12E+08	1.77E+08
5.475	1.67E+08			6.23E+07	9.91E+07	1.59E+08
5.405				5.62E+07	8.91E+07	1.42E+08
5.325				5.10E+07	8.01E+07	1.28E+08
5.255				4.68E+07	7.23E+07	1.16E+08

5.175		1.10E+08		4.36E+07	6.59E+07	1.05E+08
5.105				4.10E+07	6.04E+07	9.53E+07
5.025			2.48E+08	3.87E+07	5.55E+07	8.69E+07
4.955				3.68E+07	5.13E+07	7.98E+07
4.875	1.25E+08			3.55E+07	4.81E+07	7.33E+07
4.805				3.42E+07	4.52E+07	6.75E+07
4.725		1.49E+08		3.33E+07	4.26E+07	6.23E+07
4.655				3.26E+07	4.07E+07	5.81E+07
4.575				3.20E+07	3.87E+07	5.42E+07
4.505			3.15E+08	3.13E+07	3.71E+07	5.10E+07
4.425				3.10E+07	3.62E+07	4.81E+07
4.355				3.04E+07	3.49E+07	4.55E+07
4.275	1.41E+08	1.41E+08		3.04E+07	3.39E+07	4.33E+07
4.205				3.00E+07	3.33E+07	4.13E+07
4.125				2.97E+07	3.26E+07	3.97E+07
4.055				2.97E+07	3.20E+07	3.81E+07
3.975			2.86E+08	2.97E+07	3.16E+07	3.71E+07
3.905				2.94E+07	3.10E+07	3.58E+07
3.825		1.15E+08		2.94E+07	3.07E+07	3.49E+07
3.755	2.28E+08			2.94E+07	3.04E+07	3.42E+07
3.675				2.94E+07	3.04E+07	3.33E+07
3.605				2.94E+07	3.00E+07	3.29E+07
3.525				2.94E+07	3.00E+07	3.23E+07
3.455			5.58E+08	2.94E+07	2.97E+07	3.16E+07
3.375		2.30E+08		2.94E+07	2.97E+07	3.13E+07
3.305				2.94E+07	2.97E+07	3.10E+07
3.225				2.94E+07	2.94E+07	3.07E+07
3.155	3.30E+08			2.94E+07	2.94E+07	3.07E+07
3.075				2.94E+07	2.94E+07	3.04E+07
3.005				2.94E+07	2.94E+07	3.00E+07
2.925		3.42E+08	4.58E+08	2.94E+07	2.94E+07	3.00E+07
2.855				2.94E+07	2.94E+07	3.00E+07
2.775				2.94E+07	2.94E+07	2.97E+07
2.705				2.94E+07	2.94E+07	2.97E+07
2.625				2.94E+07	2.94E+07	2.97E+07
2.555	1.28E+08			2.94E+07	2.94E+07	2.94E+07
2.475		1.76E+08		2.94E+07	2.94E+07	2.94E+07
2.405			4.66E+08	2.94E+07	2.94E+07	2.94E+07
2.325				2.94E+07	2.94E+07	2.94E+07
2.255				2.94E+07	2.94E+07	2.94E+07
2.175				2.94E+07	2.94E+07	2.94E+07
2.105				2.94E+07	2.94E+07	2.94E+07
2.025	2.86E+08	9.66E+07		2.94E+07	2.94E+07	2.94E+07
1.955				2.94E+07	2.94E+07	2.94E+07
1.875			7.16E+08	2.94E+07	2.94E+07	2.94E+07
1.805				2.94E+07	2.94E+07	2.94E+07

1.725				2.94E+07	2.94E+07	2.94E+07
1.655				2.94E+07	2.94E+07	2.94E+07
1.575		1.79E+08		2.94E+07	2.94E+07	2.94E+07
1.505				2.94E+07	2.94E+07	2.94E+07
1.425	1.68E+08			2.94E+07	2.94E+07	2.94E+07
1.355			1.05E+09	2.94E+07	2.94E+07	2.94E+07
1.275				2.94E+07	2.94E+07	2.94E+07
1.205				2.94E+07	2.94E+07	2.94E+07
1.125		2.95E+08		2.94E+07	2.94E+07	2.94E+07
1.055				2.94E+07	2.94E+07	2.94E+07
0.975				2.94E+07	2.94E+07	2.94E+07
0.905	3.89E+08			2.94E+07	2.94E+07	2.94E+07
0.825			1.52E+09	2.94E+07	2.94E+07	2.94E+07
0.755				2.94E+07	2.94E+07	2.94E+07
0.675		7.20E+08		2.94E+07	2.94E+07	2.94E+07
0.605				2.94E+07	2.94E+07	2.94E+07
0.525				2.94E+07	2.94E+07	2.94E+07
0.455				2.94E+07	2.94E+07	2.94E+07
0.375				2.94E+07	2.94E+07	2.94E+07
0.305	6.86E+08		1.41E+09	2.94E+07	2.94E+07	2.94E+07
0.225		8.17E+08		2.94E+07	2.94E+07	2.94E+07
0.155				2.94E+07	2.94E+07	2.94E+07
0.075				2.94E+07	2.94E+07	2.94E+07
0.005				2.94E+07	2.94E+07	2.94E+07

Wissenschaftlicher Bildungsgang

Robert Christian Damiano Bauer

geboren am 19.10.1977 in München

- 1996 Abitur am Kurt-Huber-Gymnasium, Gräfelfing
- 1997-2003 Biologiestudium an der Technischen Universität München; mündliche Abschlußprüfungen in den Fächern Mikrobiologie, Genetik, und Geologie und Paläontologie. Abschlußarbeit am Lehrstuhl für Mikrobiologie bei Prof. Dr. Karl-Heinz Schleifer. Arbeitstitel: Untersuchung zur Verbreitung der Oberflächenstrukturproteine Fimbrien, cable pili und Flagellen innerhalb des *Burkholderia cepacia* Komplexes.
- 2003-2007 Promotion in der Geomikrobiologie an der Geowissenschaftlichen Fakultät, Eberhard-Karls-Universität Tübingen, bei Prof. Dr. Rainer Meckenstock, Prof. Dr. Peter Grathwohl und Prof. Dr. Stefan Haderlein.
- Akademische Lehrer: Dr. Christian Griebler
 Prof. Dr. Rainer Meckenstock
 Prof. Dr. Piotr Maloszewski

Publications:

- Bauer R. D., Kürzinger P., Rolle M., Meckenstock R. U., Griebler C. Two-dimensional sediment microcosms – versatile test systems to study biodegradation processes in porous media. *In preparation*.
- Bauer R. D., Rolle M., Eberhardt C., Grathwohl P., Bauer S., Kolditz O., Meckenstock R. U., Griebler C. Enhanced biodegradation via flow focusing of contaminant plumes in high-conductivity lenses. *In preparation*.
- Rolle M., Bauer R. D., Bauer S., Kolditz O., Meckenstock R. U., Griebler C. Biodegradation of a toluene plume in homogeneous and heterogeneous porous media. *submitted to Groundwater Qual Proc*.
- Bauer R. D., Maloszewski P., Zhang Y., Meckenstock R. U., Griebler G. (2007) Mixing-controlled biodegradation in a toluene plume – results from two-dimensional laboratory experiments. *J Contam Hydrol*, in press.
- Bauer R., Anneser B. & Griebler C. Das Schadstofffahnenrand-Konzept – Ökologie und Biochemie des biologischen Abbaus in organisch kontaminierten Grundwasserökosystemen. *Deutsche Gesellschaft für Limnologie (DGL) – Tagungsbericht 2006 (Dresden)*, accepted.
- Bauer R. D., Meckenstock R. U., Griebler C. Two-dimensional model aquifer – Effects of sulphide on aerobic and anaerobic degradation of toluene at the fringe of anoxic plumes. *Soil remediation series No. 7. International summer school 2005, Genoa, Italy*. Eds.: Prof. Pietro Canepa, Prof. Fabio Fava. ISBN 88-88214-32-1.
- Eckert P., Richters L., Wisotzky F., Schulte U., Eisenberg V., Griebler C., Bauer R., Anneser B. Projekt 2.2: Monitoring und Bewertung von stimulierten Selbstreinigungsprozessen (ENA) im Vergleich zu natürlichen Selbstreinigungsprozessen (NA) an einem BTEX- und PAK-belasteten Porengrundwasserleiter. *KORA Statusseminar-Band 2005*, S. 83-99, Herausgeber: Dechema, Frankfurt a. M. ISBN 3-89746-071-X.
- Bauer R., Eckert P., Frentjen H., Griebler C., Hellige K., Irmischer R., Kluge M., Meckenstock R., Richters L., Schulte U, Wisotzky F. Projekt 2.2: Monitoring und Bewertung von stimulierten Selbstreinigungsprozessen (ENA) im Vergleich zu natürlichen Selbstreinigungsprozessen (NA) an einem BTEX- und PAK- belasteten Porengrundwasserleiter. *KORA Statusseminar-Band 2004*, S. 62-75, Herausgeber: Dechema, Frankfurt a. M.

Selected Posters and Presentations:

- Bauer R.D., Meckenstock R.U., Griebler C. What limits microbial growth in groundwater contaminant plumes? University of Virginia (Dept. of Civil Engineering), Charlottesville, USA, May, 2007. Oral Presentation.
- Bauer R.D., Meckenstock R.U., Griebler C. Degradation of organic contaminants in porous aquifers – is it heterogeneity that matters? European Geosciences Union Meeting, Vienna, Austria, Apr., 2007. Oral Presentation.
- Bauer R.D., Meckenstock R.U., Griebler C. Investigation of contaminant plumes in a two-dimensional model aquifer – biodegradation at the fringe of anoxic toluene plumes by bacterial communities. Dechema Tagung, Frankfurt, Nov., 2006. Poster.
- Bauer R.D., Meckenstock R.U., Griebler C. Investigation of Microbial degradation in toluene plumes – recent studies in 2-D model aquifers. PhD-seminars Applied Geosciences, Universität Tübingen, Nov., 2006. Oral Presentation.
- Bauer R.D., Meckenstock R.U., Griebler C. Investigation of contaminant plumes in a two-dimensional model aquifer – biodegradation at the fringe of anoxic toluene plumes. HydroEco Meeting, Karlovy Vary, Czech Republic, Sep., 2006. Poster.
- Bauer R.D., Meckenstock R.U., Griebler C. Investigation of contaminant plumes in a two-dimensional model aquifer – Influence of sulphide to aerobic and anaerobic degradation of toluene at the fringe of anoxic plumes. VAAM-Meeting, Göttingen, Mar., 2005. Oral Presentation.
- Bauer R.D., Meckenstock R.U., Griebler C. Plume studies in a 2D-model aquifer – First results on the influence of sulphide on the thickness of the reactive zone for aerobic degradation at the fringe of an anoxic toluene plume. KORA-Seminartagung, Leipzig, Oct., 2004. Poster.